ABSTRACT

HE, JIAN. Development and Evaluation of Earth System Models on Global and Regional Scales: Aerosol Chemistry and Dynamics, Air-Sea Interactions, and Retrospective Decadal Applications. (Under the direction of Drs. Yang Zhang and Ruoying He.)

Earth system models have been used for climate predictions in recent years due to their capabilities to include coupled and interactive representations of Earth's components (e.g., atmosphere, ocean, land, and sea ice). The Intergovernmental Panel on Climate Change (IPCC) Fifth Assessment Report (AR5) indicated that the uncertainties associated with cloud, aerosol, and their feedbacks, as well as uncertainties in near- and long-term projections from earth system models are emerging issues to be addressed by the scientific community. The Community Earth System Model (CESM) is a global Earth system model that has been developed to simulate the entire Earth system by coupling physical climate system with chemistry, biogeochemistry, biology, and human systems, and it has been applied to simulate global climate change as part of IPCC-AR5. In this work, to reduce the uncertainties associated with predicted aerosol impacts on climate, several advanced chemistry and aerosol treatments are implemented to Community Atmosphere Model (CAM), which is the atmospheric component of CESM. Those treatments include two new gas-phase chemical mechanisms (i.e., the 2005 Carbon Bond Mechanism with Global Extension (CB05_GE), and the Model for OZone and Related chemical Tracers version 4 with extension (MOZART-4x)), and several advanced inorganic aerosol treatments for condensation of volatile species, ion-mediated nucleation, and explicit inorganic aerosol thermodynamics. CESM/CAM with advanced chemistry and aerosol treatments is applied for decadal (2001-2010) global climate predictions. The results demonstrate that the improved model is capable of predicting meteorology, radiation, and aerosol components, although large biases remain

in predictions on cloud variables, likely due to the uncertainties in cloud dynamics and thermodynamics in the model. Sensitivity simulations using CESM/CAM with different gas-phase mechanisms (i.e., CB05_GE and MOZART-4x) are also conducted to examine the differences in the secondary organic aerosols (SOA) predictions resulted from the two mechanisms and study the sensitivity of air quality and climate predictions to different gas-phase mechanisms. The results show that MOZART-4x can predict better secondary organic aerosols (SOA) than CB05_GE at four sites over continental U.S., but both largely underpredict total organic carbon over Europe. The two gas-phase mechanisms result in a global average difference of 0.5 W m^{-2} in simulated shortwave cloud radiative forcing, with significant differences (e.g., up to 13.6 W m^{-2}) over subtropical regions.

Regional Earth system modeling is also important since fine scale feedbacks associated with interactions among Earth's components can substantially influence regional air quality and climate. The Coupled Ocean-Atmosphere-Wave-Sediment Transport (COAWST) Modeling System enables integration of oceanic, atmospheric, wave and morphological processes in the coastal ocean. In this work, to investigate the impacts of air-sea interactions on regional air quality predictions, Weather Research and Forecasting model with chemistry (WRF/Chem) turns on the option of1-D ocean mixed layer (OML) treatment and is coupled with the 3-D Regional Ocean Modeling System (ROMS) within COAWST. The sensitivity simulations are conducted over southeastern U.S. for July 2010. The results show that compared to WRF/Chem without ocean treatments, the changes in the sea surface temperature (SST) by WRF/Chem-OML and WRF/Chem-ROMS are 0.1 ^{o}C and 1.0 ^{o}C, respectively, and the differences in surface O_3 and $PM_{2.5}$ can be as large as 17.3 ppb and 7.9 μg m^{-3}, respectively. The largest changes in surface O_3 and $PM_{2.5}$ occur not only along coast

and remote ocean, but also over inland area, indicating the significant impacts of air-sea interactions on chemical predictions. With coupling of 3-D ocean model, WRF/Chem-ROMS predictions of most clouds and radiative variables are improved, especially over ocean. WRF/Chem-ROMS predictions of surface chemical species such as SO_2, HNO_3, Max 1-h and 8-h O_3, SO_4^{2-}, NH_4^+, NO_3^-, and PM_{10} are also improved.

Development and Evaluation of Earth System Models on Global and Regional Scales: Aerosol Chemistry and Dynamics, Air-Sea Interactions, and Retrospective Decadal Applications

by
Jian He

A dissertation submitted to the Graduate Faculty of
North Carolina State University
in partial fulfillment of the
requirements for the degree of
Doctor Philosophy

Marine, Earth, and Atmospheric Sciences

Raleigh, North Carolina

2015

APPROVED BY:

Dr. Yang Zhang Committee Chair	Dr. Ruoying He Co-Chair of Advisory Committee
Dr. Nicholas Meskhidze	Dr. H. Christopher Frey

BIOGRAPHY

Jian He was born in Nantong, Jiangsu Province, China. She finished her elementary, middle, and high schools in her hometown and was admitted to Nanjing University in 2004. As a freshman, she was admitted to a national program of Geographical Science funded by the National Nature Science Foundation of China. During her undergraduate, she developed an interest in Earth system study, with a focus on the land surface and hydrological processes.

Upon receiving her B.S. degree in 2008, Jian was admitted as an M.S. student to the Graduate School of Nanjing University with an honor of exam waiver. Her Master thesis research focused on the sediment dynamics in coastal systems using short-lived radioisotopes. She participated in several national projects through field studies and laboratory measurements. She also published two papers based on her Master's research. Over the years her interests in Earth system study spread from land to ocean, and now move to atmosphere.

In August 2011, Jian began her study in the Department of Marine, Earth, and Atmospheric Sciences at the North Carolina State University. She was fortune enough to have her thesis advisors, Drs. Yang Zhang and Ruoying He, provide her with broad topics of numerical modeling of atmospheric chemistry and air-sea interactions. They were new and challenging topics for her as she did not have numerical modeling background. But it was also a great opportunity and transition for her from marine sciences to atmospheric sciences. Her Ph.D. research focused on the improvement and development of the Community Earth System Model (CESM), which is a global Earth System Model that enables the simulation of

the entire Earth system by coupling physical climate system with chemistry, biogeochemistry, biology, and human systems.

During her Ph.D. research, Jian attended several conferences and workshops and received several awards and fellowships, including Travel Awards from CESM Workshop and A&WMA, and a fellowship award from the NCAR's Advanced Study Program. At present, she has 2 first-author papers published, 1 first-author paper submitted, 1 first-author paper in preparation, and several co-author papers published and in review. She also has presented 7 first-author posters, 1 first-author oral presentation, and 8 co-author posters.

ACKNOWLEDGMENTS

I would first like to thank my advisory committee: Drs. Yang Zhang, Ruoying He, Nicholas Meskhidze, and H. Christopher Frey for their guidance and help with this work. I would especially like to thank Dr. Yang Zhang for her efforts and patience with this extensive research project. Dr. Yang Zhang has provided me a lot of opportunities, great ideas and professional training during my Ph.D. study, which will benefit me a lot throughout my career life. Special thanks are also due to Dr. Ruoying He, who is willing to serve as my co-advisor, and provided me great ideas and guidance in modeling air-sea interactions. Thanks are also due to the following people, Drs. Simone Tilmes, Louisa Emmons, Jean-Francois Lamarque, Alma Hodzic, and Francis Vitt at NCAR, who provided scientific contributions and support during my intern research at NCAR.

In addition, I also want to thank the project sponsors for my research by the U.S. National Science Foundation EaSM program AGS-1049200, and the high-performance computing support from Yellowstone (ark:/85065/d7wd3xhc) provided by NCAR's Computational and Information Systems Laboratory, sponsored by the U.S. National Science Foundation.

I also wish to thank the current and former group members of the Air Quality Forecasting Lab, and also my friends during my stay at NCSU, Drs. Kai Wang, Patrick Campbell, Duan Kai, Shuai Zhu, and Brett Gantt, Khairunnisa Yahya, Timothy Glotfelty, Ying Chen, Xue Feng, and Nan Zhang for their encouragement and help during these four years. Without them, I probably cannot finish my Ph.D. on time.

Lastly, I would like to thank my parents, who have been always there supporting me and encouraging me. It has been a very interesting and challenging time since August, 2011, I have learned a lot during my experience here at North Carolina State University. This is a very valuable and unforgettable memory in my life.

TABLE OF CONTENTS

LIST OF TABLES

LIST OF FIGURES

LIST OF ACRONYMS

Acronym	Definition
1-D	One dimensional
3-D	Three dimensional
α	the mass accommodation coefficient
AACD	Acetic and higher carboxylic acids
ACCMIP	the Atmospheric Chemistry and Climate Model Intercomparison Project
AirBase	the European air quality database
AIRS-AQS	the Aerometric Information Retrieval System-Air Quality System
ALD2	Acetaldehyde
ALDX	Propionaldehyde and higher aldehydes
ALKH	Long-chain alkanes
AMWG	the Atmospheric Model Working Group
ANN/ANU	Annual
AOD	Aerosol optical depth
APIN	α-pinene
AQMEII	the Air Quality Modeling Evaluation International Initiative Phase II
ARCPAC	the Aerosol, Radiation, and Cloud Processes affecting Arctic Climate
ARCTAS	the Arctic Research of the Composition of the Troposphere from Aircraft and Satellites
ASOA	Anthropogenic secondary organic aerosol
AUS	Australia
AVOCs	Anthropogenic volatile organic compounds
BC	Black carbon
BCARY	Beta-caryophyllene + other sesquiterpenes
BDQA	Base de Données sur la Qualité de l'Air
BIGALK	Lumped alkanes C > 3
BIGENE	Lumped alkenes C > 3
BPIN	β-pinene
BSOA	Biogenic secondary organic aerosol
BVOCs	Biogenic volatile organic compounds
$C_2H_2O_2$/GLY	Glyoxal
C_3H_6	Propene
Ca^{2+}	Calcium
CalNex	California Nexus
CAMx	the Comprehensive Air Quality Model with Extensions

CASTNET	the Clean Air Status and Trends Network
CB05	the 2005 Carbon Bond Mechanism
CB05_GE	the 2005 Carbon Bond Mechanism with Global Extension
CCN	Cloud condensation nuclei
CCN5	Cloud condensation nuclei at supersaturation of 5%
CDNC	Cloud droplet number concentration
CERES	the Clouds and Earth's Radiant Energy System
CERES-SYN1deg	the CERES Synoptic product at 1^{o} spatial resolution
CF	Cloud fraction
CF_2Cl_2	Dichlorodifluoromethane
CF_2ClBr	Bromochlorodifluoromethane
CF_3Br	Bromotrifluoromethane
$CFCl_3$	Trichlorofluoromethane
CH_3Cl	Chloromethane
Cl^-	Chloride
$ClNO_2$	Nitryl chloride
CMAQ	the Community Multi-scale Air Quality
CMIP5	the Coupled Model Intercomparison Project Phase 5
CO	Carbon monoxide
CO_2	Carbon dioxide
COAWST	the Coupled Ocean-Atmosphere-Wave-Sediment Transport
CONUS	Continental U.S.
Corr	Correlation coefficient
COT	Cloud optical thickness
CRES	Cresol and higher molecular weight phenols
D_g	the gas diffusivity
DJF	December, January, and February
DMS	Dimethyl sulfide
Dp	the particle diameter
DU	Dobson unit
EC	Elemental carbon
EDGAR	the Emission Database for Global Atmospheric Research
EMEP	the European Monitoring and Evaluation Program
ETH	Ethene
ETHA	Ethane
ETOH	Ethanol

FACD	Formic acid
FLDS/LWD	Downwelling longwave radiation at surface
FLNS	Net longwave radiation at surface
FLUT/OLR	Outgoing longwave radiation at top of atmosphere
FMCL	Formyl fluoride
FORM/HCHO	Formaldehyde
FSDS/SWD	Downwelling shortwave radiation at surface
FSNS	Net shortwave radiation at surface
GCMs	Global climate models
GEOS-5	the Goddard Earth Observing System Model, Version 5
GEOS-Chem	the Goddard Earth Observing System-Chemistry model
GFDL-ESM2	the Geophysical Fluid Dynamics Laboratory (GDFL) Earth System Model version 2
GLSOA	Secondary organic aerosol from glyoxal
GOME	the Global Ozone Monitoring Experiment
GPCP	the Global Precipitation Climatology Project
GU-WRF/Chem	the Global-through-Urban Weather Research and Forecasting model with Chemistry
H_2	Hydrogen gas
H_2O	Water
H_2O_2	Hydrogen peroxide
H_2SO_4	Sulfuric acid
HadGEM2-A	the Hadley Centre Global Environmental Model version 2 atmosphere model
HadGEM2-ES	the Hadley Centre Global Environmental Model version 2 including Earth system components
HCl	Hydrochloric acid
Hg	Mercury
Hg(0)	Elemental Hg
Hg(II)	Divalent gaseous Hg
HNO_3	Nitric acid
HO_2	Hydroperoxyl radical
HOA	Hydrocarbon-like organic aerosol
HO_x	$OH + HO_2$
HTAP	Hemispheric Transport of Air Pollution
HONO	Nitrous acid
HUM	Humulene
I_{cond}	the uptake rate

IMN	Ion-mediated nucleation
IMPROVE	the Interagency Monitoring of Protected Visual Environments
I_{net}	the gas condensation rate
IOLE	Internal olefin carbon bond (R-C=C-R)
ISOP	Isoprene
ISPD	Isoprene product (lumped methacrolein, methyl vinyl ketone, etc.)
J	Particle formation rate
JJA	June, July, and August
K^+	Potassium
KMOE	the Korean Ministry of Environment
Kn	the Knudsen number
LHFLX	Latent heat flux
LIM/LIMON	Limonene
LWCF	Longwave cloud radiative forcing
LWP	Cloud liquid water path
MACCity	the Monitoring Atmospheric Composition and Climate/CityZen
MAM	March, April, and May
MAM3	the modal aerosol model with three lognormal modes
MAM7	the modal aerosol model with seven lognormal modes
MB	Mean bias
MEGAN	the Model of Emissions of Gases and Aerosols from Nature
MEIC	the Multi-resolution Emission Inventory for China
MEOH	Methanol
MEPC	the Ministry of Environmental Protection of China
MEPX	Methylhydroperoxide
MESA	the Multicomponent Equilibrium Solver for Aerosols
Mg^{2+}	Magnesium
MGLY	Methylglyoxal and other aromatic products
MIT-IGSM	the Massachusetts Institute of Technology Integrated Global System Model
MODIS	Moderate Resolution Imaging Spectroradiometer
MOPITT	the Measurements Of Pollution In The Troposphere
MOZART-4	the Model of OZone and Related chemical Tracers version 4
MOZART-4x	the Model of OZone and Related chemical Tracers version 4 with extension
MPI-ESM	the new Max-Planck-Institute Earth System Model
MYRC	Myrcene
N_2O	Nitrous oxide
N_2O_5	Dinitrogen pentoxide

Na^+	Sodium
NAM	North America
NARR	North American Regional Reanalysis
NCAR	National Center for Atmospheric Research
NCDC	the National Climatic Data Center
NCEP	the National Centers for Environmental Prediction
NDBC	the National Data Buoy Center
NEI	the National Emission Inventory
NH_3	Ammonia
NH_4^+	Ammonium
NIESJ	the National Institute for Environmental Studies of Japan
NMB	Normalized mean bias
NME	Normalized mean error
NO	Nitric oxide
NO_2	Nitrogen dioxide
NO_3	Nitrate radical
NO_3^-	Nitrate
NOAA/CDC	the National Oceanic and Atmospheric Administration Climate Diagnostics Center
NO_x	$NO+NO_2$
NO_y	the reactive nitrogen species
NTR	Organic nitrate
O	Oxygen atom in the O^3 (P) electronic state
O1D	Oxygen atom in the O^1 (D) electronic state
OAFlux	the Objectively Analyzed Air-Sea Fluxes
OC	Organic carbon
OCI	Ocimene
OH	Hydroxyl radical
OLE	Terminal olefin carbon bond (R-C=C)
OMI/MLS	the Aura Ozone Monitoring Instrument in combination with Aura Microwave Limb Sounder
OOA	Oxygenated organic aerosol
OPEN	Aromatic ring opening product
PACD	Peroxyacetic and higher peroxycarboxylic acids
PAH	Polycyclic aromatic hydrocarbons
PAN	Peroxyacetyl nitrate
PANX	C3 and higher peroxyacyl nitrates

PAR	Paraffin carbon bond (C-C)
PBLH	Planetary boundary layer height
PM_{10}	Particulate matter with diameter less than 10 μm
$PM_{2.5}$	Particulate matter with diameter less than 2.5 μm
PNA	Peroxynitric acid
POA	Primary organic aerosol
POC	Primary organic carbon
POM	Primary organic matter
Precip	Precipitation
PWV	Precipitative water vapor
Q2	Specific humidity at 2-meter
RCP	the Representative Concentration Pathway
RH	Relative humidity
RH2	Relative humidity at 2-meter
RMSE	Root mean squared error
ROMS	the Regional Ocean Model System
ROOH	Higher organic peroxide
RRTMG	the Rapid Radiative Transfer Model for GCMs
S/IVOCs	the Semi/intermediate volatility compounds
SAF	South Africa
SAM	South America
SCIAMCHY	the SCanning Imaging Absorption spectroMeter for Atmospheric CHartographY
SEA	Southeast Asia
SHFLX	Sensible heat flux
SO_2	Sulfur dioxide
SO_4^{2-}	Sulfate
SOA	Secondary organic aerosol
SOAG	Lumped secondary organic aerosol gaseous precursors
SON	September, October, and November
SST	Sea surface temperature
STN	the Speciation Trends Network
SVSOA	Semi-volatile secondary organic aerosol
SWCF	Shortwave cloud radiative forcing
T2	Temperature at 2-meter
TAQMN	Taiwan Air Quality Monitoring Network
TC	Total carbon

TER	Terpinene
TERP	Lumped-terpene
TMPA	the Multi-satellite Precipitation Analysis from the Tropical Rainfall Measuring Mission
TOA	Total organic aerosol
TOL	Toluene and other monoalkyl aromatics
TOMS/SBUV	the Total Ozone Mapping Spectrometer/the Solar Backscatter UltraViolet
TOR	Tropospheric ozone residual
VBS	volatility-basis-set
VOCs	Volatile organic compounds
VSOA	Volatile secondary organic aerosol
WRF	the Weather Research and Forecasting model
WRF/Chem	the Weather Research and Forecasting model with Chemistry
WS10	Wind speed at 10-meter
XYL	Xylene and other polyalkyl aromatics

CHAPTER 1. INTRODUCTION

1.1 Background

Atmospheric gases and aerosols play important roles in climate change due to their ability to directly or indirectly alter the Earth's radiation balance. Atmospheric chemistry determines the distribution of important oxidants and gaseous precursors for secondary air pollutants such as ozone (O_3) and fine particular matter. Aerosols can influence the Earth's radiative balance by directly scattering and absorbing radiation and indirectly affecting cloud properties through acting as cloud condensation nuclei (CCN) and ice nuclei. The aerosol effects on radiation depend critically on their chemical composition and physical properties. Meanwhile, climate change can strongly influence atmospheric chemistry and air quality (Jacob and Winner, 2009). Due to the nonlinear relationships between chemistry, aerosols, and climate, it is important to accurately represent their interactions in a three-dimensional global model.

Earth system models have been used for climate predictions in recent years due to their capabilities to include coupled and interactive representations of Earth's components (e.g., atmosphere, ocean, land, and sea ice). The Community Earth System Model (CESM) is a global Earth system model and used in this work for decadal and global climate predictions due to its capability of simulating the entire Earth system by coupling physical climate system with chemistry, biogeochemistry, biology, and human systems. It can also quantify the certainties and uncertainties in Earth system feedbacks on time scales up to centuries and longer and has been applied to simulate climate change as part of the Intergovernmental Panel on Climate Change (IPCC) Fifth Assessment Report (AR5). However, due to the

complexities in physical and chemical processes of aerosols, uncertainties remain in the model treatments. In this work, several advanced chemistry and inorganic aerosol treatments are implemented into the Community Atmosphere Model version 5.1, the atmospheric component of CESM version 1.0.5, to reduce the uncertainties associated with some of those model treatments and the resultant predictions of aerosol impacts on climate.

Compared to global atmospheric models, regional atmospheric models have higher grid resolution and allow more detailed treatments for gaseous and aerosol physical and chemical processes. 3-D regional atmospheric models, such as the Weather Research and Forecasting model with chemistry (WRF/Chem, Grell et al., 2005; Fast et al., 2006), the Community Multi-scale Air Quality (CMAQ, Binkowski and Roselle, 2003; Byun and Schere, 2006) model, and the Comprehensive Air Quality Model with Extensions (CAMx, ENVIRON, 1998, 2010) are often used for regional air quality studies. Most regional models consist of an atmospheric component coupled with a land surface scheme and forced by prescribed sea surface temperature (SST) over ocean. However, SST patterns can impact precipitation patterns and therefore affect atmospheric heating through latent heat flux. As a result, boundary layer conditions are impacted through air-sea interactions, resulting in changes in the planetary boundary height, surface temperature, and surface wind. For example, along coastal areas, air-sea interactions associated with the transfer of momentum, heat, and moisture at the interface of the atmosphere and ocean can affect the distribution and concentration of pollutants in the air and in the ocean, which can have significant impacts on human health, environment, and ecology. Therefore, it is also important to include the interactions among Earth components in the regional models based on geographical

characteristics of the studying area, which makes regional earth system modeling important. As a first step towards this goal, a Coupled Ocean-Atmosphere-Wave-Sediment Transport (COAWST) Modeling System is used in this work for simulating the dynamic processes of coastal zones (Warner et al., 2010). In this coupled system, the atmosphere model, WRF, provides wind stresses, shortwave radiation, and net surface heat flux to the Regional Ocean Modeling System (ROMS), and the resulting SST is fed back to WRF. In this work, building on existing coupled WRF-ROM in COAWST, WRF/Chem is coupled with ROMS in COAWST to study the effects of air-sea interactions on regional air quality and climate in order to improve the predictions of air quality and climate over coastal zones

1.2 Objectives

The objectives of my Ph.D. research are:

(1) To reduce uncertainties associated with predicted aerosol impacts on climate through improving the model's representations of atmospheric gases and aerosols in CESM/CAM;

(2) To evaluate the model's capability in reproducing observations of climate and air quality and characterize their long-term variation trends through applying CESM/CAM for retrospective decadal simulations;

(3) To examine the differences in the secondary organic aerosols (SOA) predictions resulted from the two gas-phase chemical mechanisms and study the sensitivity of air quality and climate predictions to different gas-phase chemical mechanisms.

(4) To improve the predictions of regional air quality and meteorology/climate over the coastal zones through coupling of a regional air quality model with a regional ocean model and enabling more accurate representations of air-sea interactions.

The ultimate goals are to enhance CESM/CAM5's capability in representing present atmosphere and projecting future climate change and demonstrate WRF/Chem-ROMS's capability in accurately predicting regional air quality and climate. In this work, we hypothesize that chemistry and aerosol processes are important for climate predictions, and fine scale feedbacks associated with air-sea interactions are important for regional air quality and climate predictions. This work can therefore help answer several scientific questions including: (1) how gas-phase chemistry, particle nucleation, and aerosol thermodynamics will affect gas and aerosol predictions as well as their impacts on climate; (2) which is the most important for model predictions among three processes; (3) how differences for SOA predictions from different gas-phase chemical mechanism; (4) how air-sea interactions will affect regional air quality and climate?

1.3 Overall Technical Approaches

The overall technical approaches are to improve an existing global earth system model and couple a regional climate/air quality model with a regional ocean model to serve as backbone for a prototype regional earth system model. The main tasks include model development, improvement, application, and evaluation. The first component of my Ph.D. research focuses on the global Earth system model development, improvement, and evaluation. The model development work includes incorporation of a new nucleation

parameterization and an inorganic aerosol thermodynamic module into CESM/CAM5.1 (see Chapter 2), and coupling of new gas phase mechanisms (i.e., the 2005 Carbon Bond Mechanism for Global Extension (CB05_GE) and the Model of OZone and Related chemical Tracers version 4 with extension, MOZART-4x) with aerosol modules (see Chapter 4). The aerosol module used in CESM/CAM5 includes independent submodules for individual aerosol process such as condensation, nucleation, and coagulation. Under this structure, new nucleation parameterization is added into existing nucleation submodule to enable the nucleation based on new parameterization. New submodule based on new aerosol thermodynamics is added into aerosol module to allow the gas-particle partitioning. The second component of my Ph.D. research focuses on the regional Earth System by coupling WRF/Chem with ROMS in the COAWST modeling system (see Chapter 5). The linkage between WRF and ROMS is already developed in the COAWST system. The interfaces between WRF and chemistry are also kept in the WRF modules. Chemistry package can be fully coupled into WRF by modifying the model configurations in the namelist. Model application and evaluation work includes the applications of CESM/CAM5.1 with those advanced treatments for 2001-2010 (see Chapter 3) and applications of WRF/Chem-ROMS for July 2010. All model simulation results are evaluated against various surface observations and satellite observations to demonstrate the improvement of model performance.

The protocols for performance evaluation for CESM/CAM5 simulations include spatial distributions and statistics. The analysis of the performance statistics focuses on mean bias (MB), normalized mean bias (NMB), normalized mean error (NME), root mean square error (RMSE), and correlation coefficient (Corr.). The meteorological and radiative variables

are evaluated annually or seasonally, including temperature at 2-m (T2), specific humidity at 2-m (Q2), and wind speed at 10-m (WS10) from NCDC; total daily precipitation rate (Precip) from GPCP; outgoing longwave radiation (OLR) from NOAA/CDC; downwelling shortwave radiation (FSDS), downwelling longwave radiation (FLDS), surface net shortwave flux (FSNS), surface net longwave flux (FLNS), shortwave cloud forcing (SWCF), and longwave cloud forcing (LWCF) from the Clouds and the Earth's Radiant Energy System (CERES); cloud fraction (CF), aerosol optical depth (AOD), cloud optical thickness (COT), precipitating water vapor (PWV), and CCN from the Moderate Resolution Imaging Spectroradiometer (MODIS), as well as CDNC and LWP from Bennartz (2007). Surface chemical predictions are evaluated against various observational sites from each network. Chemical concentrations evaluated include seasonal and annual averaged concentrations of carbon monoxide (CO), O_3, sulfur dioxide (SO_2), ammonia (NH_3), nitrogen dioxide (NO_2), nitric acid (HNO_3), particulate matter (PM) with aerodynamic diameter less than 10 μm (PM_{10}) and 2.5 μm ($PM_{2.5}$), and its major components (i.e., sulfate (SO_4^{2-}), nitrate (NO_3^-), and ammonium (NH_4^+), black carbon (BC), organic carbon (OC), and total carbon (TC) for CONUS and Europe). The chemical observations over East Asia are very limited, and only include surface concentrations of CO, SO_2, NO_2, O_3, and PM_{10}. Column concentrations of tropospheric CO, NO_2, SO_2, and formaldehyde (HCHO), and tropospheric O_3 residual (TOR) are evaluated for the globe.

The protocols for performance evaluation for WRF/Chem simulations include temporal variations, spatial distributions, column abundances, and performance statistics for meteorological variables, radiative variables, and chemical concentrations from WRF/Chem

output, and temporal and variability of meteorological and surface fluxes from ROMS output. The chemical species evaluated for WRF/Chem are as the same as for CAM5, but with additional species such as maximum 1-h and 8-h O_3, and hourly $PM_{2.5}$. Air-sea interaction related variables are evaluated including SST and WS10 from the National Data Buoy Center (NDBC); planetary boundary layer height (PBLH) derived from the National Centers for Environmental Prediction (NCEP)/North American Regional Reanalysis (NARR); SST, sensible heat flux (SHFLX) and latent heat flux (LHFLX) derived from the Objectively Analyzed Air-Sea Fluxes (OAFlux).

Earth system models have been used to simulate climate over decadal to centennial time scales to project Earth system changes in the coming decades. However, due to the uncertainties in the model treatments, it remains a challenge to project those changes accurately. This work can help reduce the uncertainties associated with atmospheric gas and aerosols and their impacts on climate, which can in turn reduce the uncertainty in predicting climate change. Applications of CESM/CAM5 with those advanced treatments can provide valuable information about the model's capability in capturing the decadal variation trend in climate and its potential in projecting future climate changes. Coupling WRF/Chem with ROMS can help link the air-sea interactions with air quality and climate and thus improve the predictions of regional air quality and climate. The coupled WRF/Chem-ROMS can serve as a backbone of a regional earth system to be used to downscale a global Earth system model such as CESM/CAM5.

CHAPTER 2. IMPROVEMENT AND FURTHER DEVELOPMENT IN CESM/CAM5: GAS-PHASE CHEMISTRY AND INORGANIC AEROSOL TREATMENTS

2.1 Introduction

Atmospheric gases and aerosols play important roles in the Earth system due to their ability to alter the Earth's radiation balance. Atmospheric chemistry determines the formation of ozone (O_3) and fine particular matter ($PM_{2.5}$) through affecting the distribution of oxidants and their gaseous precursors. Different chemical reactions and kinetic parameters can lead to differences in the predictions of gases, secondary aerosols, new particle formation rate (J), as well as climatic variables such as cloud condensation nuclei (CCN), cloud droplet number concentration (CDNC), and radiative forcing (Faraji et al., 2008; Zhang et al., 2012a). Meanwhile, climate change can strongly influence atmospheric chemistry and air quality.

Aerosol can influence the Earth's radiative balance by directly scattering and absorbing radiation and indirectly affecting cloud properties through acting as CCN and ice nuclei (IN). Therefore, it is important to accurately simulate aerosol size distribution, chemical composition, and properties, which can determine the magnitude of aerosol radiative forcing (Koloutsou-Vakakis et al., 1998). Aerosol and its influence on climate have been included in many global climate models (GCMs) such as the Community Climate System Model (CCSM) (Collins et al., 2006), the 5th generation of global climate model modified from European Centre for Medium-Range Weather Forecasts in Hamburg (ECHAM5) (Stier et al., 2005), and Earth system models such as the Community Earth System Model (CESM) (Ghan et al., 2012; Liu et al., 2012), the Integrated Global System

Model (IGSM) (Dutkiewicz et al., 2005; Sokolov et al., 2005), and the Earth System Model (ESM) (Dunne et al., 2012). However, due to the complexity of aerosol microphysical processes and their interactions with cloud processes, it remains a challenge to accurately represent those properties and processes in GCMs.

Inorganic aerosols comprise 25-50% of fine aerosol mass (Heintzenberg, 1989), which mainly includes sulfate (SO_4^{2-}), ammonium (NH_4^+), nitrate (NO_3^-), chloride (Cl^-), and sodium (Na^+). Major gas-to-particle conversion processes of inorganic aerosols include condensation, nucleation, and thermodynamics. An important factor that determines the condensation of gases is the mass accommodation coefficient (α), which can be measured through laboratory experiments. The measured α values, however, are subject to large uncertainty and may vary in several orders of magnitudes under different laboratory conditions. To simulate aerosol condensational growth, a constant value of α is therefore often assumed in GCMs, which is a source of uncertainty in model predictions.

Homogeneous nucleation of sulfuric acid (H_2SO_4) vapor produces new particles that can grow to form CCN. Different nucleation parameterizations are used in GCMs or global aerosol models. For example, Sihto et al. (2006) derived empirical power laws with the first- or second-order dependencies of new particle formation rates (J) on H_2SO_4 vapor concentration from observations based on cluster-activation or barrierless kinetic mechanisms, which have been used in the Community Atmosphere Model (CAM) (Wang and Penner, 2009), the Global-through-Urban Weather Research and Forecasting model with Chemistry (GU-WRF/Chem) (Zhang et al., 2012b), and Global Model of Aerosol Processes (GLOMAP) (Spracklen et al., 2006). An ion-mediated nucleation (IMN) model was

developed to calculate J based on ambient atmospheric conditions, H_2SO_4 vapor concentrations, ionization rate, and surface area of preexisting particles. It has been used in GEOS-Chem (Yu et al., 2008), CAM (Yu et al., 2012), and GU_WRF/Chem (Zhang et al., 2012b). Different nucleation parameterizations lead to significant differences in J predictions by regional and global models (Zhang et al., 2010a) and CCN/CDNC (Zhang et al., 2012b; Yu et al., 2012). Limited observations make it difficult to validate predicted J values and appropriateness of various parameterizations.

A number of thermodynamic aerosol modules have been developed to understand physical and chemical properties of inorganic aerosols. For example, EQUISOLV II (Jacobson, 1999) has been used in a one-way nested (from global to local scales) gas, aerosol, transport, radiation, general circulation, mesoscale, and ocean model (GATOR-GCMOM) (Jacobson, 2010). EQUISOLV II uses analytical equilibrium iteration and mass flux iteration to solve equilibrium problems (Jacobson, 1999), which requires relatively large computational cost. SCAPE2 is used in the California Institute of Technology (CIT) model (Meng et al., 1998). ISORROPIA (Nenes et al., 1998) has been used in several global models such as GEOS-Chem (Bey et al., 2001), the GISS Caltech (Liao et al., 2003), and the GU-WRF/Chem (Zhang et al., 2012b) and regional models such as the Community Multiscale Air Quality model (CMAQ) (Byun and Schere, 2006) and the Comprehensive Air Quality Model with Extensions (CAMx) (ENVIRON, 2010). An updated version, ISORROPIA II (Fountoukis and Nenes, 2007), has also been implemented in recent versions of CMAQ (e.g., CMAQ v4.7-Dust (Wang et al., 2012) and CMAQ v5.0, Appel et al., 2013) and GEOS-Chem (Fountoukis and Nenes, 2007). The Multicomponent Equilibrium Solver for Aerosols

(MESA) (Zaveri et al., 2005) has been used in the mesoscale WRF/Chem (Fast et al., 2006). These modules assume that particles simulated in a given particle size range have the same composition (i.e., internal mixture). Different aerosol thermodynamic models can lead to different aerosol predictions (Nenes et al., 1998; Zhang et al., 2000; Zaveri et al., 2005). Zhang et al (2000) reported average absolute differences of 7.7% - 12.3% in total PM predictions between different thermodynamic modules under 400 test conditions but the differences could be as large as 68% under some cases (e.g., high nitrate/chloride and low/medium relative humidity, RH). Fountoukis and Nenes (2007) found the largest discrepancies between ISORROPIA II and SCAPE2 in water concentration predictions exist under low RH conditions (RH < 60%), primarily from differences in the treatment of water uptake and solid state composition. The 3-D atmospheric models with these modules include explicit thermodynamic treatments for sulfate, ammonium, nitrate, sodium, and chloride. The equilibrium assumption, however, is not valid under some conditions (e.g., coarse particles and cooler conditions) (Meng and Seinfeld, 1996). Kinetic approaches are therefore needed to treat gas/particle mass transfer under such conditions. Kinetic approaches, on the other hand, are computationally expensive (Zhang et al., 2004; Hu et al., 2008) and have only been implemented in a few 3-D models (e.g., Meng and Seinfeld, 1996; Jacobson, 2005; Zhang and Wexler, 2006; Zaveri et al., 2008). A hybrid approach that assumes equilibrium for fine particles and solves gas/particle mass transfer for coarse particles has been thus developed, which provides the best compromise between numerical accuracy and computational efficiency (Capaldo et al., 2000; Kelly et al., 2010). A simple approach for gas/particle mass transfer used in some GCMs, such as CAM5 is to treat sulfate and ammonium only with a

full neutralization (the NH_4^+/SO_4^{2-} molar ratio of 2 for a mode) through an irreversible condensation.

In this section, a comprehensive gas-phase chemical mechanism and detailed inorganic aerosol treatments for nucleation and aerosol thermodynamics are incorporated into CAM version 5.1 (CAM5.1) in the CESM version 1.0.5 (CESM1.0.5). Several modifications are also made to the existing treatments such as condensation and aqueous-phase chemistry. The objectives are to improve the representations of gas-phase chemistry and inorganic aerosol treatments in CESM/CAM5.1, and reduce associated uncertainties. The improved model with enhanced capabilities can be applied for decadal simulations to study interactions among atmospheric chemistry, aerosols, and climate change.

2.2 Model Development and Improvement

CESM is a fully-coupled global Earth system model, which includes land, ocean, atmosphere, and sea ice components. The atmosphere component used in this study is CAM5.1. Existing and new model treatments related to this study are described in this section. Further details on CAM5.1 can be found at http://www.cesm.ucar.edu/models/cesm1.0/cam/.

2.2.1 Existing Gas-Phase Chemistry and Aerosol Treatments in CESM/CAM5.1

CAM5.1 uses a simple gas-phase chemistry for sulfur species, which includes 1 photolytic reaction and 7 kinetic reactions among 6 gas-phase species (i.e., hydrogen peroxide (H_2O_2), H_2SO_4, sulfur dioxide (SO_2), dimethylsulfide (DMS), ammonia (NH_3), and semi-volatile organic gas, SOAG). A more comprehensive gas-phase mechanism with 40 photolytic reactions and 172 kinetic reactions among 103 species, i.e., the Model of OZone

and Related chemical Tracers version 4 (MOZART-4) of Emmons et al. (2010), has been incorporated into the official released CAM5.1. It was only coupled with the bulk aerosol module (BAM) in CAM5.1 implemented in CESM 1.0.5 that is used in this work (It was coupled with MAM in CESM v1.1). In addition to BAM, CAM5.1 contains the modal aerosol model (MAM) that is based on modal representations of aerosols. In this study, MAM is used because it can represent more accurate size distributions as compared to BAM. There are two versions of MAM, one with seven lognormal modes (MAM7), and the other with three lognormal modes (MAM3) (Liu et al., 2012), and both are coupled with the simple gas-phase chemistry in the default model. MAM7 is used in this study because it contains explicit treatments for ammonium and size distributions for dust, sea-salt, and primary carbon compared to MAM3. MAM7 explicitly treats sulfate, ammonium, sea-salt, dust, black carbon (BC), primary organic matter (POM), and secondary organic aerosol (SOA). It simulates condensational growth of aerosol, nucleation, coagulation, dry deposition, wet removal, and water uptake. Condensation is simulated based on a kinetic approach, in which MAM7 treats H_2SO_4, NH_3, and methanesulfonic acids (MSA) as completely non-volatile species and treats SOAG as a volatile species, using a constant accommodation coefficient of 0.65 for all these condensing species based on Adams and Seinfeld (2002). NH_3 condensation stops when the NH_4^+/SO_4^{2-} molar ratio of a particle mode reaches 2 (i.e., fully neutralized by SO_4^{2-} ions). The net uptake rate, I_{net}, due to gas to particle mass transfer for each species to each mode is simulated as,

$$I_{net} = \int dx \frac{dN}{dx} I_{cond} \quad (1)$$

$$I_{cond} = 2 \times \pi \times D_g \times D_p \times F(Kn, \alpha) \quad (2)$$

$$F(Kn, \alpha) = \frac{0.75 \times (1 + Kn)}{Kn \times \left(\frac{1 + Kn}{\alpha} + 0.283 \right) + 0.75} \quad (3)$$

where D_p is the particle diameter; x is the logarithmic diameter of particle, = $ln(D_p)$; dN/dx is the log-normal particle number density distribution; I_{net} is the gas condensation rate; Kn is the Knudsen number; α is the accommodation coefficient of condensable vapor; D_g is the gas diffusivity, and F(Kn, α) is the Fuchs-Sutugin correction factor that describes the resistance to uptake caused by gas-phase diffusion. Equation (1) is solved using the Gauss-Hermite quadrature of order 2. Based on Eq. (3), as α approaches zero, F(Kn, α) approaches zero. Consequently, I_{cond} (i.e., the uptake rate) approaches zero in Eq. (1).

There are three nucleation parameterizations in MAM7. The empirical power law of Wang and Penner (2009) (WP09) is used in the planetary boundary layer (PBL), which includes a first-order dependence on H_2SO_4 vapor with a prefactor of 1×10^{-6}. The binary H_2SO_4-H_2O homogeneous nucleation of Vehkamaki et al. (2002) (VE02) and ternary H_2SO_4-NH_3-H_2O homogeneous nucleation of Merikanto et al. (2007) (ME07) are used above PBL. MAM7 also only considers the neutralization of SO_4^{2-} by NH_4^+ during condensational growth. A more detailed description of MAM can be found in Liu et al. (2012).

2.2.2 New and Modified Model Treatments Implemented in This Work

Highly simplified gas-phase mechanism as used in default CAM5.1 can result in large uncertainties in the predictions of oxidants and gaseous precursors for secondary aerosols. Therefore, a new gas-phase mechanism, the 2005 Carbon Bond Mechanism for Global

Extension (CB05_GE) (Karamchandani et al., 2012) has been implemented into CAM5.1 using the same chemical preprocessor as MOZART-4 (Lamarque et al., 2012) and coupled with both MAM3 and MAM7. CB05_GE was developed to simulate major chemical reactions for global-through-urban applications as illustrated in Zhang et al. (2012b). A more detailed description of CB05_GE can be found in Karamchandani et al. (2012). In this study, gas precursors for SOA in CB05_GE are mapped to SOAG to make it compatible in MAM7. As the first study of CESM/CAM5.1 with CB05_GE, this work focuses on the impact of gas-phase chemistry. The heterogeneous chemistry on the surface of aerosol is turned off. CB05_GE implemented in CESM/CAM5 contains a total of 273 reactions including 50 photolytic reactions and 223 kinetic reactions among 93 gas-phase species in this study. The gas-phase chemical system is solved using an implicit backward Euler method.

Ions generated by cosmic radiation and natural radioactive decay have been studied for a long time as an important source to enhance nucleation (Raes et al., 1986). An IMN model is developed by Yu (2010) (Yu10) for H_2SO_4-H_2O system, and explicitly solves the dynamic equations in terms of temperature, RH, H_2SO_4 vapor concentration, ionization rate, and surface area of preexisting particles. Different from classic binary nucleation theory, which is based on the minimization of changes in Gibbs free energy (Seinfeld and Pandis, 2006), IMN is based on a kinetic model that considers the interactions among ions, neutral and charged clusters, vapor molecules, and preexisting particles (Yu, 2010). The global ionization rates due to cosmic rays are calculated based on the schemes given in Usoskin and Kovaltsov (2006) and the contribution of radioactive materials from soil to ionization rates is parameterized based on the profiles given in Reiter (1992). To reduce the computing cost

using IMN in 3-D models, Yu et al. (2008) developed lookup tables with simple interpolation subroutines to calculate nucleation rates under typical atmospheric conditions. In this work, IMN based on YU10 is implemented into MAM7 and combined with default nucleation parameterizations (VE02, ME07, and WP09) in order to improve the J predictions and aerosol number concentrations in upper troposphere. The J value above PBL is taken as the maximum value among predictions from IMN (YU10) and homogeneous nucleation (VE02 or ME07), and the J value within PBL is taken as the maximum value among predictions from IMN (YU10), homogeneous nucleation (VE02 or ME07), and the first-order parameterization (WP09).

Gas-particle partitioning is an important process in the formation and evolution of secondary aerosols. Several factors affect gas-particle partitioning, such as temperature, RH, saturation vapor pressures of species, the physical state of the condensed-phase, and the interactions among aerosol components (Zuend et al., 2010). Most models focus on inorganic aerosols. Fountoukis and Nenes (2007) developed a computationally-efficient thermodynamics equilibrium model, ISORROPIA II, for the magnesium (Mg^{2+}) - potassium (K^+) - calcium (Ca^{2+}) - NH_4^+ - Na^+ - SO_4^{2-} - NO_3^- - Cl^- - H_2O aerosol system. An important difference between ISORROPIA II and most other thermodynamics equilibrium models is that ISORROPIA II simulates crustal species, such as Mg^{2+}, K^+, and Ca^{2+}, which are important constituents of atmospheric aerosols, in particular, mineral dust. Therefore, to explicitly simulate aerosol thermodynamics, ISORROPIA II has been implemented into MAM7 and applied for accumulation, Aitken, fine sea-salt, and fine dust modes to explicitly simulate thermodynamics of SO_4^{2-}, NH_4^+, NO_3^-, Cl^-, and Na^+ as well as the impact of crustal

species associated with fine dust modes on aerosol thermodynamics. The concentrations of K^+, Ca^{2+}, and Mg^{2+} as the input for ISORROPIA II are calculated from dust concentrations, using the mass ratios of 1.022×10^{-3}, 1.701×10^{-3}, and 7.084×10^{-4}, respectively (Van Pelt and Zobeck, 2007). The resulted concentrations of aerosol components from ISORROPIA are mapped back to fine aerosol modes based on their mass ratios to the total mass over all fine modes at the previous time step.

Aerosol thermodynamics involving coarse particles (in coarse sea-salt and dust modes) is currently not treated explicitly in this work, given the high computational cost (by at least a factor of 3 compared to the cost for fine particles) for solving the non-equilibrium system involving coarse particles. Instead, the simple kinetic approach used in the default CAM5.1 is used to simulate the condensation of inorganic gases onto coarse modes (see section 2.2.4). For fine mode particles, before thermodynamic calculation using ISORROPIA II, the condensation and nucleation processes are simulated to allow a more realistic allocation of gaseous H_2SO_4 between these two competing processes. Such a treatment for fine mode particles is similar to the kinetic approach used in regional air quality models, except that the condensation is assumed to be irreversible with lower limit values of mass accommodation coefficients in this work.

MAM 7 does not treat NO_3^- and it treats NaCl as one species. In this work, MAM7 is modified to explicitly simulate NO_3^-, Cl^-, and Na^+ using a similar method to the condensation of H_2SO_4 and NH_3. NO_3^- and Cl^- are simulated in all modes except for primary carbon mode. Na^+ is simulated in sea-salt modes. The source of Na^+ is calculated based on the mass ratio of Na and Cl from sea-salt emissions. The source of Cl^- includes sea-salt emissions, and the

condensation of HCl resulted from HCl emissions and gas-particle partitioning of total chloride.

Species-dependent accommodation coefficients are used for H_2SO_4, NH_3, HNO_3, and HCl, with the values of 0.02, 0.097, 0.0024, and 0.005 (Zhang et al., 1998; Sander et al., 2003), respectively. Since by default the model treats the condensation of inorganic volatile gas species as irreversible process (no evaporation) (see Eq.1), the lower limit values of mass accommodation coefficients are used for these species to represent their net fluxes from the gas-phase to the liquid/solid phases. Such lower limit values correspond to uptake coefficients, which represent the net fluxes and are smaller than mass accommodation coefficients. To ensure electroneutrality in each mode after kinetically condensing H_2SO_4, NH_3, HNO_3, and HCl at different condensation (or uptake) rates, the condensation of NH_3 will stop when the mole concentration of cations (i.e., NH_4^+) is equal to sum of those of anions (i.e., $[NH_4^+] = 2\times[SO_4^{2-}]+[NO_3^-]+[Cl^-]$). While such an approach allows the gas/particle portioning of those volatile species over both fine and coarse modes, the irreversible condensation with lower limit mass accommodation coefficients assumed in this work, however, may contribute to model biases in simulating condensation of volatile species on coarse mode particles. A more accurate method (i.e., reversible condensation) should be used for volatile species for future work. The original MAM7 treats $NH_3(g)/NH_4^+$ in cloud water. In this work, the dissolution and dissociation of HNO_3 and HCl to produce NO_3^- and Cl^- in cloud water are added in the model based on Marsh and McElroy (1985) and Seinfeld and Pandis (2006), i.e.,

$$\boldsymbol{HNO_{3\,(g)} \rightleftharpoons HNO_3(aq) \rightleftharpoons H^+ + NO_3^-}$$

$$HCl_{(g)} \rightleftharpoons HCl_{(aq)} \rightleftharpoons H^+ + Cl^-$$

The concentration of H^+ (thus the pH value of the solution) is obtained by solving the electro-neutrality equation using the bisection method. The aqueous-phase chemical system is solved analytically.

2.3 Model Configurations and Evaluation Protocols

2.3.1 Model Setup and Simulation Design

Table 2.1 summarizes the CESM/CAM5.1 simulations that are designed to examine the impacts of individual new and modified treatments on model predictions. The first set of simulations includes two simulations with the same default MAM7 coupled with different gas-phase mechanisms: one uses the simple gas-phase chemistry (MAM_SIM) with a total of 37 prognostic species and one uses the CB05_GE (MAM_CB05_GE) with a total of 127 prognostic species. A comparison of the two simulations provides an estimate of the impacts of gas-phase chemical mechanisms. The second set of simulations consists of five simulations that use the same CB05_GE gas-phase mechanism but with modified and new aerosol treatments individually and jointly. The first one is MAM_CON that uses an explicit treatment for NO_3^-, Cl^-, and Na^+ and species-dependent mass accommodation coefficients for condensation and that includes the aqueous-phase chemistry of HNO_3/NO_3^- and HCl/Cl^-. This simulation includes a total of 139 prognostic species. The second one is MAM_CON/IMN that uses the same treatments as MAM_CON but with IMN as one of the nucleation mechanisms and a prefactor of 1.0×10^{-8} in WP09. The third one is MAM_CON/ISO that uses the same treatments as MAM_CON but with ISORROPIA II for

aerosol thermodynamics assuming metastate equilibrium (i.e., liquid only). The fourth one is MAM_NEWA that uses the same treatments as MAM_CON but with all new and modified aerosol treatments and a prefactor of 1.0×10^{-9} for WP09. The fifth one is MAM_NEWB that uses the same treatments as MAM_NEWA, but with ISORROPIA II assuming a stable condition (i.e., solid and liquid coexist). A comparison of MAM_CB05_GE with MAM_CON indicates the impact of modified condensation and aqueous-phase chemistry. A comparison of MAM_CON/IMN, MAM_CON/ISO, and MAM_NEWA with MAM_CON indicates the impacts of IMN, ISORROPIA II, and combined new and modified aerosol treatments, respectively. Comparison of MAM_NEWB with MAM_NEWA indicates the impacts of thermodynamic conditions on gas-aerosol partitioning. The 3rd set of simulation includes one simulation using the same configuration as MAM_NEWA but with adjusted emissions (MAM_NEW/EMIS). Its comparison with MAM_NEWA indicates the impacts of uncertainties in emissions on model predictions. The 4th set of simulation includes one simulation using the same configuration as MAM_SIM but with prescribed SST for a 5-year period during 2001-2005 (MAM_SIM_5Y), and two simulations both using the same configuration as MAM_NEW/EMIS for 2001-2005, but one with prescribed SST (MAM_NEW_5YA), and the other in a fully-coupled mode (MAM_NEW_5YB).

All these simulations use the same approach for photolytic rates calculations based on Lamarque et al. (2012), the same aqueous-phase chemistry of Barth et al. (2000), and the same physical options as those in MAM_SIM. Major physical options include the cloud microphysics parameterization of Morrison and Gettelman (2008), the moisture PBL scheme of Bretherton and Park (2009), the shallow convection scheme and deep convection scheme

of Park and Bretherton (2009) and Zhang and McFarlane (1995), respectively, the aerosol activation parameterization of Abdul-Razzak and Ghan (2000), and the Rapid Radiative Transfer Model for GCMs (RRTMG) of Iacono et al. (2003, 2008) for long and short-wave radiation. The land surface processes are simulated by the Community Land Model (CLM) of Lawrence et al. (2011) in CESM that is coupled with CAM5.1.

All simulations except for MAM_SIM_5Y and MAM_NEW_5YA are performed with fully-coupled CESM1.0.5 with standard B_1850-2000_CAM5_CN configuration, which represents 1850 to 2000 transient conditions and includes all active components in CESM with biogeochemistry in the land model. MAM_SIM_5Y and MAM_NEW_5YA are performed with standard F_AMIP_CAM5 configuration, which uses a climatological dataset for SST provided by NCAR for ocean model. The simulations are conducted for the full-year of 2001 and 2001-2005 at a horizontal resolution of $0.9^{o}\times1.25^{o}$ and a vertical resolution of 30 layers for CAM5.1. The initial conditions for ice and ocean models are from CESM default settings. The initial conditions for the land model are based on the output from the NCAR's CESM/CAM4 B_1850-2000_CN simulation. The initial conditions for CAM5 are derived from a 10-yr (1990-2000) CAM5 standalone simulation with the MOZART chemistry provided by NCAR. A 1-year (January 1-December 31, 2000) CESM/CAM5 simulation using NCAR's CESM B_1850-2000_CAM5_CN component set is performed as spinup to provide the initial conditions for meteorological variables and chemical species that are treated in both MOZART and CB05_GE. An additional 3-month (October 1-December 31, 2000) CESM/CAM5 simulation based on a 10-month (January-October, 2000) CESM/CAM5 output using initial conditions from NCAR's CESM B_1850-

2000_CAM5_CN is performed as spinup to provide initial conditions for chemical species that are treated in CB05_GE but not in MOZART. All production simulations of 2001 are from January 1 - December 31, 2001 and those of 2001-2005 are from January 1, 2001-December 31, 2005. The offline anthropogenic emissions used in all simulations except for MAM_NEW/EMIS are taken from Zhang et al. (2012b) (see Table 2 of Zhang et al. (2012b) for the sources of those anthropogenic emissions). Anthropogenic emissions used in MAM_NEW/EMIS are adjusted emissions based on those of Zhang et al. (2012b), with adjustment factors of 0.7, 0.5, and 1.2 for SO_2 over CONUS, Europe, and Asia, respectively, and 1.2 for NH_3, BC, and organic carbon (OC), and 1.3 for carbon monoxide (CO) over all three regions. Those emissions are adjusted based on the comparison with the emission inventories from the Representative Concentration Pathways (RCPs), the MOZART version 4 (MOZART-4), the Reanalysis of the TROpospheric chemical composition (RETRO), the Global Fire Emissions Database (GFED) version 2, and preliminary evaluation of CESM/CAM5.1 with modified and new gas and aerosol treatments using available observations. The online emissions include biogenic volatile organic carbon (Guenther et al., 2006), mineral dust (Zender et al., 2003), and sea-salt (Martensson et al., 2003).

2.3.2 Available Measurements for Model Validation

A number of observational datasets from surface networks and satellites are used for model evaluation. They are summarized along with the variables to be evaluated in Table 2.2. Global surface networks include the Baseline Surface Radiation Network (BSRN) and the National Oceanic and Atmospheric Administration Climate Diagnostics Center (NOAA/CDC). The satellite datasets include the Moderate Resolution Imaging

Spectroradiometer (MODIS), the Clouds and Earth's Radiant Energy System (CERES), the Total Ozone Mapping Spectrometer/the Solar Backscatter UltraViolet (TOMS/SBUV), the Measurements Of Pollution In The Troposphere (MOPITT), and the Global Ozone Monitoring Experiment (GOME). Other satellite-based data include the MODIS-derived CDNC from Bennartz (2007) (BE07).

Regional observational networks include the Clean Air Status and Trends Network (CASTNET), the Interagency Monitoring of Protected Visual Environments (IMPROVE), and the Speciation Trends Network (STN) over CONUS; the European Monitoring and Evaluation Program (EMEP), the Base de Données sur la Qualité de l'Air (BDQA), and the European air quality database (AirBase) over Europe; the Ministry of Environmental Protection of China (MEP of China), the National Institute for Environmental Studies of Japan (NIES of Japan), and Taiwan Air Quality Monitoring Network (TAQMN) over East Asia. The observational data for particle formation rate J is compiled from Kulmala et al. (2004) and Yu et al. (2008), which include land-, ship-, and aircraft-based measurements.

2.3.3 Evaluation Protocol

The protocols for performance evaluation include spatial distributions and statistics, following the approach of Zhang et al. (2012b). The analysis of the performance statistics will focus on mean bias (MB), normalized mean bias (NMB), normalized mean error (NME), and root mean square error (RMSE). The radiative variables are evaluated annually, including downwelling shortwave radiation (SWD) and downwelling longwave radiation (LWD) from BSRN; outgoing longwave radiation (OLR) from NOAA/CDC; shortwave cloud forcing (SWCF) from CERES; cloud fraction (CF), aerosol optical depth (AOD), cloud

optical thickness (COT), cloud water path (CWP), precipitating water vapor (PWV), and CCN from MODIS; as well as CDNC from BE07. Chemical concentrations evaluated include seasonal and annual averaged concentrations of CO, O_3, SO_2, NH_3, nitrogen dioxide (NO_2), nitric acid (HNO_3), PM, and its major components (i.e., SO_4^{2-}, NO_3^-, and NH_4^+, BC, OC, total carbon (TC) for CONUS and Europe). The chemical observations over East Asia are very limited, and they only include surface concentrations of CO, SO_2, NO_2, O_3, and PM_{10}. Column concentrations of tropospheric CO and NO_2, and tropospheric O_3 residual (TOR) are evaluated for globe.

All observational data used for evaluating 2001 simulations are based on 2001 only except for particle formation rates (J) that are based on different years compiled from Kulmala et al. (2004) and Yu et al. (2008). All observational data used for evaluating 2001-2005 simulations are based on 2001-2005.

2.4 Model Evaluation for MAM_SIM Based on Original Model Treatments

Tables 2.3a and b show MBs and NMBs of radiative/cloud and chemical predictions, respectively. The model performance of the baseline simulation, MAM_SIM, is discussed below, and that for all other simulations will be discussed in section 2.5.

As shown in Table 2.3a, radiative variables such as LWD and SWD are underpredicted by 3.4 W m^{-2} (~ -1.1%) and 2.0 W m^{-2} (~ -1.1%), respectively, whereas OLR and SWCF are overpredicted by 8.8 W m^{-2} (~ 4.1%) and 3.2 W m^{-2} (~ 7.9%) respectively. Cloud variables such as CF and PWV are slightly underpredicted, whereas COT, CWP, column CCN at a supersaturation of 0.5% (CCN5), and CDNC are largely underpredicted,

with NMBs of -77.8% to -55.6%, which is likely due to the limitations in the current model treatments of cloud microphysics and aerosol-cloud interactions in CAM5.1.

AOD is also underpredicted by 36.1%, which is likely due to inaccurate predictions of aerosol concentrations and uncertainties in the assumed hygroscopicity of aerosol components in the calculation of optical properties and water uptake. For example, as shown in Table 2.3b, $PM_{2.5}$ concentrations over CONUS and Europe, and PM_{10} concentrations over CONUS, Europe, and East Asia are underpredicted, with NMBs of -67.5% to -31.8%, which is due to the inaccurate predictions of SO_4^{2-}, NH_4^+, and organic aerosols, and missing major inorganic aerosol species such as nitrate and chloride. The concentrations of BC, OC, and TC are underpredicted (by ~ 50%), which is likely due to the uncertainties in the BC and primary OC emissions as well as treatments for SOA formation. In particular, the SOA treatment used in CAM5.1 is based on a highly-simplified aerosol yield approach with a single lumped semi-volatile organic gas (i.e., SOAG). For gaseous species, SO_2 concentrations over CONUS and Europe are significantly overpredicted by 10.3 μg m^{-3} (~ 264.8%) and 6.6 μg m^{-3} (~ 97.5%), respectively, whereas SO_2 concentrations over East Asia are largely underpredicted by 7.9 μg m^{-3} (by ~63.0%). NH_3 concentrations over Europe are also largely underpredicted by 82.0%. These large biases in SO_2 and NH_3 are likely due in part to the uncertainties in the emissions of SO_2 and NH_3, which in turn affect the predictions of SO_4^{2-} and NH_4^+. The J values in PBL are highly underpredicted by 99.6%, which is mainly due to the inaccurate calculation of H_2SO_4 vapor concentration that participates in the nucleation and uncertainties in the nucleation parameterizations used in the default CESM/CAM5.1.

2.5 Sensitivity Simulations

2.5.1 Impacts of New Gas-Phase Chemistry

Compared to simple gas-phase chemistry, many more gaseous species and chemical reactions simulated in CB05_GE can affect secondary aerosol formation through gas-to-particle mass transfer and aqueous-phase chemistry and affect climatic variables through chemistry feedbacks to the climate system. Figure 2.1a shows the absolute differences of H_2O_2, SO_2, SO_4^{2-}, and SOA between MAM_CB05_GE and MAM_SIM. MAM_CB05_GE treats more gaseous species and chemical reactions than MAM_SIM, leading to large changes in the concentrations of gaseous and PM species. Compared with MAM_SIM, MAM_CB05_GE predicts higher H_2O_2 by 0.4 ppb, SO_2 by 7.3 ppt, SO_4^{2-} by 0.01 μg m^{-3}, and SOA by 0.06 μg m^{-3} in terms of global mean. Those changes are mainly caused by different gas-phase chemical mechanisms used in MAM_SIM and MAM_CB05_GE. While MAM_CB05_GE explicitly simulates OH, HO_2, NO_3, and O_3, MAM_SIM uses climatology data for these species. OH simulated by MAM_CB05_GE is lower than that prescribed by MAM_SIM by up to 2.8×10^6 molecules cm^{-3}, or higher by up to 3.0×10^6 molecules cm^{-3} in different regions (Figure not shown), with a higher global mean by MAM_CB05_GE. MAM_SIM includes the production of H_2O_2 from the self-destruction of HO_2 and the loss of H_2O_2 through its photolytic reaction and its reaction with OH. Higher H_2O_2 in MAM_CB05_GE is mainly due to greater production of H_2O_2 from additional chemical reactions (e.g., OH+OH) than loss of H_2O_2 through the reactions of OH + H_2O_2, O + H_2O_2, Cl + H_2O_2, and Hg + H_2O_2. Different predictions in H_2O_2 can in turn affect OH mixing ratios in MAM_CB05_GE but not in MAM_SIM. In addition, the photolytic reactions of VOCs (e.g., HCHO, peroxyacyl nitrates (PAN), and peroxyacetic and higher peroxycarboxylic

acids, PACD) and other gases (e.g., HNO_3, HONO, HNO_4, HOCl, and HOBR) treated in MAM_CB05_GE can produce OH. Figure 2.1b shows the absolute differences between the mixing ratios of major oxidants predicted from MAM_CB05_GE and climatology values used in MAM_SIM. The global mean mixing ratios of oxidants are higher in MAM_CB05_GE than climatology data in MAM_SIM, leading to more oxidation of VOCs and therefore more SOA in MAM_CB05_GE. Higher O_3 predicted from MAM_CB05_GE over most of the domain is mainly due to more O_3 precursors (e.g., NO_2 and VOCs) treated in the model. Despite higher OH mixing ratios in MAM_CB05_GE, many gaseous species such as NO_x, SO_2, HNO_3, HONO, and other VOCs are oxidized by OH to form secondary inorganic and organic aerosols. Those oxidation reactions compete for limited OH, leading to less oxidation of SO_2, thus higher SO_2 mixing ratios over most land areas by MAM_CB05_GE. Lower SO_2 mixing ratios over the oceanic areas in MAM_CB05_GE is due to the combined effects of less production of SO_2 from lower DMS mixing ratios (due to increased OH levels) and greater SO_2 oxidation from higher OH mixing ratios.

The changes in the concentrations of PM and its components are due to the change in the mixing ratios of gaseous precursors. CB05_GE contains more photolytic reactions, which affect the mixing ratios of OH, SO_2, and H_2SO_4, and subsequently the concentration of SO_4^{2-} through condensation and homogeneous nucleation. Higher SO_2 mixing ratios in MAM_CB05_GE result in more H_2SO_4 thus more SO_4^{2-}. For example, both SO_2 mixing ratios and SO_4^{2-} concentrations are higher over eastern China in MAM_CB05_GE. More SO_4^{2-} over the oceanic areas is mainly due to more oxidation of SO_2 by OH. Due to the simplification of aerosol thermodynamics in default MAM7, the concentrations of SO_4^{2-} can

affect the concentrations of NH_4^+ directly and therefore NH_3 mixing ratios and PM number concentrations (PM_{num}). For example, the increase of SO_4^{2-} results in an increase in NH_4^+ and PM_{num}, and a decrease in NH_3. The increase of SO_4^{2-} and PM_{num} can increase AOD, CF, COT, CWP, PWV, and CDNC and therefore affect radiation by increasing LWD and SWD (Figures not shown, see changes in performance statistics of these affected variables in Table 2.3a). The increase of SOA is due to the inclusion of more gaseous precursor emissions (e.g., isoprene, terpene, xylene, and toluene) in MAM_CB05_GE, which contribute to SOAG and thus SOA through gas-to-particle conversion.

Figure 2.2 shows the spatial distributions of CO, O_3, NO_2, HNO_3, hydrochloric acid (HCl), and isoprene (ISOP) that can be predicted by MAM_CB05_GE but not by MAM_SIM. CO mixing ratio is higher in most Asia, central Africa, South Africa, and eastern U.S., which is mainly due to higher CO emissions in those regions and the production of CO from the photolytic reactions of VOCs (e.g., formaldehyde, acetaldehyde, and isoprene). Higher O_3 mixing ratios in the northern hemisphere than southern hemisphere are mainly due to much higher mixing ratios of O_3 precursors. Higher O_3 mixing ratios over Mediterranean Sea are mainly due to the transport of O_3 and its precursors from source regions and less deposition onto ocean surface. Higher O_3 mixing ratios over Tibet are mainly due to the stratospheric influences from high altitude and no titration of O_3 due to low NO mixing ratios (< 0.2 ppb) in this region. Higher mixing ratios of NO_2 over most Asia, eastern U.S, Europe, and Central Africa are mainly due to higher NO_x emissions over those regions, which also result in higher HNO_3 in those regions. Higher mixing ratios of HCl over Europe, India, and East Asia are mainly due to the higher anthropogenic HCl emissions in

those regions. In addition, MAM_CB05_GE includes oceanic emissions of HCl, leading to higher HCl over ocean. Higher isoprene mixing ratios over South Africa, central Africa, and Oceania are mainly due to higher isoprene emissions in those regions, which also contribute to the formation of SOA in those regions.

The aforementioned changes in the concentrations of gaseous species and PM due to new gas-phase chemistry implemented in the model and its feedbacks to radiation through the climate system result in a change in predicted cloud properties and radiation balance that in turn affect the predictions of all chemical species during subsequent time steps. As a consequence of interwoven changes due to complex feedback mechanisms, the two simulations perform differently, with noticeable improvement by MAM_CB05_GE. As shown in Table 2.3a, compared with MAM_SIM, MAM_CB05_GE reduces MB of LWD by 17.6%, OLR by 8.0%, CF by 28.6%, COT by 1.0%, PWV by 28.0%, AOD by 5.5%, and CDNC by 1.8%, leading to 0.3-2.2% absolute reduction in their NMBs. Although MAM_CB05_GE increases MB of SWD by 26.2%, the increases in their NMBs are only 1.2%. Table 2.4 shows the probability of differences in radiative/cloud predictions between paired-simulation. As shown in Table 2.4, the changes in most cloud and radiative variables between MAM_SIM and MAM_CB05_GE are statistically significant. As shown in Table 2.3b, MAM_CB05_GE also reduces MBs of SO_2 by 2.5% and PM_{10} by 8.1% over East Asia, NH_3 by 1.3% and SO_4^{2-} by 12.5% over Europe, OC by 11.1%, TC by 8.3%, and $PM_{2.5}$ by 3.3% over CONUS, leading to 0.8-6.5% absolute reductions in NMBs. Despite the model improvement by CB05_GE, large biases still remain for some chemical species. For example, CO over East Asia is largely underpredicted with an NMB of -82.1% (see Table

2.3b), which results from the uncertainties in the CO emissions over East Asia. However, the column CO over globe is predicted very well, with an NMB of -5.7%. Large biases in SO_2 predictions over CONUS, Europe, and East Asia are mainly due to the uncertainties in the SO_2 emissions over those regions. Large biases in O_3 over Europe are likely due to the uncertainties in the O_3 precursor emissions (e.g., NO_x) and inaccurate predictions of radiation over Europe. In particular, the large underpredictions in NO_2 concentrations (likely due to the uncertainties in the NO_x emissions and overpredictions in radiation, see section 5.5 for more detailed discussions) indicate insufficient NO_x for titration of O_3, leading to a large overprediction in O_3 concentrations in Europe. The large biases in HNO_3 are due to no treatment for gas-particle partitioning in both simulations.

2.5.2 Impacts of Condensation and Aqueous-Phase Chemistry

The mass accommodation coefficient (α) for H_2SO_4 vapor is subject to considerable uncertainty. The default condensation module with a default α value of 0.65 gives a very low concentration of H_2SO_4, resulting in very low nucleation rates and aerosol number concentrations. Considering that the original model treats H_2SO_4 and NH_3 condensation as an irreversible process, the default α value of 0.65 for H_2SO_4 and NH_3 is reduced to 0.02 and 0.097, respectively, based on Zhang et al. (1998). This change in α value provides sufficient H_2SO_4 and NH_3 for nucleation with a typical H_2SO_4 concentration range of 10^6~10^8 molecules cm^{-3}. Because HNO_3 and HCl are semi-volatile species, the lower limits of α (0.0024 and 0.005, respectively) based on Sander et al. (2002) are selected for their irreversible condensation process. NH_4^+ from NH_3 condensation will be constrained by the available SO_4^{2-}, NO_3^-, and condensed Cl^- to neutralize the system.

Figure 2.3 shows the absolute differences of NH_3, SO_2, HNO_3, HCl, H_2SO_4, total particulate ammonium (TNH_4), total particulate sulfate (TSO_4), total particulate nitrate (TNO_3), and total particulate chloride (TCL) in all the modes except primary carbon mode, and $PM_{2.5}$ between MAM_CON and MAM_CB05_GE in June, July, and August (JJA), 2001. Due to the inclusion of HNO_3 and HCl condensation in MAM_CON, the concentrations of HNO_3 and HCl decrease by 0.1 ppb (~72%) and 0.097 ppb (~84%), respectively. NO_3^- is not simulated in the original model and the concentration of NO_3^- is assumed as zero in MAM_CB05_GE. Therefore, the concentration of NO_3^- increases due to the condensation of HNO_3 in MAM_CON. The concentration of TCL in MAM_CB05_GE is calculated from the mass ratio of chloride in sea-salt. Over land, TCL increases significantly due to the condensation of HCl to form Cl^-. The change of TCL over ocean is mainly due to the change of sea-salt emissions. The changes of SO_2 mixing ratios are mainly due to the differences in mixing ratios of species in sulfur chemistry in the two simulations. For example, compared to MAM_CB05_GE, the increase of SO_2 over eastern U.S. in MAM_CON is likely due to less SO_2 oxidation in clouds (Figure not shown), which results from lower CF. The decrease of SO_2 mixing ratios over most oceanic areas is likely due to the combined effects of DMS oxidation and SO_2 oxidations in MAM_CON. More SO_2 can result in more H_2SO_4 and therefore more SO_4^{2-} through condensation and homogeneous nucleation of H_2SO_4. The changes in H_2SO_4 concentrations are the results of changes of SO_2 mixing ratios. The mass accommodation coefficient of H_2SO_4 is reduced significantly (by a factor of 32.5), allowing more H_2SO_4 to participate in binary/ternary homogeneous nucleation and produce more secondary SO_4^{2-}, improving predictions of SO_4^{2-} over CONUS but degrading the

performance of SO_4^{2-} over Europe (see Table 2.3b). Although the mass accommodation coefficient of NH_3 is reduced significantly (by a factor of 67), more available NH_3 can participate in the ternary homogeneous nucleation and produce secondary NH_4^+. Meanwhile, the secondary NH_4^+ formed from NH_3 condensation is also constrained by available SO_4^{2-}, NO_3^-, and condensed Cl^-. As a result, the concentrations of NH_3 decrease and those of NH_4^+ increase. Due to more available H_2SO_4 participating in the nucleation, J has been improved significantly, reducing the NMB from -99.5% to -12.8%. With an inclusion of the dissolution and dissociation of HNO_3 and HCl in cloud water, more NH_3 is required to dissolve to maintain cation-anion equilibrium in the cloud water, which further reduces the mixing ratios of NH_3, HNO_3, and HCl.

As shown in Table 2.3b, compared with MAM_CB05_GE, MAM_CON gives better performance against observations in terms of CO, NO_2, O_3, HNO_3, $PM_{2.5}$, and PM_{10} over Europe, CO and PM_{10} over East Asia, O_3, HNO_3, SO_4^{2-}, NH_4^+, BC, OC, TC, and $PM_{2.5}$ over CONUS, and column CO, column NO_2, TOR, and J over globe. As also shown in Table 2.3a, the improved chemical predictions improve the predictions of OLR, SWCF, CF, COT, CWP, AOD, and CDNC. As shown in Table 2.4, the changes in most cloud /radiative variables between MAM_CB05_GE and MAM_CON are statistically significant, indicating the significant impacts of the modified condensation and aqueous-phase chemistry treatments on radiation. Treating condensation and aqueous-phase chemistry of HNO_3 and HCl enables an explicit simulation of NO_3^- and Cl^- in MAM7. However, the mass concentrations of SO_2 remain significant overpredictions, with NMBs of 301.2% for CONUS, and 123.0% for Europe, mainly because of the uncertainties in SO_2 emissions over those regions. Due to the

simplified irreversible treatment for gas condensation, the mass concentrations of SO_4^{2-}, NH_4^+, NO_3^-, and Cl^- are overpredicted, although the lower limit of mass accommodation coefficient for each precursor is used in MAM_CON. As shown in Table 2.3b, the concentrations of SO_4^{2-}, NH_4^+, NO_3^-, and Cl^- from MAM_CON are overpredicted by 1.7%, 20.0%, 198.2%, and 359.9%, respectively, for CONUS, and 40.3%, 85.0%, 67.8%, and 102.8%, respectively, for Europe. The large NMBs of NO_3^- and Cl^- in MAM_CON are due to the small observed values for NO_3^- (i.e., 1.0 μg m^{-3} over CONUS and 2.0 μg m^{-3} over Europe) and Cl^- (i.e., 0.1 μg m^{-3} over CONUS and 0.7 μg m^{-3} over Europe), the uncertainties in treating HNO_3 and HCl as non-volatile species using their lower limits of accommodation coefficients, and lack of treatments for NO_3^- and Cl^- thermodynamics.

2.5.3 Impacts of New Particle Formation

Figure 2.4 shows the annual-mean vertical distributions of particle formation rate (J) values and aerosol number concentrations, and simulated J values averaged between the ground level and 1000-m overlaid with observations within the same layers. In MAM_CON/IMN, IMN is combined with three default nucleation parameterizations to predict J throughout the atmosphere. In MAM_CON, J over ocean is overpredicted by factors of 5-50, despite a seeming good NMB of -12.8% in the globe mean (see Table 2.3b). J values at several sites over land are underpredicted by factors of 1-10, which compensates the large overpredictions at most sites over ocean. The large underpredictions at those sites are likely due to the uncertainties in SO_2 emissions and nucleation parameterizations, and the missing species that may have participated in nucleation. For example, several other species may contribute to the new particle formation, including methanesulfonic acid (van Dingenen and

Raes, 1993), hydrochloric acid (Arstila et al., 1999), organic compounds (Berndt, et al., 2014), iodine-containing compounds (Hoffmann et al., 2001), and amines (Berndt et al., 2014). Limited observations also introduce some uncertainties in the model validation. The overprediction of J over ocean is mainly due to the use of the prefactor of 1×10^{-6} in WP09. This prefactor is derived from limited in-situ measurements (Sihto et al., 2006). It can vary by up to 3-4 orders of magnitude based on measurements in different areas and seasons (Zhang et al., 2010a), introducing a large uncertainty for its application to the global scale. In MAM_CON/IMN, a prefactor of 1×10^{-8} is used in WP09 in PBL over the globe, which then decreases J and aerosol number concentrations in PBL (see Figure 2.4). J in PBL is very sensitive to the prefactor in WP09, and the uncertainty of the prefactor can result in a large bias in predictions of J and aerosol number in PBL. With the implementation of IMN, J values in the troposphere increase by factors of 2-10, which in turn increase the aerosol number concentrations in the troposphere. Due to a stronger radiation in the upper layer, more available ions can contribute to the new particle formation, therefore increasing the aerosol number concentrations in the middle/upper troposphere and lower stratosphere by factors of 2-4.

Figure 2.5 shows the absolute differences of $PM_{2.5}$, AOD, column CCN5, CF, SWCF, and SWD between MAM_CON and MAM_CON/IMN for 2001. Aerosol number can directly affect CCN, which can affect cloud formation and properties as well as radiation. Changes of PM concentrations also have impacts on AOD, CCN, CF, COT, and SWCF through both aerosol direct and indirect effects. As a net result of all those interwoven changes initially triggered by the increase of aerosol number concentrations in

troposphere/stratosphere, AOD and column CCN5 increase by 0.004 (or by 3.3%) and 2.1×10^7 cm^{-2} (or by 11.9%), respectively, and SWCF and SWD decrease by 0.1 W m^{-2} (or by 0.2%) and 0.8 W m^{-2} (or by 0.5%), respectively, in terms of global mean. As shown in Table 2.4, the changes in SWD, AOD, and cloud variables such as column CCN5, CDNC, and COT between MAM_CON and MAM_CON/IMN are statistically significant, indicating the significant impacts of IMN on aerosol number concentration and cloud prediction.

Compared with MAM_CON, IMN (MAM_CON/IMN) improves the predictions of SO_2, NO_3^-, and $PM_{2.5}$ over CONUS, SO_2, SO_4^{2-}, NH_4^+, NO_3^-, Cl^-, $PM_{2.5}$, and PM_{10} over Europe, PM_{10} over East Asia (see Table 2.3b). The improved performance in aerosol concentrations and increased aerosol numbers in the troposphere and lower stratosphere contribute to the improved performance of aerosol and cloud parameters, with increased AOD, CCN, and CDNC, and consequently increased CF, COT, CWP, and SWCF, as shown in Table 2.3a. However, there are still large biases for some chemical species predictions. For example, CO mixing ratio is underpredicted over East Asia, which is mainly due to the uncertainty in CO emissions in this region. Large biases in SO_2 predictions over CONUS, Europe, and East Asia are mainly due to the uncertainties in SO_2 emissions in those regions. Large biases in NO_2 and HNO_3 predictions over Europe are mainly due to the uncertainties in NO_x emissions and inaccurate predictions of radiation over this region. The performance of J degrades with NMBs from -21.8% to -49.6% in the globe, which is due to the use of a smaller prefactor of WP09 in MAM_CON/IMN than in MAM_CON. J in PBL is very sensitive to the prefactor in WP09. Although the prediction of J over ocean in PBL has been improved in MAM_CON/IMN, J over land areas in PBL is largely underpredicted by factors

of 1-100, resulting in degraded J performance in terms of globe mean. The underprediction of J over land in PBL is likely due to the uncertainties in the nucleation parameterizations (e.g., the missing species as mentioned previously). Large NMBs still remain for COT, CWP, and CCN, indicating the uncertainties in the treatments of related atmospheric processes such as cloud microphysics and aerosol-cloud interactions.

2.5.4 Impacts of Gas-Aerosol Partitioning

The inclusion of ISORROPIA II changes the mass concentrations of major $PM_{2.5}$ species and their gaseous precursors. Changes in PM concentrations then affect predictions of cloud variables and therefore radiation. Changes of radiation can also affect SO_2 oxidation by OH, which affects H_2SO_4 concentrations. Figure 2.6a and b show the absolute differences of H_2SO_4, fine particulate sulfate (SO4f), NH_3, fine particulate ammonium (NH4f), HNO_3, fine particulate nitrate (NO3f), HCl, and fine particulate chloride (CLf) for summer (June, July, August, JJA) and winter (December, January, and February, DJF) 2001 between MAM_CON and MAM_CON/ISO. Compared to MAM_CON, MAM_CON/ISO gives higher H_2SO_4 mixing ratios but lower SO4f concentrations. SWD increases with the global mean of 8.9 W m^{-2} (~ 5.8%) in MAM_CON/ISO, which allows more production of OH from photolytic reactions of VOCs, HONO, HNO_3, HNO_4, H_2O_2, HOCl, and HOBr, and therefore enhanced oxidation of SO_2 to form H_2SO_4. As shown in Figure 2.6a, the mixing ratios of H_2SO_4 either increase up to 0.76 ppt or decrease as large as 1.14 ppt, leading to a net increase of 0.002 ppt in terms of global mean. The mass concentration of SO4f is mainly affected by H_2SO_4 condensation. Although the mixing ratios of H_2SO_4 increase with the global mean change of 0.002 ppt, SO4f concentrations decrease with the global mean of 0.02 μg m^{-3},

which are mainly due to less condensation of H_2SO_4 under higher temperature conditions. In summer, the increase or decrease of H_2SO_4 can result in an increase or a decrease of SO4f (e.g., over most oceanic areas). However, the decrease of SO4f with the increase of H_2SO_4 over the India Ocean is mainly due to less H_2SO_4 condensation. For the regions where SO4f increases over land, the increase of SO4f is due to more oxidation of SO_2 by OH. Compared to MAM_CON, the concentrations of NH_3, HNO_3, and HCl increase significantly over most land areas, whereas NH4f, NO3f, and Clf decrease significantly over most land areas in MAM_CON/ISO. Such changes can be explained based on the chemical regimes and their spatial distributions as shown in Figure 2.7.

The chemical regimes is the controlling factor for gas-aerosol equilibrium partitioning, which is determined based on the ratio of SO_4^{2-} molar concentrations to total molar concentrations of cations and their respective gases (referred to as TCAT/TSO4) (Zhang et al., 2000). Three regimes are defined based on the values of TCAT/TSO4: (1) if TCAT/TSO4 < 2, the system contains excess sulfate and is in a sulfate-rich regime; (2) if TCAT/TSO4 = 2, the system contains just sufficient sulfate to neutralize the cation species and is in sulfate-neutral regime; (3) if TCAT/TSO4 > 2, the system contain insufficient sulfate to neutralize the cation species and is in sulfate-poor regime. Over land, the major cation is NH_4^+, and there are also crustal species (K^+, Ca^{2+}, and Mg^{2+}) associated with dust emissions, whereas over ocean, the major cation is Na^+, which is a non-volatile species. Therefore, the gas-aerosol equilibrium partitioning behaves differently over land and over ocean. Figure 2.7 shows the distributions of TCAT/TSO4 in MAM_CON and MAM_CON/ISO, and their absolute differences for summer and winter, 2001. In summer,

compared to MAM_CON, TCAT/TSO4 in MAM_CON/ISO either increases up by 80.1 (mostly over ocean) or decreases up by 51.8 (over both land and ocean), leading to a net increase of 0.7. In MAM_CON, most regions are in sulfate-poor regime, whereas Greenland, southeast U.S., North Africa, a small portion of Asia and North Atlantic Ocean, and some areas in North Pole are in sulfate-rich regime in summer. However, due to the simplified thermodynamics treatment in MAM_CON, NH_3 is underpredicted and NH_4^+ is overpredicted (see Table 2.3b). With the inclusion of ISORROPIA II, most sulfate-poor regions over land and over part of Pacific Ocean and most Atlantic Ocean become less sulfate-poor. The sulfate-poor regime can drive HNO_3/HCl to produce NO_3^-/Cl^- by neutralizing excess NH_4^+. If the amount of NO_3^-/Cl^- is insufficient to neutralize NH_4^+, sulfate-poor regime can drive NH_4^+ to the gas phase to produce NH_3. Therefore, the increase of NH_3 and decrease of NH_4^+ in MAM_CON/ISO are mainly due to insufficient NO_3^-/Cl^- to neutralize NH_4^+ under sulfate-poor regime. Insufficient NO_3^-/Cl^- results from the thermodynamic partitioning under higher temperature conditions that favors the production of HNO_3 and HCl from NO_3^-/Cl^- to produce HNO_3 and HCl under higher temperature conditions. The slight increase of NO_3^- over Pacific Ocean and South Atlantic Ocean is due to much higher Na^+ concentrations yet insufficient SO_4^{2-} in those regions compared with those over the land areas. Unlike a sulfate-poor regime, a sulfate-rich regime (e.g., small portion of North Atlantic Ocean, South China Sea, and Greenland), requires more cations such as NH_4^+ and Na^+ to neutralize excess SO_4^{2-} in the system and the thermodynamics favors the partitioning of volatile species such as NO_3^- and Cl^- in the gas phase as HNO_3 and HCl. Therefore, despite the increased temperatures, the decrease of NH_4^+ due to its evaporation back to the gas-phase is not as significant as that of

NO_3^- and Cl^-, because NH_4^+ needs to stay in the system to neutralize SO_4^{2-}. In winter, as shown in Figure 2.6b, compared with MAM_CON, the mixing ratios of H_2SO_4 in MAM_CON/ISO either increase by up to 4.3 ppt, or decrease by up to 1.0 ppt, leading to a net increase with the global mean of 0.001 ppt. NH_3 increases over most regions except Europe, eastern China, and some regions in North Pole. HNO_3 decreases over most oceanic areas, Northeastern China, and East Europe, whereas increases over South Asia, North Pole, southern U.S., Africa, and most land areas in southern hemisphere. HCl increases over most areas except the northeastern portion of Asia and eastern Europe.

Compared with MAM_CON, MAM_CON/ISO predicts higher HNO_3 and HCl over some land areas. As shown in Figure 2.7, in MAM_CON, most regions are in sulfate-poor regime, whereas Greenland, North Pole, North Africa, some portions of Asia and western Pacific Ocean are in sulfate-rich regime. For example, northeastern China is in sulfate-poor regime, driving HNO_3 and HCl partitioning to the aerosol phase to neutralize excess NH_4^+. This results in an increase in NO3f and Clf, changing sulfate-poor regime to less sulfate-poor. North Pacific Ocean and southern oceanic areas are also in sulfate-poor regime, and the increase of NO3f is due to the partitioning HNO_3 to the aerosol phase to neutralize Na^+, whose concentration is relatively higher compared to that over land areas. Therefore, more anions such as NO_3^- are needed to neutralize the system. However, the decrease Cl^- over these regions is due to the equilibrium state of HCl under different atmospheric conditions. The western Pacific Ocean is in sulfate-rich regime, driving NO_3^- and Cl^- partition to the gas phase, which results in a decrease in NO3f and Clf, and an increase in HNO_3 and HCl over

this region. With the inclusion of ISORROPIA II, the western Pacific Ocean changes from sulfate-rich regime to less sulfate-rich regime.

Figure 2.8 shows the absolute differences of major inorganic gas and aerosol species between metastable (MAM_NEWA) and stable (MAM_NEWB) conditions. Compared with MAM_NEWA, the global average changes predicted by MAM_NEWB are overall small (within 5%) for most gaseous and aerosol species. For example, the global average changes are 0.01 μg m^{-3} (by 4.2%) for SO_4^{2-}, 0.005 μg m^{-3}(by 12.8%) for NH_4^+, 0.006 μg m^{-3}(by -0.01%) for NO_3^-, and -4×10^{-4} μg m^{-3} (by 2.0%) for Cl^-. The increase of SO_4^{2-} results in an increase in NH_4^+ (e.g., East Asia and Northeast U.S.). The differences between stable and metastable conditions may be more significant under low RH conditions (RH < 50% for nitrate, Fountoukis et al., 2009). However, based on the simulated global annual mean RH values, most regions have RH values > 60-70% (exceptions are over desert/arid regions such as Australia, the northern Africa, Arabian Desert, northwestern China, and western U.S.). These results indicate that the assumption of metastable conditions is not a significant sources of uncertainty for global model predictions of gaseous and aerosol species.

Compared to MAM_CON, the prediction of SWD in MAM_CON/ISO is improved with the NMB decreasing from -6.5% to -2.2%. The predictions of involved species such as NH_4^+, NO_3^-, and Cl^- are improved significantly by 13.6%~345.4%, although there is a slight degradation in the predictions of SO_4^{2-} and O_3 over CONUS, CO, O_3, $PM_{2.5}$, and PM_{10} over Europe, PM_{10} over East Asia, and column CO, NO_2, TOR, and J over globe. MAM_CON/ISO improves the predictions of HNO_3, NH_4^+, NO_3^-, Cl^-, BC, OC, TC, and $PM_{2.5}$ over CONUS, SO_2, NH_3, NO_2, SO_4^{2-}, NH_4^+, NO_3^-, and Cl^- over Europe, and CO and

SO_2 over East Asia, which leads to improved performance in SWD, column CCN5, and SWCF over globe, as shown in Table 2.3a. As shown in Table 2.4, the changes in most radiative and cloud variables between MAM_CON and MAM_CON/ISO are statistically significant, indicating the significant impacts of ISORROIA II on the predictions of radiation, aerosol, and cloud. ISORROPIA II calculates gas-aerosol partitioning under different atmospheric conditions, significantly improving predictions of major gas precursor (e.g., HNO_3) over CONUS and secondary aerosols (e.g., NO_3^- and Cl^-) over CONUS and Europe. Large decreases in the concentrations of NO_3^- and Cl^- result in a decrease in NH_4^+, $PM_{2.5}$, and PM_{10}, thus decreasing CCN, CDNC, AOD, and the absolute value of SWCF.

MAM_CON/ISO assumes metastable conditions (i.e., assuming all salts in an aqueous solution), which may introduce errors in gas/particle partitioning. The validity of this assumption is examined by taking the absolute differences of the concentrations of major inorganic gas and aerosol species between metastable (MAM_NEWA) and stable (MAM_NEWB) conditions (i.e., Figure 2.8). Compared with MAM_NEWA, the global average changes predicted by MAM_NEWB are within 5% for most gaseous and aerosol species over non-desert/arid regions, indicating that the assumption of metastable conditions is not a significant sources of uncertainty in this work. However, the irreversible gas-to-particle mass transfer treatment for coarse particles can potentially overpredict the concentrations of coarse particles (e.g., overpredictions of Cl^- and NO_3^- over Europe).

2.5.5 Overall Impacts of All New and Modified Model Treatments

Compared to MAM_CB05_GE, the simulations with modified or new aerosol treatments (MAM_CON, MAM_CON/IMN, MAM_CON/ISO, MAM_NEWA) slightly

degrade the prediction of LWD (increasing NMB from -0.9% to -1.4%), but improve the predictions of OLR, CF, COT, and CWP slightly (with 0.6% - 10.4% decreases in their NMBs) and CDNC significantly (reducing NMBs from -57.5% up to -13.4%). Although the CCN predictions are somewhat degraded in MAM_CON and MAM_CON/IMN, they are improved significantly in MAM_CON/ISO and MAM_NEWA (reducing NMBs from -61.6% to 1.8-6.3%). As shown in Table 2.4, changes in most radiative and cloud variables between MAM_SIM and MAM_NEWA are statistically significant, indicating the significant impacts of new and modified treatments on predictions of radiation and cloud. Among all new and modified model treatments, the new gas-phase chemistry simulates more gaseous species and improves the predictions of NH_3 over Europe, $PM_{2.5}$ over CONUS and PM_{10} over East Asia. The modified condensation and aqueous-phase chemistry simulate more aerosol species (NO_3^- and Cl^-) and improve the prediction of HNO_3. MAM_CON also improves J in the PBL due to more available H_2SO_4 involved in the homogeneous nucleation using an accommodation coefficient of 0.02 for H_2SO_4 condensation, and improves the predictions of CDNC and AOD significantly. MAM_CON/IMN increases PM_{num} above PBL and $PM_{2.5}$ and PM_{10} over Europe and improves the prediction of $PM_{2.5}$ over CONUS and Europe. MAM_CON/ISO improves the predictions of HNO_3, NH_4^+, $PM_{2.5}$, NO_3^-, and Cl^- over CONUS, NO_3^- and Cl^- over Europe, and CCN over globe, and improves the predictions of SWCF most (with an NMB of 1.6%).

Large biases in some variables remain in MAM_NEWA due to uncertainties in model inputs (e.g., meteorology and emissions) and model treatments (e.g., multi-phase chemistry, dust emission scheme, cloud microphysics, aerosol activation, SOA formation, and dry and

wet deposition). The large NMBs of CO and SO_2 over East Asia, SO_2, NH_3, and NO_2 over Europe, SO_2, and BC over CONUS are likely due to the uncertainties of emissions and the interpolation of emissions from a fine-grid scale in the original emission inventories (e.g., county-based emissions over CONUS) to a large-grid scale used in this work, which can result in large NMBs in secondary aerosols (e.g., SO_4^{2-}, NH_4^+, NO_3^-, thus $PM_{2.5}$ and PM_{10}). Heterogeneous reactions are not included in this work, which may help explain to some extent less oxidation and underpredictions for PM species predictions (e.g., sulfate and nitrate) and overpredictions for gaseous species. The large NMB of O_3 predictions over Europe in MAM_NEWA (with an NMB of 62.7%) is mainly due to a lack of NO_x titration (as indicated by large underpredictions in NO_2) and more production of O_3 from the photolytic reaction of NO_2 resulted from overpredictions of SWD particularly in autumn and winter. Table 2.5 shows the seasonal statistics for O_3, NO_2, and HNO_3 over Europe in MAM_NEWA. During autumn and winter, O_3 is overpredicted by about 100% ~ 140%, whereas NO_2 is underpredicted by about -85% ~ -20%, indicating insufficient NO_x for titration of O_3 titration. SWD is overpredicted by 45.0 W m^{-2} (or by 58.4%), favoring the photolytic reactions of NO_2 to produce O_3.Due to the uncertainties in the NO_x emissions, NO_2 is underpredicted, causing less NO_2 to be oxidized to produce HNO_3, which results in an underprediction of HNO_3 in winter. In autumn, SWD is overpredicted by 42.8 W m^{-2} (or by 37.9%). However, in autumn, although NO_2 is underpredicted due to the uncertainties in the NO_x emissions, HNO_3 mixing ratios are overpredicted. SWD is stronger in autumn than in winter, and mixing ratios of OH are higher due to photolytic reactions of overpredicted O_3 and additional photolytic reactions of VOCs. Therefore, OH can oxidize NO_2 to produce

HNO_3, resulting in the overprediction of HNO_3. Simple aqueous-phase chemistry is included in this work, which could result in high uncertainty in predicting aerosols in clouds. Decreased aerosol number concentrations can result in a decrease of CCN and AOD directly. The underpredictions of CDNC are likely due to uncertainties in the model treatments for aerosol activation and cloud microphysics, which then result in large NMBs in COT and CWP. The large biases in OC and TC indicate the uncertainties in the emissions of BC and primary OC, and the treatments for SOA formation. The large NMB in particle formation rate J is likely due to uncertainties in model inputs (e.g., SO_2 emissions) and model treatments (e.g., the accommodation coefficient of H_2SO_4 and missing participants in the current nucleation schemes).

2.5.6 Impacts of Adjusted Emissions

The evaluation and analyses of MAM_NEWA indicate that some large biases are caused by inaccuracies in the emissions of CO, SO_2, BC, OC, and NH_3. The sensitivity simulation with adjusted emissions of CO, SO_2, BC, OC, and NH_3 (MAM_NEW/EMIS) is performed to further look into such impacts. For example, with 30% increase in CO emissions and 20% increase in NH_3 emissions over Europe, the NMBs of surface concentrations of CO and NH_3 change from-3.4% to 12.1%, -84.3% to -77.5%, respectively. On a global scale, the increased CO emissions result in 3.0% absolute reduction in the NMB of column CO. The 30% reduction in SO_2 emissions and 20% increase in OC and BC emissions over CONUS result in 139.6%, 8.6%, and 24.9% absolute reduction in their NMBs. The 30% increase in CO emissions and 20% increase in SO_2 over East Asia result in 3.3% and 7.8% absolute reduction in their NMBs.

As shown in Table 2.3b, compared with MAM_NEWA, MAM_NEW/EMIS shows an improved performance in the concentrations of SO_2, HNO_3, SO_4^{2-}, NH_3, and NH_4^+ over Europe, SO_2, HNO_3, BC, OC, TC, NO_3^-, and Cl^- over CONUS, CO and SO_2 over Asia, and column CO over globe. However, it degrades to some extent the performance of SO_4^{2-} and NH_4^+ over CONUS, $PM_{2.5}$ and PM_{10} over Europe, PM_{10} over Asia, and J over globe. Decreased SO_2 emissions over CONUS result in a decrease of H_2SO_4 and therefore a decrease of SO_4^{2-}. Based on aerosol thermodynamic treatments, decreased SO_4^{2-} will result in decreased NH_4^+. Therefore, $PM_{2.5}$ and PM_{10} decrease as well. Adjusted emissions can affect secondary aerosol formations and therefore radiative variables can be affected due to the direct and indirect effects of aerosols. As shown in Table 2.3a, compared with MAM_NEWA, MAM_NEW/EMIS reduces MB of LWD by 9.3%, SWD by 37.5%, and CF by 18.9%, leading to 0.1% - 1.6% absolute reduction in their NMBs. This illustrates the sensitivity of radiation to the perturbations in emissions through chemistry feedbacks to the climate system. As shown in Table 2.4, only column CCN5 and AOD are significantly different between MAM_NEWA and MAM_NEW/EMIS, indicating the impacts of emissions are more significant on predictions of gas and aerosol than radiative variables.

2.6 Evaluation of the Five-Year Simulations

2.6.1. Performance Evaluation

Tables 2.6a and b show the statistical performance for radiative/cloud variables and chemical predictions, respectively, from the 5-year simulations using three different configurations. Compared with MAM_SIM_5Y, MAM_NEW_5YA improves the predictions of aerosol and cloud variables such as AOD, COT, CWP, CCN5, and CDNC

(with 4.8% to 23.4% absolute reduction in their NMBs), and radiative variables such as SWD, LWD, OLR, and SWCF (with 0.4-4.2% absolute reduction in their NMBs). MAM_NEW_5YA also shows slight improvement for the predictions of SO_4^{2-} and BC over CONUS and SO_2 over East Asia (with 0.3-2.3% absolute reduction in their NMBs), but moderate-to-large improvements for the predictions of OC, TC, and $PM_{2.5}$ over CONUS, PM_{10} over East Asia, and SO_2, $PM_{2.5}$, and PM_{10} over Europe (with 5.2-20.1% absolute reduction in their NMBs). Compared to TOR calculated based on O_3 climatology used in MAM_SIM_5Y, TOR predicted from MAM_NEW_5YA is slightly improved with 1.2%, 1.3%, and 0.3 absolute reduction in its NMB, NME, and RMSE, respectively. Tables 2.7a and b show the evaluation of major radiative/cloud variables and chemical predictions are also conducted for June, July, and August (JJA) of 2001-2005. Compared with full 5-year (2001-2005) average, the simulation for JJA gives similar predictions for chemical species but better model predictions for radiation (e.g., LWD, SWD, and OLR) and cloud (e.g., COT, CWP, column CCN5, and CDNC) variables.

Tables 2.6a and b also show the performance of MAM_NEW_5YB in which CAM5 is fully coupled with land, ocean, and ice models. The performance is overall similar for all radiative variables and most chemical species between MAM_NEW_5YA and MAM_NEW_5YB (most within 5% differences in the absolute values of their NMBs). The performance of HNO_3 over CONUS and Europe, NH_4^+, NO_3^-, and Cl^- over Europe, PM_{10} over Europe and East Asia is improved appreciably (with 4.2-17.9% reduction in the absolute values of their NMBs), and that of SO_2 over CONUS and Europe and NH_4^+, NO_3^-, and Cl^- over CONUS degrades appreciably (with 4.3-8.5% increase in the absolute values of their

NMBs). Those changes are mainly due to the interactions among Earth's components, particularly at the interface of earth components (e.g., air-sea, air-land, and sea-ice interfaces) and feedbacks to the climate system, which in turn affects gaseous and aerosol concentrations in the coupled system.

Large biases remain for some variables in MAM_NEW_5YA and MAM_NEW_5YB due to uncertainties in model inputs (e.g., meteorology and emissions) and model treatments (e.g., multi-phase chemistry, dust emission scheme, cloud microphysics, aerosol activation, SOA formation, and dry and wet deposition), which have been illustrated in Section 5.5. Large biases in Cl^- predictions over Europe are likely due to the combined effects of a low concentration of observed Cl^-, uncertainties in HCl emissions, and inaccurate predictions of coarse Cl^- in the model since ISORROPIA II is only implemented for fine particles. Uncertainties in the mass accommodation coefficients of volatile gas species can also result in uncertainties in predictions of condensable gases.

2.6.2 Impact of New and Modified Treatments on 2001-2005 Simulations

Figure 2.9a shows the absolute differences of surface SO_2, NH_3, SO_4^{2-}, NH_4^+, TC, $PM_{2.5}$, PM_{10}, J, and aerosol number (PM_{num}) and Figure 2.9b shows the absolute differences of radiative variables between MAM_SIM_5Y and MAM_NEW_5YA. The new and modified model treatments in MAM_NEW_5YA cause changes in the concentrations of PM and precursor gases, which affect radiative variables through aerosol direct and indirect effects. The changes in radiative variables in turn affect gas-phase chemistry and aerosol processes. As shown in Figure 2.7, the difference of SO_2 between the two simulations varies from -1.7 to 3.8 ppb, with a global mean difference of 4.2 ppt. The decrease of SO_2 over

most oceanic area is mainly due to the decrease of DMS resulted from less oxidation by OH radicals. The increase of SO_4^{2-} over East Asia and eastern U.S. drives more NH_3 from gas-phase to particulate phase to form NH_4^+ through thermodynamic equilibrium, increasing the concentrations of NH_4^+ over these regions. However, the concentrations of SO_4^{2-} decrease over Europe due in part to less oxidation of SO_2. Despite such a decrease, the concentrations of NH_4^+ are higher over Europe due to the neutralization of NH_3 by Cl^- and NO_3^- that are treated in MAM_NEW_5YA but not treated in in MAM_SIM_5Y. Compared with MAM_SIM_5Y, J from MAM_NEW_5YA increases over globe with a global mean difference of 0.066 cm^{-3} s^{-1}, due to the use of a lower mass accommodation coefficient of H_2SO_4 in MAM_NEW_5YA, resulting in more available H_2SO_4 vapor participating in nucleation. The increases in J result in an increase in aerosol mass and number concentrations and thus higher concentrations of $PM_{2.5}$ and PM_{10} (which improve appreciably their performance, see Table 2.6b).

As shown in Figure 2.9b, compared with MAM_SIM_5Y, AOD increases by 0.007, column CCN5 increases by 3.8×10^7 cm^{-2}, and CDNC increases by 16.1 cm^{-3} in MAM_NEW_5YA. Higher PM_{num} in MAM_NEW_5YA allows more aerosol to grow into the CCN size, leading to higher CCN in MAM_NEW_5YA. Higher aerosol concentrations in MAM_NEW_5YA result in higher AOD. The increased aerosol number and mass concentration result in an increase in the predictions of cloud variables through the aerosol-cloud interactions. For example, with all the modified and new treatments, COT increases by 0.8, CWP increases by 4.1 g m^{-2}, and PWV increases by 0.026 cm on global average. Due to the aerosol direct and indirect effects, the difference in simulated SWD varies from -19.3 to

10.4 W m^{-2} and decreases by 3.4 W m^{-2} (~ 2.0%) on a global average. The difference in LWD varies from -4.2 to 8.5 W m^{-2} and increases by 1.0 W m^{-2} (~ 0.4%) on a global average (Figure not shown). The difference in SWCF varies from -8.4 to 17.9 W $m^{-2,}$ with a net increase of 2.7 W m^{-2} (~ 6.4%) on a global average.

Figure 2.10a shows the absolute differences of surface SO_2, NH_3, SO_4^{2-}, NH_4^+, TC, $PM_{2.5}$, PM_{10}, J, and PM_{num} and Figure 2.10b shows the absolute differences of cloud and radiative variables between MAM_SIM_5Y and MAM_NEW_5YA for JJA average of 2001-2005. Compared with MAM_SIM_5Y, MAM_NEW_5YA predicts lower SO_2 and NH_3 over East Asia with higher SO_4^{2-} and NH_4^+ in this region. More SO_2 is oxidized to form SO_4^{2-}, leading to enhanced acidity, which drives more NH_3 partitioning into NH_4^+ to neutralize the system in this region. SO_4^{2-} decreases over CONUS whereas NH_4^+ increases, driving more HNO_3 and HCl partitioning into NO_3^- and Cl^- to neutralize NH_4^+. Therefore, the concentrations of $PM_{2.5}$ and PM_{10} increase over CONUS. The overprediction of NH_4^+ over Europe and CONUS is mainly due to additional anions (NO_3^- and Cl^-) in the system, leading to perturbations in the thermodynamic equilibrium. Similar to Figure 2.9a, J and PM_{num} increase near the surface, resulting in an increase in AOD and cloud variable predictions such as column CCN5, CDNC, and COT (see Figure 2.10b). As shown in Figure 2.10b, SWD decreases by 3.2 W m^{-2} in global mean, which is due to the increased cloud predictions (e.g., column CCN5, CDNC, and COT). Due to aerosol direct and indirect effects, SWCF increases by 2.6 W m^{-2} in global mean. Compared with 5-year annual average (ANU), the absolute change of most radiative variables are smaller in JJA. The absolute changes of PM_{10}

are larger in ANU than in JJA, which is mainly due to the dust events during other months (e.g., March-May over East Asia).

2.6.3 Global Burden Analysis

Table 2.8 shows the simulated global burdens of major gas and aerosol species for 2001-2005. The global burdens of most gaseous precursors of aerosol are higher in MAM_NEW_5YA than MAM_SIM_5Y (except for NH_3), due mainly to the incorporation of ISORROPIA II in MAM_NEW_5YA. The global burden of tropospheric O_3 is higher in MAM_NEW_5YA than MAM_SIM_5Y, which is due to higher mixing ratios of O_3 precursors (e.g., NO_2 and VOCs) that are simulated in MAM_NEW_5YA. The global burdens of most gas species are comparable with previous studies (Horowitz et al., 2006; Lamarque et al., 2005; Williams et al., 2009; Liu et al., 2012) with absolute differences of less than 20%. One exception is H_2SO_4, which is higher by a factor 5 in MAM_NEW_5YA than in MAM_SIM_5Y. The higher burden of H_2SO_4 in MAM_NEW_5YA is likely due to the less condensation of H_2SO_4 resulted from the use of a lower mass accommodation coefficient. SO_4^{2-} burden is higher by 8.3% in MAM_NEW_5YA than MAM_SIM_5Y, which is likely due to greater SO_2 oxidation in MAM_NEW_5YA. Higher SO_4^{2-} burden results from higher SO_2 burden. Higher SO_2 burden leads to more SO_2 to be oxidized to produce SO_4^{2-}, which overweighs the impacts from less H_2SO_4 condensation due to lower mass accommodation coefficient. More SO_4^{2-} result in more NH_4^+. The burdens of BC and POM are lower by 16.5% and 23.8%, respectively, in MAM_NEW_5YA than in MAM_SIM_5Y, which is likely due in part to greater dry deposition fluxes and in part to a slower primary carbon aging rate resulted from reduced condensation of gas species in

MAM_NEW_5YA. Condensation onto the primary carbon mode produces aging of the particles in this mode. A lower accommodation coefficient is used in MAM_NEW_5YA, which results in less condensation. Therefore, the fraction of aged particles has decreased. The global burdens of most aerosol species are in the range of previous studies. For example, global burdens of SO_4^{2-} and NH_4^+ from MAM_SIM_5Y and MAM_NEW_5YA are 23.4% and 17.0%, respectively, and 16.7% and 12.5%, respectively, lower than Liu et al. (2012), which is likely because MAM_SIM_5Y contains no SO_4^{2-} emissions but Liu et al. (2012) included additional SO_4^{2-} emissions of 1.66 Tg S yr^{-1}. Higher SO_4^{2-} emission leads to more SO_4^{2-} concentrations thus more NH_4^+ in Liu et al. (2012). Compared with Horowitz et al. (2006), global burdens of BC and OC from MAM_NEW_5YA are lower by 72.9% and 52.3%, respectively. Compared with Liu et al. (2012), MAM_NEW_5YA gives comparable BC and POM burdens but much lower SOA (by a factor of 3.0). Compared with Textor et al. (2006), POM burden is a factor of 3.5 lower in MAM_NEW_5YA. The lower BC, OC, POM, and SOA burdens are likely due to the uncertainties in the BC and OC emissions used as well as differences in the model treatments for SOA formation and POM aging.

2.7 Summary

In this section, a new gas-phase chemistry mechanism and several advanced inorganic aerosol treatments have been incorporated into CESM/CAM5.1-MAM7. These include (1) the CB05_GE gas-phase chemical mechanism coupled with MAM7; (2) the condensation and aqueous-phase chemistry involving HNO_3/ NO_3^- and HCl/ Cl^-; (3) an ion-mediated nucleation (IMN) parameterization for the new particle formation from ions, (4) an inorganic thermodynamic module, ISORROPIA II, that explicitly simulates thermodynamics of SO_4^{2-},

NH_4^+, NO_3^-, Cl^-, and Na^+ as well as the impact of crustal species, such as Ca^{2+}, K^+, and Mg^{2+}, on aerosol thermodynamics. CB05_GE with new and modified inorganic aerosol treatments in MAM7 simulates 139 species with 273 chemical reactions, which is more accurate than simple gas chemistry coupled with default MAM7. Seven 1-yr simulations for 2001 and three 5-year simulations for 2001-2005 with different model configurations are performed to evaluate the capabilities of the original and improved CESM/CAM5 and the mechanisms underlying differences among model predictions.

Comparing to the simple gas-phase chemistry, the 2001 simulation with CB05_GE can predict many more gaseous species, and give improved performance for predictions of organic carbon and $PM_{2.5}$ over CONUS, NH_3 and SO_4^{2-} over Europe, SO_2 and PM_{10} over East Asia, and cloud properties such as CF, CDNC, and SWCF on the global scale. MAM_CON simulates NO_3^- and Cl^-, which are important inorganic aerosols. With species-dependent accommodation coefficients for gas condensation, more H_2SO_4 can participate in homogeneous nucleation, resulting in the improvement of predictions of $PM_{2.5}$, PM_{10}, J, CDNC, and SWCF. IMN can increase the predictions of J and PM_{num} in the upper atmosphere and thus improve the predictions of AOD, CCN, and cloud properties, and SWCF over globe, $PM_{2.5}$ over CONUS and Europe, PM_{10} over Europe and East Asia, and PM composition over Europe. The 2001 simulation with ISORROPIA II can improve the predictions of major gas and aerosol species significantly, including HNO_3, NH_4^+, NO_3^-, Cl^-, BC, OC, TC, and $PM_{2.5}$ over CONUS, SO_2, NH_3, NO_2, SO_4^{2-}, NH_4^+, NO_3^-, and Cl^- over Europe, and CO and SO_2 over East Asia. Such improvements lead to improved predictions of SWD, SWCF, and CCN5 over globe. The 2001 simulation with the new and modified

inorganic aerosol treatments appreciably improve the predictions of OLR, CF, COT, CWP, PWV, CCN, CDNC, SWCF, J on the global scale, and HNO_3 (CONUS and Europe), NH_4^+ (CONUS), $PM_{2.5}$ (CONUS and Europe), and PM_{10} (Europe and East Asia). The 2001 sensitivity simulation with adjusted emissions further improves model predictions of CO and SO_2 over East Asia, SO_2, HNO_3, NO_3^-, Cl^-, BC, OC, and TC over CONUS, SO_2, NH_3, NH_4^+, HNO_3, NO_3^-, and Cl^- over Europe, and column CO and SWD over globe. The change of emissions can affect primary gaseous precursors directly, and secondary gaseous species indirectly through gas-phase chemistry. Meanwhile, secondary aerosols can be affected by gaseous precursors, and therefore have impacts on cloud properties as well as direct and indirect effects on radiation. Reducing the uncertainty of emissions can thus help reduce the model biases significantly.

The comparison of the 5-year simulations with prescribed SST shows that MAM_NEW_5YA with CB05_GE can appreciably improve the predictions of AOD, COT, CWP, CCN5, CDNC, SWD, LWD, OLR, and SWCF on global scale and OC, TC, and $PM_{2.5}$ over CONUS, PM_{10} over East Asia, and SO_2, $PM_{2.5}$, and PM_{10} over Europe. The performance is overall similar for all radiative variables and most chemical species between MAM_NEW_5YA with prescribed SST and MAM_NEW_5YB in a fully-coupled mode.

In addition to uncertainties in emissions, additional uncertainties exist in the model treatments. For example, the large biases in the predictions of O_3 over Europe and East Asia are mainly due to insufficient NO_x titration resulting from the uncertainties in the NO_x emissions. The large biases in PM_{10} over East Asia and Europe may be mainly due to the inaccurate predictions of dust. The large bias in Cl^- over Europe may be due to the inaccurate

predictions of HCl and coarse Cl^-, resulted from the irreversible condensation of HCl over coarse mode particles, and the uncertainty in the mass accommodation coefficient of HCl used. A reversible condensation treatment should be used for volatile species in the future, which can more accurately simulate the gas/particle partitioning of those volatile species over coarse mode particles. Assumptions associated with equilibrium partitioning for fine particles such as metastable conditions may be responsible for biases over desert/arid regions under low RH conditions. In the default and modified nucleation treatments, it only considers H_2SO_4, NH_3, H_2O, and ions involved in the new particle formation. Missing species (e.g., organics, iodine compounds, and DMS) may also contribute to the new particle formation. Uncertainties in treating organic gas-aerosol partitioning may contribute to the inaccurate predictions of SOA, OC, TC, and PM. The large biases in CDNC, COT, and CWP indicate the uncertainties in cloud microphysics schemes and aerosol-cloud interaction parameterizations, which also limit the ability of climate and Earth system models to quantify aerosol indirect effects (Stephens, 2005; Gettelman et al., 2008). In addition to uncertainties in the model treatments, uncertainties in the model simulation settings such as the use of a coarse grid resolution and a large model time step of 1800 seconds for solving the chemical system in this work may contribute to the model biases. The representations of some of the aforementioned uncertain processes in CESM/CAM5.1 are being further improved by the authors' group. Decadal simulations using improved CESM/CAM5.1 will be conducted in the future to study the interactions among atmospheric chemistry, aerosol, and climate change and reduce associated uncertainties.

Table 2.1. Simulation design and purposes

Index Run	Model Configuration	Purpose
MAM_SIM	Simple gas-phase chemistry coupled with default MAM7	A baseline run for the 1st set of simulations (see text)
MAM_CB05_GE	CB05_GE coupled with default MAM7	Differences of MAM_SIM and MAM_CB05_GE indicate the impacts of gas-phase chemical mechanisms
MAM_CON	Same as MAM_CB05_GE, but with explicit treatments for NO_3^-, Cl^-, and Na^+; HNO_3 and HCl condensation and aqueous-phase chemistry; species-dependent accommodation coefficients	A baseline run for the 2nd set of simulations; differences of MAM_SIM and MAM_CB05_GE indicate the impact of modified condensation and aqueous-phase chemistry treatments
MAM_CON/IMN	Same as MAM7_CON, but combine IMN with modified default nucleation parameterizations with a prefactor of 1.0×10^{-8}	Differences of MAM_CON and MAM_CON/IMN indicate the impacts of IMN and the lower prefactor for WP09
MAM_CON/ISO	Same as MAM7_CON, but with ISORROPIA II for aerosol thermodynamics under metastable conditions	Differences between MAM_CON and MAM_IMN/ISO indicate the impacts of explicit aerosol thermodynamics
MAM_NEWA	Same as MAM7_CON, but with all modified and new treatments and using a prefactor of 1.0×10^{-9} for default nucleation parameterization	Differences between MAM_CB05_GE and MAM_NEWA indicate the impacts of all new and modified treatments for inorganic aerosols
MAM_NEWB	Same as MAM_NEWA, but with ISORROPIA II under stable condition	Differences between MAM_NEWA and MAM_NEWB indicate the impacts of thermodynamic conditions on gas-aerosol partitioning
MAM_NEW/EMIS	Same as MAM7_NEW, but with adjusted emissions of SO_2, NH_3, BC, POM, and CO over CONUS, Europe, and East Asia	Differences between MAM_NEWA and MAM_NEW/EMIS indicate the impact of emissions
MAM_SIM_5Y	Same as MAM_SIM, but with prescribed SST for 2001-2005	A baseline run for 4th set of simulations
MAM_NEW_5YA	Same as MAM_NEW/EMIS, but with prescribed SST for 2001-2005	Differences between MAM_SIM_5Y and MAM_NEW_5YA indicate the indicate the impacts of all new and modified treatments for inorganic aerosols
MAM_NEW_5YB	Same as MAM_NEW/EMIS, but with fully-coupled model for 2001-2005	Difference between MAM_NEW_5YB and MAM_NEW_5YA indicate the impacts of processes from component models in the fully-coupled Earth system

Table 2.2. Datasets for model evaluation

Species/Variables	Dataset
Downwelling longwave radiation (LWD)	BSRN
Downwelling shortwave radiation (SWD)	BSRN
Outgoing longwave radiation (OLR)	NOAA/CDC
Cloud fraction (CF), Cloud optical thickness (COT) Cloud water path (CWP), Precipitating water vapor (PWV), Aerosol optical depth (AOD), Column cloud condensation nuclei (ocean) at S = 0.5% (CCN5)	MODIS
Cloud droplet number concentration (CDNC)	BE07
Shortwave cloud radiative forcing (SWCF)	CERES
Carbon monoxide (CO)	Europe: EMEP East Asia: NIES of Japan, TAQMN
Ozone (O_3)	CONUS: CASTNET Europe: Airbase, BDQA, EMEP East Asia: TAQMN
Sulfur dioxide (SO_2)	CONUS: CASTNET Europe: Airbase, BDQA, EMEP East Asia: MEP of China, NIES of Japan, TAQMN
Nitric acid (HNO_3)	CONUS: CASTNET Europe: EMEP
Ammonia (NH_3)	Europe: Airbase, EMEP
Nitrogen dioxide (NO_2)	Europe: Airbase, BDQA, EMEP East Asia: NIES of Japan, TAQMN
Sulfate (SO_4^{2-})	CONUS: CASTNET, IMPROVE, STN Europe: Airbase, EMEP
Ammonium (NH_4^+)	CONUS: CASTNET, IMPROVE, STN Europe: Airbase, EMEP
Nitrate (NO_3^-)	CONUS: CASTNET, IMPROVE, STN Europe: Airbase, EMEP
Chloride (Cl^-)	CONUS: IMPROVE Europe: Airbase, EMEP
Organic carbon (OC), Black carbon (BC), Total carbon (TC)	CONUS: IMPROVE, STN
Particulate matter with diameter less than 2.5 μm ($PM_{2.5}$)	CONUS: IMPROVE, STN Europe: BDQA, EMEP
Particulate matter with diameter less than 10 μm (PM_{10})	Europe: Airbase, BDQA, EMEP East Asia: MEP of China, NIES of Japan, TAQMN
Column CO	Globe: MOPITT
Column NO_2	Globe: GOME
Tropospheric ozone residual (TOR)	Globe: TOMS/SBUV
New particle formation rate (J)	Globe: Kulmala et al. (2004); Yu et al. (2008)

BSRN: Baseline Surface Radiation Network; NOAA/CDC: National Oceanic and Atmospheric Administration Climate Diagnostics Center; MODIS: Moderate Resolution Imaging Spectroradiometer; BE07: Bennartz, 2007; CERES: Clouds and Earth's Radiant Energy System; TOMS/SBUV: the Total Ozone Mapping Spectrometer/the Solar Backscatter UltraViolet; MOPITT: the Measurements Of Pollution In The Troposphere; GOME: Global Ozone Monitoring Experiment; CASTNET: Clean Air Status and Trends Network; IMPROVE: Interagency Monitoring of Protected Visual Environments; STN: Speciation Trends Network; EMEP: European Monitoring and Evaluation Program; BDQA: Base de Données sur la Qualité de l'Air; AirBase: European air quality database; MEP of China: Ministry of Environmental Protection of China; TAQMN: Taiwan Air Quality Monitoring Network; NIES of Japan: National Institute for Environmental Studies of Japan.

Table 2.3a. Mean bias (MB) and normalized mean bias (NMB, in %) of radiative/cloud predictions for the 2001 simulations

Species/Variables	Dataset	Obs.	Simulations						
			MAM_ SIM	**MAM_ CB05_GE**	**MAM_ CON**	**MAM_ CON/IMN**	**MAM_ CON/ISO**	**MAM_ NEWA**	**MAM_ NEW/EMIS**
LWD (W m^{-2})[a]	BSRN	312.5	309.2/ -3.4/-1.1c	309.6/ -2.9/-0.9	308.4/ -4.2/-1.3	308.0/ -4.5/-1.4	308.3/ -4.2/-1.3	308.7/ -3.8/-1.2	309.1/ -3.5/-1.1
SWD (W m^{-2})[b]	BSRN	181.2	179.2/ -2.0/-1.1	177.0/ -4.2/-2.3	169.4/ -11.8/-6.5	170.2/ -11.0/-6.1	177.3/ -3.9/-2.2	174.5/ -6.8/-3.7	177.0/ -4.2/-2.3
OLR (W m^{-2})	NOAA-CDC	214.4	223.2/ 8.8/4.1	222.4/ 8.1/3.8	219.3/ 4.9/2.3	219.3/ 4.9/2.3	220.7/ 6.2/2.9	221.2/ 6.9/3.2	221.2/ 6.9/3.2
SWCF (W m^{-2})	CERES	-41.0	-37.8/ -3.2/-7.9	-38.4/ -2.7/-6.5	-43.2/ 2.2/5.3	-43.3/ 2.3/5.6	-40.4/ -0.7/-1.6	-40.7/ -0.4/-0.9	-40.5/ -0.6/-1.4
CF (%)	MODIS	66.9	65.6/ -1.4/-2.0	65.9/ -1.0/-1.5	67.5/ 0.5/0.8	67.6/ 0.7/1.0	66.4/ -0.5/-0.8	66.5/ -0.4/-0.6	66.6/ -0.3/-0.5
COT	MODIS	17.1	6.9/ -10.2/-59.5	7.1/ -10.1/-58.8	8.7/ -8.4/-49.2	8.8/ -8.3/-48.4	7.7/ -9.4/-55.1	7.7/ -9.4/-54.9	7.7/ -9.4/-55.2
CWP (g m^{-2})	MODIS	148.1	33.0/ -115.1/ -77.7	33.5/ -114.7/ -77.4	42.3/ -105.8/ -71.4	42.7/ -105.4/ -71.2	36.4/ -111.7/ -75.4	36.5/ -111.7/ -75.4	36.2/ -111.9/ -75.5
PWV (cm)	MODIS	1.9	1.9/ -2.5×10^{-2}/ -1.3	1.9/ -1.8×10^{-2}/ -0.9	1.9/ -3.3×10^{-2}/ -1.7	1.9/ -3.9×10^{-2}/ -2.0	1.9/ -1.8×10^{-2}/ -0.9	1.9/ -1.4×10^{-2}/ -0.7	1.9/ -1.2×10^{-2}/ -0.6
AOD	MODIS	1.5×10^{-1}	9.8×10^{-2}/ -5.5×10^{-2}/ -36.1	1.0×10^{-1}/ -5.2×10^{-2}/ -33.9	1.2×10^{-1}/ -3.0×10^{-2}/ -19.8	1.3×10^{-1}/ -2.6×10^{-2}/ -17.1	1.0×10^{-1}/ -5.3×10^{-2}/ -34.4	1.0×10^{-1}/ -5.0×10^{-2}/ -32.9	1.0×10^{-1}/ -5.2×10^{-2}/ -34.0
Column CCN5 (ocean) (cm^{-2})	MODIS	2.4×10^{8}	5.8×10^{7}/ -1.9×10^{8}/ -76.4	5.2×10^{7}/ -1.9×10^{8}/ -78.6	1.8×10^{8}/ -6.7×10^{7}/ -27.5	2.0×10^{8}/ -4.6×10^{7}/ -18.8	9.1×10^{7}/ -1.5×10^{8}/ -62.7	8.5×10^{7}/ -1.6×10^{8}/ -65.3	8.2×10^{7}/ -1.6×10^{8}/ -66.6
CDNC (cm^{-3})	BE07	113.1	45.5/ -67.7/-59.9	46.7/ -66.5/-58.8	89.7/ -23.4/-20.7	93.1/ -20.0/-17.7	65.0/ -48.1/-42.5	66.7/ -46.4/-41.0	67.0/ -46.1/-40.8

[a]The pair of observation and simulation is removed in the statistical calculation if the observed LWD value is lower than 50 W m^{-2} or higher than 700 W m^{-2} (http://www.pangaea.de).

[b]The pair of observation and simulation is removed in the statistical calculation if the observed SWD value is lower than -10 or higher than 3000 W m^{-2} (http://www.pangaea.de).

[c]The values of modeled results (Sim), MBs, and NMBs are expressed as Sim/MB/NMB.

Table 2.3b. Mean bias (MB) and normalized mean bias (NMB, in %) of chemical predictions for the 2001 simulations

Species/ variables[a]	Domain	Obs.	Simulations							
			MAM_SIM	MAM_CB05_GE	MAM_CON	MAM_CON/IMN	MAM_CON/ISO	MAM_NEWA	MAM_NEWB	MAM_NEW/ EMIS
CO	Europe	123.0	-	112.4/-10.6/-8.6	115.0/-8.0/-6.5	107.9/-15.1/-12.3	114.0-9.0/-7.3	118.8/-4.2/-3.4	113.6/-9.4/-7.6	137.9/14.9/12.1
	East Asia	0.6	-	0.1/-0.5/-82.1	0.1/-0.5/-82.0	0.1/-0.5/-81.8	0.1/-0.5/-81.8	0.1/-0.5/-82.0	0.1/-0.5/-81.7	0.1/-0.5/-78.7
SO_2	CONUS	3.9	14.2/10.3/264.8[b]	14.4/10.5/270.1	15.6/11.7/301.2	15.1/11.2/286.1	15.4/11.5/295.8	15.3/11.4/291.8	15.3/11.4/293.0	9.8/5.9/152.2
	Europe	6.8	13.4/6.6/97.5	13.8/7.0/103.2	15.2/8.4/123.0	13.6/6.8/100.3	14.6/7.8/114.7	15.7/8.9/130.7	14.5/7.7/114.0	6.8/0.0/0.3
	East Asia	12.5	4.6/-7.9/-63.0	4.8/-7.7/-61.3	4.8/-7.7/-61.4	4.8/-7.7/-61.8	4.9-7.6/-61.0	4.8/-7.7/-61.2	4.8/-7.7/-61.2	5.8/-6.7/-53.4
NH_3	Europe	9.4	1.7/-7.7/-82.0	1.8/-7.6/-80.8	1.2/-8.2/-86.8	1.1/-8.3/-87.8	1.4/-8.0/-84.7	1.5/-7.9/-84.3	1.1/-8.3/-84.0	2.1/-7.3/-77.5
NO_2	Europe	20.2	-	4.6/-15.6/-77.0	5.2/-15.0/-74.1	4.7/-15.5/-76.5	5.0/-15.2/-75.2	5.2/-15.0/-74.1	4.9/-15.3/-75.7	4.9/-15.3/-75.9
	East Asia	14.0		1.6/-12.4/-88.4/	1.7/-12.3/-88.0	1.7/-12.3/-88.2	1.6/-12.4/-88.4	1.7/-12.3/-88.3	1.6/-12.4/-88.5	1.7/-12.3/-88.2
O_3	CONUS	34.6	-	44.6/10.0/28.9	42.6/8.0/23.0	42.5/7.9/22.7	44.4/9.8/28.4	44.1/9.5/27.4	43.7/9.1/26.4	44.4/9.8/28.1
	Europe	53.5	-	90.2/36.7/68.6	84.4/30.9/57.7	84.5/31.0/58.0	87.6/34.1/63.7	87.0/33.5/62.7	87.7/34.2/63.9	88.4/34.9/65.2
	East Asia	26.4		42.8/16.4/62.2	42.7/16.3/61.7	40.7/14.3/54.3	42.6/16.2/65.9	42.1/15.7/59.6	43.0/16.6/63.0	42.5/16.1/61.2
HNO_3	CONUS	1.5	-	2.5/1.0/68.1	0.6/-0.9/-60.2	0.6/-0.9/-59.7	1.7/0.2/15.8	1.8/0.3/17.7	1.8/0.3/19.0	1.6/0.1/4.1
	Europe	0.5	-	1.8/1.3/268.5	0.3/-0.2/-34.1	0.3/-0.2/-35.8	0.9/0.4/86.1	0.9/0.4/83.6	1.0/0.5/103.8	0.9/0.4/73.8
SO_4^{2-}	CONUS	2.6	2.5/-0.1/-5.1	2.4/-0.2/-7.2	$2.6/4.4\times10^{-2}$/1.7	$2.6/4.2\times10^{-2}$/1.6	2.4/-0.2/-7.9	2.4/-0.2/-6.3	2.5/-0.1/-5.5	1.9/-0.7/-28.4
	Europe	2.2	3.0/0.8/36.5	2.9/0.7/33.1	3.1/0.9/40.3	3.0/0.8/35.8	2.9/0.7/32.6	3.1/0.9/39.4	3.0/0.8/36.8	2.0/-0.2/-7.2
NH_4^+	CONUS	1.4	1.0/-0.4/-32.1	0.8/-0.6/-39.6	1.7/0.3/20.0	1.7/0.3/19.7	1.3/-0.1/-6.4	1.3/-0.1/-6.5	1.3/-0.1/-4.3	1.2/-0.2/-13.1
	Europe	1.2	1.1/-0.1/-9.1	1.0/-0.2/18.3	2.2/1.0/85.0	2.0/0.8/65.7	1.8/0.6/49.4	1.9/0.7/54.8	1.7/0.5/37.7	1.6/0.4/32.5
NO_3^-	CONUS	1.0	-	-	3.0/2.0/198.2	2.9/1.9/192.7	$1.0/-4.8\times10^{-2}$/-4.8	0.9/-0.1/-9.6	$1.0/-2.2\times10^{-2}$/-2.1	$1.0/4.0\times10^{-3}$/0.4
	Europe	2.0	-	-	3.4/1.4/67.8	3.0/1.0/49.4	1.9/-0.1/-4.3	$2.0/-4.0\times10^{-2}$/-2.0	1.8/-0.2/-12.5	2.1/0.1/5.2
Cl^-	CONUS	0.1	-	-	0.5/0.4/359.9	0.5/0.4/373.1	$0.1/-1.5\times10^{-2}$/-14.5	$0.1/-1.8\times10^{-2}$/-17.5	$0.1/-1.5\times10^{-2}$/-12.1	$0.1/-2.8\times10^{-3}$/-2.8
	Europe	0.7	-	-	1.4/0.7/102.8	1.3/0.6/89.9	$0.7/2.1\times10^{-3}$/0.3	$0.7/1.4\times10^{-2}$/2.0	0.6/-0.1/-14.5	-4.7×10^{-2}/-6.7
BC	CONUS	0.6	0.3/-0.3/-54.6	0.3/-0.3/-55.8	0.3/-0.3/-54.7	0.3/-0.3/-54.6	0.3/-0.3/-53.8	0.3/-0.3/-54.3	0.3/-0.3/-54.9	0.4/-0.2/-29.4
OC	CONUS	1.1	0.8/-0.3/-22.7	1.0/-0.1/-12.1	1.0/-0.1/-11.4	1.0/-0.1/-11.9	1.0/-0.1/-8.6	1.0/-0.1/-9.1	1.0/-0.1/-11.3	$1.0/5.6\times10^{-3}$/0.5
TC	CONUS	2.5	1.3/-1.2/-47.9	1.4/-1.1/-43.1	1.4/-1.1/-42.2	1.4/-1.1/-42.5	1.4/-1.0/-40.9	1.5/-1.0/-41.1	1.4/-1.1/-42.5	1.6/-0.9/-35.0
$PM_{2.5}$	CONUS	7.9	4.9/-3.0/-37.6	5.0/-2.9/-36.8	9.5/1.6/20.1	6.6/1.3/16.7	7.8/-0.1/-1.7	6.9/-1.0/-13.2	7.2/-0.7/-8.8	6.8/-1.1/-13.5
	Europe	14.5	8.4/-6.1/-41.8	7.9/-6.6/-45.3	13.7/-0.8/-5.5	14.4/-0.1/-0.9	11.0/-3.5/-24.4	11.9/-2.6/-17.7	10.9/-3.6/-24.9	10.6/-3.9/-27.2
PM_{10}	Europe	25.7	17.5/-8.2/-31.8	16.5/-9.2/-35.8	22.5/-3.2/-12.3	23.0/-2.7/-10.5	20.1/-4.8/-18.5	21.4/-4.3/-16.6	20.7/-5.0/-19.4	20.9/-4.8/-18.8
	East Asia	118.5	38.5/-80.0/-67.5	44.9/-73.6/-62.1	55.9/-62.6/-52.8	58.8/-57.7/-48.7	48.5/-70.0/-59.1	65.5/-53.0/-44.7	55.6/-62.9/-53.1	48.2/-70.3/-59.3
Col.CO	Globe	1.3×10^{18}	-	1.2×10^{18}/ -7.4×10^{16}/-5.7	1.2×10^{18}/ -5.7×10^{16}/-4.4	1.2×10^{18}/ -6.3×10^{16}/-4.8	1.2×10^{18}/ -6.4×1016/-4.9	1.2×10^{18}/ -6.3×1016/-4.8	1.2×10^{18}/ -5.6×1016/-4.3	1.2×10^{18}/ 2.3×1016/1.8
Col.NO_2	Globe	4.7×10^{14}	-	6.7×1014/ 1.9×1014/40.5	6.2×1014/ 1.4×1014/30.4	6.2×1014/ 1.4×1014/30.0	6.5×1014/ 1.8×10^{14}/37.5	6.5×1014/ 1.8×10^{14}/37.2	6.5×1014/ 1.8×10^{14}/37.9	6.5×1014/ 1.8×10^{14}/37.3
TOR	Globe	30.3	29.8/-0.5/1.6	29.2/-1.1/-3.7	27.6/-2.7/-9.0	27.4/-2.9/-9.6	28.8/-1.5/-4.9	28.7/-1.6/-5.2	28.6/-1.5/-5.0	28.6-1.5/-4.9
J	Globe	0.6	0.003/-0.6/-99.6	0.1/-0.5/-99.5	0.5/-0.1/-12.8	0.3/-0.3/-49.6	0.8/0.2/36.1	0.3/-0.3/-53.1	0.3/-0.3/-51.7	0.3/-0.3/-62.0

[a]The units are CO, ppb (over Europe) and ppm (over East Asia); SO_2, ppb (over East Asia) and μg m^{-3} (over CONUS and Europe); O_3, ppb (over CONUS) and μg m^{-3} (over Europe); column CO and NO_2, molecules cm^{-2}; TOR, DU; J, $cm^{-3}s^{-1}$. All other concentrations are in μg m^{-3}. [b]The values of modeled results (Sim), MBs, and NMBs are expressed as Sim/MB/NMB.

Table 2.4. Probability of differences in radiative/cloud predictions between paired-simulation

Species/Variables	Paired-simulation					
	MAM_SIM/ MAM_CB05_GE	**MAM_CB05_GE/ MAM_CON**	**MAM_CON/ MAM_CON/IMN**	**MAM_CON/ MAM_CON/ISO**	**MAM_SIM/ MAM_NEWA**	**MAM_NEWA/ MAM_NEW/EMIS**
LWD	0.7	0.6	0.2	0.8	0.5	0.7
SWD	8.1×10^{-3}	0	0.03	5.1×10^{-12}	1.3×10^{-12}	0.3
OLR	4×10^{-4}	0	0.9	1.6×10^{-10}	4.6×10^{-13}	0.8
SWCF	2×10^{-4}	1.2×10^{-12}	0.4	0	5.7×10^{-12}	0.2
CF	8.7×10^{-5}	1.2×10^{-12}	0.05	5.3×10^{-12}	0	0.4
COT	2.3×10^{-3}	0	3.9×10^{-3}	1.5×10^{-12}	2.3×10^{-12}	0.3
CWP	3.7×10^{-3}	0	0.06	5.4×10^{-12}	6.8×10^{-13}	0.2
PWV	0.4	0.08	0.5	0.1	0.2	0.9
AOD	7.9×10^{-5}	0	3.1×10^{-6}	3.8×10^{-13}	1.8×10^{-11}	0.03
Column CCN5 (ocean)	5.3×10^{-12}	0	3.3×10^{-12}	0	0	0
CDNC	2.7×10^{-10}	2.6×10^{-12}	9.8×10^{-9}	0	6.4×10^{-13}	0.5

*Probability value is expressed in fraction, with a minimum value of 0 and a maximum value of 1. A value less than 0.05 (i.e., 5%) indicates that the differences between the simulation pairs are statistically significant at the 95% confidence level.

Table 2.5. The observed values and the mean bias (MB) and normalized mean bias (NMB, in %) of predictions of O_3, NO_2, and HNO_3 mixing ratios over Europe in MAM_NEWA

	Network		Obs ($\mu g\ m^{-3}$)	Sim ($\mu g\ m^{-3}$)	MB/NMB
Winter	Airbase	O_3	37.7	75.2	37.5/99.6[a]
		NO_2	26.0	7.6	-18.4/-70.9
	BDQA	O_3	31.0	74.2	43.2/139.2
		NO_2	30.6	5.6	-25.0/-81.9
	EMEP	O_3	50.7	75.7	25.0/49.3
		NO_2	9.0	8.3	-0.7/-7.8
		HNO_3	0.5	0.5	-4.9×10^{-3}/1.0
Spring	Airbase	O_3	63.1	100.8	37.7/59.7
		NO_2	20.0	4.6	-15.4/-77.1
	BDQA	O_3	59.6	98.9	39.3/65.9
		NO_2	23.6	3.1	-20.5/-87.0
	EMEP	O_3	75.0	101.9	26.9/35.9
		NO_2	5.9	4.9	-1.0/-17.2
		HNO_3	0.4	0.9	0.5/144.5
Summer	Airbase	O_3	64.9	93.5	28.6/44.0
		NO_2	16.2	4.4	-11.8/-72.8
	BDQA	O_3	64.5	94.5	30.0/46.5
		NO_2	18.7	3.6	-15.1/-80.9
	EMEP	O_3	72.2	91.2	19.0/26.3
		NO_2	4.7	4.4	-0.3/-6.2
		HNO_3	0.5	1.3	0.8/169.6
Autumn	Airbase	O_3	40.5	79.5	39.0/96.4
		NO_2	21.7	5.3	-16.4/-75.6
	BDQA	O_3	35.7	80.9	45.2/126.5
		NO_2	24.8	3.7	-21.1/-85.2
	EMEP	O_3	51.7	78.2	26.5/51.2
		NO_2	6.6	5.2	-1.4/-21.1
		HNO_3	0.6	0.9	0.3/45.0

[a]The values of MBs and NMBs are expressed as MB/NMB.

Table 2.6a. Statistical performance of radiative/cloud predictions (average of the 2001-2005 simulations)

Species/Variables	Dataset	Obs.	Simulations		
			MAM_SIM_5Y	MAM_NEW_5YA	MAM_NEW_5YB
LWD (W m^{-2})[a]	CERES	307.6	302.9/-4.7/-1.5/2.9/11.6[c]	303.9/-3.6/-1.1/2.8/11.3	304.4/-3.1/-1.0/2.9/11.3
SWD (W m^{-2})[b]	CERES	163.9	169.9/5.9/3.6/7.0/14.1	166.5/2.5/1.5/6.5/13.8	167.0/3.1/1.9/6.7/13.7
OLR (W m^{-2})	NOAA-CDC	215.9	222.5/6.6/3.1/3.5/8.9	220.7/4.8/2.2/3.4/9.1	221.4/5.5/2.6/3.5/9.0
SWCF (W m^{-2})	CERES	-41.0	-38.8/2.2/-5.4/-21.5/12.0	-41.5/-0.5/1.2/-21.4/12.5	-40.8/0.2/-0.5/-22.2/12.4
CF (%)	MODIS	67.1	66.6/-0.6/-0.8/15.2/13.3	67.3/0.2/0.3/14.7/13.0	66.6/-0.6/-0.9/15.5/13.7
COT	MODIS	17.3	7.1/-10.3/-59.3/70.2/15.1	7.9/-9.4/-54.5/65.7/14.6	7.8/-9.6/-55.2/65.6/14.5
CWP (g m^{-2})	MODIS	86.0	38.2/-47.8/-55.5/55.7/52.9	43.2/-42.8/-49.8/50.0/49.2	43.4/-42.6/-49.5/49.7/49.2
PWV (cm)	MODIS	1.93	1.96/0.03/1.5/11.6/0.3	1.99/0.06/2.9/10.9/0.3	1.97/0.04/1.8/13.8/0.3
AOD	MODIS	0.2	0.1/-0.07/-44.1/54.5/0.1	0.1/-0.06/-39.2/51.3/0.1	0.1/-0.06/-36.3/49.5/0.1
Column CCN5 (ocean) (cm^{-2})	MODIS	2.5×10^8	5.3×10^7/-1.9×10^8/ -78.6/78.6/5.7×10^8	8.6×10^7/1.6×10^8/ -65.2/65.2/5.5×10^8	8.6×10^7/1.6×10^8/ -65.3/65.3/5.5×10^8
CDNC (cm^{-3})	BE07	112.6	44.2/-68.3/-60.7/61.6/84.3	69.2/-43.4/-38.6/44.2/66.8	68.8/-43.8/-38.9/45.5/67.9

[a] The pair of observation and simulation is removed in the statistical calculation if the observed LWD value is lower than 50 W m^{-2} or higher than 700 W m^{-2} (http://www.pangaea.de).

[b]The pair of observation and simulation is removed in the statistical calculation if the observed SWD value is lower than -10 or higher than 3000 W m^{-2} (http://www.pangaea.de).

[c]The values are expressed as Sim/MB/NMB/NME/RMSE. Sim: simulated values; MB: mean bias; NMB: normalized mean bias (%); NME: normalized mean error (%); RMSE: root mean squared error.

Table 2.6b. Statistical performance of chemical predictions (average of the 2001-2005 simulations)

Species/ variables[a]	Domain	Obs.	Simulations		
			MAM_SIM_5Y	MAM_NEW_5YA	MAM_NEW_5YB
CO	East Asia	562.0	-	139.7/-422.3/-75.1/75.1/451.8[b]	137.0/-425.0/-75.6/75.6/454.0
SO_2	CONUS	3.4	9.6/6.2/183.9/184.6/9.9	10.1/6.7/198.8/199.1/10.6	10.3/6.9/203.1/203.5/10.9
	Europe	6.6	6.0/-0.6/-9.3/73.3/7.9	6.6/-0.06/-0.9/77.2/8.3	6.2/-0.4/-5.5/74.6/8.0
	East Asia	3.4	3.4/0.04/1.1/76.0/5.0	3.4/0.01/0.4/76.2/5.0	3.4/-0.05/-1.6/73.1/4.8
NH_3	Europe	6.3	3.0/-3.3/-52.0/81.0/25.3	2.4/-3.9/-61.3/79.7/25.3	2.4/-3.9/-62.0/79.3/25.3
NO_2	Europe	23.5	-	5.8/-17.7/-75.4/76.5/21.5	5.5/-18.0/-76.7/77.7/21.7
	East Asia	13.5	-	2.3/-11.2/-83.3/83.3/12.2	2.3/-11.2/-83.6/83.6/12.2
O_3	CONUS	35.1	-	43.9/8.8/25.1/27.3/11.3	44.1/9.0/25.7/27.7/11.6
	Europe	52.7	-	86.6/33.9/64.5/64.6/36.4	89.2/36.5/69.3/69.4/38.8
	East Asia	27.4	-	45.6/18.2/66.4/66.4/19.2	45.5/18.1/66.0/66.0/19.1
HNO_3	CONUS	1.4	-	1.6/0.2/16.3/39.5/0.7	1.6/0.2/12.1/38.2/0.7
	Europe	0.7	-	1.0/0.3/45.8/83.5/0.8	1.0/0.3/37.9/79.8/0.8
SO_4^{2-}	CONUS	2.6	2.3/-0.3/-13.4/26.9/1.0	2.3/-0.3/-13.1/23.0/0.8	2.3/-0.3/-12.8/24.2/0.9
	Europe	2.3	2.3/-0.04/-1.9/37.3/1.4	2.0/-0.3/-11.1/34.1/1.3	2.0/-0.3/-13.0/35.5/1.4
NH_4^+	CONUS	1.2	0.9/-0.3/-20.8/33.4/55.0	1.5/0.3/22.2/43.2/0.8	1.5/0.3/26.4/44.3/0.8
	Europe	1.0	0.8/-0.2/-16.8/36.9/0.5	1.6/0.6/62.8/68.7/0.9	1.5/0.5/53.8/60.3/0.8
NO_3^-	CONUS	1.1	-	1.6/0.5/41.3/85.4/1.4	1.6/0.5/49.8/90.2/1.5
	Europe	1.8	-	2.3/0.5/30.3/51.1/1.2	2.2/0.4/24.7/47.0/1.1
Cl^-	CONUS	0.1	-	$0.1/3.1\times10^{-3}$/2.7/105.8/0.4	$0.1/8.7\times10^{-3}$/7.8/110.1/0.4
	Europe	0.3	-	2.4/2.1/681.2/681.2/2.9	2.3/2.0/663.3/663.6/2.8
BC	CONUS	0.4	0.3/-0.1/-17.9/44.4/0.3	0.3/-0.1/-15.6/44.0/28.2	0.3/-0.1/-17.7/44.3/0.2
OC	CONUS	1.2	0.9/-0.3/-23.2/59.3/1.0	1.1/-0.1/-7.7/56.7/1.0	1.1/-0.1/-11.0/54.3/0.9
TC	CONUS	3.1	1.4/-1.7/-54.4/62.8/2.8	1.7/-1.4/-45.7/57.1/2.6	1.6/-1.5/-47.1/57.1/2.7
$PM_{2.5}$	CONUS	8.8	7.2/-1.6/-17.9/37.0/4.3	9.2/0.4/4.1/33.5/3.9	8.7/-0.1/-1.1/29.4/3.6
	Europe	14.6	6.7/-7.9/-53.9/54.6/10.6	9.7/-4.9/-33.8/37.6/8.6	10.0/-4.6/-31.7/36.1/8.4
PM_{10}	Europe	26.3	15.1/-11.2/-42.6/46.8/15.9	18.7/-7.6/-28.8/36.1/13.9	19.9/-6.4/-24.4/33.5/13.1
	East Asia	107.9	45.4/-62.5/-58.0/59.3/70.7	52.5/-57.4/-53.2/54.2/66.0	57.8/-50.1/-46.5/50.0/61.6
Col.CO	Globe	1.4×10^{18}	-	1.3×10^{18}/-1.4×10^{17}/ -10.2/16.5/3.1×10^{17}	1.2×10^{18}/-1.5×10^{17}/ -11.0/17.2/3.2×10^{17}
Col.NO_2	Globe	5.3×10^{14}	-	8.4×10^{14}/3.1×10^{14}/ 59.2/70.0/5.4×10^{14}	8.3×10^{14}/3.0×10^{14}/ 57.6/69.2/5.4×10^{14}
TOR	Globe	30.4	29.9/-0.5/1.6/16.3/6.1	30.5/0.1/0.4/15.0/5.8	29.9/-0.5/-1.7/16.4/6.1

[a]The units are CO, ppm (over East Asia); SO_2, ppb (over East Asia) and μg m^{-3} (over CONUS); O_3, ppb (over CONUS) and μg m^{-3} (over Europe); column CO and NO_2, molecules cm^{-2}; TOR, DU. All other concentrations are in μg m^{-3}.
[b]The values are expressed as Sim/MB/NMB/NME/RMSE. MB: mean bias; NMB: normalized mean bias (%); NME: normalized mean error (%); RMSE: root mean square error.

Table 2.7a. Statistical performance of radiative/cloud predictions during JJA, 2001-2005

Species/Variables	Dataset	Obs	Simulations		
			MAM_SIM_5Y	**MAM_NEW _5YA**	**MAM_NEW _5YB**
LWD (W m^{-2})	CERES	320.3	317.3/-3.0/-0.9/3.0/13.0[a]	318.0/-2.3/-0.7/3.0/12.8	318.1/-2.2/-0.7/2.9/12.6
SWD (W m^{-2})	CERES	192.4	197.9/5.5/2.9/9.7/25.1	194.1/1.7/0.9/9.5/24.3	196.2/3.8/2.0/9.5/23.6
OLR (W m^{-2})	NOAA-CDC	220.6	227.0/6.4/2.9/4.4/11.8	224.9/4.3/2.0/4.0/11.1	224.9/4.3/2.0/4.0/11.1
SWCF (W m^{-2})	CERES	-41.3	-40.1/1.2/-2.8/-25.9/16.4	-42.8/-1.5/3.6/-26.4/16.6	-41.2/0.1/-0.3/-26.3/16.2
CF (%)	MODIS	69.9	65.3/-4.6/-6.5/13.7/12.5	66.0/-3.9/-5.6/13.0/12.2	65.5/-4.4/-6.3/13.6/12.3
COT	MODIS	17.1	8.5/-8.6/-50.6/65.1/14.9	9.4/-7.7/-45.0/60.7/14.5	9.0/-8.1/-47.5/60.0/14.1
CWP (g m^{-2})	MODIS	87.9	41.7/-46.2/-52.6/53.3/54.5	47.2/-40.7/-46.3/47.4/50.7	46.6/-41.3/-47.0/47.8/51.4
PWV (cm)	MODIS	2.1	2.1/0.05/2.4/12.8/36.0	2.1/0.07/3.2/12.1/34.2	2.1/0.01/0.6/13.2/37.0
AOD	MODIS	0.2	0.2/-0.06/-34.1/54.5/0.2	0.2/-0.05/-29.0/51.3/0.2	0.2/-0.04/-25.0/48.7/0.2
Column CCN5 (ocean) (cm^{-2})	MODIS	2.3×10^{8}	6.1×10^{7}/-1.7×10^{8}/ -74.2/74.7/2.6×10^{8}	9.1×10^{7}/-1.4×10^{8}/ -59.8/61.9/2.3×10^{8}	9.1×10^{7}/-1.4×10^{8}/ -60.2/62.0/2.3×10^{8}
CDNC (cm^{-3})	BE07	117.4	48.5/-68.9/-58.8/61.1/87.7	69.5/-47.9/-40.8/49.7/76.2	67.7/-49.7/-42.3/50.8/77.1

[a] The values are expressed as Sim/MB/NMB/NME/RMSE, where Sim is modeled value; MB is mean bias; NMB is normalized mean bias (%); NME is normalized mean error (%); and RMSE is root mean square error.

Table 2.7b. Statistical performance of chemical predictions during JJA, 2001-2005

Variables[a]	Domain	Obs.	Simulations		
			MAM_SIM_5Y	MAM_NEW_5YA	MAM_NEW_5YB
CO	East Asia	535.4	-	119.4/-416.1/-77.7/77.7/441.1[b]	114.8/-420.6/-78.6/78.6/444.7
SO_2	CONUS	2.0	8.3/6.3/309.8/312.1/9.6	8.2/6.2/309.0/311.4/9.6	8.0/6.0/297.5/299.9/9.3
	Europe	5.3	6.0/0.7/12.4/85.2/7.1	6.0/0.7/13.3/87.3/7.3	6.3/1.0/19.2/90.1/7.5
	East Asia	3.7	2.3/-1.4/-37.2/57.6/2.5	3.2/-0.5/-12.6/59.2/3.5	3.2/-0.5/-14.9/58.0/3.6
NH_3	Europe	6.0	2.7/-3.2/-54.4/84.0/18.0	2.2/-3.8/-62.9/82.6/18.0	2.4/-3.5/-59.1/82.7/18.0
NO_2	Europe	18.5	-	4.2/-14.3/-77.4/78.2/17.8	4.4/-14.1/-76.4/77.3/17.6
	East Asia	13.2	-	2.1/-11.1/-84.2/84.2/12.1	2.1/-11.1-84.5/84.5/12.1
O_3	CONUS	39.4	-	47.4/8.0/20.2/23.9/11.7	46.9/7.5/19.2/22.9/11.2
	Europe	64.9	-	93.8/28.9/44.5/44.6/32.0	96.2/31.3/48.2/48.3/34.4
	East Asia	21.7	-	34.2/12.5/57.5/57.5/13.7	33.9/12.2/56.4/56.4/13.3
HNO_3	CONUS	1.6	-	1.8/0.2/10.5/40.9/0.9	1.6/0.04/2.5/38.7/0.8
	Europe	1.0		1.8/0.8/87.4/118.0/1.3	1.9/0.9/94.8/125.8/1.4
SO_4^{2-}	CONUS	3.6	3.2/-0.5/-12.4/22.1/1.1	3.2/-0.4/-10.3/19.9/1.0	3.1/-0.5/-12.7/19.1/0.9
	Europe	2.4	2.9/0.5/20.5/46.7/1.6	2.8/0.4/17.4/42.2/1.5	2.9/0.5/22.0/44.7/1.5
NH_4^+	CONUS	1.3	1.3/-0.02/-1.3/20.2/0.4	1.4/0.1/9.8/31.8/0.6	1.4/0.1/11.0/28.1/0.5
	Europe	0.8	1.0/0.2/30.3/46.8/0.6	1.6/0.8/95.0/99.7/1.1	1.6/0.8/96.0/100.6/1.1
NO_3^-	CONUS	0.5	-	0.7/0.2/37.8/84.5/0.6	0.8/0.3/57.1/97.9/0.7
	Europe	1.3	-	1.5/0.3/22.0/55.1/1.0	1.5/0.3/26.5/52.2/1.0
Cl^-	CONUS	0.1	-	$0.1/-4.0\times10^{-3}$/-5.3/98.5/0.2	$0.1/-4.0\times10^{-3}$/-5.4/101.2/0.2
	Europe	0.1		1.1/1.0/650.0/650.0/1.4	1.1/1.0/666.8/666.8/1.4
BC	CONUS	0.4	0.4/-0.02/-5.0/42.3/0.2	0.4/-0.02/-4.8/42.3/0.2	0.4/-0.02/-5.7/41.3/0.2
OC	CONUS	1.7	1.1/-0.6/-34.8/50.5/1.1	1.5/-0.2/-13.6/50.6/1.1	1.4/-0.3/-15.6/45.9/1.0
TC	CONUS	3.5	1.5/-1.9/-55.8/60.0/2.5	2.1/-1.4/-40.6/49.7/2.2	2.0/-1.5/-42.8/50.3/2.2
$PM_{2.5}$	CONUS	10.6	8.4/-2.2/-20.5/35.5/4.9	10.0/-0.6/-5.6/27.0/4.1	9.9/-0.7/-6.3/19.4/2.6
	Europe	13.1	8.7/-4.4/-33.6/34.8/5.4	10.1/-3.0/-23.0/30.4/5.0	11.9/-1.1/8.7/26.1/4.3
PM_{10}	Europe	25.9	16.4/-9.5/-36.6/41.4/12.5	18.3/-7.6/-29.4/34.5/11.7	21.6/-4.3/-16.7/26.6/9.7
	East Asia	85.4	31.5/-54.0/-63.2/65.0/59.0	39.9/-45.6/-53.3/54.6/51.2	45.4/-40.0/-46.8/51.3/48.4
Col.CO	Globe	1.3×10^{18}	-	1.2×10^{18}/-1.1×10^{17}/ -8.2/26.8/4.4×10^{17}	1.2×10^{18}/-1.3×10^{17}/ -10.0/28.1/4.7×10^{17}
Col.NO_2	Globe	5.9×10^{14}	-	9.0×10^{14}/3.1×10^{14}/ 52.2/65.0/5.2×10^{14}	8.8×10^{14}/2.9×10^{14}/ 48.9/62.4/5.1×10^{14}
TOR	Globe	32.1	29.8/-2.3/-7.4/18.9/6.9	31.1/-1.0/-3.0/14.2/5.9	30.4/-1.7/-5.4/15.4/6.2

[a]The units are CO, ppm (over East Asia); SO_2, ppb (over East Asia) and μg m^{-3} (over CONUS); O_3, ppb (over CONUS) and μg m^{-3} (over Europe); column CO and NO_2, molecules cm^{-2}; TOR, DU. All other concentrations are in μg m^{-3}.

[b]The values are expressed as Sim/MB/NMB/NME/RMSE, where Sim is modeled value, MB is mean bias; NMB is normalized mean bias (%); NME is normalized mean error (%); RMSE is root mean squared error

Table 2.8. Global burdens of major gaseous and aerosol species from the 2001-2005 simulations

	MAM_SIM_5Y	MAM_NEW_5YA	Previous studies
Tropospheric CO (Tg) [a]	N.A.[c]	322.06	337-354 [d]
Tropospheric O_3 (DU) [a]	29.7 [c]	30.5	34.04 [e]
Tropospheric O_3 (Tg) [a]	324.14 [c]	332.87	372 [e]
DMS (Tg S)	0.051	0.058	0.067 [f]
SO_2 (Tg S)	0.276	0.281	0.34 [f]
H_2SO_4 (Tg S)	3.8×10^{-4}	1.9×10^{-3}	4.2×10^{-4} [f]
Tropospheric NO_x [a, b]	N.A. [c]	0.116 Tg N (8.24×10^{14} molecules cm^{-2})	7.6×10^{14} molecules cm^{-2} [g]
NOy (Tg N) [b]	N.A. [c]	3.26	N.A. [c]
NH3 (Tg N)	0.074	0.059	0.064 [f]
VOCs (Tg C) [b]	N.A. [c]	7.63	N.A. [c]
Tropospheric HCHO (Tg C) [a]	N.A. [c]	0.391	0.335-0.349 [d]
SO_4^{2-} (Tg S)	0.36	0.39	0.84 [e] ,0.47 [f], 0.66 [h]
NO_3^- (Tg N)	N.A. [c]	0.11	0.01-0.14 i
NH_4^+ (Tg N)	0.20	0.21	0.24 [f] , (0.27-0.44) [i]
Na^+ (Tg)	2.93	3.04	2.98 [e] , (0.38-5.19) [i]
Cl^- (Tg)	4.52	4.47	4.60 [e] , (0.59-8.02) [i]
BC (Tg)	0.091	0.076	0.28 [e] , 0.093 [f]
OC (Tg)	0.45	0.61	1.28 [e]
POM (Tg)	0.63	0.48	0.68 [f] , 1.70 [h]
SOA (Tg)	N.A. [c]	0.38	1.15 [f] , 0.59 [j]
Dust (Tg)	25.78	26.43	24.7 [f] , (7.9-35.9) [i]

[a] CESM/CAM5 simulations use 30 model layers, with atmospheric pressures from ~1000 mb (layer 30) to ~3 mb (layer 1). Troposphere refers to model layers below tropopause height.

[b] NO_x = NO + NO_2; NO_y = NO_x + nitrogen trioxide (NO_3) + dinitrogen pentoxide (N_2O_5) + nitrous acid (HONO) + nitric acid (HNO_3) + pernitric acid (HNO_4) + peroxyacyl nitrate (PAN) + ≥C_3 peroxyacyl nitrate (PANX) + other organic nitrate (NTR); VOCs-volatile organic compounds including acetaldehyde (ALD2), carboxylic acid(AACD), long-chain alkanes (ALKH), Cresol and higher phenols (CRES), ethene (ETH), ethane (ETHA), ethanol (ETOH), formaldehyde (FORM), internal olefinic carbon bond (IOLE), methanol (MEOH), olefinic carbon bond (OLE), paraffin carbon bond (PAR), polycyclic aromatic hydrocarbons (PAH), toluene (TOL), xylene (XYL), isoprene (ISOP), and terpene (TERP).

[c] N.A – not available, it refers to the species that are not treated in MAM_SIM_5Y or species having no burden data from previous studies. Tropospheric O_3 burden in MAM_SIM_5Y is from climatology. N.A. in SOA is due to no SOAG emission for MAM_SIM_5Y.

[d] Williams et al. (2009)

[e] Horowitz et al. (2006)

[f] Liu et al. (2012)

[g] Lamarque et al. (2005)

[h] Textor et al. (2006)

[i] Tsigaridis et al. (2006)

[j] Heald et al. (2008)

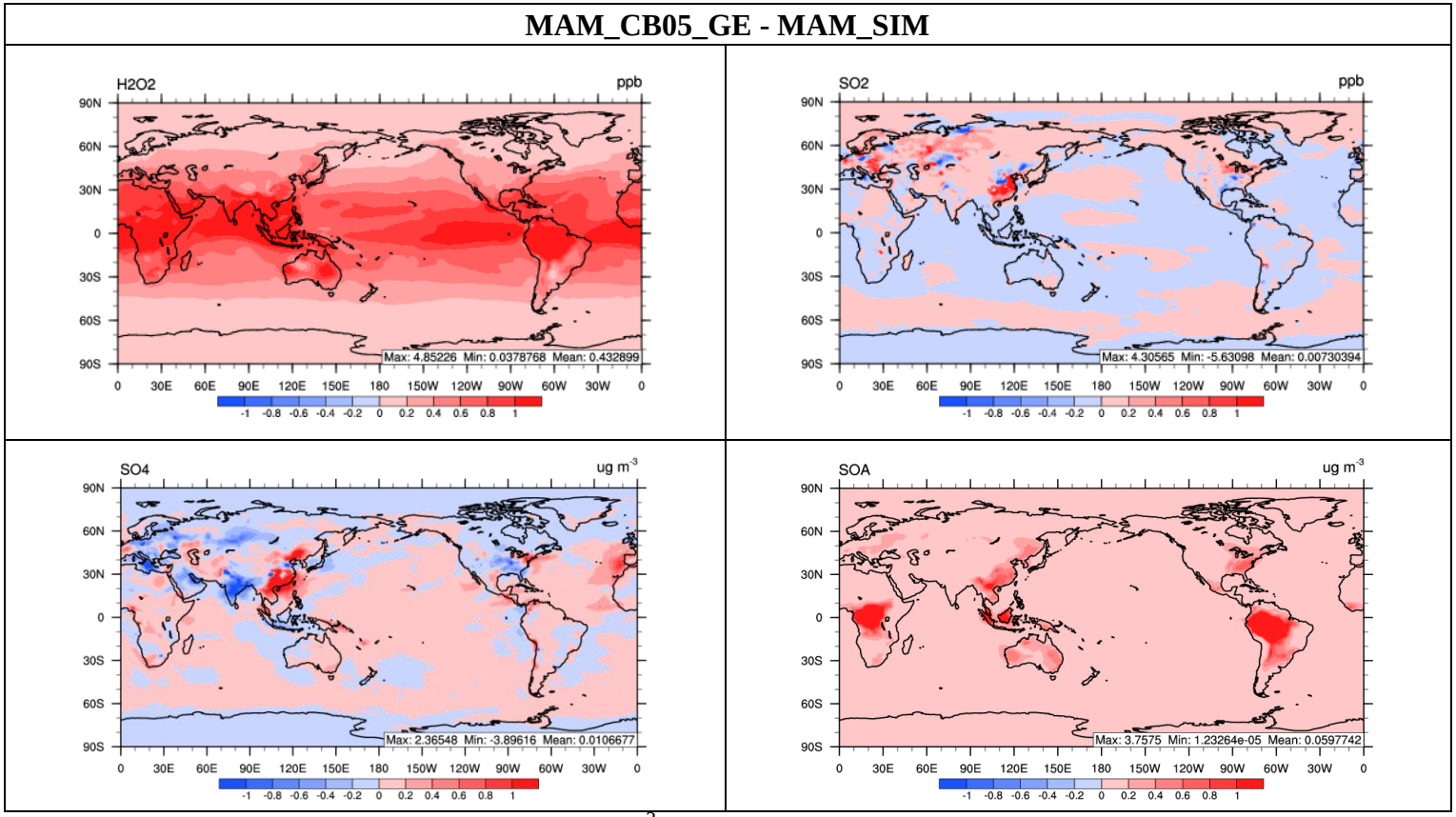

Figure 2.1a. Absolute differences of H_2O_2, SO_2, SO_4^{2-}, and SOA between MAM_CB05_GE and MAM_SIM for 2001.

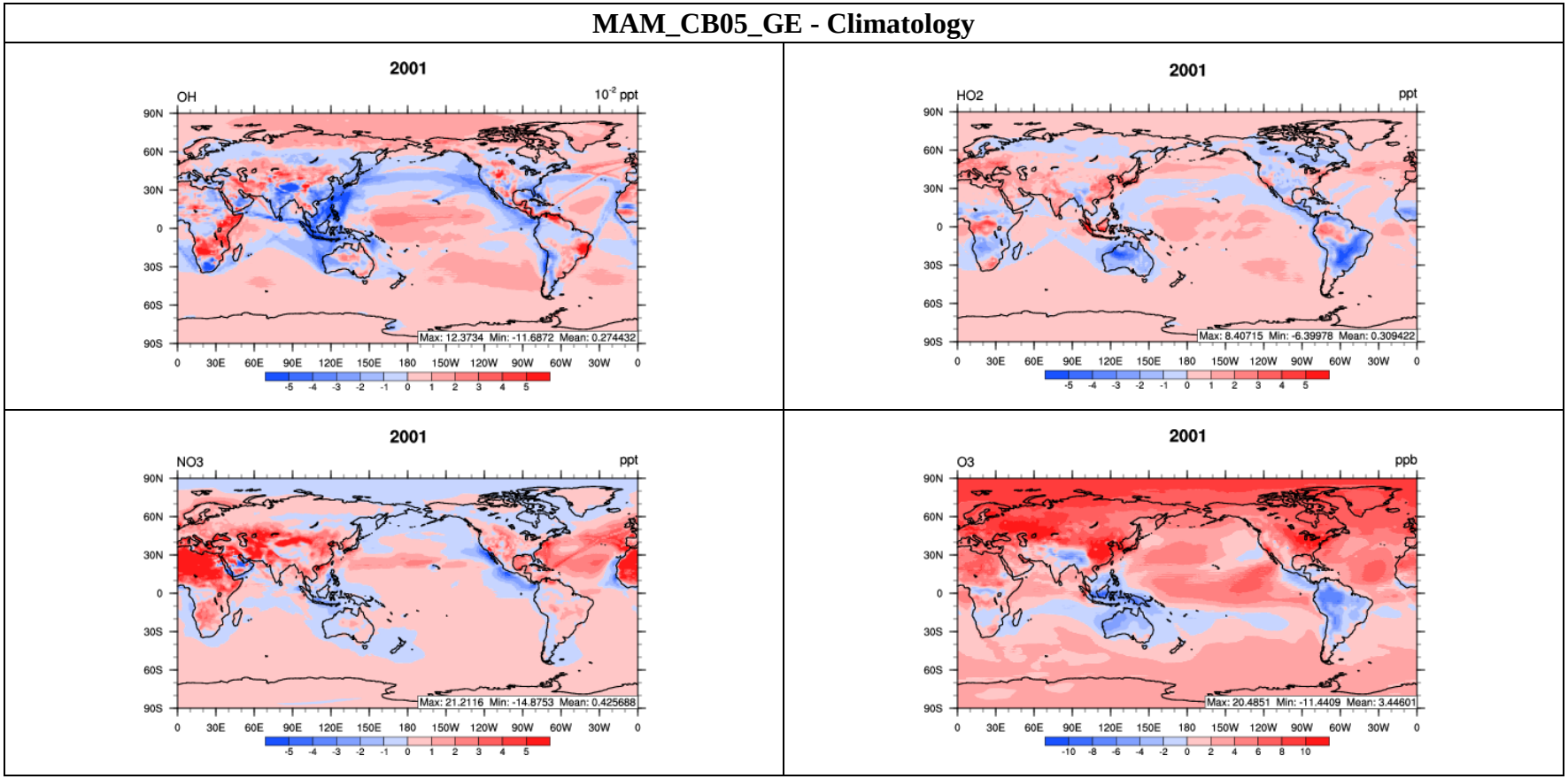

Figure 2.1b. Absolute differences between the mixing ratios of surface OH, HO_2, NO_3, and O_3 predicted from MAM_CB05_GE and climatology values used in MAM_SIM for 2001.

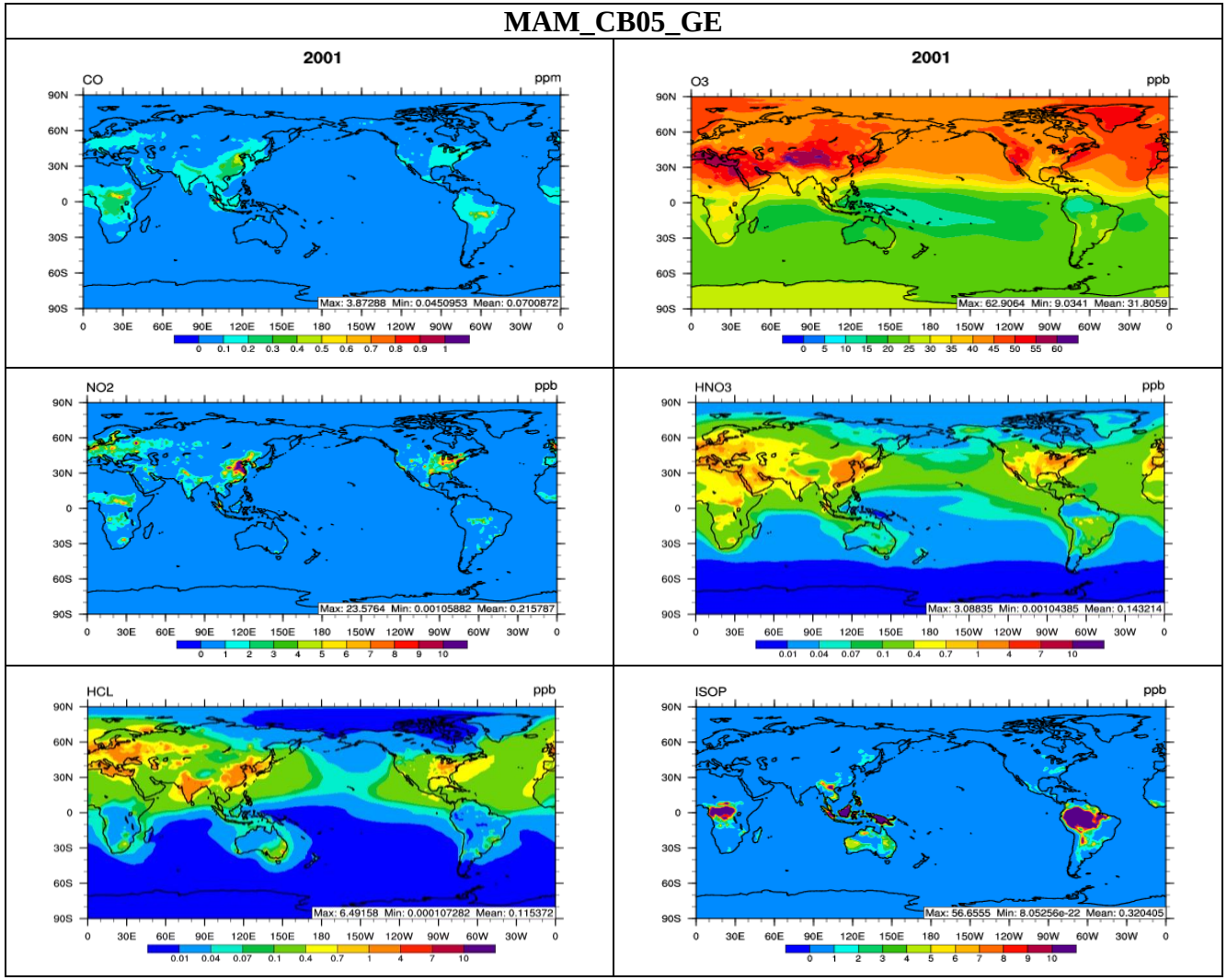

Figure 2.2. Surface distribution of CO, O_3, NO_2, HNO_3, HCl, and isoprene (ISOP) in MAM_CB05_GE for 2001.

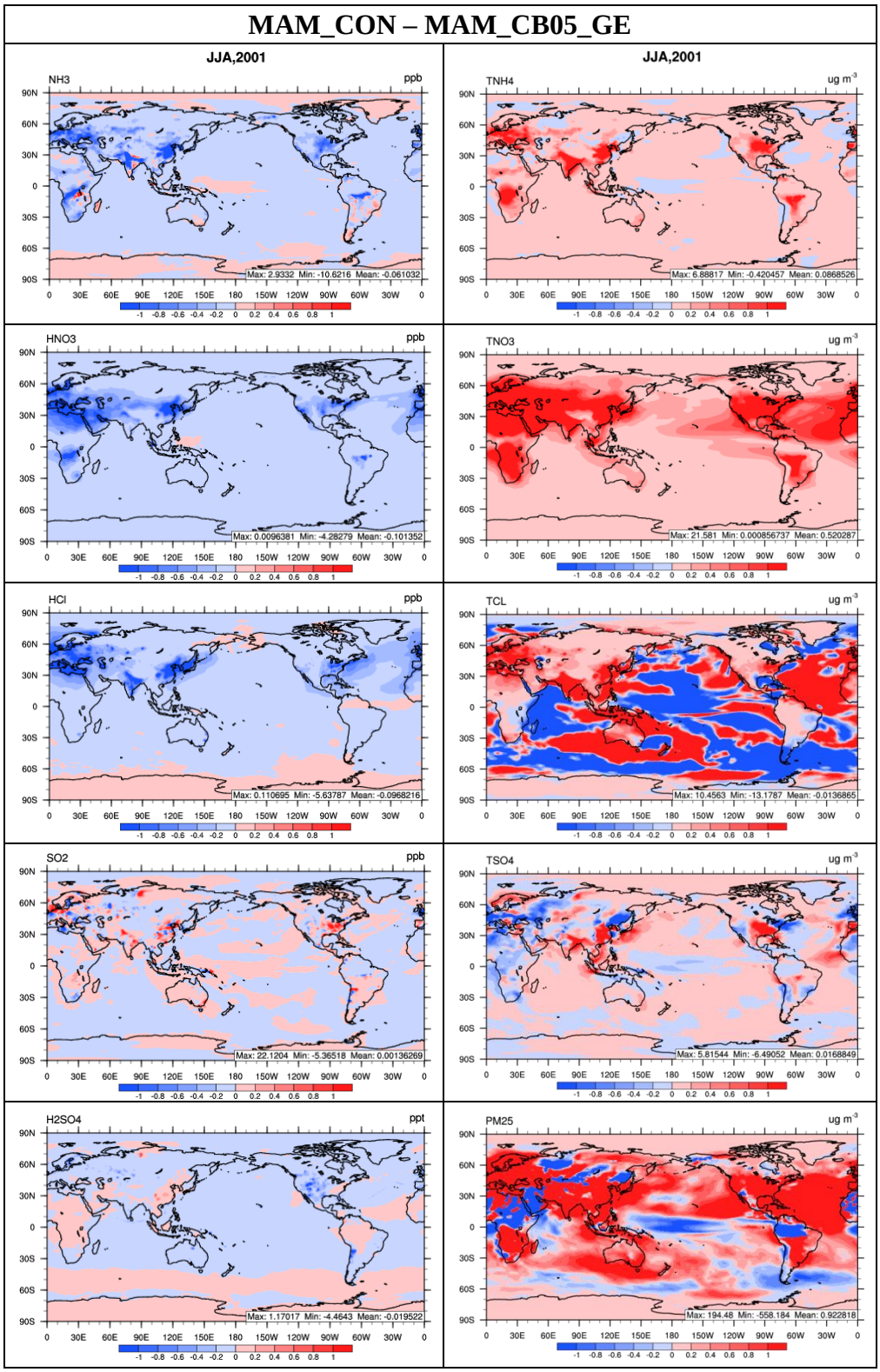

Figure 2.3. Surface distribution of total ammonium, total sulfate, total nitrate, total chloride, $PM_{2.5}$, NH_3, SO_2, H_2SO_4, HNO_3, and HCl between MAM_CON and MAM_CB05_GE for summer (June, July, and August, JJA), 2001.

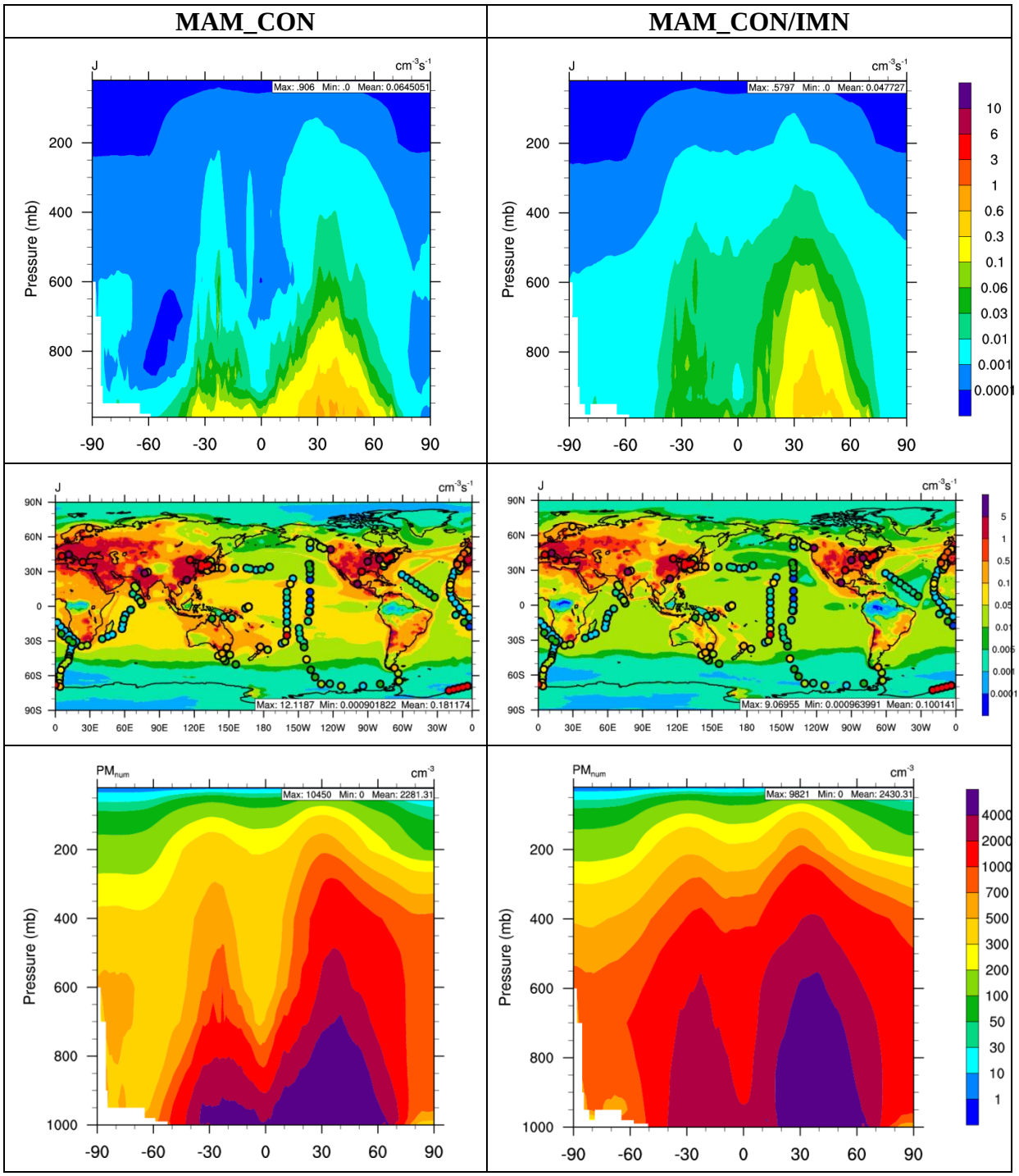

Figure 2.4. Vertical distribution of new particle formation rate (J) and aerosol number (PMnum) simulated by MAM_CON/IMN for 2001. The overlay plots show the distribution of J in bottom 1000-m. Circles on overlay plots represent observations for J. Different colors of circles represent different values of J, using the same color scale as simulated J.

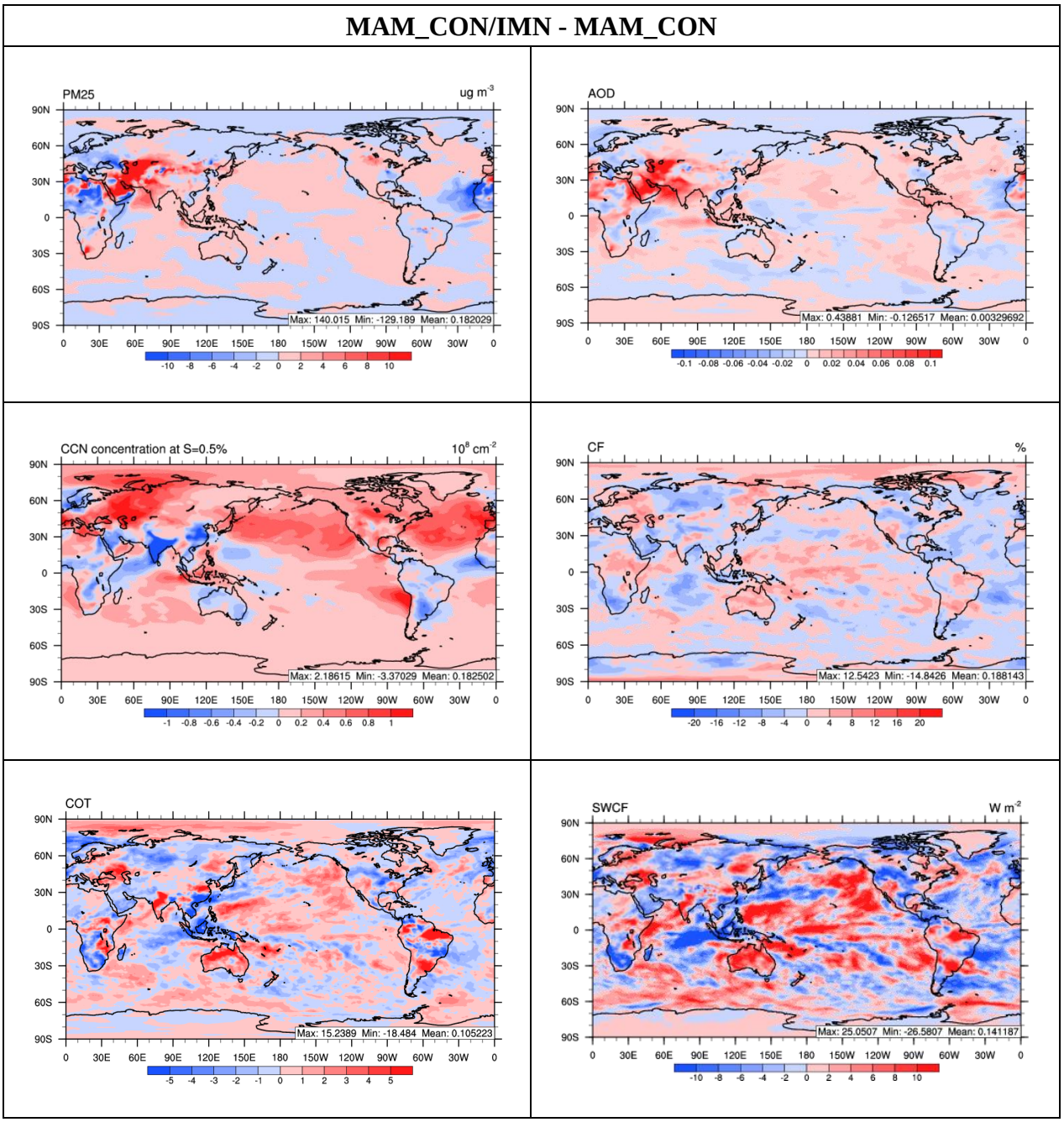

Figure 2.5. Absolute differences of $PM_{2.5}$, AOD, column CCN5, CF, COT, and SWCF between MAM_CON/IMN and MAM_CON for 2001.

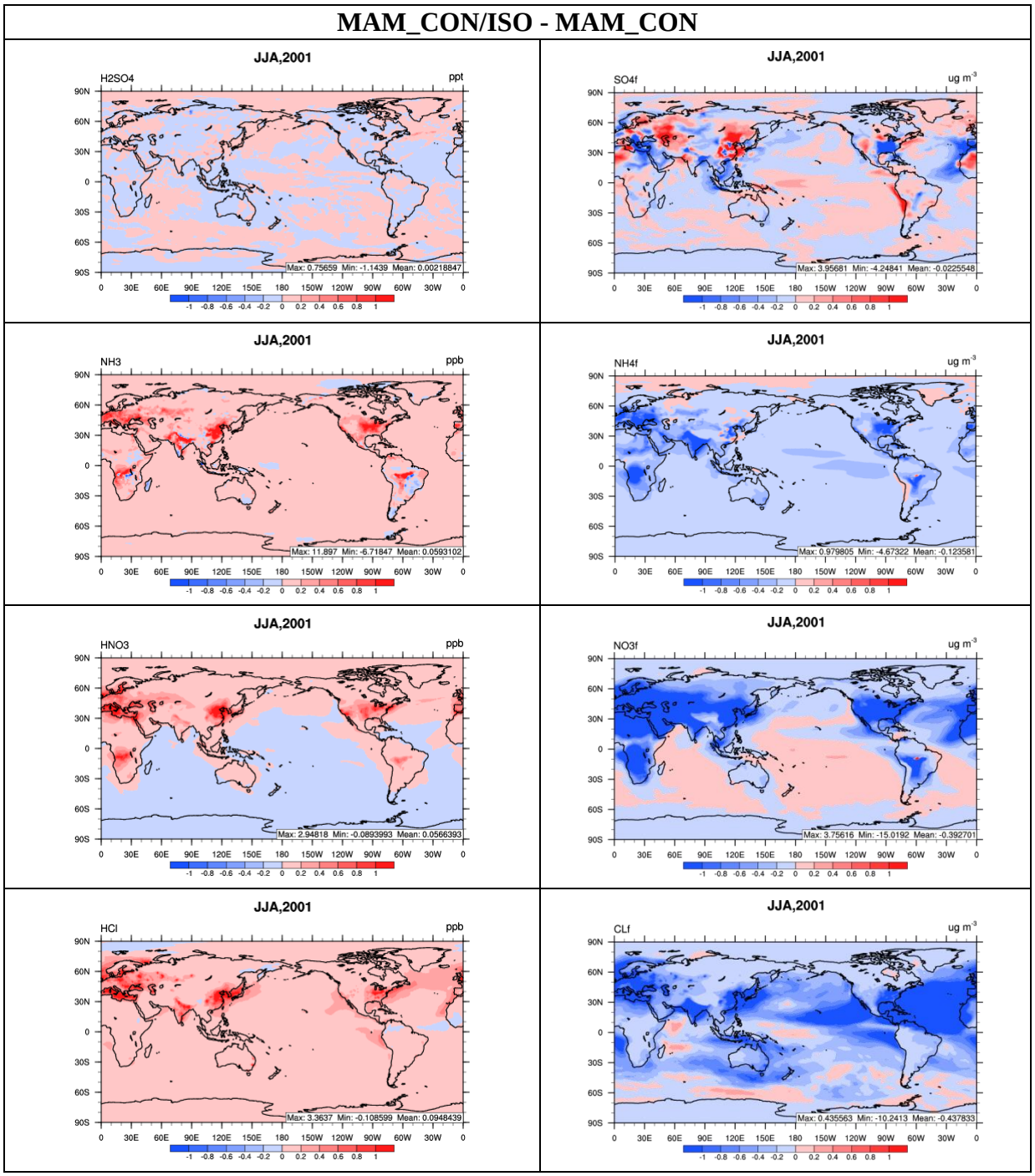

Figure 2.6a. Absolute differences of major PM species and their gas precursors between MAM_CON/ISO and MAM_CON for summer, 2001.

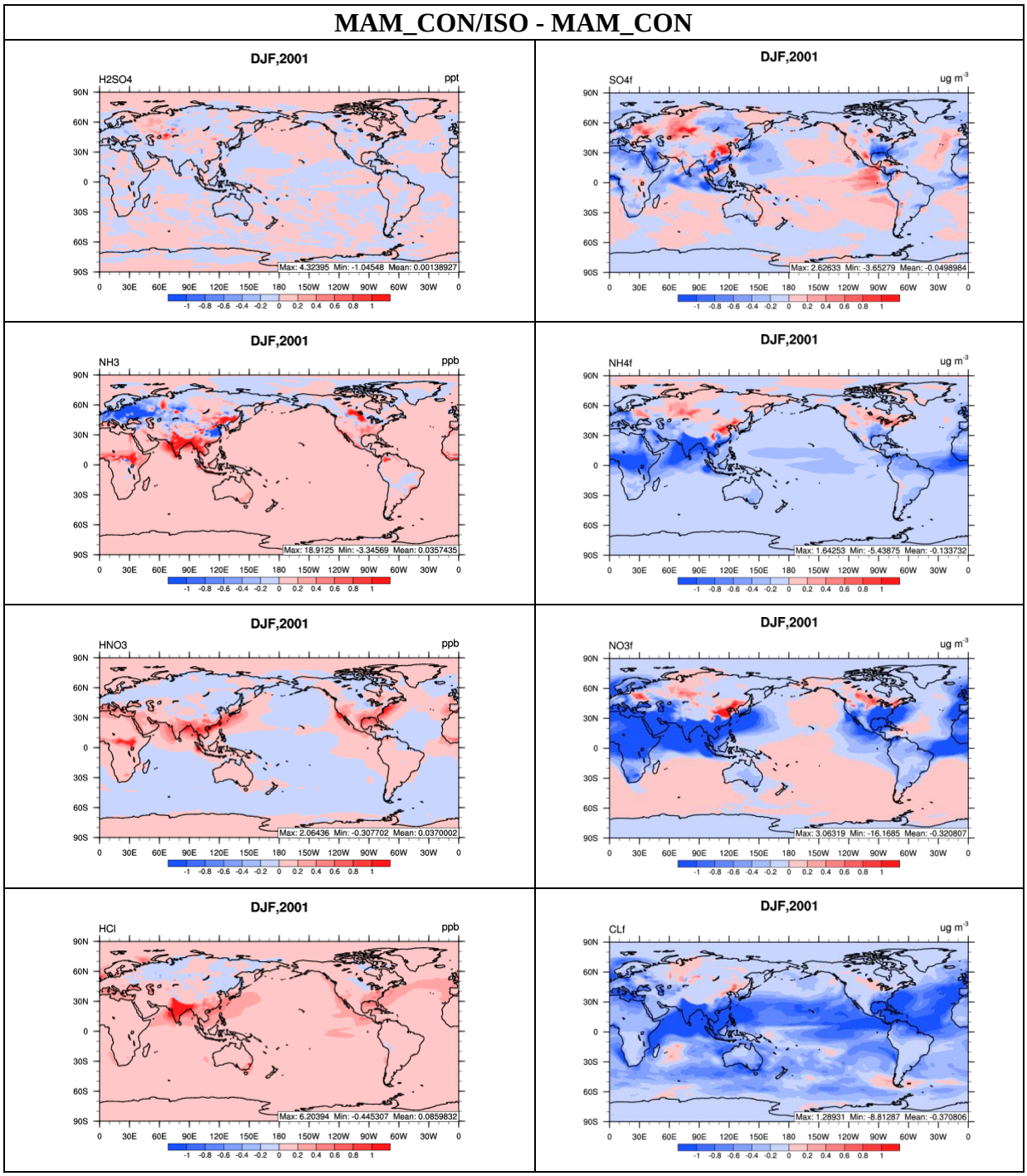

Figure 2.6b. Absolute differences of major PM species and their gas precursors between MAM_CON/ISO and MAM_CON for winter, 2001.

	JJA, 2001	DJF, 2001
MAM_CON	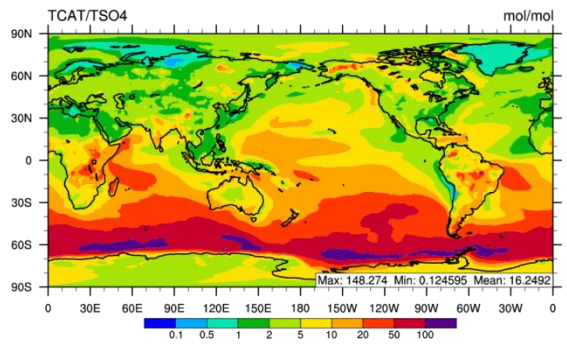	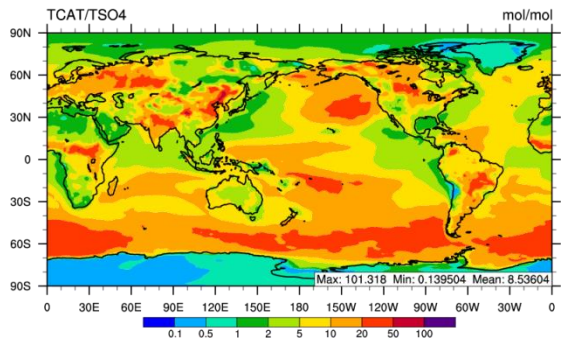
MAM_CON/ISO	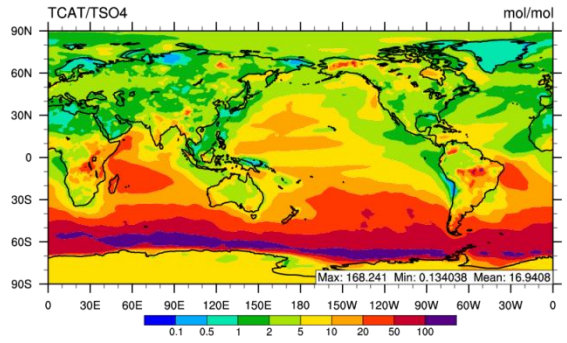	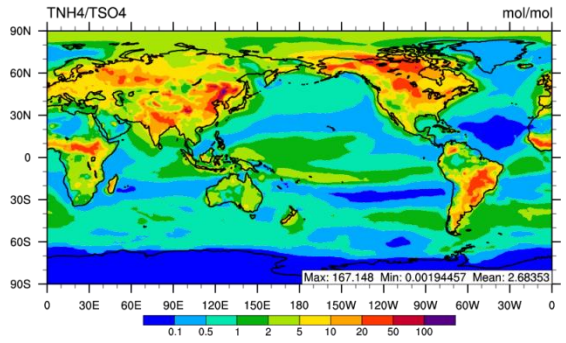
MAM_CON/ISO - MAM_CON	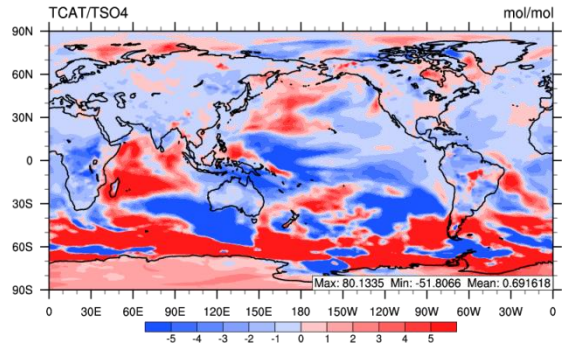	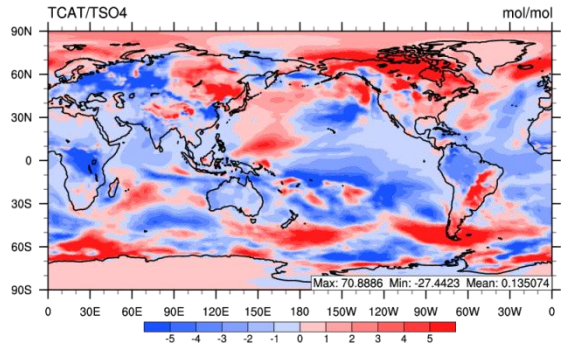

Figure 2.7. Surface distribution of TCAT/TSO4 in MAM_CON and MAM_CON/ISO and absolute differences of TCAT/TSO4 between MAM_CON/ISO and MAM_CON for summer and winter, 2001.

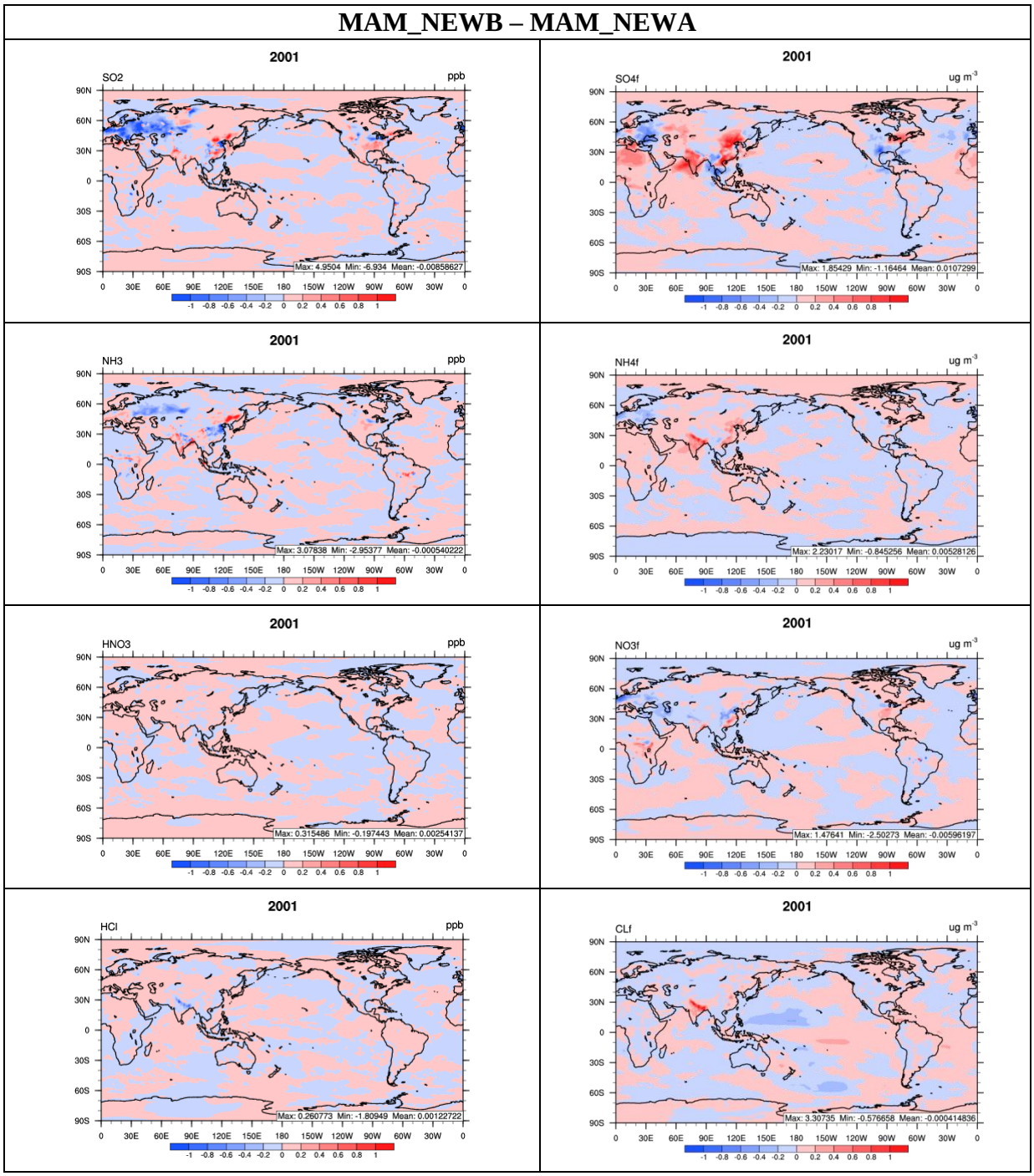

Figure 2.8. Absolute differences of major aerosol species and their gas precursors between metastable and stable conditions.

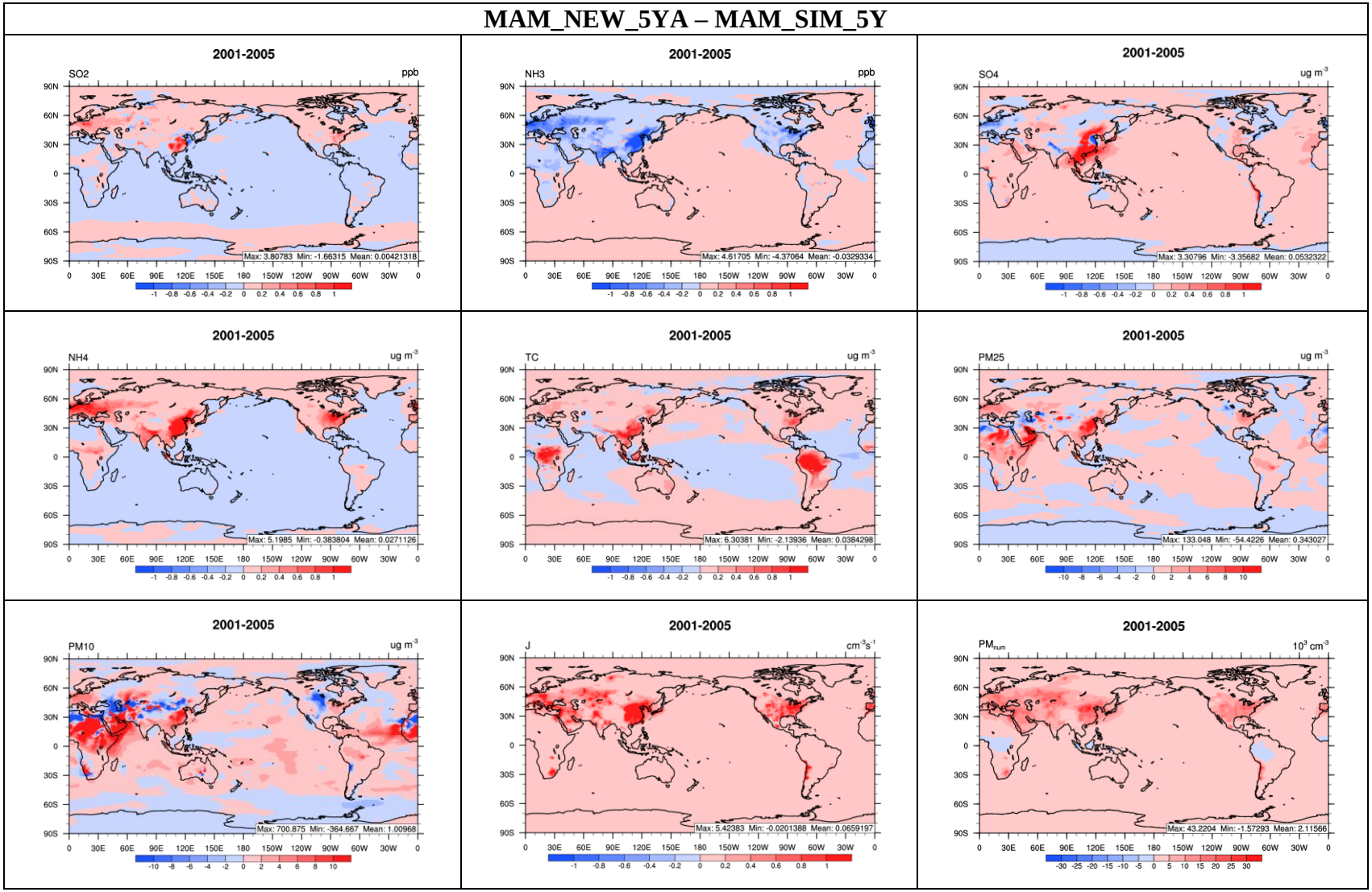

Figure 2.9a. Absolute differences of major aerosol species and their gas precursors, new particle formation rate (J), and aerosol number between MAM_NEW_5YA and MAM_SIM_5Y for 2001-2005.

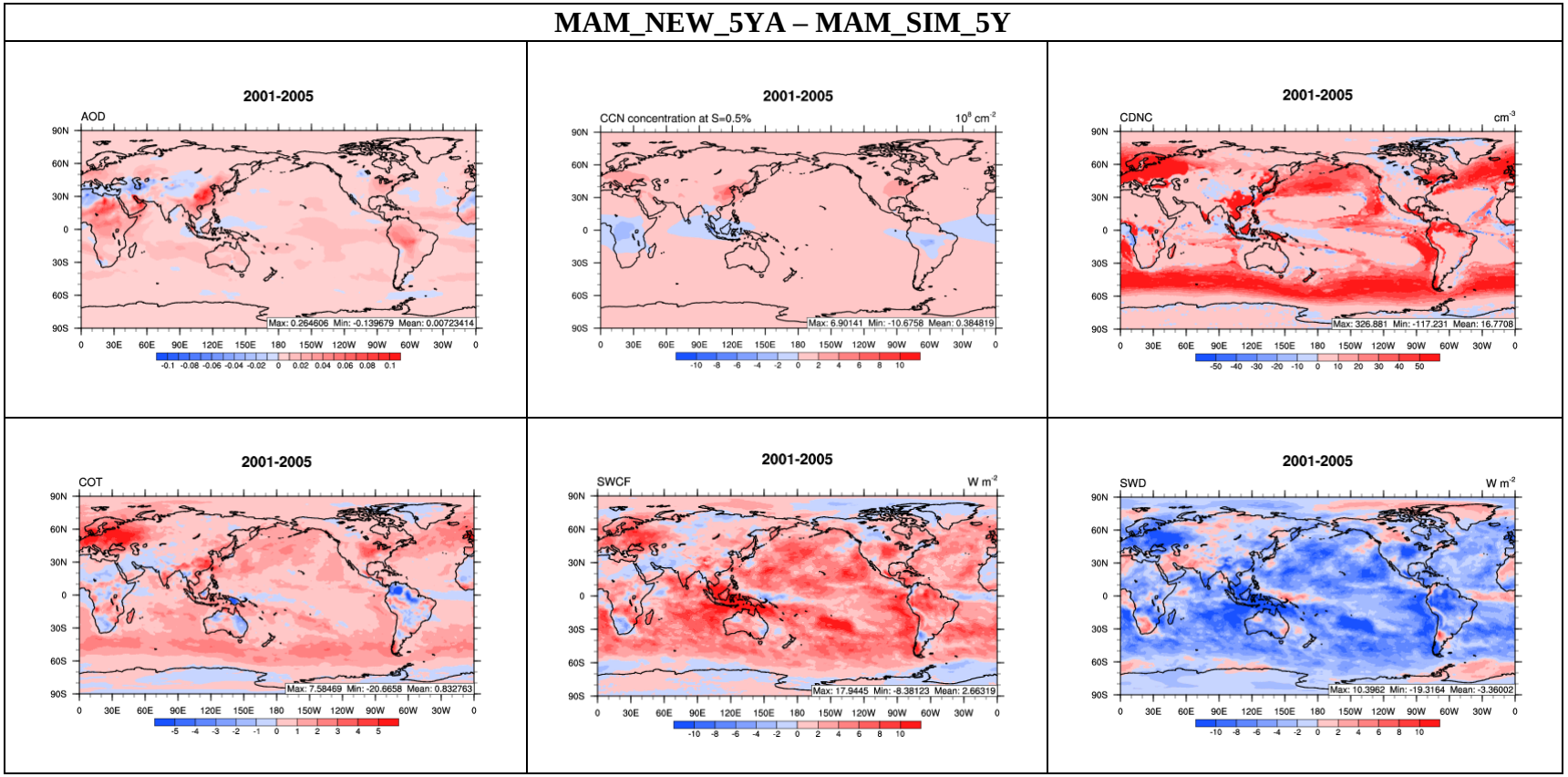

Figure 2.9b. Absolute differences of major cloud and radiative variables between MAM_NEW_5YA and MAM_SIM_5Y for 2001-2005.

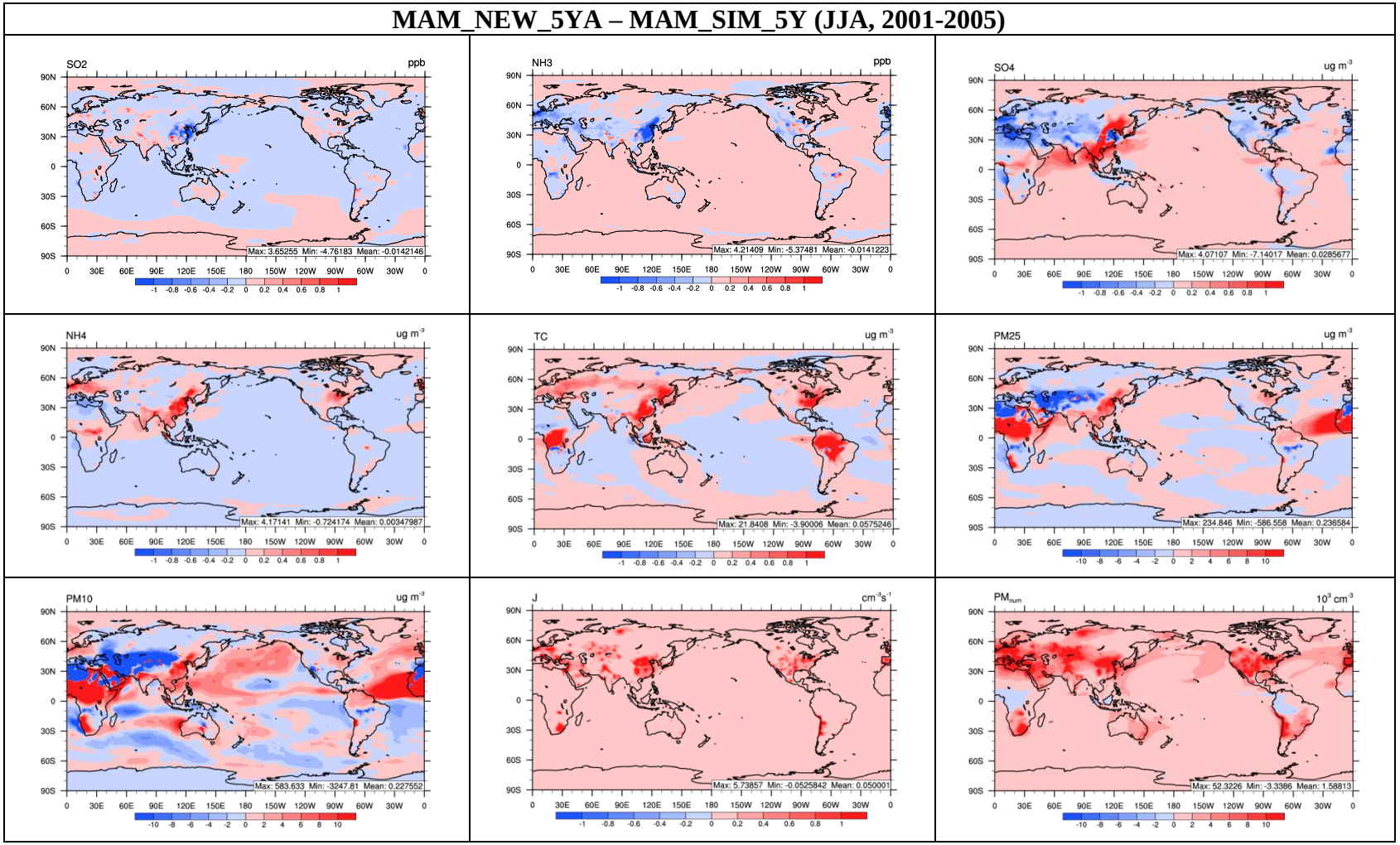

Figure 2.10a. Absolute differences of major aerosol species and their gas precursors, new particle formation rate (J), and aerosol number between MAM_NEW_5YA and MAM_SIM_5Y for June, July, and August (JJA), 2001-2005.

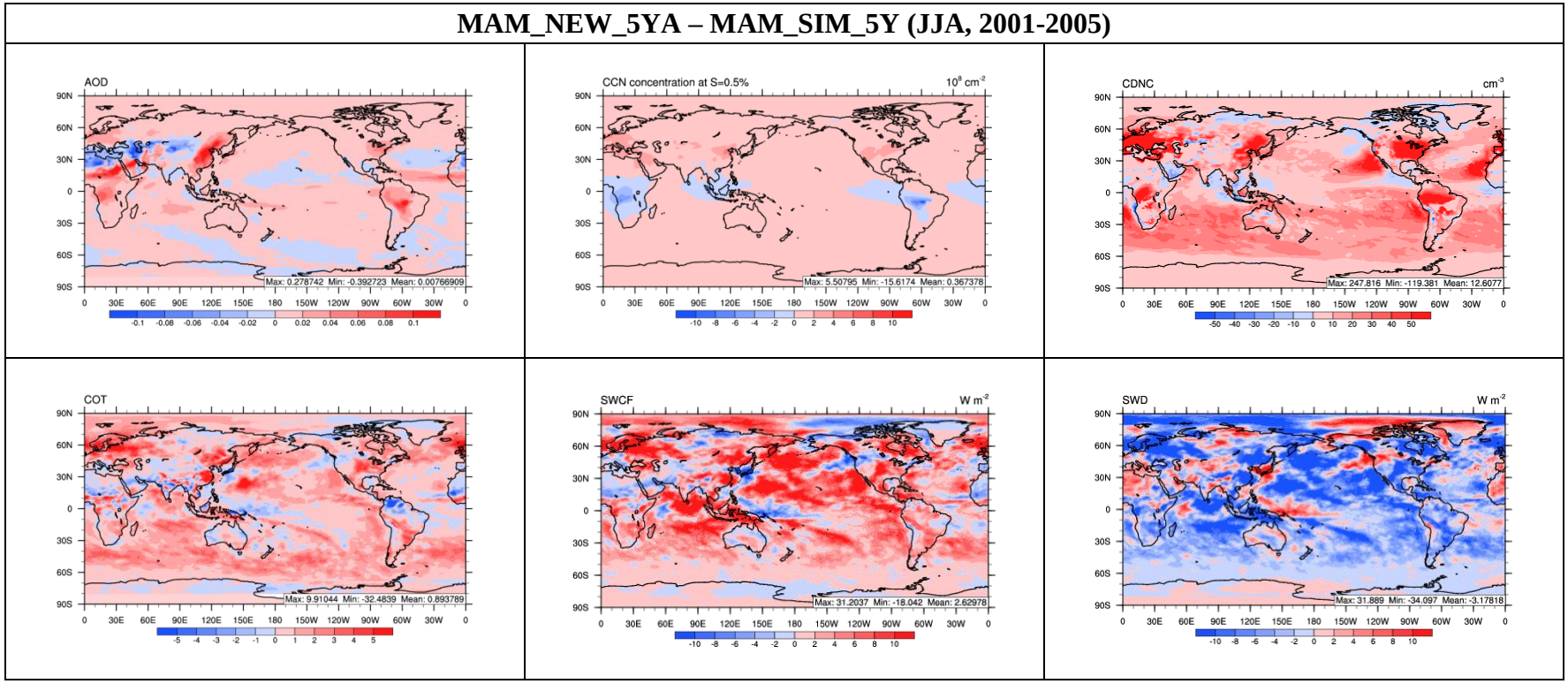

Figure 2.10b. Absolute differences of major cloud and radiative variables between MAM_NEW_5YA and MAM_SIM_5Y for June, July, and August (JJA), 2001-2005.

CHAPTER 3. DECALDAL SIMULATION AND COMPREHENSIVE EVALUATION OF CESM/CAM5 WITH ADVANCED CHEMISTRY, AEROSOL MICROPHYSICS, AND AEROSOL-CLOUD INTERACTIONS

3.1 Introduction

A number of Earth system models have been developed in recent years to understand climate change and variability by including biogeochemical cycles, human impacts, as well as coupled and interactive representations of Earth system components (e.g., atmosphere, ocean, land, and sea ice). Table 3.1 summarizes current Earth system models that are used in the community. The Hadley Centre Global Environmental Model version 2 including Earth system components (HadGEM2-ES, Collins et al., 2011a) developed by U.K. Met Office Hadley Centre is designed for simulating and understanding the centennial-scale evolution of climate including physical, chemical, and biological processes among Earth system components. Bellouin et al. (2011) evaluated HadGEM2-ES 1860-2100 simulations in terms of aerosols and discussed the importance of aerosols in the climate system. The Earth System Model version 2 (ESM2, Dunne et al., 2012, 2013) developed by the Geophysical Fluid Dynamics Laboratory (GDFL) was designed to study carbon-climate interactions and feedbacks within climate systems under the diverse anthropogenic perturbations (e.g., fossil fuel emissions, agriculture and forestry, and aerosol chemistry) within a single self-consistent system. Dunne et al. (2012) evaluated the GDFL-ESM2 100-year simulations and discussed the impacts of ocean dynamics on climate variability. The new Max-Planck-Institute Earth System Model (MPI-ESM, Giorgetta et al., 2013) developed by the Max Planck Institute for Meteorology is designed through diverse model configurations for a series of climate change

experiments to estimate climate sensitivity and transient climate change. MPI-ESM simulations through diverse model configurations and experiments associated with different climate forcings have contributed to the Coupled Model Intercomparison Project phase 5 (CMIP5, Giorgetta et al., 2013). The Integrated Global System Model (IGSM, Dutkiewicz et al., 2005; Sokolov et al., 2005) developed by the Massachusetts Institute of Technology (MIT) consists of an economic model, a coupled atmosphere-ocean-land surface model with interactive chemistry, and natural ecosystem models. It is designed to analyze the global environmental changes that may result from anthropogenic causes, quantify the uncertainties associated with the projected changes, and assess the costs and environmental effectiveness of proposed policies to mitigate climate risk. Since IGSM consists of a two-dimensional atmospheric component, Monier et al. (2013) coupled IGSM with the Community Atmosphere Model (CAM) developed by the National Center for Atmospheric Research (NCAR) to address regional climate change.

As one of the recent Earth system models, the Community Earth System Model (CESM, Hurrell et al., 2013) developed by NCAR consists of component models with many capabilities that can be coupled in different configurations for different purposes. These capabilities include interactive carbon-nitrogen cycling, human impacts on vegetation and land use change, a marine ecosystem-biogeochemical module, and new chemical and physical processes to study both the direct and indirect effects of aerosols on climate. CESM can simulate the entire Earth system by coupling the physical climate system with chemistry, biogeochemistry, biology, and human systems. It can also quantify the certainties and uncertainties in Earth system feedbacks on time scales up to centuries and longer. It has been

applied to simulate climate change as part of the Intergovernmental Panel on Climate Change (IPCC) Fifth Assessment Report (AR5). However, due to the complexities in physical and chemical processes of aerosols, significant uncertainties remain in the treatments of such processes in the models. For example, many Earth system models do not include chemistry or use prescribed or highly simplified gas/aerosol treatments in the model simulations. However, gas-phase chemistry and subsequent gas-to-particle conversion processes (e.g., new particle formation, condensation, and thermodynamic partitioning) have large impacts on climate as they influence the amounts and distributions of gaseous precursors and secondary aerosols. Aerosols can influence the Earth's radiative balance by directly scattering and absorbing radiation and indirectly affecting cloud properties through acting as cloud condensation nuclei (CCN) and ice nuclei (IN). Therefore, it is important to accurately simulate aerosol size distribution, chemical composition, and physical and chemical properties, which determine the magnitude of the aerosol radiative forcing (Koloutsou-Vakakis et al., 1998). Uncertainties associated with aerosol-cloud interactions as well as their feedbacks are also among the emerging issues that are to be addressed by the scientific community. To reduce the uncertainties associated with some of those model treatments and the resultant predictions of aerosol impacts on climate, advanced treatments for chemistry and inorganic aerosol (He and Zhang, 2014), secondary organic aerosol (SOA, Glotfelty et al., 2013), as well as aerosol activation (Gantt et al., 2014) have recently been implemented into the Community Atmosphere Model version 5.1 (CAM5.1), the atmospheric component of CESM version 1.0.5 (CESM1.0.5), by North Carolina State University (NCSU, referred to as CESM_NCSU in Table 3.1).

A comprehensive model evaluation must be performed to assess the model's capability to reproduce the current atmosphere before it can be applied to project future climate change. Most Earth system model evaluations have been performed for a single species or component model. For example, Keppel-Aleks et al. (2013) evaluated CO_2 variability predicted by CESM. Lamarque et al. (2012) evaluated the chemistry model in CESM. Liu et al. (2012) and Ghan et al. (2012) evaluated the aerosol model and aerosol radiative forcing in CAM5. Lipscomb et al. (2013) evaluated the Glimmer Community ICE Sheet model in CESM. He and Zhang (2014) implemented advanced gas-phase mechanism and inorganic aerosol treatments into CESM/CAM5 and evaluated the chemistry/aerosol performance from the model simulations with a fully coupled mode and with prescribed SST. Gantt et al. (2014) implemented an advanced aerosol activation scheme and evaluated the model performance in simulating aerosol and cloud properties and their impacts on climate using CESM/CAM5 with the advanced aerosol activation scheme. Simulations with each of the updates in the model's representations of chemistry, aerosol, and aerosol-cloud interactions used in this work have been evaluated in He and Zhang (2014) and Gantt et al. (2014) to illustrate the individual impact of each updated treatment on the overall model predictions.

In this section, a comprehensive evaluation of multiple variables and species from CESM/CAM5.1 is conducted through applying the CESM/CAM5.1 with advanced chemistry/aerosol treatments and their interactions with clouds for retrospective decadal simulations during 2001-2010. The objectives of this work are to comprehensively evaluate the capability of the fully-coupled CESM with advanced chemistry/aerosol treatment in

reproducing observations (or re-analyses) of climate and air quality variables in 2001-2010, characterize their seasonal and interannual variability, and study interactions among atmospheric chemistry, aerosols, and clouds, as well as their impacts on climate via atmospheric radiation and aerosol direct/indirect effects. Such comprehensive evaluations can provide information to assess the appropriateness of the model for future climate simulations and identify uncertainties/limitations for future model improvement. Through this work, several scientific questions will be addressed. For example, can the improved CESM-CAM5 reproduce the meteorological and chemical observations and their time evolution during a decade-long period? How is its skill for decadal climate modeling compared to the skill of CESM-CMIP5? What are additional uncertainties/limitations in the model treatment for accurate model predictions? What are the contributions of anthropogenic emissions to global radiation and climate for a present-day atmosphere?

3.2 Model Description

CESM/CAM5.1 used in this work, is based on version 1.0.5 that was released by NCAR and further developed and improved at NCSU (Glotfelty et al., 2013; He and Zhang, 2014; Gantt et al., 2014). The gas-phase chemical mechanism is based on the 2005 Carbon Bond Mechanism for Global Extension (CB05_GE) of Karamchandani et al. (2012). The aerosol module used in the NCSU's version is based on the 7-mode modal aerosol module (MAM7) of CESM/CAM5.1, but with several modifications. First, the new particle formation treatments include a combination of the default nucleation parameterizations of Vehkamaki et al. (2002) and Merikanto et al. (2007), a newly added ion-mediated aerosol nucleation (Yu, 2010) above the planetary boundary layer (PBL), and a combination of the

three and an additional parameterization of Wang and Penner (2009) in the PBL. Second, the inorganic aerosol thermodynamics is based on ISORROPIA II of Fountoukis and Nenes (2007) which explicitly simulates the thermodynamics of sulfate (SO_4^{2-}), ammonium (NH_4^+), nitrate (NO_3^-), sodium (Na^+), and chloride (Cl^-) in the Aitken, accumulation, and fine sea-salt modes, as well as the impact of crustal species associated with the fine dust mode. Other updates to the chemistry and aerosol treatments include splitting sea-salt aerosol in MAM7 into sodium and chloride to enable chlorine chemistry in ISORROPIA II, the addition of aqueous-phase dissolution and dissociation of nitric acid (HNO_3) and hydrochloric acid (HCl), and the use of species-dependent accommodation coefficients for sulfuric acid (H_2SO_4), ammonia (NH_3), HNO_3, and HCl, with values of 0.1, 0.097, 0.0024, and 0.005, respectively. For aerosol-cloud interactions, the NCSU version of CESM/CAM5.1 contains an advanced aerosol activation scheme based on Fountoukis and Nenes (2005, hereinafter FN05) with additional updates based on Kumar et al. (2009, hereinafter K09) and Barahona et al. (2010, hereinafter B10) by Gantt et al. (2014, hereafter referred to as the FN05 series parameterization). FN05 is based on Nenes and Seinfeld (2003) and includes explicit calculations of mass transfer, condensation coefficient, integration over the aerosol size distribution, and kinetic limitations. K09 accounts for insoluble adsorption, which leads to the activation of some particles that would not easily activate under Köhler theory. B10 parameterization accounts for the slow condensation upon internally-limited droplets in the calculation of the droplet surface area and maximum supersaturation in a cloud updraft. With all those updates, the advanced aerosol activation scheme accounts for adsorption activation from insoluble CCN and giant CCN equilibrium timescale on aerosol activation. More

detailed descriptions of the NCSU version of CESM/CAM5 can be found in He and Zhang (2014) and Gantt et al. (2014).

In this work, several additional developments and updates have been performed in the NCSU version of CESM/CAM5.1. First, the heterogeneous chemistry has been implemented into CB05 based on Karamchandani et al. (2012); it includes 14 heterogeneous reactions on aerosol particles/cloud droplets and 10 heterogeneous reactions in polar stratospheric clouds (PSCs). Additionally, six kinetic reactions pertaining to the oxidation of anthropogenic and biogenic volatile organic compounds (VOCs) by OH are included in this work; the products of those reactions are linked with the organic gas/aerosol partitioning for SOA formation. Second, a volatility-basis-set (VBS) approach has been implemented into CAM5.1 (Glotfelty et al., 2013) to provide an advanced treatment for SOA, which can potentially improve model performance with respect to organic aerosols (OA). VBS provides an empirical representation of the aging and volatility of the OA and its precursors (Donahue et al., 2006; Lane et al., 2008; Andreae, 2009; Jimenez et al., 2009; Ahmadov et al., 2012). Using VBS, VOCs are oxidized primarily by OH to form semi volatile organic compounds (SVOCs). The SVOCs partition in both the gas- and the condensed phases. The SOA formed from these SVOCs is represented with different volatility bins defined by different effective saturation concentrations. Over time, the SVOCs will be oxidized further and move from the higher volatility bins to the lower volatility bins, where they are more likely to condense to the particulate phase. This approach has been extended to a two-dimensional model that accounts for changes in the oxidation state indicated by the O:C ratio (Donahue et al., 2011, 2012). The increases in the O:C ratio increase the likelihood that the SVOC will condense and

increase the hygroscopicity of the OA formed (Jimenez et al., 2009). These improvements include the VBS representation of biogenic SOA and anthropogenic SOA formation and the linking of the volatility of SOA to the hygroscopicity of the aerosol. Compared to the work of He and Zhang (2014), the version of CESM/CAM5.1-MAM7 used in this work includes the above updates and the aforementioned FN05 series parameterization for aerosol activation as implemented by Gantt et al. (2014).

3.3 Model Configurations and Evaluation Protocols

3.3.1 Model Setup and Inputs

The simulation is performed with fully coupled CESM1.0.5 with standard B_1850-2000_CAM5_CN configuration, which represents 1850 to 2000 transient conditions and includes all active component models in CESM with biogeochemistry in the land model. The simulation is conducted for 2001-2010 at a horizontal resolution of $0.9^{o}\times1.25^{o}$ and a vertical resolution of 30 layers for CAM5.1.

The initial conditions for ice and ocean models are from CESM default settings. The initial conditions for the land model are based on the output from the NCAR CESM/CAM4 B_1850-2000_CN simulation. The initial conditions for CAM5.1 are derived from a 10-yr (1990-2000) CAM5.1 standalone simulation with the MOZART chemistry provided by NCAR. A 1-year (January 1-December 31, 2000) CESM/CAM5.1 simulation using the NCAR CESM B_1850-2000_CAM5_CN component set is performed as a spin-up to provide the initial conditions for the meteorological variables and chemical species that are treated in both MOZART and CB05_GE. An additional 3-month (October 1-December 31, 2000) CESM/CAM5.1 simulation based on a 10-month (January-October, 2000) CESM/CAM5.1

output using initial conditions from NCAR's CESM B_1850-2000_CAM5_CN is performed as a spin-up to provide initial conditions for chemical species that are treated in CB05_GE but not in MOZART.

Table 3.2 shows the emission inventories that are used for the 2001-2010 simulations. The emissions representative of three time periods are used for the CESM simulations of 2001-2003, 2004-2006, and 2007-2010, respectively. Emissions for the first period are based on Zhang et al. (2012) with adjustment factors of 0.7, 0.5, and 1.2 for sulfur dioxide (SO_2) over the continental U.S. (CONUS), Europe, and East Asia, respectively, and 1.2 for ammonia (NH_3), black carbon (BC), and organic carbon (OC), and 1.3 for carbon monoxide (CO) over all three regions. Those emissions are adjusted based on the comparison with several global emission inventories and preliminary evaluation of the NCSU CESM/CAM5.1 against available observations. Emissions for the second period are based on the 2005 Emission Database for Global Atmospheric Research (EDGAR), with regional updates based on the 2006 emissions from Air Quality Modeling Evaluation International Initiative Phase II (AQMEII) over North America and the 2006 emissions from the Multi-resolution Emission Inventory for China (MEIC) over China. Emissions for the third period are based on the 2008 EDGAR emissions, with regional updates from the 2010 AQMEII emissions over North America and Europe, and from the 2010 MEIC emissions over China. The emissions for missing species in EDGAR (e.g., dimethyl sulfide (DMS) and hydrogen gas, H_2) are based on Zhang et al. (2012) with inclusion of DMS and H_2 emissions from biomass burning, which are from the Atmospheric Chemistry and Climate Model Intercomparison Project (ACCMIP). The online emissions include those of biogenic VOCs simulated with the Model

of Emissions of Gases and Aerosols from Nature version 2 (MEGAN 2, Guenther et al., 2006), mineral dust (Zender et al., 2003), and sea-salt (Martensson et al., 2003).

The simulation includes a total of 139 prognostic species in tracer advection. The simulation calculates photolysis rates based on Lamarque et al. (2012) and uses the aqueous-phase chemistry described by He and Zhang (2014). Major physical options include the cloud microphysics parameterization of Morrison and Gettelman (2008), the moisture PBL scheme of Bretherton and Park (2009), the shallow and deep convection schemes of Park and Bretherton (2009) and Zhang and McFarlane (1995), respectively, and the Rapid Radiative Transfer Model for GCMs (RRTMG) of Mlawer et al. (1997) and Iacono et al. (2003, 2008) for long and short-wave radiation. The land surface processes are simulated by the Community Land Model (CLM) of Lawrence et al. (2011) in CESM that is coupled with CAM5.1. A sensitivity simulation of 2001-2010 using CESM-CAM5 with the same configurations as baseline but with 80% reductions in the anthropogenic emissions is also conducted. The results from this sensitivity simulation are compared with the baseline simulation to quantify the impacts of chemical species including both gases and aerosol species on climate through various feedbacks mechanisms.

3.3.2 Available Measurements

A number of observational datasets from surface networks and satellites are used for model evaluation. They are summarized along with the variables to be evaluated in Table 3.3. Global surface networks include the National Climatic Data Center (NCDC), the Global Precipitation Climatology Project (GPCP), and the National Oceanic and Atmospheric Administration Climate Diagnostics Center (NOAA/CDC). The National Centers for

Environmental Prediction (NCEP) reanalysis data are from a joint project between the NCEP and NCAR. The satellite datasets include the Moderate Resolution Imaging Spectroradiometer (MODIS), the Clouds and Earth's Radiant Energy System (CERES), the Total Ozone Mapping Spectrometer/the Solar Backscatter UltraViolet (TOMS/SBUV), the Aura Ozone Monitoring Instrument in combination with Aura Microwave Limb Sounder (OMI/MLS), the Measurements Of Pollution In The Troposphere (MOPITT), the Global Ozone Monitoring Experiment (GOME), and the SCanning Imaging Absorption spectroMeter for Atmospheric CHartographY (SCIAMACHY). Other satellite-based data include the MODIS-derived cloud droplet number concentration (CDNC) and cloud liquid water path (LWP) from the University of Wisconsin-Madison (UW-M), which are derived based on Bennartz (2007).

Regional observational networks include the Clean Air Status and Trends Network (CASTNET), the Interagency Monitoring of Protected Visual Environments (IMPROVE), and the Speciation Trends Network (STN) over CONUS; the European Monitoring and Evaluation Program (EMEP), the Base de Données sur la Qualité de l'Air (BDQA), and the European air quality database (AirBase) over Europe; the Ministry of Environmental Protection of China (MEPC), the National Institute for Environmental Studies of Japan (NIESJ), Taiwan Air Quality Monitoring Network (TAQMN), and the Korean Ministry Of Environment (KMOE) over East Asia. Traffic and industrial sites from AirBase and BDQA are excluded for the chemical evaluation because the horizontal grid resolution used in this work is too coarse to reproduce observations at those sites.

3.3.3 Evaluation Protocols

The protocols for performance evaluation include spatial distributions and statistics, following the approach of Zhang et al. (2012). The analysis of the performance statistics focuses on mean bias (MB), normalized mean bias (NMB), normalized mean error (NME), root mean square error (RMSE), and correlation coefficient (Corr.). The meteorological and radiative variables are evaluated annually or seasonally, including temperature at 2-m (T2), specific humidity at 2-m (Q2), and wind speed at 10-m (WS10) from NCDC; vertical temperature profile, vertical relative humidity (RH) profile, and vertical specific humidity (Q) profile from NCEP/NCAR reanalysis data; total daily precipitation rate (Precip) from GPCP; outgoing longwave radiation (OLR) from NOAA/CDC; downwelling shortwave radiation (FSDS), downwelling longwave radiation (FLDS), surface net shortwave flux (FSNS), surface net longwave flux (FLNS), shortwave cloud forcing (SWCF), and longwave cloud forcing (LWCF) from CERES; cloud fraction (CF), aerosol optical depth (AOD), cloud optical thickness (COT), precipitating water vapor (PWV), and CCN from MODIS; and CDNC and LWP from UW-M. CDNC is calculated as an average value of layers between 850 and 960 mb for comparison with the satellite-derived values of UW-M. Surface chemical predictions are evaluated against various observational sites from each network (see Table 3.3). Chemical concentrations evaluated include seasonal and annual averaged concentrations of CO, ozone (O_3), SO_2, NH_3, nitrogen dioxide (NO_2), HNO_3, particulate matter (PM) with aerodynamic diameter less than 10 μm (PM_{10}) and 2.5 μm ($PM_{2.5}$), and its major components (i.e., SO_4^{2-}, NO_3^-, NH_4^+, BC, OC, and total carbon (TC) for CONUS and Europe). The chemical observations over East Asia are very limited, and only include surface concentrations of CO, SO_2, NO_2, O_3, and PM_{10}. Column concentrations of tropospheric CO,

NO_2, SO_2, and formaldehyde (HCHO), and tropospheric O_3 residual (TOR) are evaluated for the globe. Following the regions suggested by Rausch et al. (2010), interannual variations of PM, column CCN at supersaturation of 5% (CCN5), AOD, and SWCF are analyzed over the marine stratocumulus regions of near Australia (AUS, 30^oS-40^oS, 88^oE-103^oE), North America (NAM, 15^oN-35^oN, 115^oW-140^oW), South East Asia (SEA, 0^oN-40^oN, 105^oW-150^oW), Southern Africa (SAF, 5^oS-25^oS, 10^oW-15^oE), and South America (SAM, 8^oS-28^oS, 70^oW-90^oW).

Model performance is also compared with CESM1-CAM5 ensemble simulations under historical and Representative Concentration Pathway (RCP) 4.5 scenarios from CMIP5. All observational data used for evaluating 2001-2010 simulations were based on 2001-2010 except for several variables with data during a limited time period including LWP from UW-M (2001-2008), chemical observations from KMOE (2006-2010), tropospheric SO_2 from SCIAMACHY (2005-2010), tropospheric HCHO from GOME (2001-2002) and SCIAMACHY (2003-2010), TOR from TOMS/SBUV (2001-2004) and OMI/MLS (2005-2010), and tropospheric NO_2 from GOME (2001-2002) and SCIAMACHY (2003-2010).

3.4 Model Evaluation and Intercomparison

3.4.1 Evaluation of Improved CESM/CAM5.1

Table 3.4a shows the statistical performance for major meteorological and radiative variables and Figure 3.1 shows the absolute differences between model simulation and observations/reanalysis data averaged for 2001-2010. Compared with NCDC observations, meteorological variables such as T2, Q2, and WS10 are underpredicted by 2.9 ^oC (~ -22.1%), 1.0 g kg^{-1} (~ -11.4%), and 0.4 m s^{-1} (~ -9.7%), respectively, whereas Precip is overpredicted

by 0.1 mm day^{-1} (~ 6.6%), with a correlation coefficient of 0.5 to 0.9. Compared with NCEP data, meteorological variables such as T2 and Q2 are underpredicted by 2.6 ^{o}C (~ -45.1%) and 1.3 g kg^{-1} (~ -15.8%), respectively, whereas WS10 is overpredicted by 2.5 m s^{-1} (~ 58.4%). The underprediction of T2 is mainly due to the underprediction of the heat flux at the surface. As shown in Figure 3.1, there are large discrepancies for T2 between model simulation and the NCEP/NCAR reanalysis data, especially over higher latitudes. There is a large cold bias (> 5 ^{o}C) between 60^{o} N and 90^{o} N, whereas there is a warm bias between 50^{o} S and 70^{o} S. The T2 biases are less than 2 ^{o}C over most continental areas and oceanic areas in the low and middle latitudes. The large underprediction of T2 over higher latitudes is due to the inaccurate predictions of the net flux (FSNS + FLNS) at the surface. Since FSNS represents the heating effect and FLNS represents the cooling effect, the combination of underpredicted FSNS (by 4.8%) and overpredicted FLNS (by 5.7%) contributes to the further underprediction of T2. Compared with NCEP/NCAR reanalysis data, Q2 is underpredicted by 0.5-4.9 g kg^{-1} (1-15%) over most regions except for the Sahara desert, western Asia, Australia, and the western U.S., whereas WS10 is overpredicted by 0.5-7.3 m s^{-1} (20-200%) over most regions especially over oceanic areas in the middle and higher latitudes. Figures 3.2a and b compare meteorological variables with NCEP over North America, South America, Africa, Asia, Europe, and Australia for December-January-February (DJF) and June-July-August (JJA), respectively. Temperature profiles from CESM agree reasonably well with NCEP for both JJA and DJF, despite some discrepancies near the surface for some regions. For example, the temperature near the surface (925 mb) from CESM is about 4 ^{o}C lower than NCEP over Asia (JJA and DJF), Africa (DJF), and North America (DJF). For

other regions, the temperature differences are less than 4 ^{o}C. Specific humidity profiles from CESM agree very well with NCEP for both JJA and DJF over six regions although there are discrepancies (< 1.2 g kg^{-1}) near the surface over Asia, Europe, and North America in JJA. The underprediction of Q2 is likely due to the overprediction of Precip. There are large discrepancies for relative humidity (RH) profiles between CESM and NCEP although their distribution patterns are similar. RH from CESM is overall higher than that from NCEP. The overprediction of RH is likely due to the underprediction of temperature and overprediction of moisture fluxes from overprediction of Precip. The different performance of WS10 against NCDC and NCEP is mainly due to different data pairs used in the model evaluation as well as the different degrees of uncertainties in the observations and reanalysis data. Due to the limited observations, observational sites in NCDC do not cover the entire global domain whereas NCEP data cover each grid cell. It is possible that some grid cells with large biases in NCEP are not taken into account in NCDC due to the unavailability of observations. On the other hand, reanalysis data are processed in global forecast models based on multiple sources of observations. Uncertainties in observations and model treatments can propagate to the reanalysis data. Smith et al. (2001) showed that there was a significant underestimation in near-surface wind speed by NCEP reanalysis data, which can partly explain the overpredictions of WS10.

Radiative variables such as OLR, FSDS, FLNS, FLDS, and FSNS show excellent agreement with observations, with NMBs within ±6%; and SWCF and LWCF show reasonably good agreement, with NMBs of 10.6% and -19%, respectively. All predicted radiation variables show high correlation with observations, with Corr values of 0.9 to 0.99.

While CF is well predicted, moderate overpredictions or underpredictions occur for CDNC, AOD, COT, and LWP, with NMBs of 26.7%, -35.4%, -41.7%, and -31.2%, respectively, and large underpredictions occur for column CCN5 over oceanic areas with an NMB of -82.2%. Due to the underpredictions of cloud variables (e.g., COT, LWP, and CCN5), OLR is slightly overpredicted by 1.4 W m^{-2} (or by 0.7%) and LWCF is underpredicted by 4.4 W m^{-2} (or by 19.4%). As shown in Figure 3.1, CDNC is largely overpredicted by 40-369 cm^{-3} (or by 40-752%) over most oceanic areas, East Asia, Europe, and eastern U.S. Cloud droplet formation is sensitive to both particle number concentration and updraft velocity (Reutter et al., 2009). The overprediction of CDNC is due partly to high activation fractions (e.g., inclusion of adsorption activation from insoluble CCN and effective uptake coefficient of 0.06 by Gantt et al., 2014) as well as the uncertainties in the model treatments for cloud microphysics (e.g., resolved clouds and subgrid-scale cumulus clouds) and satellite retrievals (e.g., error propagation of the input variables to derive CDNC) (Bennartz, 2007). For example, a constant condensation coefficient of water vapor with a value of 0.06 is used to determine size-dependent water vapor diffusivity in FN05. However, this value is uncertain and may vary by a factor of five for pure water (i.e., 0.1-0.3) (Ghan et al., 2011; FN05). It varies from 0.04 to 0.06 for aged atmospheric droplet and can be further reduced by the presence of organic films (Chuang, 2003; Ghan et al., 2011; FN05). In K09, empirical constants of A_{FHH} (e.g., 2.25 used in this work) and B_{FHH} (e.g., 1.20 used in this work) are used to determine the water vapor saturation ratio of an insoluble particle in equilibrium with surrounding water vapor. However, A_{FHH} and B_{FHH} have been found to vary from 0.1 to 3.0 and from 0.5 to 3.0, respectively, from experimental studies (Sorjamaa and Laaksonen, 2007; K09). Therefore,

these constant parameters used in this work may contribute to the uncertainties in predicting CDNC. On the other hand, MODIS is known to provide very high values for the retrieved effective radius, especially over those remote oceanic areas that are dominated by broken cumulus clouds. This possibly is a retrieval artifact caused by cloud inhomogeneites (Zhang and Platnick, 2011) or drizzle/rain contamination (Nakajima et al., 2010). Such a high bias in effective radius would result in an underestimation of MODIS-derived CDNC, which is based on the retrieved MODIS effective radii (Bennartz, 2007). The statistical evaluation of CDNC over land and oceanic areas indicates that most overpredictions occur over ocean, due mainly to the underestimated MODIS-CDNC. The underpredictions of AOD over oceanic areas can be attributed to the uncertainties in the sea-salt emissions as well as inaccurate predictions of other PM components (e.g., marine organic aerosols) over the ocean and overestimation of oceanic AOD in the MODIS collection 5.1 (Levy et al., 2013). COT is largely overpredicted by 5-77 (or by 20-529%) over Southeast Asia, South Africa, South America, and northern Australia, and slightly overpredicted over western Europe and eastern U.S., whereas it is largely underpredicted by 10-48 (or by 50-100%) over continents of 50^{o} N - 90^{o} N and regions within 60^{o} S - 90^{o} S. Overpredictions in CDNC and COT can increase cloud albedo and therefore, increase SWCF, leading to its overpredictions by 10-99.6 W m^{-2} (or by 20-250%) mainly over the low and middle latitudes. The underpredictions in COT and LWP may be caused by limitations and uncertainties associated with the microphysics treatments for resolved and cumulus clouds. The large underpredictions of LWP and COT over polar regions can be also attributed to the uncertainties in plane-parallel visible-near-infrared retrievals with low solar zenith angle (Seethala and Horváth, 2010) as well as the

influence of radiatively active snow on overlying cloud fraction (Kay et al., 2012). Underpredictions in COT can decrease SWCF as well, leading to underpredictions of SWCF over higher latitudes. The opposite performance of CDNC (overprediction) and COT (underprediction) is likely due to the fact that COT (i.e., mixed-phase clouds) is affected by both aerosol activation and ice nucleation (Lance et al., 2011; Xie et al., 2013). CDNC is evaluated between 850 and 950 mb, whereas COT is evaluated over entire model layers. Uncertainties in ice clouds predictions can result in uncertainties in COT predictions. The moderate and poor correlation coefficients of cloud variables (e.g., CCN5, COT, CDNC, and LWP) suggest the uncertainties both in the model treatments for microphysics and in the satellite retrievals.

Figures 3.3-3.5 compare AOD, CDNC, and SWCF with observations for the 10-year average of 2001-2010 (ANU), December-January-February (DJF), March-April-May (MAM), June-July-August (JJA), and September-October-November (SON). AOD is underpredicted over most regions except North Africa, the tropical Atlantic Ocean, and West Asia for MAM, JJA, and SON. The model captures the hot spots for observed AOD over East Asia, North Africa, the tropical Atlantic Ocean, and West Asia (e.g., in MAM and JJA), whereas it fails to predict the hot spot for South Africa in SON. The hot spots for AOD are mainly due to the high concentration of dust, indicating the uncertainties in the dust emissions. The underprediction of AOD over 40^{o}S - 70^{o}S is mainly due to a bias in satellite products (i.e., MODIS Collection 5.1), which does not account for the wind speed-dependent whitecap and foam fraction on the ocean surface (Levy, 2013). Unlike AOD, CDNC is overpredicted over most regions. The model can also capture the hot spots for observed

CDNC over Europe, East Asia, and East U.S. (e.g., in DJF, MAM, and SON). The hot spots for CDNC are mainly due to the high PM concentrations over those regions. The overpredictions of CDNC are likely due to uncertainties in the treatment of insoluble CCN activations (e.g., BC and dust) and effective uptake coefficient used for aerosol activation as well as the uncertainties in the model treatments for cloud microphysics (e.g., resolved clouds and subgrid-scale cumulus clouds) and satellite retrievals as discussed previously. Similar to CDNC, SWCF is also overpredicted in all seasons especially over oceanic areas in low and middle latitudes as well as land areas such as East Asia, eastern U.S., Europe, South America, South Africa, and Australia. Due to the overpredictions of CDNC over these regions, cloud albedo increases and more solar radiation is reflected, resulting in overpredictions of SWCF. However, SWCF over polar regions is underpredicted, especially in JJA. The underpredictions of SWCF over the polar regions are likely due to the underpredictions of COT over those regions (see Figure 3.1).

Table 3.4b shows the statistical performance for major chemical species and Figure 3.6 compares simulated and observed surface concentrations of chemical species over various sites from different surface networks including CASTNET, IMPROVE, EMEP, MEPC, TAQMN, and NIESJ. CO mixing ratios and NO_2 concentrations over East Asia are largely underpredicted with NMBs of -56.1% and -82.7%, respectively; these results are likely due to uncertainties in the CO and NO_x emissions over this region. SO_2 concentrations are moderately underpredicted with absolute NMBs less than 20% over Europe (but the NMBs can be as high as 244.7% over the EMEP sites as shown in Figure 3.6) and East Asia (with an NMB of 18% over the NIESJ sites), but largely overpredicted with an NMB of

219.1% over CONUS (with an NMB of 244.7% over the CASTNET sites), which is likely due to uncertainties in the SO_2 emissions and wet deposition, and measurements. He and Zhang (2014) investigated the sensitivity of the chemical predictions to emissions; the results showed that with a 30% reduction in SO_2 emissions, the NMB of SO_2 predictions is reduced by about half, from 291.8% to 152.2%. Precip is also underpredicted over the middle/eastern U.S., resulting in less SO_2 wet deposition. NO_2 concentrations are largely underpredicted over Europe, with an NMB of -77.7%, whereas NH_3 and HNO_3 concentrations are overpredicted over Europe, with NMBs of 31.9% and 41.8%, respectively The biases of predictions in NH_3 and NO_2 concentrations could be due to the uncertainties in NH_3 and NO_x emissions. The overprediction of HNO_3 over Europe is likely due in part to overestimated oxidation of NO_2 resulted from overestimated OH concentrations, and/or underestimated dry deposition of HNO_3. FSNS is overpredicted over Europe (see Figure 3.1), allowing more photolytic reactions to produce OH (e.g., photolytic reactions of O_3 and VOCs), and therefore more OH can oxidize NO_2 to produce HNO_3. In addition, the observed surface OH concentrations vary from 0 to 6 $\times 10^6$ molecules cm^{-3}, with a mean maximum value of 4.2×10^6 molecule cm^{-3} in summer over Europe (Michoud et al., 2012). The summer (JJA) average of simulated OH over Europe is about 0.05-0.35 ppt (or 1-7 $\times 10^6$ molecules cm^{-3}),indicating possible OH overpredictions. O_3 concentrations are predicted reasonably well over CONUS with an NMB of 16.2%, whereas they are largely overpredicted over Europe and East Asia, with NMBs of 47.8% and 48.5%, respectively. As shown in Figure 3.6, surface O_3 is overpredicted by 5.7 ppb (or by 16.2%) over the CASTNET sites, whereas it is overpredicted by 15 μg m^{-3} (or by 23.0%) over the EMEP sites and overpredicted by 10.5

ppb (or by 36.6%) over the TAQMN sites. The overpredictions of O_3 over Europe and East Asia are likely due to the underprediction of O_3 titration resulting from the underprediction of NO_x. SO_4^{2-} concentrations are predicted reasonably well over CONUS and Europe, whereas NH_4^+ and NO_3^- concentrations are overpredicted over these regions, with NMBs of 37.4-59.8% to 44.8-93.2%. The overpredictions of HNO_3 concentrations over CONUS and Europe result in the overpredictions of NO_3^- concentrations over these regions. The overpredictions of NH_4^+ concentrations over CONUS and Europe are due possibly to the uncertainties in NH_3 emissions as well as overpredictions of HNO_3 over these regions, which can partition into NO_3^- to neutralize excess NH_4^+ through thermodynamic equilibrium. Cl^- concentrations are well predicted over CONUS but are largely overpredicted over Europe with an NMB of 376.0%, which is likely due to the uncertainties in the HCl and sea-salt emissions as well as treatments for coarse particulate chloride. The model only treats gas/particle equilibrium thermodynamics for fine inorganic particles and the condensation of major inorganic volatile gases (e.g., H_2SO_4, NH_3, HNO_3, and HCl) onto all aerosol modes is treated as irreversible, which can result in overpredictions of inorganic aerosol concentrations in the coarse mode, thus overpredictions of inorganic aerosol concentrations over all the modes (e.g., NH_4^+, NO_3^-, and Cl^- over Europe). The concentrations of OC, BC, and $PM_{2.5}$ are well predicted over CONUS, with absolute NMBs less than 16% whereas TC concentrations are underpredicted with an NMB of 37.9%. The discrepancy between OC/BC and TC performance is mainly due to the different observational datasets used for the evaluation. The OC observations are from IMPROVE, whereas BC and TC observations are from IMPROVE and STN. $PM_{2.5}$ and PM_{10} concentrations are moderately underpredicted over Europe and East Asia, with an NMB of -

37.2% to -6.3%. As shown in Figure 3.6, the surface $PM_{2.5}$ concentration is underpredicted by 1.0 μg m^{-3} (or by 16.1%) over the IMPROVE sites and underpredicted by 1.3 μg m^{-3} (or by 11.2%) over the EMEP sites, whereas the surface PM_{10} concentration is underpredicted by 39.25 μg m^{-3} (or by 36.2%) over the MEPC sites. The underpredictions of $PM_{2.5}/PM_{10}$ are likely due to the underpredictions of organic aerosol concentrations. The underpredictions of organic aerosol concentrations can be attributed in part to the uncertainties in the VOCs and OC emissions. Several studies indicated the uncertainties in the emission data used over CONUS, Europe, and Asia. For example, power plant and industry NO_x emissions over eastern U.S. have decreased by 50% between 1999 and 2003/2004 (Frost et al., 2006; Hudman et al., 2007). It is not clear whether the U.S. National Emission Inventory has included such information. Langmann et al. (2008) suggested an updated emission by considering the changes in heating practices in Europe to improve the SOA predictions. The anthropogenic NO_x emissions over mainland China have increased from 3.8 TgN yr^{-1} in 2000 (Zhang et al., 2007) to 6.3 TgN yr^{-1} in 2006 (Zhang et al., 2009). Emission inventories over all those regions, on the other hand, are not updated on a yearly basis. For example, the U.S. EPA updates the NEI every 3-4 years. In this work, emissions during 3 years, i.e., 2001, 2005, and 2008 are used to represent emissions for 2001-2010 based on the best available emissions from global and regional emission inventories. The lack of yearly varied emissions may lead to some inaccuracies in representing the emission interannual variations of the individual species, and therefore explaining some uncertainties in the model predictions. In He and Zhang (2014), a sensitivity simulation with emission adjustment was conducted to investigate the impacts of emissions on model predictions, which indicated that

anthropogenic emissions on major chemical species, such as CO, SO_2, NO_2, NH_3, OC, and BC have significant impacts on the model predictions. The underpredictions of organic aerosol concentrations may also be attributed in part to the uncertainties in the model treatments for SOA formation. The current VBS representation for SOA formation included in this work only includes biogenic VOCs and anthropogenic VOCs partitioning in both the gas- and the condensed phases without consideration of SVOC and aging and volatility of POA. Including SVOC emissions and their subsequent oxidation has been shown to have a considerable impact on OC predictions over Europe (Couvidat et al., 2012, 2013a). Furthermore, the aqueous-phase oxidation of VOCs in clouds is not taken into account; although it is not a major SOA formation pathway, it can contribute several % in some areas and seasons over Europe (Couvidat et al., 2013b).

The global tropospheric SO_2 column is underpredicted with NMB of -28.4%, which is likely due to uncertainties in SO_2 emissions. Tropospheric CO and NO_2 columns are largely overpredicted whereas surface concentrations of CO and NO_2 are underpredicted, suggesting the uncertainties in CO and NO_2 emissions in terms of spatial allocations as well as convective transport treatments. The global TOR is slightly underpredicted with an NMB of -3.5%. The global tropospheric HCHO column is largely underpredicted with an NMB of -44.6%, which is likely due partly to no biogenic HCHO emissions as well as uncertainties in biogenic isoprene emissions and its secondary HCHO formation. Figure 3.7 shows emission trends for SO_2, NH_3, NO_x, primary OC (POC), and BC. Emissions of SO_2, NH_3, and POC decrease from 2001 to 2008, whereas CO and NO_x emissions are higher in 2005 than 2001 and 2008, and BC emissions are lower in 2005 than 2001 and 2008. The corresponding

aerosol burdens such as SO_4^{2-}, NH_4^+, NO_3^-, OC, and BC have strong correlations with the emission trends of SO_2, NH_3, NO_x, OC, and BC, respectively, due to the impacts of emissions on aerosol predictions. Meanwhile, other processes can affect chemical species predictions, such as kinetic reactions, condensation, and dry/wet deposition. For example, the reaction rate for oxidation of CO by OH is likely to decrease due to underpredictions of temperature, resulting in smaller loss of CO and OH and higher CO column concentrations. In addition, the uncertainties in the model treatments for dry and wet deposition can result in uncertainties in the removal of chemical species through those processes. For example, precipitation is underpredicted over 30^o N - 60^o N, which can result in overpredictions of chemical concentrations in this region, whereas it is overpredicted over 30^oS - 30^oN, which can result in underpredictions of chemical concentrations. The accommodation coefficients are usually measured under laboratory conditions, therefore, uncertainties may exist when they are extrapolated to ambient atmospheric conditions to simulate the formation of secondary aerosols through condensation of gaseous precursors under different atmospheric conditions and at the global scale.

Table 3.5 shows the simulated 10-year average global burdens of major gaseous and aerosol species for three emission periods. The global burdens of some gaseous species (e.g., tropospheric O_3, HCHO, NO_x, and NO_y, and total column of DMS, SO_2, and NH_3) are within 25% of differences comparing with previous studies, whereas there are large differences for other gaseous species such as CO, H_2SO_4, and HNO_3. Compared with the results of He and Zhang (2014), the 10-yr mean global CO burden is about 105.5% higher but that of H_2SO_4 burden is about 69.5% lower in this work. The higher CO burden is likely due to the different

kinetic reaction rate calculation for CO+OH used in this work, which is based on superfast chemistry in default CAM5. However, it turned out there was a typographical error in the rate constant for CO+OH in default CAM5 (Lamarque et al., 2013, supporting information), which could result in underprediction of CO loss from CO+OH and overprediction of CO burden. Precipitation, especially over 30^{o} N - 60^{o} N (e.g., Europe and the middle/eastern U.S.), is underpredicted by 10-50%, resulting in low wet deposition. The reaction rate of oxidation CO by OH is affected by temperature and pressure. Temperature is underpredicted, decreasing the reaction rate of oxidation, which is likely to increase the CO burden. The lower H_2SO_4 burden is due to greater condensation of H_2SO_4 resulting from a larger mass accommodation coefficient of 0.1 compared to the value of 0.02 that was used by He and Zhang (2014). However, compared with other studies, the H_2SO_4 burden is still relatively higher (e.g., a mass accommodation coefficient of 0.65 is used in Liu et al., 2012), indicating the uncertainties in the H_2SO_4 condensation associated with its mass accommodation coefficient. The HNO_3 burden in this work is comparable with that from He and Zhang (2014), but it is about 76% lower than William et al. (2009). The lower HNO_3 burden is likely due in part to the uncertainties in the NO_x emissions and overprediction of Precip in the low and middle latitudes.

As shown in Figure 3.7, chemical burdens are strongly correlated with emissions. In Table 3.4, the SO_4^{2-} and NH_4^{+} burdens decrease during 2001-2010, whereas the NO_3^{-} burden increases from 2001-2003 to 2004-2006 and then decreases to 2007-2010. Most inorganic aerosol burdens are in the range of previous studies except those of SO_4^{2-} and NH_4^{+}. The SO_4^{2-} burden is slightly lower, which is likely due to the lower SO_2 emissions compared to

the study of Liu et al. (2012) and missing SO_4^{2-} emissions. The lower SO_4^{2-} burden results in lower NH_4^+ burden. Compared with Horowitz et al. (2006), global burdens of BC and OC are lower by 76.1% and 59.4%, respectively. Compared with Liu et al. (2012), global burdens of BC, primary organic matter (POM), and SOA are lower by 28.5%, 48.5%, and 89.6%, respectively. The lower BC, OC, POM, and SOA burdens are likely due to uncertainties in the BC and OC emissions used in the model as well as differences in the model treatments for SOA formation and POM aging. For example, Liu et al. (2012) used the default CAM5 SOA formation treatments, whereas the VBS representation of SOA formation is included in this work. Condensation onto the primary carbon mode produces aging of the particles in this mode. A lower accommodation coefficient is used in this work compared to Liu et al. (2012), resulting in less condensation. Therefore, the fraction of aged particles has decreased, which affects BC and POM concentrations.

3.4.2 Impacts of the Anthropogenic Emissions

To quantify the overall impacts of anthropogenic emissions on air quality and climate through atmospheric radiation and aerosol direct/indirect effects, anthropogenic emissions of both gaseous and PM species are reduced by 80% to represent the clean/background chemical conditions. Figures 3.8a-c compare the CESM simulations with baseline emissions and with 20% of anthropogenic emissions from the baseline emissions. Primary aerosols such as BC and OC can be directly affected by the emissions. Secondary aerosols can be affected through chemical reactions and gas-particle partitioning. As shown in Figure 3.8a, with 80% higher anthropogenic emissions, the 10-year average domainwide-mean surface concentrations of SO_4^{2-}, SOA, and POM increase by 0.4 μg m^{-3} (or by 79.8%), 0.07 μg m^{-3}

(or by 86.0%), and 0.23 μg m^{-3} (or by 81.4%), respectively. As a result, the surface concentrations of $PM_{2.5}$ and PM_{10} increase by 1.1 μg m^{-3} (or by 20.7%) and 1.5 μg m^{-3} (or by 6.1%) in the global mean. The smaller increase of PM_{10} compared to that of $PM_{2.5}$ is mainly due to the changes in online dust and sea-salt emissions through feedbacks from meteorology (e.g., WS10). Aerosol can be activated as CCN and therefore affect cloud properties. With 80% higher anthropogenic emissions, as shown in Figure 3.8b, domainwide column CCN5, CDNC, and COT increase by 2.8×10^{7} cm^{-2} (or by 52.7%), 39.3 cm^{-3} (or by 40.4%), and 1.6 (or by 14.7%) in the global mean. Due to more clouds from more aerosols, domainwide SWCF increases by 3.2 W m^{-2} (or by 3.1%) in the global mean. Because of more reflection from aerosols and clouds, as shown in Figure 3.8c, FSDS decreases by 4.7 W m^{-2} (or by 2.9%), resulting in a domainwide decrease in T2 by 1.0 ^{o}C (or by 47.6%) in the global mean. WS10 is not affected significantly (Figure not shown), but there is a 5% decrease in Precip in the global mean, PBLH is also affected, with increases as large as 101.6 m (or by 24.6%) or decreases as large as 169.2 m (or by 61.7%), and with a net decrease of 2.8 m (or by 0.8%) in the global mean.

3.4.3 Intercomparison of Simulations With Improved CESM/CAM5.1 and Simulations With CMIP5

Figure 3.9 shows the Taylor diagram (Taylor, 2001) comparing the model performance of CESM-NCSU with that of the CESM1-CAM5 output from CMIP5. The similarity between the two patterns is quantified in terms of their correlations (i.e., angle), their standard deviations (i.e., y axis), and the ratio of their variances (i.e., x axis). Compared with CESM-CMIP5, the bias of meteorological variables such as T2 and Q2 predicted by

CESM-NCSU are larger whereas the bias of WS10 is similar and the bias of Precip is smaller. The larger biases of T2 and Q2 in CESM-NCSU are mainly due to the perturbations to the climate system resulting from higher aerosol concentrations as well as higher cloud predictions in CESM-NCSU. The bias of radiative variables from CESM-NCSU and CESM-CMIP5 are within the same range except for OLR, which shows a smaller bias in CESM-NCSU. The biases of CF, LWP, and AOD are smaller in CESM-NCSU than in CESM-CMIP5. The standardized deviations of most variables are lower in CESM-CMIP5 than in CESM-NCSU, especially for LWP and AOD. The lower standard deviation in CESM-CMIP5 is likely due to the lower variability from CESM-CMIP5 ensemble simulations. Compared with observations, the correlation coefficients for LWP and AOD are higher in CESM-NCSU than in CESM-CMIP5. The different model performance between CESM-NCSU and CESM-CMIP5 indicates the sensitivity of the climate system to perturbations in different model inputs (e.g., emissions) and model configurations (e.g., prescribed chemistry used in CESM-CMIP5 simulations), as well as the effect of the incorporation of new model treatments in CESM-NCSU.

Figure 3.10 compares zonal mean predictions from CESM-NCSU with CESM-CMIP5 against observations or reanalysis data. T2 and Q2 predicted by CESM-NCSU overall agree well with those by CESM-CMIP5, although T2 and Q2 from CESM-NCSU are lower than those from CESM-CMIP5 in tropical regions and the Northern Hemisphere. Compared with NCEP, the biases of T2 and Q2 from CESM-CMIP5 are smaller than those from CESM-NCSU. Precipitation predicted by CESM-NCSU overall agrees well with those predicted by CESM-CMIP5, although Precip from CESM-NCSU is lower than that from

CESM-CMIP5 in 30^{o} N - 60^{o} N. Compared with NCEP, the bias of Precip from CESM-CMIP5 is smaller than that from CESM-NCSU. Both CESM-NCSU and CESM-CMIP5 underpredict FSDS over tropical regions by 5-30 W m^{-2}. Compared with CERES observations, FLDS from CESM-NCSU is overall underpredicted (especially over higher latitudes in the Southern Hemisphere and the entire Northern Hemisphere), whereas CESM-CMIP5 underpredicts FLDS mainly over higher latitudes in the Northern Hemisphere (Figure not shown). The underpredictions of FLDS and FSDS result in the underprediction of T2. OLR from CESM-NCSU overall agrees well with that from CESM-CMIP5, although it is about 5-10 W m^{-2} lower in the Northern Hemisphere. Compared with NOAA/CDC observations, the bias of OLR (1.5 W m^{-2}) from CESM-NCSU is smaller than that from CESM-CMIP5 (5.8 W m^{-2}).

CF from CESM-NCSU agrees well with that from CESM-CMIP5, although it is higher in Northern Hemisphere, especially over the North Pole. Compared with MODIS data, CF from CESM-NCSU and CESM-CMIP5 are lower over low-mid latitudes whereas they are higher over the polar regions. AOD predicted by CESM-NCSU is higher over 10^{o}N - 40^{o} N but agrees better with satellite observations than CESM-CMIP5, due in part to higher dust concentrations in CESM-NCSU. However, AOD is still underpredicted especially over 50^{o} S - 90^{o} S and 40^{o} N - 90^{o} N. The underprediction of AOD can be due to the uncertainties in the optical properties and uncertainties in predictions of aerosol concentrations as well in the retrievals of oceanic AOD from MODIS data. The aerosol optical properties are defined for each mode of the MAM as described by Ghan and Zaveri (2007). Hygroscopicity characteristics are specified for soluble species. For each shortwave band calculation, aerosol

extinction, single scattering albedo, and asymmetry parameter are specified. For each longwave band, mass specific absorption is specified. These optical properties are species-dependent. Composition of organic aerosol and soil dust is highly complex and variable, resulting in uncertainties in their optical properties. All such uncertainties can contribute to the uncertainty in AOD predictions. While simulated and observed SWCF agree reasonably well, large discrepancies exist between observed CDNC, COT, and LWP and simulated values from CESM_NCSU, in particular, in the polar regions. This can be attributed in part to the bias in these variables from MODIS at high latitudes and model's limitation in simulating cloud-related treatments.

Figure 3.11 shows the comparison of spatial distributions of T2, Precip, AOD, and FSDS from observations, CESM-CMIP5, and CESM-NCSU. Compared with NCEP/NCAR reanalysis data, T2 from CESM-CMIP5 agrees better than that from CESM-NCSU especially over the tropical ocean (e.g., tropical Indian Ocean and tropical Pacific Ocean). T2 from CESM-NCSU is underpredicted ($< 2\ ^{o}C$) over these regions, which is due to the underpredictions of SST. The underprediction of SST is due partly to the underprediction of FSDS as well as the uncertainties in the ocean initial conditions. Precip from CESM-CMIP5 and CESM-NCSU agree well with that from GPCP. However, both CESM-CMIP5 and CESM-NCSU overpredict the Intertropical Convergence Zone (ITCZ) in the Northern Hemisphere and predict another ITCZ around 5-15^{o}S. The double ITCZ has been identified as a systematic error in most climate models, including those CMIP5 models. FSDS from CESM-CMIP5 and CESM-NCSU agree well with that from CERES. However, both CESM-CMIP5 and CESM-NCSU underpredict FSDS by 5-10 W m^{-2} over the tropical oceans, which

is likely due to the overprediction of CDNC over these regions. Both CESM-CMIP5 and CESM-NCSU capture hot spots for observed AOD over the Sahara and the Mediterranean Sea, whereas CESM-CMIP5 failed to predict AOD over East Asia and CESM-NCSU largely underpredicted AOD over most oceanic areas. The large underprediction of AOD is mainly due to the inaccurate predictions of aerosol concentrations.

3.5 Interannual Variability

Figure 3.12a shows the time evolution along with interannual variations of tropospheric column mass abundances of ozone, NO_2, HCHO, and $PM_{2.5}/PM_{10}$ over AUS, NAM, SAF, SAM, and SEA, and Figure 3.12b shows similar plots for AOD, column CCN5, CDNC, and SWCF over the same five regions. The model in general can capture the interannual variations of tropospheric ozone column and NO_2, column with some exceptions (e.g., TOR over SAF and SAM, and column NO_2 over AUS and NAM). Compared with TOMS/SBUV and OMI/MLS data, the tropospheric ozone column is relatively well predicted over AUS, where it is slightly overpredicted over NAM and SEA and largely underpredicted over SAF and SAM. The correlation between simulated and observed time evolution of TOR is relatively well over AUS and SEA. The TOMS/SBUV and OMI/MLS data show decreases of TOR during 2001-2010 over NAM and SEA indicated, however, the model fails to predict the decreasing trend over NAM but captures the decreasing trend over SEA. Compared with the SCIAMACHY data, the tropospheric NO_2 column is slightly overpredicted over SAM and SEA and largely overpredicted over AUS and NAM. The tropospheric NO_2 column is much higher over SEA than other regions, which is mainly due to the higher NO_x emissions over this region. The correlation of simulated and observed time

evolution of tropospheric NO_2 column is relatively good over SAF, SAM, and SEA. The SCIAMACHY data indicate an increasing trend of tropospheric NO_2 over SEA during 2001-2010, which is also captured in the model. Compared with the GOME and SCIAMACHY data, the correlation of simulated and observed time evolution of tropospheric HCHO column is relatively poor over AUS, NAM, SAF, and SAM. The HCHO column increases over AUS, SAF, and SAM during 2001-2010, but the model fails to capture this trend. While the model can capture interannual variations of tropospheric HCHO column in terms of the annual crests over SEA, it largely underpredicts the annual troughs. The model largely underpredicts tropospheric HCHO column over all five regions, which is mainly due to the uncertainties in the emissions of HCHO and its precursors (e.g., biogenic emissions) as well as HCHO retrievals.

The $PM_{2.5}/PM_{10}$ burdens over SAF and SEA are higher than those over AUS, NAM, and SAM, with mean concentrations of 21.3/66.8 and 27.7/67.5 mg m^{-2}, respectively. The higher PM burden with mass fraction of coarse particles of 68.1% over SAF is mainly due to the dust emissions, whereas the higher PM burden with a mass fraction of coarse particles of 59.0% over SEA is due partly to the emissions of dust, sea-salt, and higher anthropogenic emissions. The higher mass fraction of coarse particles over AUS, NAM, and SAM are mainly from sea-salt over oceanic areas. Higher PM burdens result in higher AOD and column CCN5.

The interannual variations of PM, column CCN5, and AOD over AUS, NAM, and SAM are not as strong as those over SAF and SEA. The variability of $PM_{2.5}/PM_{10}$ is larger over SAF and SEA than AUS, NAM, and SAM, with standard deviations (SD) of 3.4/6.7 and

3.1/9.6, respectively. Variation of AOD and column CCN5 over SAF and SEA correlates strongly with PM, whereas CDNC does not always correlate with PM, which is likely due to the impacts from other processes such as droplet nucleation, evaporation, and precipitation. Compared with MODIS data, the model can capture the interannual variations of AOD and CCN5, although the model underpredicts the magnitudes of AOD and CCN5 over most regions. The underpredictions of AOD over SAF and SEA are mainly due to the uncertainties in the model treatment of dust emissions. The underpredictions of CCN5 are mainly due to the underpredictions of PM as well as uncertainties in the cloud microphysics. Compared with the MODIS-derived CDNC data, the model in general can capture the interannual variations of CDNC, however, it largely overpredicts CDNC over all five regions. The overpredictions of CDNC are mainly due to the uncertainties in the model treatment (e.g., aerosol activation and cloud microphysics) as well as satellite data retrieval that have been discussed previously. Compared with the CERES data, the model can capture the interannual variation of SWCF very well over all five regions, although it slightly to moderately overpredicts SWCF over NAM and SEA. The variability of SWCF is larger over AUS and NAM than SAF, SAM, and SEA, with SD of 4.7 and 5.5, respectively, whereas the mean SWCF is higher in NAM, SAM, and SEA, with regional mean of -75.5 W m^{-2}, -72.2 W m^{-2}, and -78.4 W m^{-2}, respectively. The variability of SWCF does not necessarily correlate with CDNC, which is mainly due to impacts from other cloud variables such as COT.

3.6 Conclusions

In this work, a comprehensive evaluation has been conducted through applying CESM/CAM5.1 with advanced chemistry-aerosol-cloud interactions treatments for

retrospective decadal simulations during 2001-2010. Meteorological and radiative variables are overall well predicted with NMBs of --14.1% to -9.7% and 0.7% to 10.8%, respectively, except T2, which is underpredicted by 22.2% compared to NCDC and 45.1% compared to NCEP/NCAR reanalysis data CF and PWV are well predicted, with NMBs of -10.5% to 0.4%, whereas CCN, LWP, and COT are moderately-to-largely underpredicted, with NMBs of -82.2% to -31.2%, and CDNC is overpredicted by 26.7%, suggesting the uncertainties in the model treatments for cloud microphysics (e.g., resolved and subgrid-scale cumulus clouds) and/or satellite retrieval algorithms (e.g., error propagations in deriving cloud variables and plane-parallel visible-near-infrared retrievals with low solar zenith angle).

Concentrations of SO_4^{2-}, Cl^-, OC, and $PM_{2.5}$ are relatively well predicted over CONUS with NMBs of -12.8% to -1.18%, whereas O_3 concentrations over CONUS are slightly overpredicted with an NMB of 16.2% and BC concentrations are slightly underpredicted with an NMB of -15.6%. Surface O_3 mixing ratios (or concentrations) are overpredicted by 5.7 ppb (or by 16.2%) over the CASTNET sites, by 15 μg m^{-3} (or by 23.0%) over the EMEP sites, and by 10.5 ppb (or by 36.6%) over the TAQMN sites. Concentrations of SO_2, SO_4^{2-}, and PM_{10} are relatively well predicted over Europe with NMBs of -20.8% to -5.2%. The surface $PM_{2.5}$ concentrations are underpredicted by 1.0 μg m^{-3} (or by 16.1%) over the IMPROVE sites and by 1.3 μg m^{-3} (or by 11.2%) over the EMEP sites, and the surface $PM_{10\ 5}$ concentrations are underpredicted by 39.25 μg m^{-3} (or by 36.2%) over the MEPC sites. SO_2 concentrations are relatively well predicted over East Asia with an NMB of -18.2%. TOR is well predicted over the globe with an NMB of -3.5%. Large biases for some chemical predictions can be attributed to uncertainties in the emissions and

model treatments. For example, SO_2 concentrations over CONUS are largely overpredicted, which is likely due to uncertainties in the SO_2 emissions and measurements, as well as less SO_2 wet deposition from underpredictions of Precip. SO_2 and PM_{10} over East Asia are underpredicted, which is likely due to uncertainties in the emissions of SO_2, PM constituents (e.g., POC, dust, and sea-salt) as well as other PM precursors. O_3 concentrations are overpredicted over Europe and East Asia, likely due to the underprediction of O_3 titration, resulting from underprediction of NO_x concentrations. The model only treats thermodynamics for fine inorganic particles and condensation is treated irreversible, which can result in overpredictions of inorganic aerosol concentration in coarse modes, and therefore inorganic aerosol concentrations over all the modes (e.g., NH_4^+, NO_3^-, and Cl^- over Europe). OC is typically underpredicted. Uncertainties in emissions of SVOCs could be a major cause of those underpredictions. Comparisons of the CESM simulation with baseline emissions and 80% reduced anthropogenic emissions indicate the significant impacts of anthropogenic emissions on radiation and climate predictions. With 80% higher anthropogenic emissions, FSDS can decrease by 4.7 W m^{-2} (or by 2.9%) domain-wide mean and as large as 14.6 W m^{-2} (or by 18.3%), and SWCF can increase by 3.2 W m^{-2} (or by 3.1%) in the global mean, and as large as 21.1 W m^{-2} (or by 68.7%). These results indicate the important role of anthropogenic emissions in the climate system and a need to develop co-benefited emission control strategies for air pollution control and climate mitigation.

Most meteorological and radiative variables predicted by CESM-NCSU overall agree well with those by CESM-CMIP5, although the bias of T2 from CESM-NCSU is larger than that from CESM-CMIP5. AOD predicted by CESM-NCSU is higher but agrees better with

satellite observations than AOD from CESM-CMIP5, due in part to higher dust concentrations in CESM-NCSU. Model inputs (e.g., emissions and ocean initial conditions), model configurations as well as model treatments differ between CESM-NCSU and CESM-CMIP5; these differences can result in different perturbations in the climate system, and thus different meteorology and radiation predictions.

The model can generally predict the interannual variations of major chemical species, such as tropospheric O_3 column and tropospheric NO_2 column with some exceptions (e.g., tropospheric O_3 over SAF and SAM, and NO_2 over AUS and NAM). The correlation of time series of tropospheric O_3 is relatively well over AUS and SEA and the model can capture the decreasing trend of tropospheric O_3 over SEA during 2001-2010. The correlation of time series of tropospheric NO_2 column is relatively good over SAF, SAM, and SEA and the model can capture the increasing trend of tropospheric NO_2 over SEA during 2001-2010. The correlation of time series of tropospheric HCHO column is relatively poor over AUS, NAM, SAF, and SAM and tropospheric HCHO column is largely underpredicted over the five regions. The interannual variations of PM, column CCN5, and AOD indicate the strong correlation of CCN and AOD with PM. CDNC does not always correlate with PM, due to the impacts from other processes such as droplet nucleation, evaporation, and precipitation. Likewise, SWCF does not always correlate with CDNC, due to the impacts from other cloud variables such as COT.

Comparing to CESM-CMIP5, the results from the 2001-2010 decadal simulations of CESM with advanced chemistry/aerosol treatment can provide a more accurate description of the interactions among chemistry, aerosol, and climate in the current atmosphere. It will

therefore be a promising model for current and future decadal climate simulations under various emission scenarios to project climate change with reduced uncertainties associated with such interactions.

Table 3.1. Atmospheric component in the Earth system models

	HadGEM2-ES [a]	GFDL-ESM2 [b]	MPI-ESM [c]	MIT-IGSM-CAM [d]	NCAR-CESM [e]	NCSU-CESM [f]
Atmosphere model	HadGEM2-A [g]	AM2 [g]	ECHAM6 [g]	CAM3 [g]	CAM5 [g]	CAM5 [g]
Gas-phase	O'Connor et al., 2014	Prescribed	Prescribed	Prescribed	(1) Simple chemistry, (2) Emmons et al. (2010), (3) Lamarque et al. (2012)	CB05_GE [g]
Aqueous-phase	SO_2 oxidation by H_2O_2	N.A.[h]	N.A.	N.A.	Barth et al. (2000)	He and Zhang (2014)
Inorganic aerosol	Bellouin et al. (2011)	Prescribed	Prescribed	Prescribed	Liu et al. (2012)	He and Zhang (2014)
SOA	Bellouin et al. (2011)	Prescribed	Prescribed	Prescribed	Liu et al. (2012)	Glotfelty et al. (2013)
Aerosol activation	N.A.	N.A.	N.A.	N.A.	Abdul-Razzak and Ghan (2000)	Gantt et al. (2014)
Supported horizontal resolution	$1.25^o \times 1.875^o$	$2^o \times 2.5^o$	1.9^o	$2^o \times 2.5^o$	$1.9^o \times 2.5^o$, $0.9^o \times 1.25^o$	$0.9^o \times 1.25^o$
Supported vertical layers	38	24	47	26	26, 30	30

[a] HadGEM2-ES: the Hadley Centre Global Environmental Model version 2 including Earth system components (Collins et al., 2011a)

[b] GFDL-ESM2: the Geophysical Fluid Dynamics Laboratory (GDFL) Earth System Model version 2 (Dunne et al., 2012, 2013)

[c] MPI-ESM: the new Max-Planck-Institute Earth System Model (Giorgetta et al., 2013)

[d] MIT-IGSM: the Massachusetts Institute of Technology Integrated Global System Model (Monier et al., 2013)

[e] NCAR-CESM: the National Center for Atmospheric Research Community Earth System Model (Hurrell et al., 2013)

[f] NCSU-CESM: the North Carolina State University Community Earth System Model used in this work

[g] HadGEM2-A: HadGEM2 atmosphere model (Martine et al., 2011); AM2: the Atmospheric Model version 2 (GFDL, Global Atmospheric Model Development Team, 2004); ECHAM6: the 6th generation of atmospheric general circulation developed by the Max Planck Institute for Meteorology (Stevens, et al., 2013); CAM3: Community Atmosphere Model version 3 (Collins et al., 2004); CAM5: Community Atmosphere Mode version 5 (Neale et al., 2012); CB05_GE: the 2005 Carbon Bond mechanism with global extension (Karamchandani et al., 2012).

[h] N.A. - not available, it refers to no description about aerosol activation treatment in the model.

Table 3.2. Sources of emission inventories used for 2001-2010 simulation

Species[1]	Sources[2]	Spatial (Temporal) Resolution	Year	Available Domain
CO_2	Zhang et al. (2012)	$1^o \times 1^o$ (monthly)	2001	Global
	EDGAR v4.2	$0.1^o \times 0.1^o$ (Annual)	2005/2008	Global
	MEIC	36 ×36 km (monthly)	2006/2010	China mainland
CO, NO_x, SO_2, NH_3, ALD2, ETH, ETHA, ETOH, FORM, IOLE, MEOH, OLE, PAR[4], TOL, XYL	Zhang et al. (2012)[3]	$1^o \times 1^o$ (monthly)	2001	Global
	EDGAR v4.2	$0.1^o \times 0.1^o$ (Annual)	2005/2008	Global
	MEIC	36 ×36 km (monthly)	2006/2010	China mainland
	AQMEII-CONUS	36 ×36 km (monthly)	2006/2010	CONUS
	AQMEII-EU	36 ×36 km (monthly)	2010	Europe
BC, OC	Zhang et al. (2012)	$1^o \times 1^o$ (monthly)	2001	Global
	EDGAR HTAPv1	$0.1^o \times 0.1^o$ (Annual)	2005	Global
	EDGAR HTAPv2	$0.1^o \times 0.1^o$ (monthly)	2008	Global
	MEIC	36 ×36 km (monthly)	2006/2010	China mainland
	AQMEII-CONUS	36 ×36 km (monthly)	2006/2010	CONUS
	AQMEII-EU	36 ×36 km (monthly)	2010	Europe
CH_4, N_2O, AACD, CRES	Zhang et al. (2012)	$1^o \times 1^o$ (monthly)	2001	Global
	EDGAR v4.2	$0.1^o \times 0.1^o$ (Annual)	2005/2008	Global
ALKH, PAH	RCP4.5	$0.5^o \times 0.5^o$ (monthly)	2000	Global
	EDGAR v4.2	$0.1^o \times 0.1^o$ (Annual)	2005/2008	Global
CH_3Cl, $ClNO_2$, FMCL, CF_2ClBr, CF_3Br, CF_2Cl_2, $CFCl_3$, Hg(0), Hg(II)	Zhang et al. (2012)	$1^o \times 1^o$ (monthly)	2001	Global
DMS, H_2	Zhang et al. (2012)	$1^o \times 1^o$ (monthly)	2001	Global
	ACCMIP (biomass burning)	$0.5^o \times 0.5^o$ (monthly)	2005/2008	Global
HCl	Zhang et al. (2012)	$1^o \times 1^o$ (monthly)	2001	Global
	AQMEII-CONUS	36 ×36 km (monthly)	2006/2010	CONUS
Biogenic VOCs	Guenther et al. (2006)	Online	N/A	Global
Mineral dust	Zender et al. (2003)	Online	N/A	Global
Sea salt	Martensson et al. (2003)	Online	N/A	Global

[1] CO_2, carbon dioxide; CO, carbon monoxide; NO_x, nitrogen oxides (nitrogen dioxide (NO_2) + nitric oxide (NO)); SO_2, sulfur dioxide; NH_3, ammonia; ALD2, acetaldehyde; ETH, ethane; ETHA, ethane; ETOH, ethanol; FORM, formaldehyde; IOLE, internal olefinic carbon bond; MEOH, methanol; OLE, olefinic carbon bond; PAR, paraffin carbon bond; TOL, toluene; XYL, xylene; BC, black carbon; OC, organic carbon; CH_4, methane; N_2O, nitrous oxide; AACD, carboxylic acid; CRES, cresol and higher phenols; ALKH, long-chain alkanes; PAH, polycyclic aromatic hydrocarbons; CH_3Cl, methyl chloride; $ClNO_2$,chlorine nitrite; FMCL, formyl chloride; CF_2ClBr, chlorobromomethane; CF_3Br, trifluorobromomethane; CF_2Cl_2, dichlorodifluoromethane; $CFCl_3$, trichlorofluoromethane; Hg(0), mercury; Hg(II), mercury; DMS, dimethyl sulfide; H_2, hydrogen gas; HCl, hydrochloric acid; VOCs, volatile organic compounds.

[2] EDGAR, Emission Database for Global Atmospheric Research; HTAP, Hemispheric Transport of Air Pollution; MEIC, Multi-resolution Emission Inventory for China; AQMEII, Air Quality Modeling Evaluation International Initiative Phase II; RCP, Representative Concentration Pathway; ACCMIP, Atmospheric Chemistry and Climate Model Intercomparison Project; CONUS, Continental U.S.

[3] Adjustment factors of 0.7, 0.5, and 1.2 for SO_2 emissions are applied over CONUS, Europe, and Asia, and 1.2 for emissions of NH_3, BC, and OC, and 1.3 for CO over all three regions[4] PAR = 0.955×Propane+0.965×Butane+0.972×Pentane+0.117×Trimethylbenzene+0.333×Propene

Table 3.3. Datasets for model evaluation

Species/Variables	**Dataset**
Temperature at 2-m (T2), Specific humidity at 2-m (Q2), Wind speed at 10-m (WS10)	NCDC
Vertical temperature profile (T), Vertical relative humidity profile (RH), Vertical specific humidity profile (Q)	NCEP/NCAR
Precipitation (Precip)	GPCP
Outgoing longwave radiation (OLR)	NOAA/CDC
Cloud fraction (CF), Cloud optical thickness (COT), Precipitating water vapor (PWV), Aerosol optical depth (AOD), Column cloud condensation nuclei (ocean) at S = 0.5% (CCN5)	MODIS
Cloud droplet number concentration (CDNC), Cloud liquid water path (LWP)	UW-M
Downwelling longwave radiation (FLDS), Downwelling shortwave radiation (FSDS), Surface net longwave flux (FLNS), Surface net shortwave flux (FSNS), Shortwave cloud radiative forcing (SWCF), Longwave cloud radiative forcing (LWCF)	CERES
Carbon monoxide (CO)	East Asia: NIESJ, TAQMN, KMOE
Ozone (O_3)	CONUS: CASTNET Europe: Airbase, BDQA, EMEP East Asia: TAQMN, KMOE
Sulfur dioxide (SO_2)	CONUS: CASTNET Europe: Airbase, BDQA, EMEP East Asia: NIESJ, TAQMN, KMOE
Nitric acid (HNO_3)	CONUS: CASTNET Europe: EMEP
Ammonia (NH_3)	Europe: EMEP
Nitrogen dioxide (NO_2)	Europe: Airbase, BDQA, EMEP East Asia: NIESJ, TAQMN, KMOE
Sulfate (SO_4^{2-}), Ammonium (NH_4^+), Nitrate (NO_3^-), Chloride (Cl^-)	CONUS: CASTNET, IMPROVE, STN Europe: EMEP
Organic carbon (OC)	CONUS: IMPROVE
Black carbon (BC), Total carbon (TC)	CONUS: IMPROVE, STN
Particulate matter with diameter less than 2.5 μm ($PM_{2.5}$)	CONUS: IMPROVE, STN Europe: Airbase, BDQA, EMEP
Particulate matter with diameter less than 10 μm (PM_{10})	Europe: Airbase, BDQA, EMEP East Asia: MEPC, NIESJ, TAQMN, KMOE
Tropospheric CO	Globe: MOPITT
Tropospheric SO_2, HCHO	Globe: SCIAMCHY
Tropospheric NO_2	Globe: GOME, SCIAMCHY
Tropospheric ozone residual (TOR)	Globe: TOMS/SBUV, OMI/MLS

NCDC: National Climatic Data Center; NCEP/NCAR: National Centers for Environmental Prediction and National Center for Atmospheric Research; GPCP: Global Precipitation Climatology Project; NOAA/CDC: National Oceanic and Atmospheric Administration Climate Diagnostics Center; MODIS: Moderate Resolution Imaging Spectroradiometer; UW-M: University of Wisconsin-Madison; CERES: Clouds and Earth's Radiant Energy System; TOMS/SBUV: the Total Ozone Mapping Spectrometer/the Solar Backscatter UltraViolet; OMI/MLS: the Aura Ozone Monitoring Instrument in combination with Aura Microwave Limb Sounder; MOPITT: the Measurements Of Pollution In The Troposphere; the Global Ozone Monitoring Experiment; SCIAMCHY: the SCanning Imaging Absorption spectroMeter for Atmospheric CHartographY; GOME: the Global Ozone Monitoring Experiment; CASTNET: Clean Air Status and Trends Network; IMPROVE: Interagency Monitoring of Protected Visual Environments; STN: Speciation Trends Network; EMEP: European Monitoring and Evaluation Program; BDQA: Base de Données sur la Qualité de l'Air; AirBase: European air quality database; MEPC: Ministry of Environmental Protection of China; TAQMN: Taiwan Air Quality Monitoring Network; NIESJ: National Institute for Environmental Studies of Japan; KMOE: Korean Ministry of Environment.

Table 3.4a. Statistical performance of meteorological/radiative variables

		Obs	Sim	MB[a]	NMB (%)[a]	NME (%)[a]	RMSE[a]	Corr[a]
T2 (^{o}C)	NCDC[b]	13.1	10.2	-2.9	-22.2	28.0	4.8	0.9
	NCEP/NCAR[c]	5.7	3.2	-2.6	-45.1	51.1	4.1	0.99
Q2 (g kg^{-1})	NCDC	8.3	7.3	-1.0	-11.4	17.4	1.9	0.9
	NCEP/NCAR	8.3	7.0	-1.3	-15.8	17.2	1.6	0.99
WS10 (m s^{-1})	NCDC	3.7	3.3	-0.4	-9.7	32.8	1.8	0.5
	NCEP/NCAR	4.3	6.8	2.5	58.4	64.3	3.3	0.6
Precip (mm day^{-1})	GPCP	2.3	2.4	0.1	6.6	26.0	1.0	0.9
OLR (W m^{-2})	NOAA/CDC	216.4	217.9	1.4	0.7	2.9	7.8	0.98
FLDS (W m^{-2})	CERES	306.3	292.6	-13.8	-4.5	4.8	18.4	0.99
FSDS (W m^{-2})	CERES	163.5	161.8	-1.7	-1.0	6.6	14.0	0.97
FLNS (W m^{-2})	CERES	-47.6	-50.3	2.7	5.7	14.2	9.0	0.9
FSNS (W m^{-2})	CERES	128.5	122.4	-6.2	-4.8	7.9	13.4	0.99
SWCF (W m^{-2})	CERES	-40.7	-45.1	4.3	10.6	26.3	14.5	0.9
LWCF (W m^{-2})	CERES	22.7	18.3	-4.4	-19.4	24.0	6.5	0.9
CCN5[d] (# cm^{-2})	MODIS	2.4×10^{8}	4.3×10^{7}	-2.0×10^{8}	-82.2	82.2	4.8×10^{8}	0.1
CF (%)	MODIS	67.2	67.5	0.3	0.4	15.3	13.6	0.7
COT	MODIS	17.0	9.9	-7.1	-41.7	57.8	13.6	-0.2
AOD	MODIS	1.6×10^{-1}	1.0×10^{-1}	-5.5×10^{-2}	-35.4	49.2	0.1	0.6
PWV (cm)	MODIS	1.9	1.7	-0.2	-10.5	17.2	0.5	0.98
CDNC (# cm^{-3})	UW-M	108.5	137.5	29.0	26.7	52.2	74.1	0.4
LWP (g m^{-2})	UW-M	85.7	59.0	-26.7	-31.2	34.2	38.3	0.5

[a] MB: mean bias; NMB: normalized mean bias (%); NME: normalized mean error (%); RMSE: root mean squared error; Corr.: correlation coefficient

[b] Results are based on NCDC sites mean

[c] Results are based on global mean.

[d] Column CCN (ocean) at supersaturation of 0.5%.

Table 3.4b. Statistical performance of chemical species

		Obs	Sim	MB[a]	NMB (%)[a]	NME (%)[a]	RMSE[a]	Corr[a]
CO (ppm)	East Asia	503.9	221.2	-282.7	-56.1	56.4	315.9	0.4
SO_2[b]	CONUS	2.7	8.7	6.0	219.1	219.6	9.5	0.8
	Europe	5.5	5.2	-0.3	-5.2	65.9	6.5	0.4
	East Asia	3.2	2.6	-0.6	-18.2	65.9	3.6	0.3
NH_3 ($\mu g\ m^{-3}$)	Europe	1.0	1.3	0.3	31.9	75.2	1.0	0.5
NO_2[c]	Europe	18.6	4.1	-14.4	-77.7	78.6	17.4	0.2
	East Asia	12.8	2.2	-10.6	-82.7	83.0	11.7	0.5
O_3[d]	CONUS	35.1	40.8	5.7	16.2	20.6	9.0	0.5
	Europe	54.9	81.2	26.2	47.8	48.7	29.0	0.3
	East Asia	28.7	42.6	13.9	48.5	49.1	15.7	0.2
HNO_3 ($\mu g\ m^{-3}$)	CONUS	1.2	1.8	0.6	48.5	60.1	0.9	0.6
	Europe	0.8	1.1	0.3	41.8	84.0	0.9	0.2
Col. CO ($molec.cm^{-2}$)	Globe	1.4×10^{18}	2.6×10^{18}	1.2×10^{18}	84.3	84.3	1.3×10^{18}	0.8
Col. NO_2 ($molec.cm^{-2}$)	Globe	5.0×10^{14}	7.2×10^{14}	1.9×10^{14}	35.5	52.2	4.5×10^{14}	0.9
Col. HCHO ($molec.cm^{-2}$)	Globe	4.2×10^{15}	2.3×10^{15}	-1.9×10^{15}	-44.6	48.0	2.7×10^{15}	0.6
Col. SO_2(DU)	Globe	0.2	0.1	-0.1	-28.4	113.3	0.4	-0.1
TOR (DU)	Globe	29.1	28.1	-1.0	-3.5	16.8	5.7	0.8
SO_4^{2-} ($\mu g\ m^{-3}$)	CONUS	2.3	2.0	-0.3	-12.8	24.3	0.8	0.9
	Europe	2.0	1.6	-0.4	-20.8	36.7	1.0	0.6
NH_4^+ ($\mu g\ m^{-3}$)	CONUS	1.1	1.5	0.4	37.4	53.2	0.9	0.7
	Europe	0.9	1.5	0.5	59.8	68.0	0.8	0.8
NO_3^- ($\mu g\ m^{-3}$)	CONUS	1.0	2.0	1.0	93.2	118.3	1.9	0.5
	Europe	1.8	2.7	0.8	44.8	72.3	1.9	0.6
Cl^- ($\mu g\ m^{-3}$)	CONUS	0.1	0.1	-3.2×10^{-3}	-3.0	100.3	0.4	0.2
	Europe	0.9	4.4	3.5	376.0	376.0	4.6	0.7
BC ($\mu g\ m^{-3}$)	CONUS	0.4	0.3	-5.7×10^{-2}	-15.6	44.3	0.3	0.5
OC ($\mu g\ m^{-3}$)	CONUS	1.1	1.1	-2.2×10^{-2}	-2.0	46.7	0.8	0.4
TC ($\mu g\ m^{-3}$)	CONUS	2.6	1.6	-1.0	-37.9	49.9	2.1	0.5
$PM_{2.5}$ ($\mu g\ m^{-3}$)	CONUS	8.4	8.3	-0.1	-1.1	31.3	3.6	0.7
	Europe	13.6	9.8	-3.9	-28.2	36.4	7.7	0.3
PM_{10} ($\mu g\ m^{-3}$)	Europe	23.1	21.7	-1.5	-6.3	38.5	13.6	0.2
	East Asia	97.1	60.9	-36.1	-37.2	43.0	49.2	0.6

[a] MB: mean bias; NMB: normalized mean bias (%); NME: normalized mean error (%); RMSE: root mean squared error; Corr.: correlation coefficient.

[b] The unit is $\mu g\ m^{-3}$ for CONUS and Europe, and ppb for East Asia.

[c] The unit is $\mu g\ m^{-3}$ for Europe and ppb for East Asia.

[d] The unit is ppb for CONUS and East Asia, and $\mu g\ m^{-3}$ for Europe.

Table 3.5. Global burdens of major gaseous and aerosol species (2001-2010)

	2001-2003	2004-2006	2007-2010	2001-2010	He and Zhang (2014)	Previous studies
Tropospheric CO (Tg) [a]	712	726	576	661.87	322.06	337-354 [d]
Tropospheric O_3 (DU) [a] Tropospheric O_3 (Tg) [a]	28.2 219.3	30.1 313.8	27.6 283.0	28.5 294.83	30.5 332.87	34.04 [e] 372 [e]
DMS (Tg S)	0.073	0.064	0.065	0.067	0.058	0.067 [f]
SO_2 (Tg S)	0.289	0.264	0.224	0.256	0.281	0.34 [f]
H_2SO_4 (Tg S)	6.2×10^{-4}	5.7×10^{-4}	5.5×10^{-4}	5.8×10^{-4}	1.9×10^{-3}	4.2×10^{-4} [f]
Tropospheric NO_x [a, b] (molec. cm^{-2})	8.9×10^{14} (0.11 Tg N)	1.1×10^{15} (0.13 Tg N)	1.0×10^{15} (0.12 Tg N)	1.0×10^{15} (0.12 Tg N)	8.2×10^{14} (0.116 Tg N)	7.6×10^{14} – 9.2×10^{14} [g]
Tropospheric NO_y (Tg N) [b]	0.83	0.96	0.85	0.88	1.02	N.A. [c]
Tropospheric HNO_3 (Tg N)	0.11	0.13	0.12	0.12	0.12	0.5[d]
NH_3 (Tg N)	0.057	0.056	0.043	0.051	0.059	0.064 [f]
VOCs (Tg C)[b]	7.14	5.97	5.89	6.29	7.63	N.A. [c]
Tropospheric HCHO (Tg C) [a]	0.340	0.321	0.293	0.315	0.391	0.335-0.349 [d]
SO_4^{2-} (Tg S)	0.42	0.38	0.32	0.37	0.39	0.84 [e], 0.47 [f], 0.66 [h]
NO_3^- (Tg N)	0.08	0.10	0.09	0.09	0.11	0.01-0.14 [i]
NH_4^+ (Tg N)	0.22	0.21	0.17	0.20	0.21	0.24 [f], (0.27-0.44) [i]
Na^+ (Tg)	3.82	3.82	3.85	3.83	3.04	2.98 [e], (0.38-5.19) [i]
Cl^- (Tg)	5.64	5.64	5.68	5.66	4.47	4.60 [e], (0.59-8.02) [i]
BC (Tg)	0.090	0.055	0.057	0.067	0.076	0.28 [e], 0.093 [f]
OC (Tg)	0.54	0.26	0.22	0.33	0.61	1.28 [e]
POM (Tg)	0.63	0.25	0.20	0.35	0.48	0.68 [f], 1.70 [h]
SOA (Tg)	0.13	0.12	0.11	0.12	0.38	1.15 [f], 0.59 [j]
Dust (Tg)	27.2	29.0	26.4	27.4	26.4	24.7 [f], (7.9-35.9) [i]

[a] Troposphere refers to model layers below tropopause height.

[b] $NO_x = NO + NO_2$; $NO_y = NO_x$ + nitrogen trioxide (NO_3) + dinitrogen pentoxide (N_2O_5) + nitrous acid (HONO) + nitric acid (HNO_3) + pernitric acid (HNO_4) + peroxyacyl nitrate (PAN) + d $_3$ peroxyacyl nitrate (PANX) + other organic nitrate (NTR); VOCs-volatile organic compounds including acetaldehyde (ALD2), carboxylic acid(AACD), long-chain alkanes (ALKH), cresol and higher phenols (CRES), ethene (ETH), ethane (ETHA), ethanol (ETOH), formaldehyde (FORM), internal olefinic carbon bond (IOLE), methanol (MEOH), olefinic carbon bond (OLE), paraffin carbon bond (PAR), polycyclic aromatic hydrocarbons (PAH), toluene (TOL), xylene (XYL), isoprene (ISOP), and terpene (TERP).

[c] N.A – not available, it refers to species having no burden data from previous studies.

[d] Williams et al. (2009)

[e] Horowitz et al. (2006)

[f] Liu et al. (2012)

[g] Lamarque et al. (2005)

[h] Textor et al. (2006)

[i] Tsigaridis et al. (2006)

[j] Heald et al. (2008)

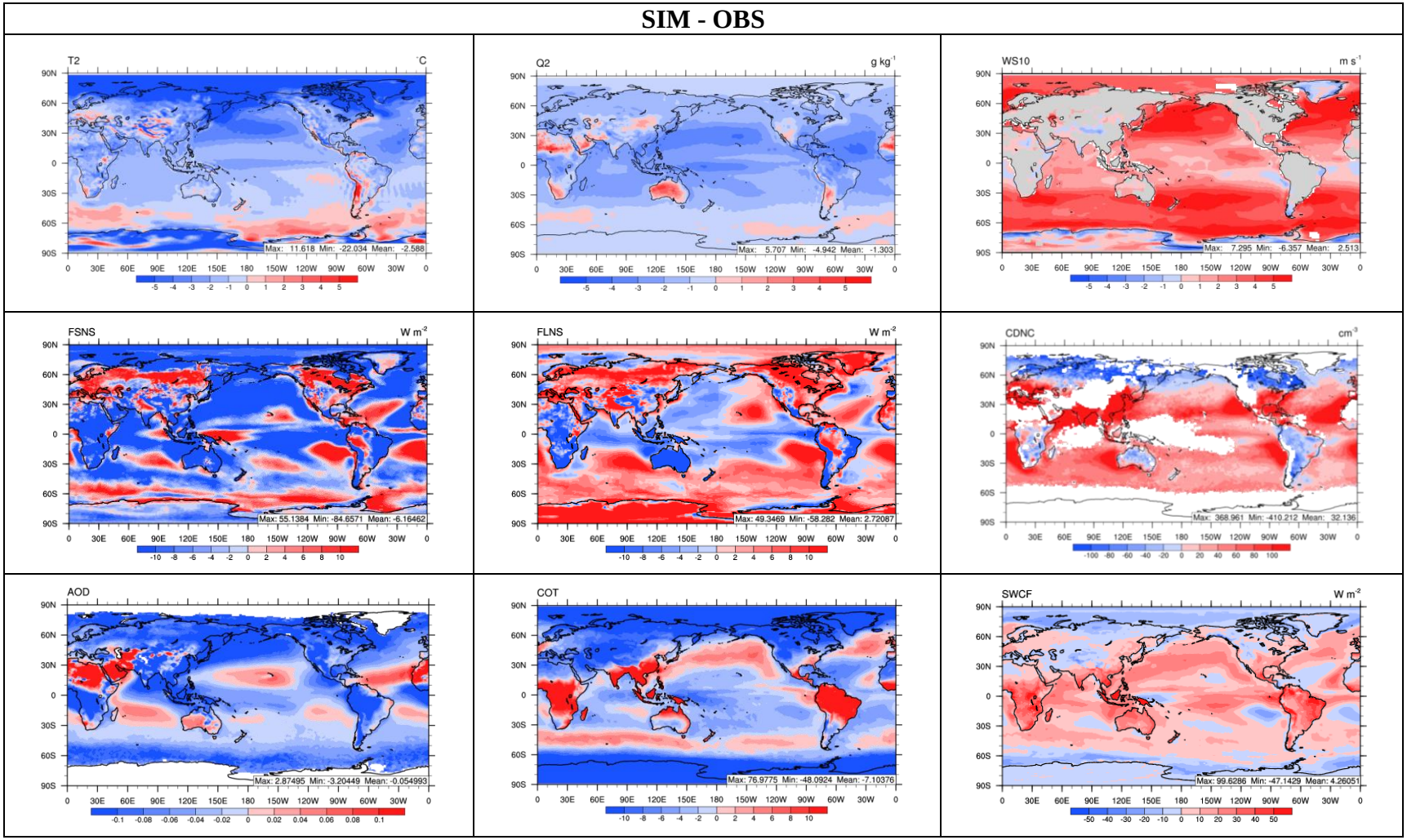

Figure 3.1. Absolute differences between simulation results from CESM_NCSU and observations/reanalysis for 2001-2010. NCEP reanalysis data is used for comparison of T2, Q2, and WS10. CERES data is used for comparison of FSNS, FLNS, and SWCF. UW-M data is used for comparison of CDNC. MODIS data is used for comparison of AOD and COT.

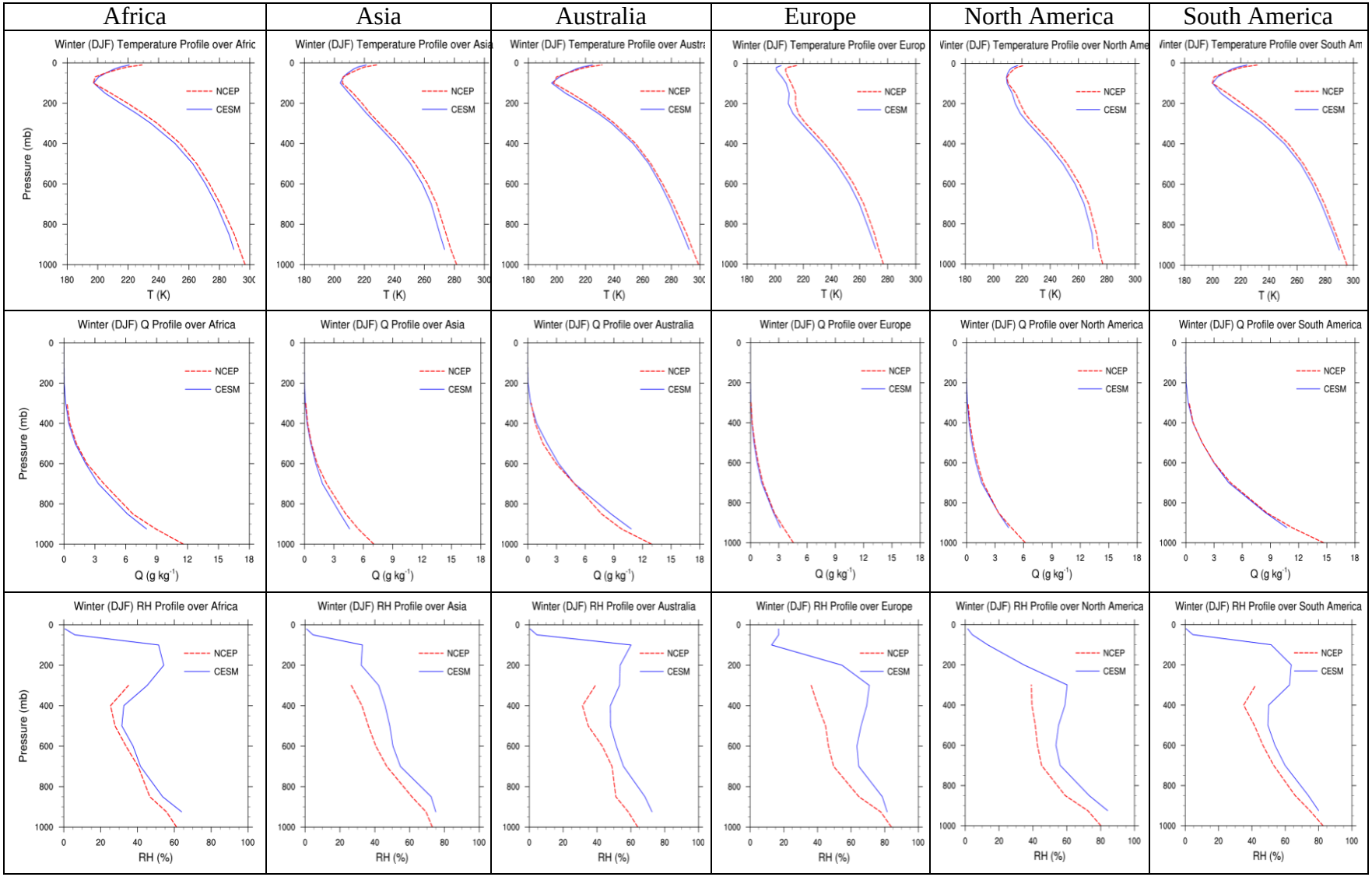

Figure 3.2a. Comparison of meteorological profiles of CESM-NCSU with NCEP over Africa, Asia, Australia, Europe, North America, and South America for December, January, and February (DJF).

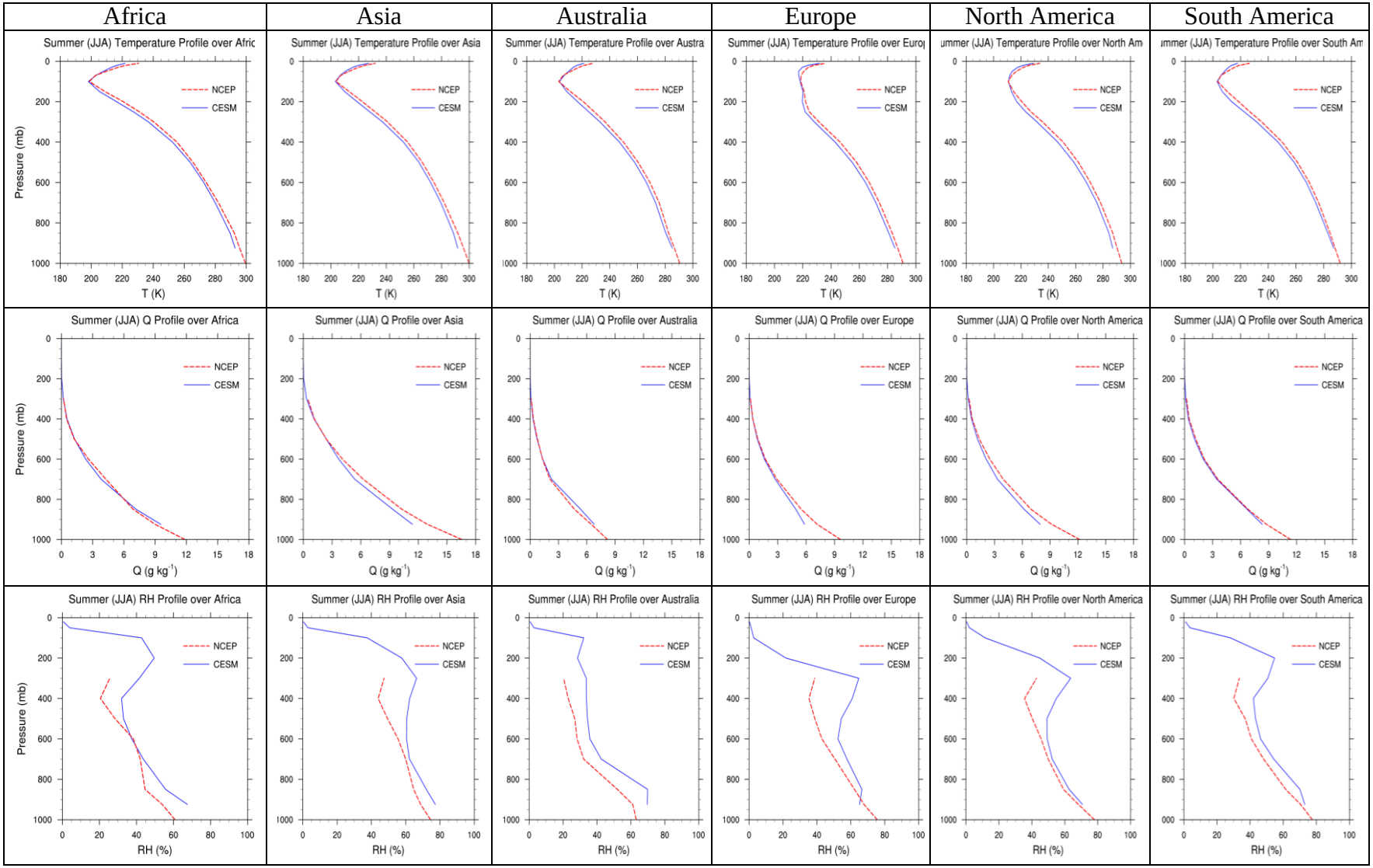

Figure 3.2b. Comparison of meteorological profiles of CESM-NCSU with NCEP over Africa, Asia, Australia, Europe, North America, and South America for June, July, and August (JJA).

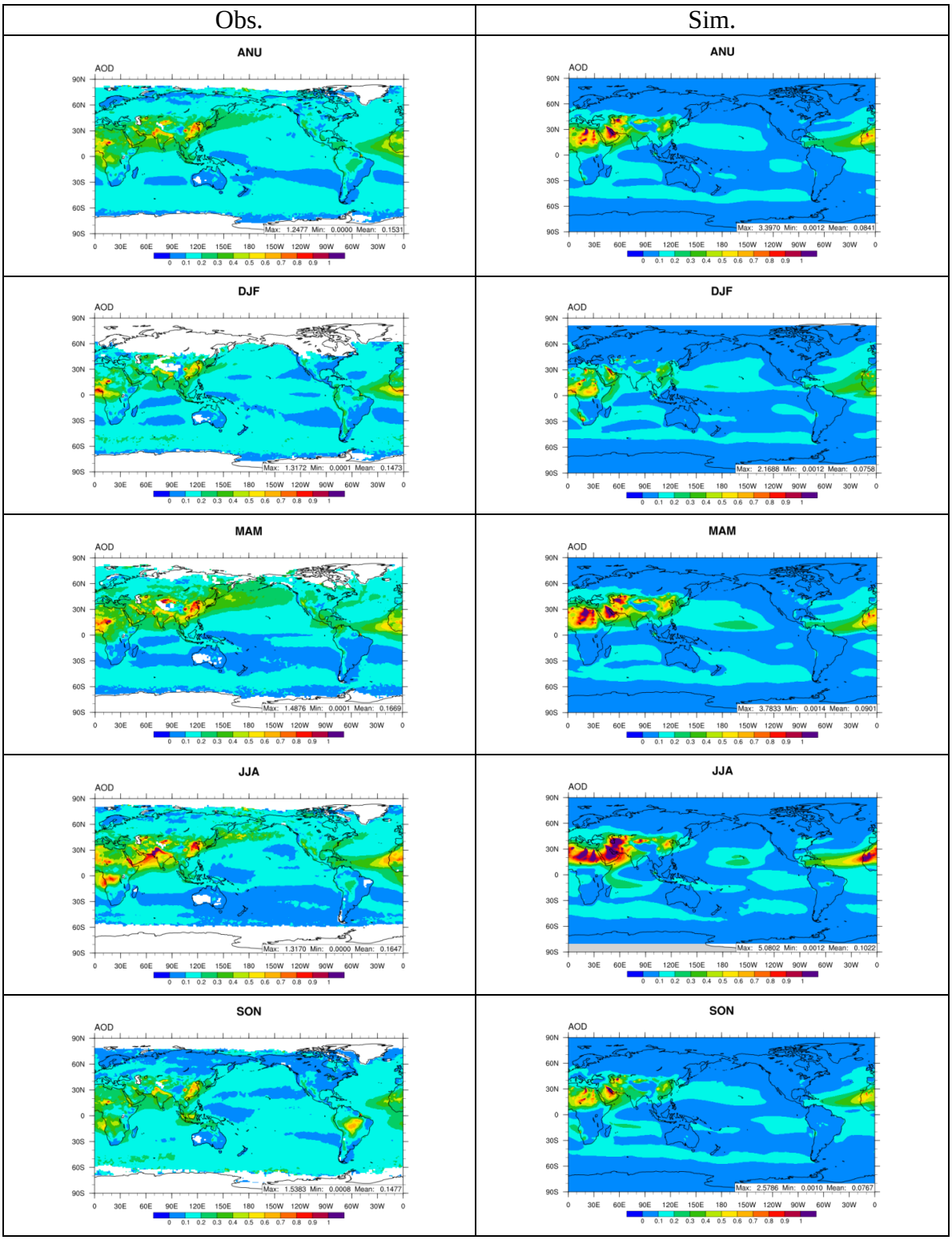

Figure 3.3. Seasonal and annual comparison of simulated AOD (Sim.) against MODIS observations (Obs.). From top to bottom: annual (ANU), December-January-February (DJF), March-April-May (MAM), June-July-August (JJA), and September-October-November (SON). The results are based on 10-year average of 2001-2010.

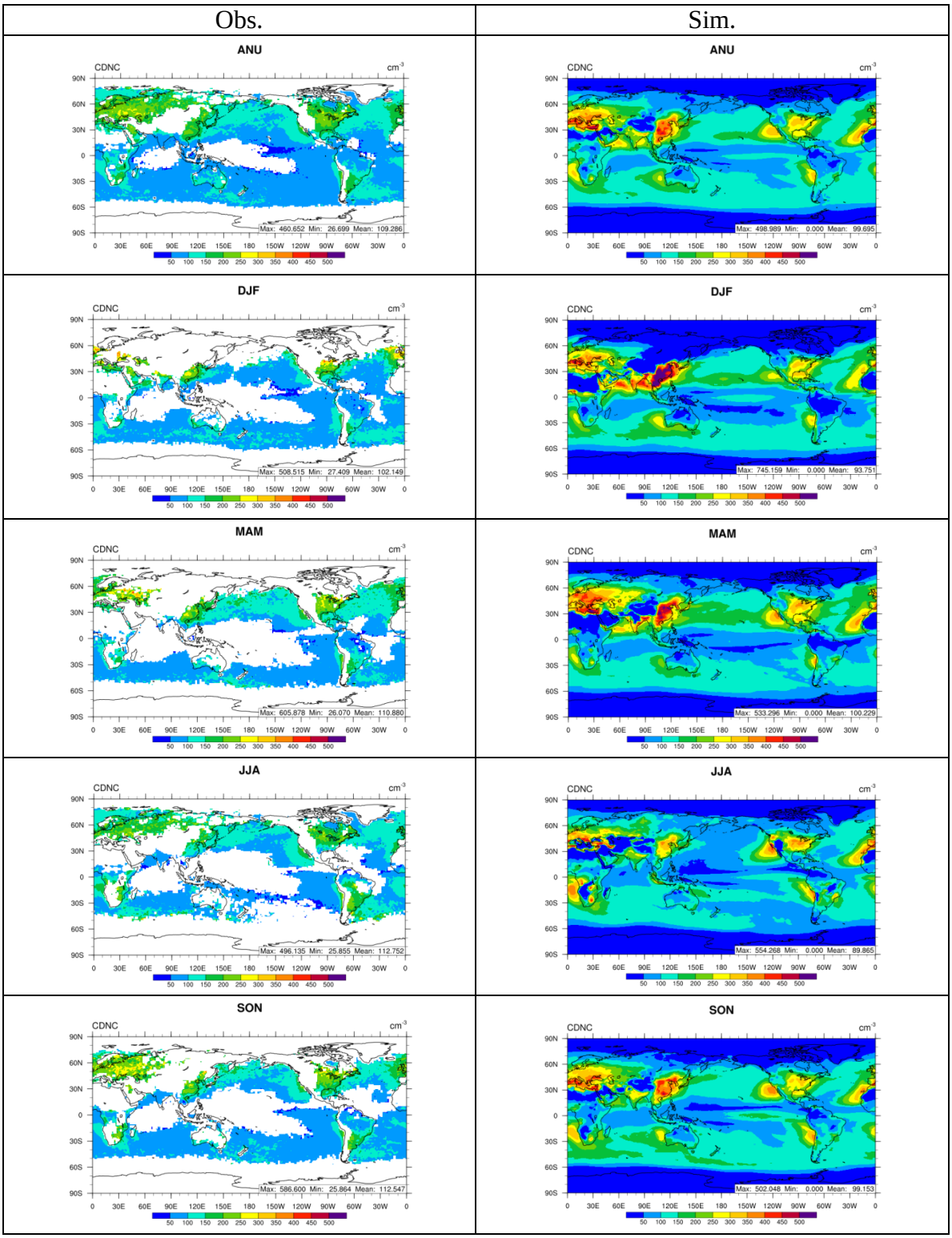

Figure 3.4. Seasonal and annual comparison of simulated CDNC (Sim.) against UW-M observations (Obs.). From top to bottom: annual (ANU), December-January-February (DJF), March-April-May (MAM), June-July-August (JJA), and September-October-November (SON). The results are based on 10-year average of 2001-2010.

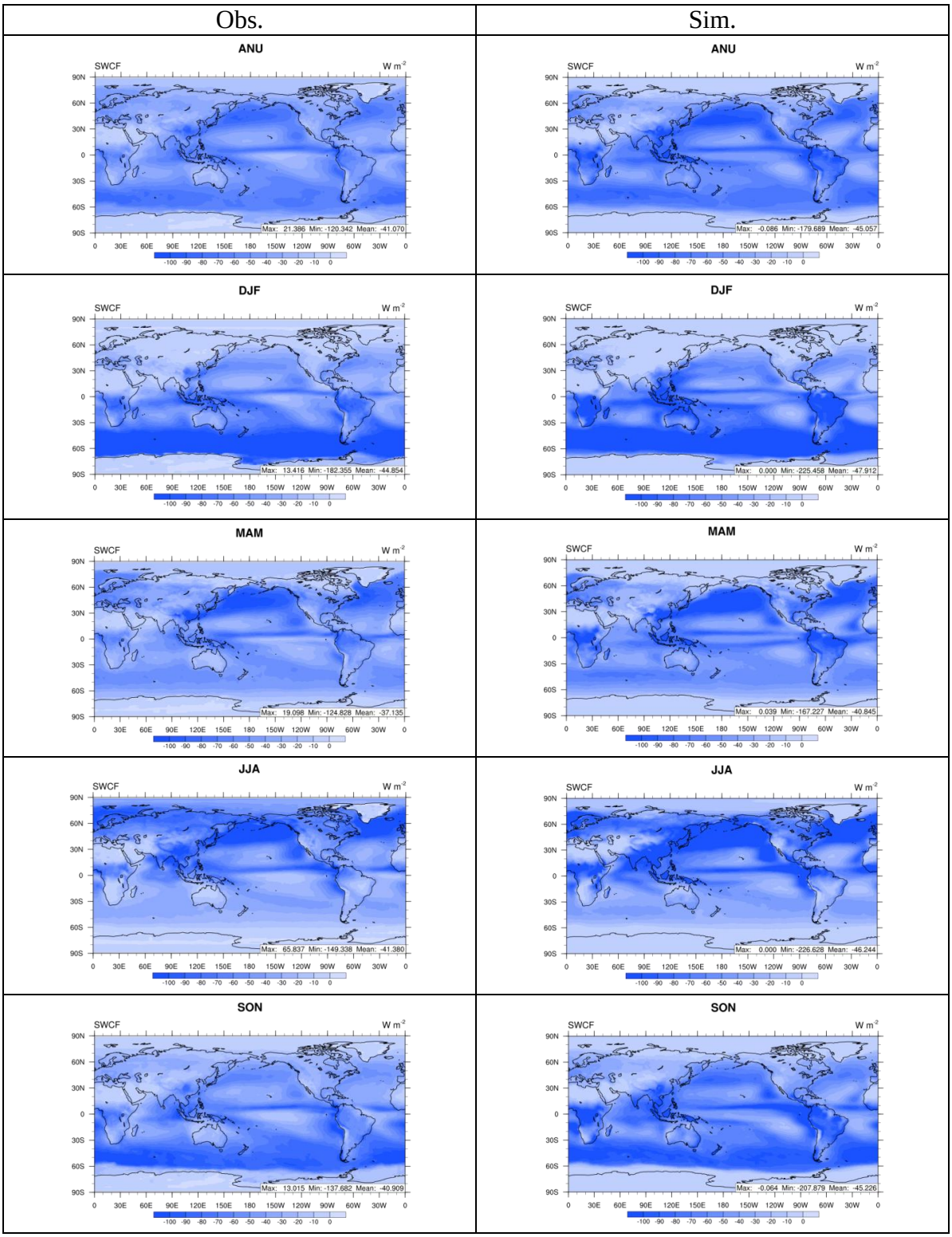

Figure 3.5. Seasonal and annual comparison of simulated SWCF (Sim.) against CERES observations (Obs.). From top to bottom: annual (ANU), December-January-February (DJF), March-April-May (MAM), June-July-August (JJA), and September-October-November (SON). The results are based on 10-year average of 2001-2010.

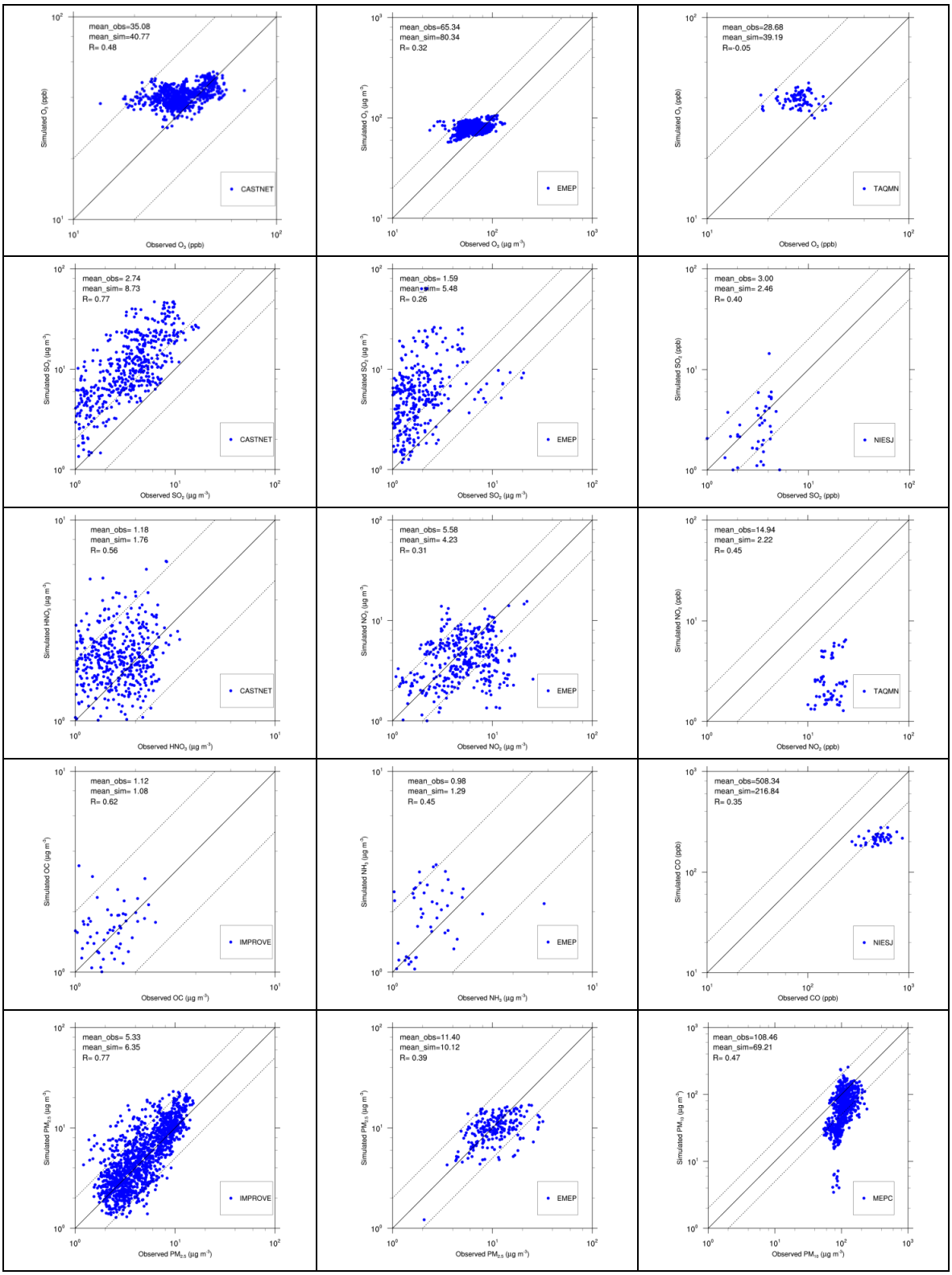

Figure 3.6. Scatter plots of major chemical species over various sites in different monitoring networks including CASTNET, IMPROVE, EMEP, MEPC, NIESJ, and TAQMN.

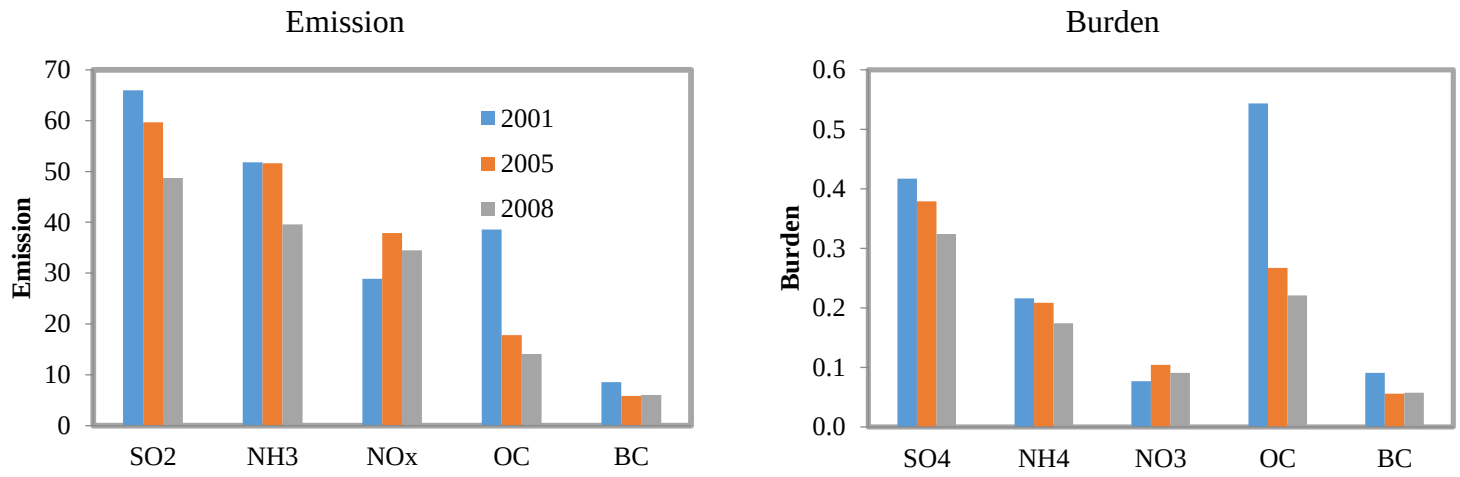

Figure 3.7. Emission trend and corresponding aerosol burden trend. Units for SO_2 emission and SO_4 burden are Tg S yr^{-1} and Tg S; units for NH_3 emission and NH_4 burden are Tg N yr^{-1} and Tg N; for NO_x emission and NO_3 burden are Tg N yr^{-1} and Tg N; units for OC/BC emission and OC/BC burden are Tg yr^{-1} and Tg.

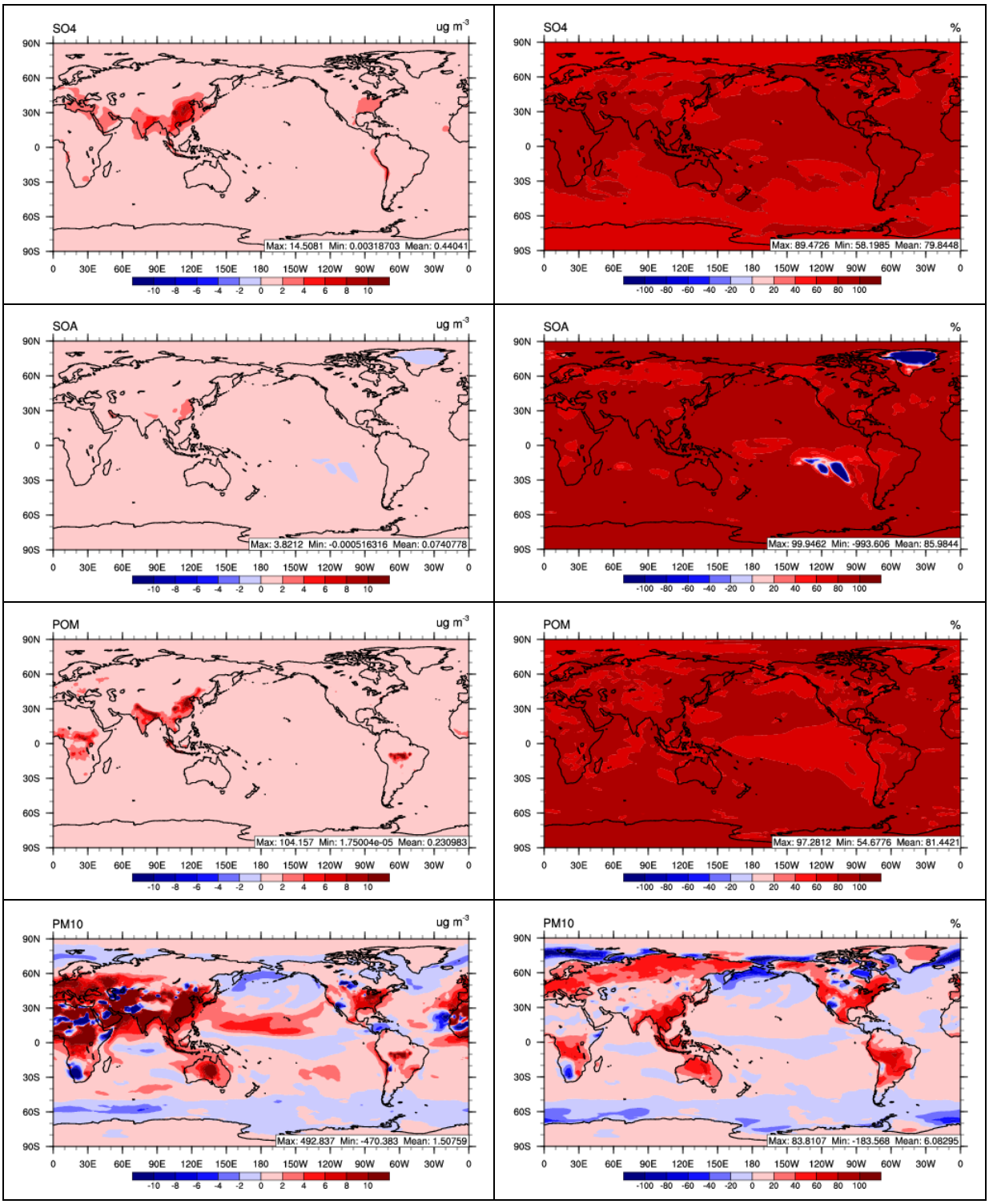

Figure 3.8a. Spatial distributions of absolute and percentage differences of SO4, SOA, POM, and PM_{10} between CESM/CAM5 simulations with baseline emissions and 20% of anthropogenic emissions from the baseline emissions.

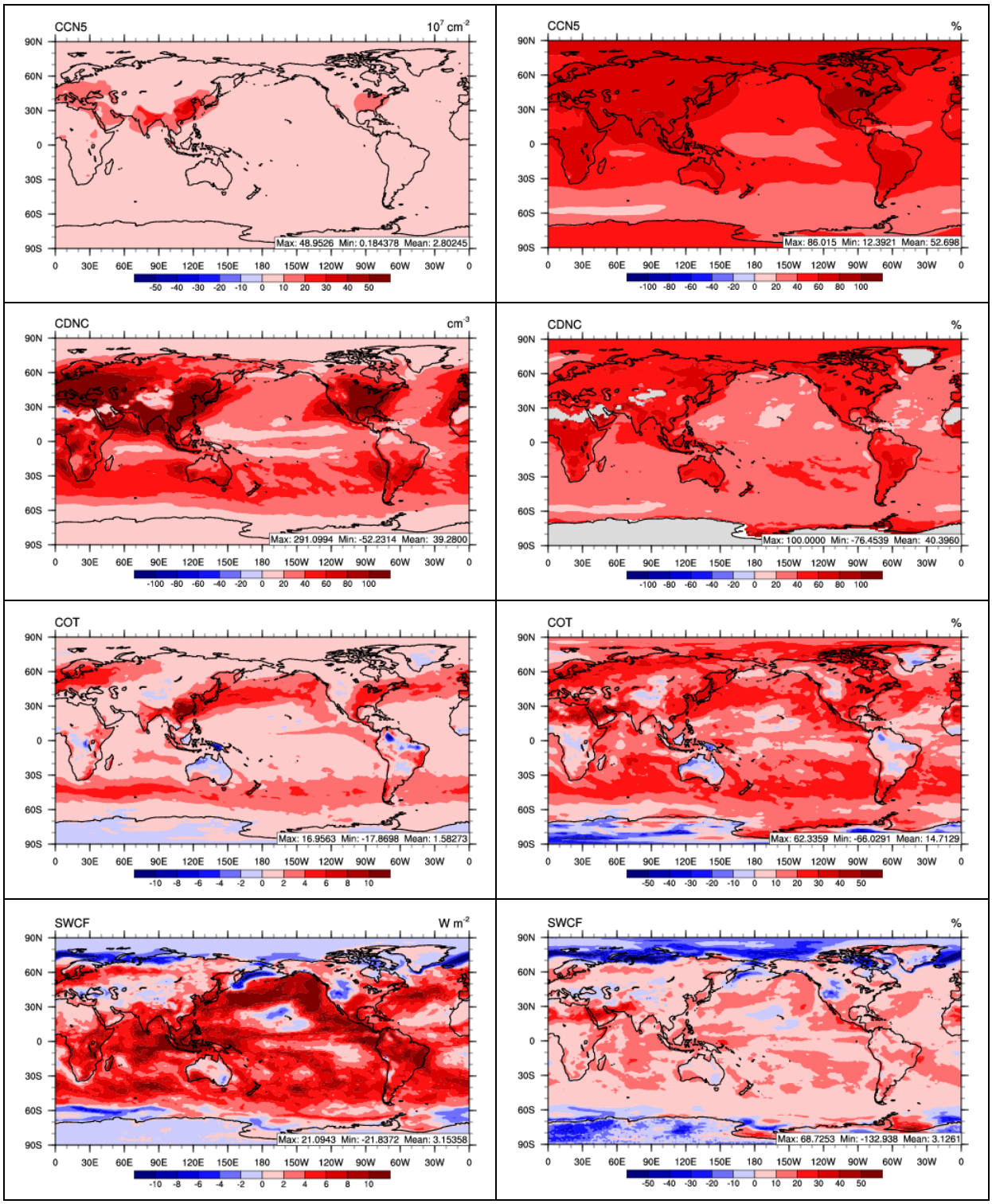

Figure 3.8b. Spatial distributions of absolute and percentage differences of CCN at s=0.5%, CDNC, COT, and SWCF between CESM/CAM5 simulations with baseline emissions and 20% of anthropogenic emissions from the baseline emissions.

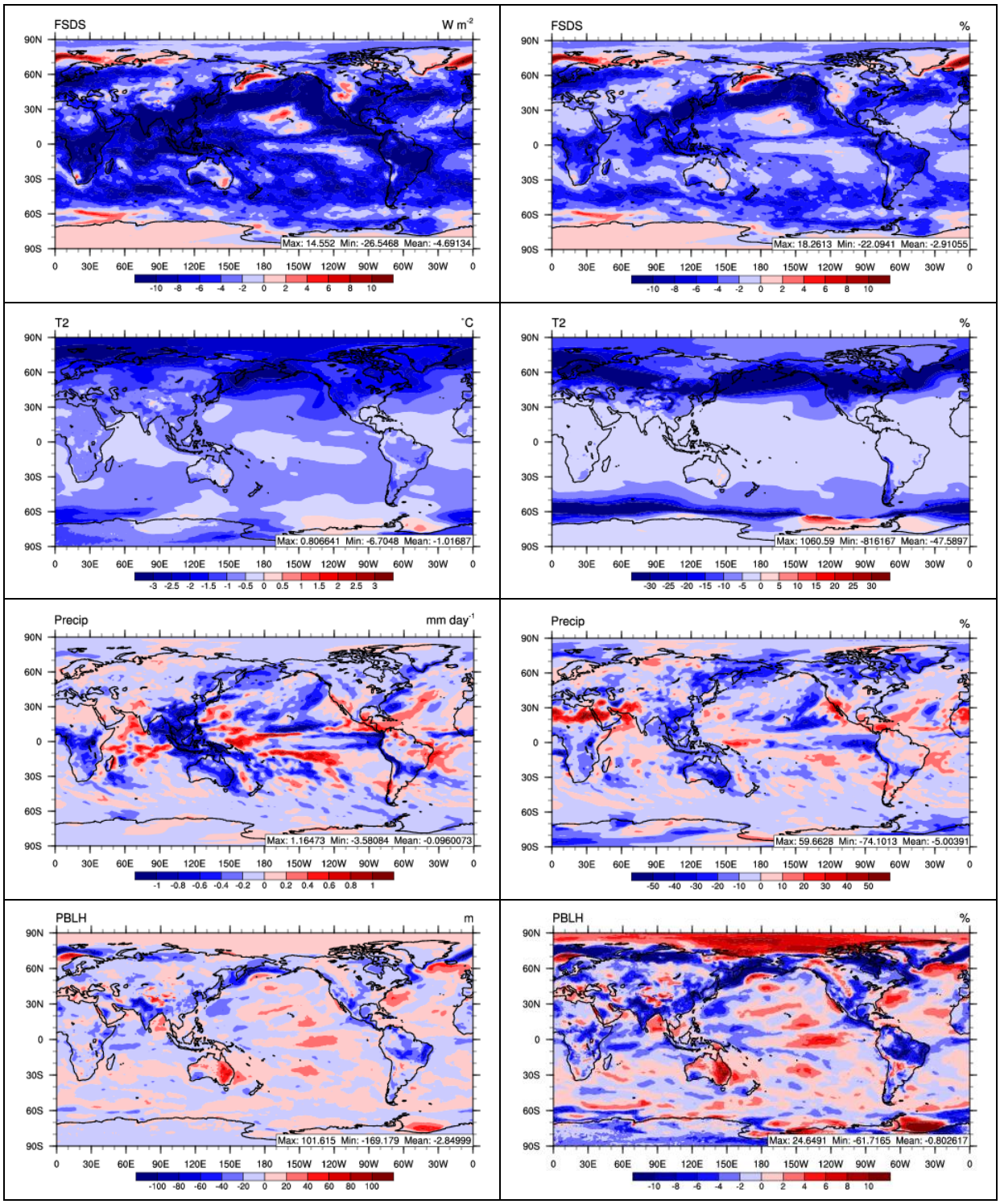

Figure 3.8c. Spatial distributions of absolute and percentage differences of FSDS, T2, Precip, and PBLH between CESM/CAM5 simulations with baseline emissions and 20% of anthropogenic emissions from the baseline emissions.

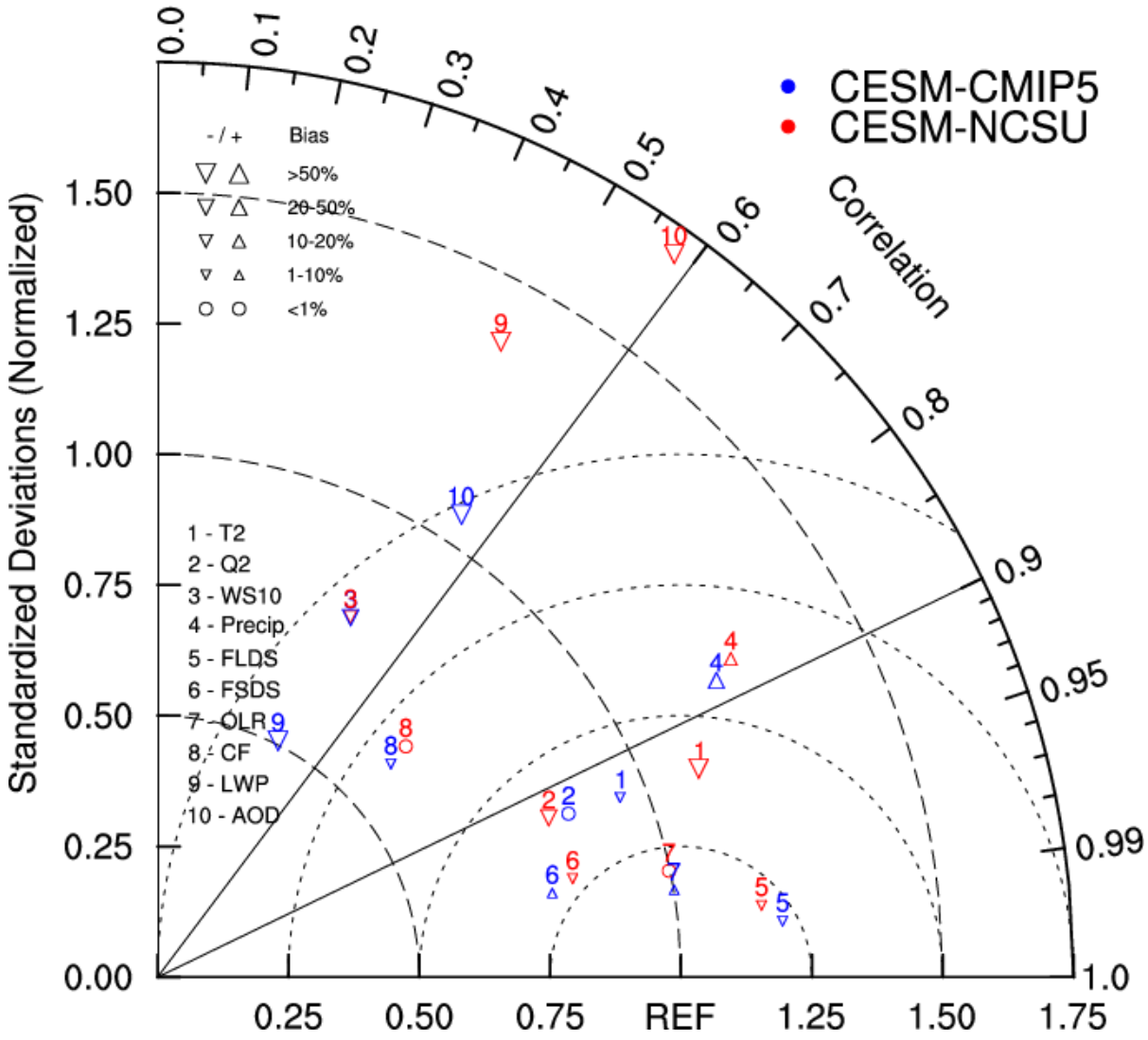

Figure 3.9. Taylor diagram of comparison between CESM-NCSU and CESM-CMIP5. The results are based on 10-year average. This diagram represents the similarity between CESM-NCSU and CESM-CMIP5. X-axis represents the ratio of variances between observations and simulations (proportional to the reference point identified as "REF"), and Y-axis represents the normalized standard deviation between the two patterns (proportional to the radial distance from the origin).

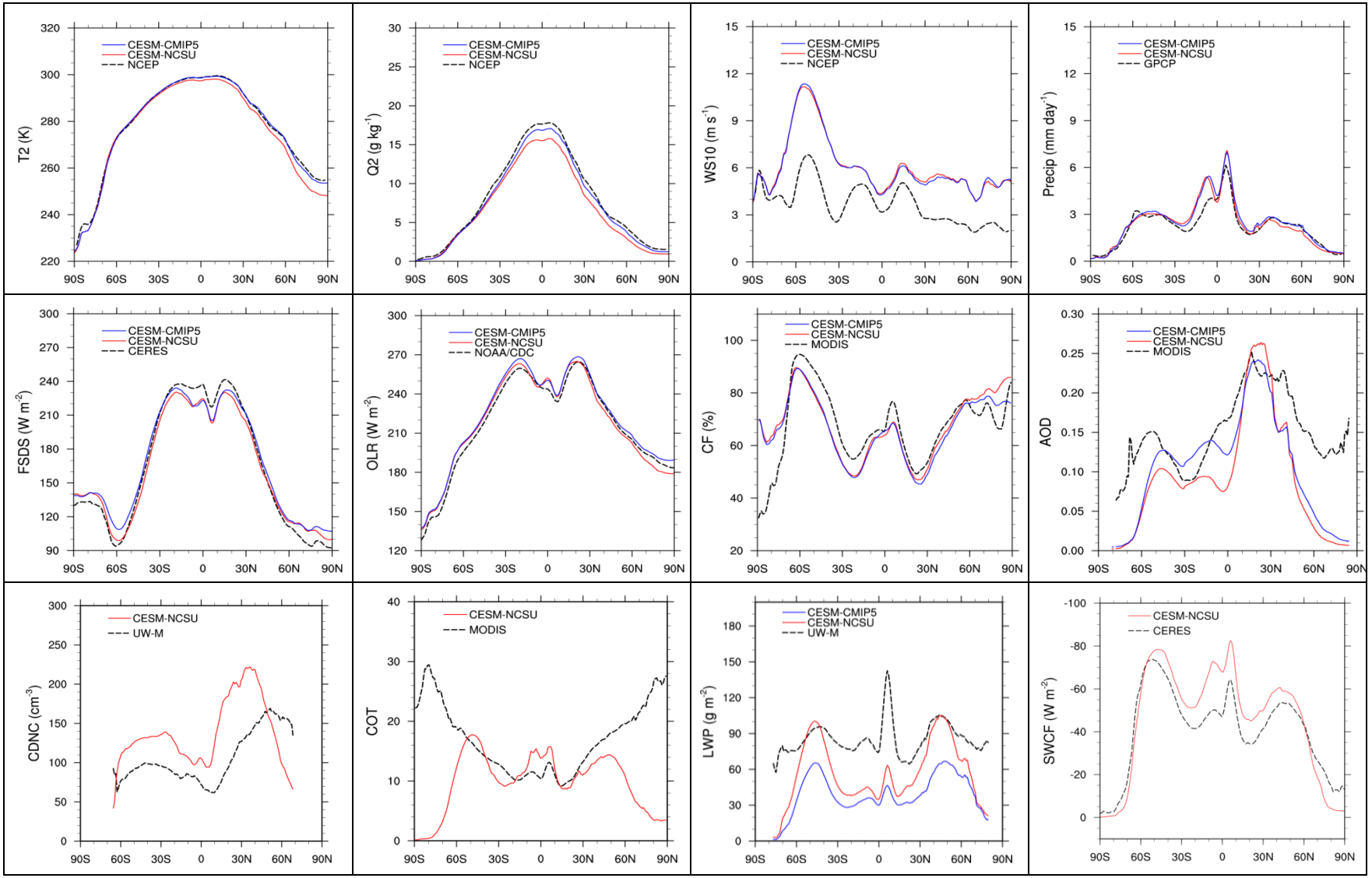

Figure 3.10. Comparison of 10-year average zonal mean predictions from CESM-NCSU and CESM-CMIP5 with observations/reanalysis data.

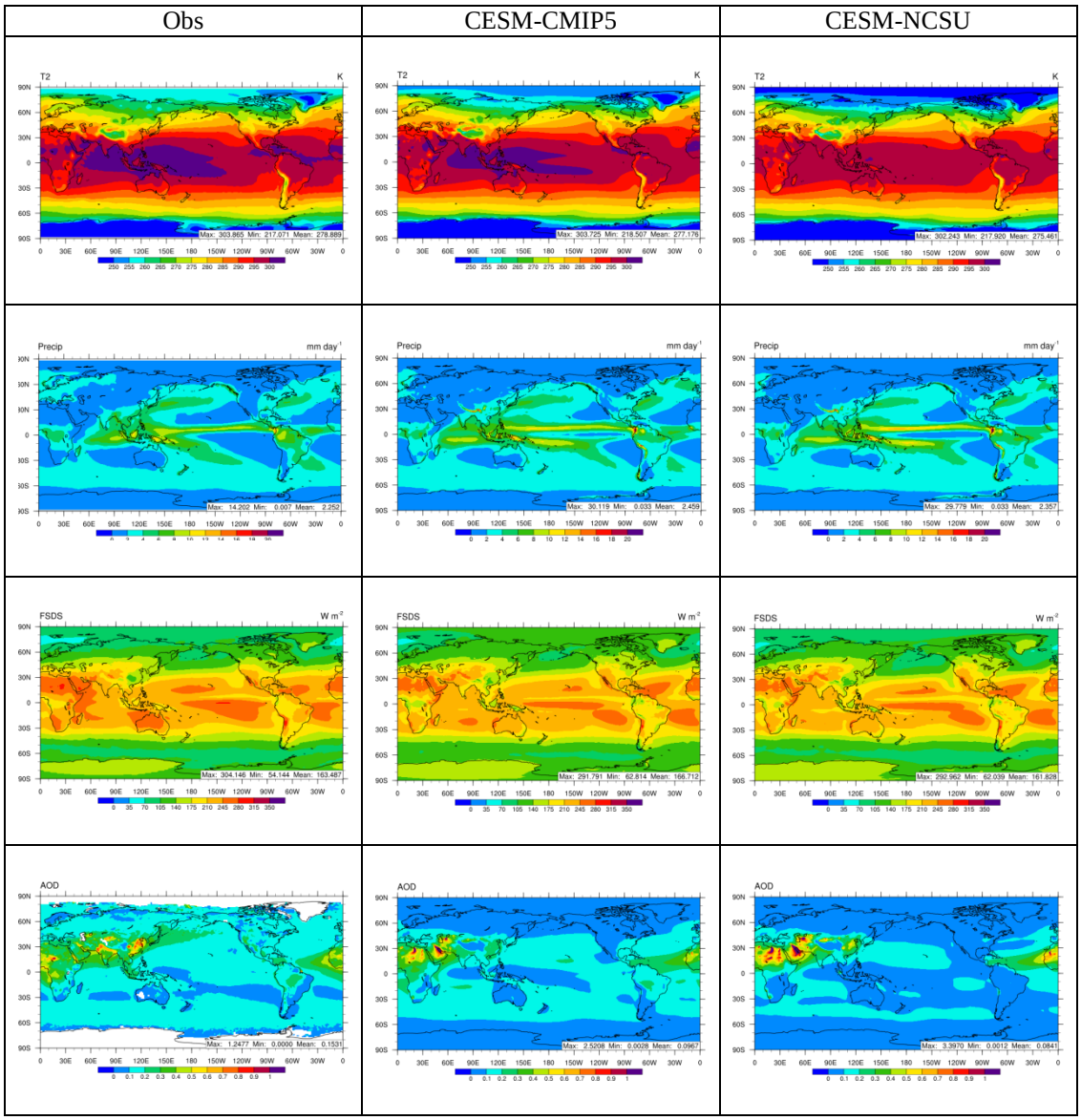

Figure 3.11. Comparison of 10-year average spatial distributions of T2, Precip, FSDS, and AOD from observations (left column), CESM-CMIP5 (middle column), and CESM-NCSU (right column).

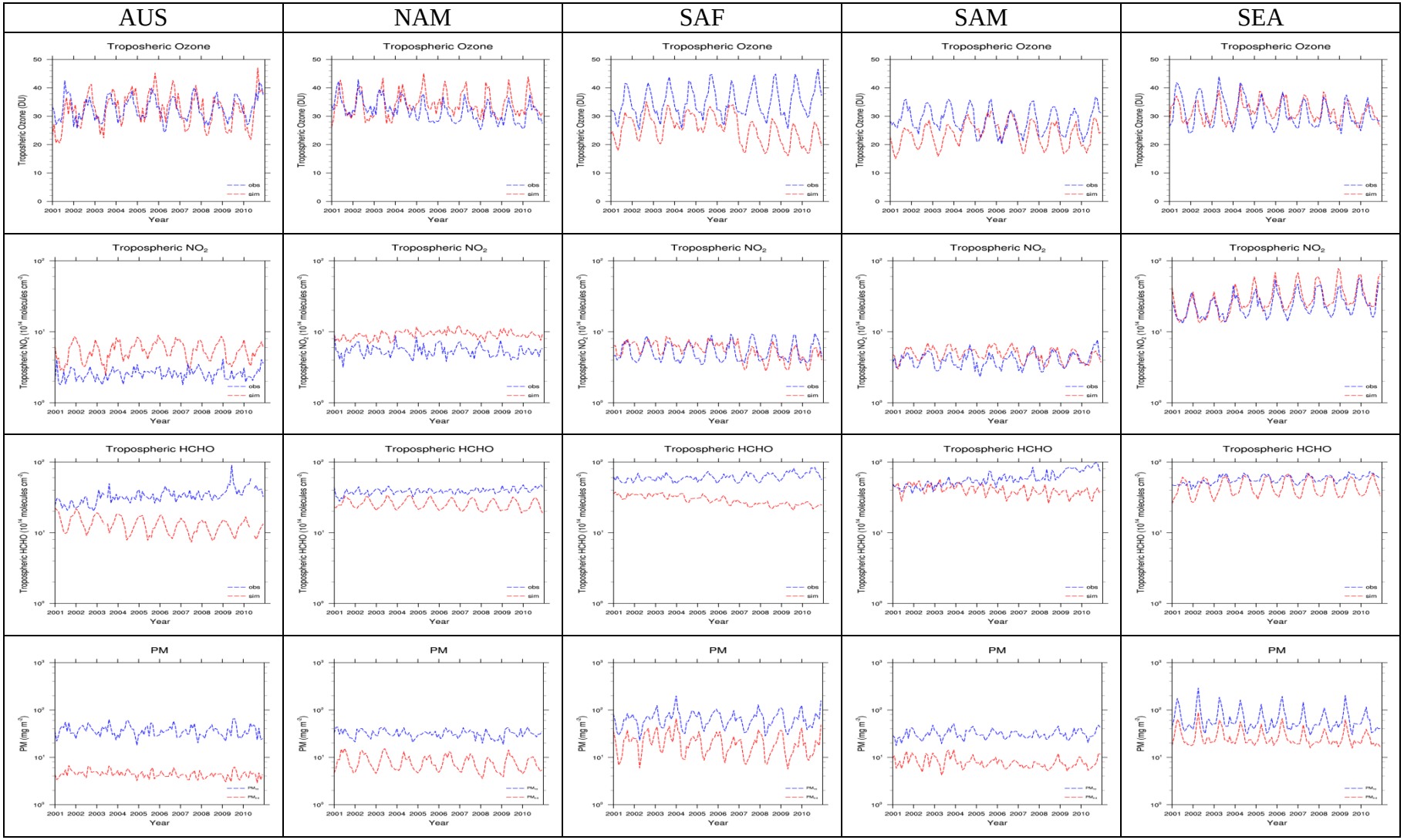

Figure 3.12a. Time series of 10-year (2001-2010) average observed and simulated tropospheric column mass abundances of O_3, NO_2, and HCHO, and simulated column concentrations of $PM_{2.5}$ and PM_{10} (note that no observations for column $PM_{2.5}$ or PM_{10} concentrations) over AUS, NAM, SAF, SAM, and SEA.

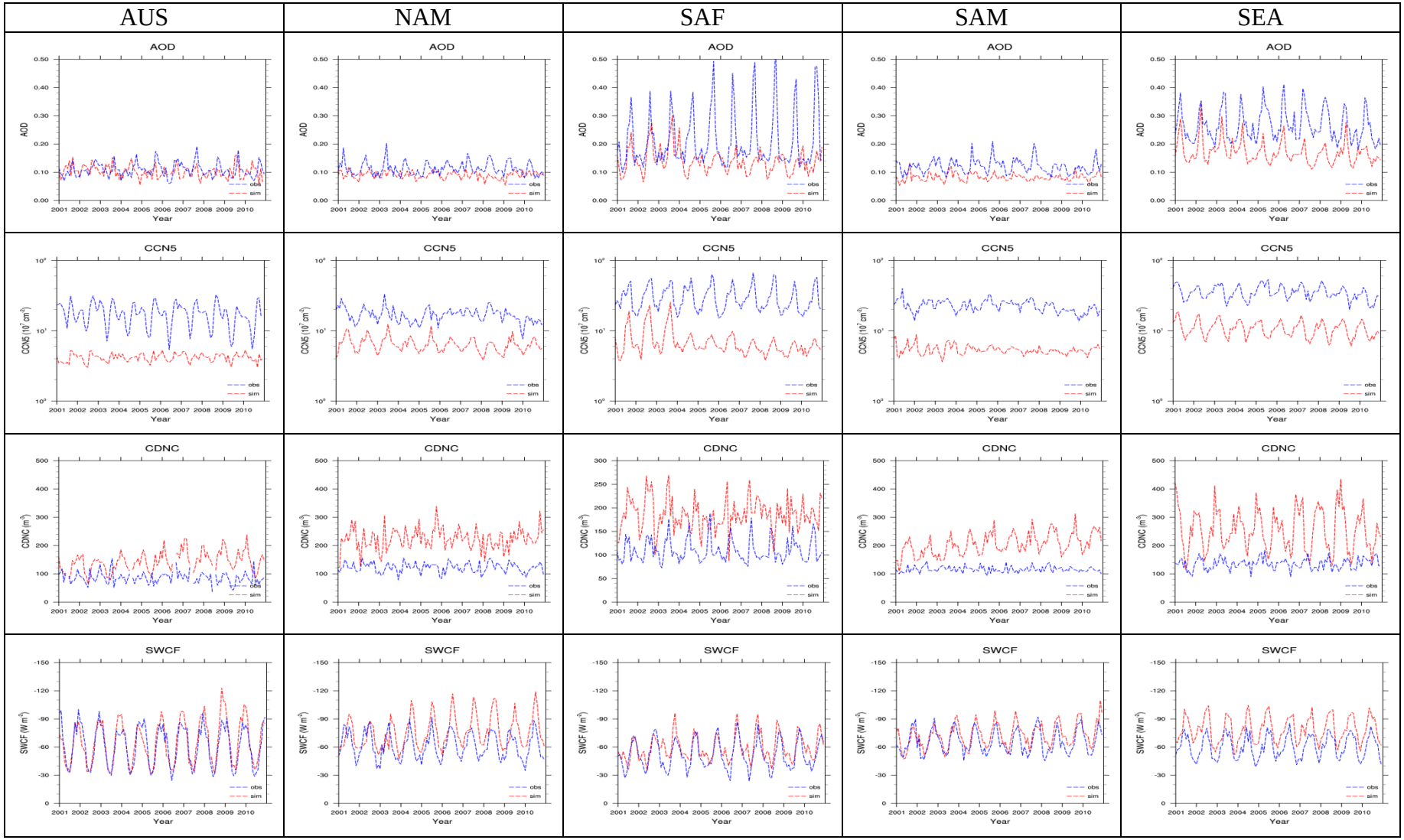

Figure 3.12b. Time series of 10-year (2001-2010) average observed and simulated AOD, column CCN5, CDNC, and SWCF over AUS, NAM, SAF, SAM, and SEA.

CHAPTER 4. CESM/CAM5 IMPROVEMENT AND APPLICATION: COMPARISON AND EVAULATION OF UPDATED CB05_GE AND MOZART-4 GAS-PHASE MECHANISMS AND ASSOCIATED IMPACTS ON GLOBAL AIR QUALITY AND CLIMATE

4.1 Introduction

Atmospheric chemistry plays an important role in the perturbation of climate system by determining the amounts and distributions of important oxidants and gaseous precursors for secondary air pollutants such as ozone (O_3) and aerosols. Aerosols can influence the Earth's radiative balance by directly scattering and absorbing radiation and indirectly affecting cloud properties through acting as cloud condensation nuclei (CCN) and ice nuclei. The aerosol effects on radiation depend critically on their chemical composition and physical properties. Therefore, atmospheric chemistry is an important component for atmospheric and Earth system models. Different chemical mechanisms (e.g., different chemical reactions and kinetic parameters) can lead to differences in the predictions of gases, secondary aerosols, as well as climatic variables such as CCN, cloud droplet number concentration (CDNC), and radiative forcings (Luecken et al., 2008; Sarwar et al., 2008; Zhang et al., 2012a; Lamarque et al., 2013).

There are generally two types of species in the gas-phase mechanisms: inorganic and organic. Although most mechanisms include the same important inorganic species (e.g., O_3, CO, HO_x, and NO_x), the predicted amounts can vary greatly among different mechanisms (Knote et al., 2014a). Some mechanisms ignore reactions with very low reaction rates since they do not affect results significantly. Also, some reactions may use different rate

coefficients with different dependence on atmospheric temperature and pressure due to the uncertainties in the laboratory measurements or the use of mechanisms that have not been updated in time. Unlike inorganic species, there are more significant differences in the representation of organic species. Light organic species with low molecular weight are often explicitly treated (e.g., methane, formaldehyde (HCHO)), whereas lumped or surrogate species are used to represent more complex mixtures of heavy organic compounds with high molecular weight (e.g., aromatics, organic nitrates). There are three most common representations of organic chemistry, including the lumped structure technique, the surrogate species approach, and the lumped species method (Zhang et al., 2004). For example, the Carbon Bond mechanism version IV (CB-IV, Gery et al., 1989), which uses the lumped structure approach for volatile organic compounds (VOCs), has been widely used in air quality modeling systems through urban to regional scales for many years. This mechanism has later been extensively updated in 2005 (CB05, Yarwood et al., 2005), and has been implemented into the Community Multiscale Air Quality model (CMAQ, Sarwar et al., 2008) and the Weather Research and Forecasting model with Chemistry (WRF-Chem, Wang et al., 2014a). CB05 has been further expanded to include more than 120 reactions that are important on global scale (CB05 with global extension (CB05_GE), Karamchandani et al., 2012) and implemented into global models, such as the Global-through-Urban WRF/Chem (GU-WRF/Chem, Zhang et al., 2012a) and the Community Atmosphere Model version 5 (CAM5), the atmospheric component of the Community Earth System Model (CESM/CAM5, He and Zhang, 2014). The Model of OZone and Related chemical Tracers version 4 (MOZART-4, Emmons et al., 2010) mechanism, which uses the lumped species

approach for VOCs, has also been used in WRF-Chem (Knote et al., 2014b), and CAM with extensive tropospheric and stratospheric chemistry (CAM-chem) Versions 4 and 5 (Lamarque et al., 2012; Tilmes et al., 2015). Different gas-phase mechanisms have also been compared in several studies, however, most of which are conducted in box models or using regional models (Kim et al., 2009; Kim et al., 2011a, b). For example, using WRF-Chem, Zhang et al. (2012b) found that three different mechanisms (i.e., the Carbon Bond Mechanism-Z (CBM-Z), the 1999 Statewide Air Pollution Research Center Mechanism (SAPRC99), and the CB05) can predict different O_3 concentrations up to 5 ppb at surface in July, 2001. Knote et al. (2014a) also compared seven chemical mechanisms using a box model and found that the differences in daytime OH radical concentrations can be up to 40%.

Climate change can also strongly influence atmospheric chemistry and aerosols and therefore air quality. For example, photolysis and temperature-dependent reactions can be directly impacted by climate change (Jacob and Winner, 2009). Due to the nonlinear relationships between chemistry, aerosols, and climate, it is important to accurately represent their interactions in a three-dimensional global model. Several studies have demonstrated the capability of CAM-chem to represent tropospheric (Aghedo et al., 2011; Lamarque et al., 2010, 2011a, b; Tilmes et al., 2015) and stratospheric (Lamarque et al., 2008; Lamarque and Solomon, 2010) conditions. The chemical mechanism used in CAM-chem is based on MOZART-4, with detailed stratospheric chemistry of Kinnison et al. (2007). In this section, two most commonly used gas-phase mechanisms: the extended MOZART-4 (with updates as described by Knote et al. (2014b) and additional updates in this work, referred to as MOZART-4x) and the CB05_GE chemical mechanisms are compared using the latest

CESM/CAM5. The objectives are to examine the differences in the secondary organic aerosols (SOA) predictions resulted from the two gas-phase chemical mechanisms and study the sensitivity of air quality and climate predictions to different gas-phase chemical mechanisms.

4.2 Model Descriptions

The CESM/CAM5 used in this work is based on CAM version 5.3 of CESM version 1.2.2, coupled to comprehensive tropospheric and stratospheric chemistry (CAM5-chem, Tilmes et al., 2015) using the 7-mode Modal Aerosol Model (MAM7, Liu et al., 2012). This version of CAM5-chem was further developed and improved at North Carolina State University (NCSU) in collaboration with NCAR, as described below. A more detailed description of this version of CESM CAM5-chem (referred to as CAM5-NCSU hereafter) used in this study can be found in He and Zhang (2014) and He et al. (2015).

4.2.1 Chemical Mechanisms

In this study, CB05_GE has been updated to include additional kinetic reactions describing interactions between functionalization and fragmentation processes during gas-phase oxidation of anthropogenic and biogenic VOCs by the hydroxyl radical, OH (Glotfelty et al., 2015). The products of those reactions are linked with the organic gas/particle partitioning for SOA formation. Heterogeneous reactions on tropospheric aerosols and stratospheric clouds are also added as same as those in MOZART-4x (Tilmes et al., 2015) with one additional pathway in CB05_GE to simulate sulfate formation through oxidation of sulfur dioxide (SO_2) by O_3 on the surface of dust particles.

MOZART-4x used in this work extends the MOZART chemical mechanism used in Lamarque et al. (2012) and Tilmes et al. (2015) to include several updates as described in Knote et al. (2014b). These updates include (1) detailed treatments of monoterpenes (α-pinene, β-pinene, and limonene) and 2-methyl-3-buten-2-ol (MBO); (2) detailed treatments of aromatics (e.g., benzene, toluene, and xylenes); (3) additional glyoxal ($C_2H_2O_2$) production from oxidized VOCs products; and (4) an updated isoprene (ISOP) oxidation scheme. In this work, the oxidation of anthropogenic and biogenic VOCs and subsequent aging processes are also included in MOZART-4x, and the products of those reactions are linked with the organic gas/particle partitioning for SOA formation.

Table 4.1 shows the gas-phase organic precursors for SOA formation treated in MOZART-4x and CB05_GE. For aromatic precursors of SOA, MOZART-4x includes benzene, toluene (TOL), xylenes, and cresol. Although CB05_GE does not include benzene, it includes polycyclic aromatic hydrocarbons (PAH) as a SOA precursor. For alkane precursors of SOA, MOZART-4x includes BIGALK (lumped alkanes with carbon (C) number > 3), whereas CB05_GE includes ALKH (long-chain alkanes, with C > 6). For anthropogenic alkene precursors of SOA, MOZART-4x includes propene (C_3H_6) and BIGENE (lumped alkenes with C >3), whereas CB05_GE includes terminal olefin (OLE) and internal olefin (IOLE). The emissions for biogenic alkene precursors are from the Model of Emissions of Gases and Aerosols from Nature version 2.1 (MEGAN2.1, Guenther et al., 2012). Both MOZART-4x and CB05_GE include alpha-pinene (APIN), beta-pinene (BPIN), limonene, and ISOP as precursors for biogenic SOA. CB05_GE also includes additional biogenic precursors such as speciated ocimene (OCI), humulene (HUM) and terpinene

(TER). However, in MOZART-4x, the species mapping for MEGAN emission calculation is slightly different. For example, α-pinene and other compounds (e.g., α-thujene, p-cymene, and o-cymene) are mapped into APIN, β-pinene and other compounds (e.g., sabinene and camphene) are mapped into BPIN, limonene and other compounds (e.g.; phellandrene and terpinene) are mapped into LIMON, myrcene and other compounds (e.g., ocimene) are mapped into MYRC, and beta-caryophyllene and other sesquiterpenes (e.g., humulene and α-bergamotene) are mapped into BCARY. Due to the different mapping for MEGAN species, biogenic emissions between MOZART-4x and CB05_GE are different, which can result in different biogenic SOA predictions. On the other hand, the rate coefficients for the oxidations of biogenic VOCs (e.g., APIN, BPIN, and limonene) are constant in CB05_GE, whereas they are temperature dependent in MOZART-4x, such a difference can result in different SOA predictions as well. In addition, there are uncertainties in the HO_x recycling associated with isoprene chemistry in CB05_GE (Karamchandani et al., 2012), whereas MOZART-4x used in this work includes OH recycling from improved isoprene chemistry. For example, in CB05_GE, ISOP is oxidized by OH to generate 91.2% molar yield of HO_2. In MOZART-4x, the isoprene peroxy radical from the oxidation ISOP by OH (i.e., ISOPO2) has different yields of HO_2 through reactions with NO, NO_3, methylperoxy radical (CH_3O_2), and acetylperoxy radical (CH_3CO_3), and it can also consume HO_2 itself. These reactions have different reaction rate coefficients. These differences can affect O_3, OH, and NO_x predictions, and thus the oxidation of VOCs.

4.2.2 Aerosol/Cloud Treatments

In CAM5-NCSU, the aerosol module is based on MAM7 of Liu et al. (2012), with improvements in terms of condensation, nucleation, aerosol thermodynamics, and aerosol activation (He and Zhang, 2014; Gantt et al., 2014). The major updates include: (1) the new particle formation treatments with a combination of the default nucleation parameterizations of Vehkamaki et al. (2002), Merikanto et al. (2007), and a newly added ion-mediated aerosol nucleation (Yu, 2010) above the planetary boundary layer (PBL), and a combination of the three and an additional parameterization of Wang and Penner (2009) in the PBL; (2) the inorganic aerosol thermodynamics based on ISORROPIA II of Fountoukis and Nenes (2007), which explicitly simulates the thermodynamics of sulfate (SO_4^{2-}), ammonium (NH_4^+), nitrate (NO_3^-), sodium (Na^+), and chloride (Cl^-) in the Aitken, accumulation, and fine sea-salt modes, as well as the impact of crustal species associated with the fine dust mode; (3) an advanced aerosol activation scheme based on Fountoukis and Nenes (2005) with additional updates based on Kumar et al. (2009) and Barahona et al. (2010), which accounts for adsorption activation from insoluble CCN and giant CCN equilibrium timescale on aerosol activation.

CAM5-NCSU also includes an advanced treatment for SOA formation based on a volatility-basis-set (VBS) approach that has been coupled with CB05_GE by Glotfelty et al. (2015) and is also coupled with MOZART-4x in this work. This approach consists of two primary components: (1) volatile SOA (VSOA) formation from anthropogenic VOCs (AVOCs) and biogenic VOCs (BVOCs) and (2) the volatility and aging of primary organic aerosol (POA) and the repartitioning of the semi/intermediate volatility compounds (S/IVOC) into SOA. The VSOA treatment is based on the treatment of Tsimpidi et al.

(2010). The products of VOC oxidation are mapped onto the volatility distribution using the aerosol mass yields listed in Tsimpidi et al. (2010) using the CB05_GE species that represent those precursor VOCs. An additional pathway for the formation of SOA from PAH is also added in CB05_GE. The SOA mass yields for PAHs are derived from the laboratory measurements of Chan et al. (2009) following the approach of Stainer et al. (2008), where the SOA mass yields for naphthalene, 1-methylnaphthalene, and 2-methylnaphthalene are averaged as surrogates for PAHs. The volatility of POA and the subsequent formation of SOA from POA vapors are based on the work of Robinson et al. (2007) and Shrivastava et al. (2008). POA emissions are distributed into nine logarithmically-spaced volatility bins with effective saturation (C*) values ranging from 10^{-2} to 10^{6} μg m^{-3}. An updated emission spectrum is used to distribute the POA emissions into the volatility bins as the emission spectrum used in Robinson et al. (2007) has been shown to be too volatile (Cappa and Jimenez, 2010; Hodzic et al., 2010; Jathar et al., 2011). This new emission spectrum maps the anthropogenic POA emissions onto the volatility distribution based on thermodenuder measurements of gasoline exhaust and also contains separate emissions fractions for biomass burning aerosol which is less volatile than anthropogenic POA (May et al., 2013a, b). The emission spectrum of Robinson et al. (2007), also assumes that the emissions of SVOCs are fully captured by the original POA emissions and missing IVOCs are assumed to be equivalent to 1.5 times the POA emissions inventory with these additional emissions placed in the three highest volatility bins. However, because the estimations of the missing IVOC emissions are poorly constrained, the 1.5 times the POA mass for IVOCs is not included in this study.

In additional to the classic 1-D VBS treatment as described above, functionalization and fragmentation treatment described in Shrivastava et al. (2013) are included in this version of VBS for both VSOA and S/IVOCs (referred to as 1.5 D VBS). In this treatment, the VSOA and S/IVOCs in each volatility bin are split into three different species representing three generations of oxidation. During the first two generations of oxidation the mass of the VSOA and S/IVOCs grows by 15%, reflecting the addition of oxygen atoms. In this aging scheme not only do the masses of VSOA and S/IVOCs increase in generation when oxidized by OH (at a rate of 1.0×10^{-11} and 4.0×10^{-11} cm^3 $molecule^{-1}$ s^{-1}, respectively) but also their volatility decrease as they are moved into smaller volatility bins. Fragmentation occurs once the VSOA and S/IVOCs have aged to the third generation. This represents the breaking of carbon bonds, which can increase volatility of the organic species thus reducing SOA formation. This is parameterized by allowing 17.25% of the organic mass to pass to the next lowest volatility bin but passing 75% of the VSOA and S/IVOC to the highest volatility bin in the VBS structure. The remaining mass is assumed to be lost to species of higher volatility than the VBS structure. A more detailed description of SOA formation from the VBS approach is summarized in Glotfelty et al. (2015).

4.3 Model Configurations and Evaluation Protocols

4.3.1 Model Setup and Inputs

The simulations are performed with specified dynamics configuration, of which winds and temperature are driven by the Goddard Earth Observing System Model, Version 5 (GEOS-5) meteorology. The internally-derived meteorological fields are nudged every time step (30 min) by 10% towards analysis fields from GEOS-5. The simulations are conducted

for a 3-year period of 2008-2010 at a horizontal resolution of $0.9^{o} \times 1.25^{o}$ and a vertical resolution of 56 layers for CAM5. The initial chemical conditions are generated with same configurations with 1-year spinup.

The offline emissions used in this work are based on those used in Tilmes et al. (2015), of which the anthropogenic and biofuel emissions are from the Monitoring Atmospheric Composition and Climate/CityZen (MACCity) emission data set (Granier et al., 2011), and biomass burning emissions are taken from the Atmospheric Chemistry and Climate Model Intercomparison Project (ACCMIP) historical emissions dataset (Lamarque et al., 2010). The ACCMIP emissions are extrapolated for 2008-2010 with the Representative Concentration Pathway (RCP) 8.5 scenario and extended for VOCs and several other species for MOZART-4x species. MOZART-4x species are then mapped into CB05_GE species to generate emissions for CB05_GE species. The online emissions include biogenic VOCs from MEGAN2.1 (Guenther et al., 2012), lightning NO_x (Price and Rind, 1992; Price et al., 1997), mineral dust (Zender et al., 2003), and sea-salt (Martensson et al., 2003).

4.3.2 Available Measurements for Model Evaluation

A number of observational datasets from surface networks and satellites are used for model evaluation. They are summarized along with the variables to be evaluated in Table 4.2. The global surface network includes data sets from the National Oceanic and Atmospheric Administration Climate Diagnostics Center (NOAA/CDC). The satellite datasets include the Moderate Resolution Imaging Spectroradiometer (MODIS) for the retrievals of cloud properties, the Clouds and Earth's Radiant Energy System (CERES), for the retrievals of radiation fluxes at surface and top of atmosphere, the Aura Ozone

Monitoring Instrument in combination with Aura Microwave Limb Sounder (OMI/MLS) for the tropospheric ozone retrieval, the Measurements Of Pollution In The Troposphere (MOPITT) for tropospheric carbon monoxide (CO) retrieval, and the SCanning Imaging Absorption spectroMeter for Atmospheric CHartographY (SCIAMACHY) for the retrievals of tropospheric nitrogen dioxide (NO_2), HCHO, and $C_2H_2O_2$. Other satellite-based data include the MODIS-derived CDNC and cloud liquid water path (LWP) by Bennartz (2007).

Regional observational networks include the Clean Air Status and Trends Network (CASTNET), the Interagency Monitoring of Protected Visual Environments (IMPROVE), the Speciation Trends Network (STN), and the Air Quality System (AQS) over CONUS; the European Monitoring and Evaluation Program (EMEP), the Base de Données sur la Qualité de l'Air (BDQA, France), and the European air quality database (AirBase) over Europe; the Ministry of Environmental Protection of China (MEPC), the National Institute for Environmental Studies of Japan (NIESJ), the Korean Ministry Of Environment (KMOE), and Taiwan Air Quality Monitoring Network (TAQMN) over East Asia. In addition to the data from the above networks, SOA measurements collected by Lewandowski et al. (2013) at four field study sites including Cleveland and Medina, OH (July-August, 2009), and Bakersfield and Pasadena, CA (May-June, 2010) are used to evaluate SOA predictions.

Aircraft measurements include aircraft campaigns from Aerosol, Radiation, and Cloud Processes affecting Arctic Climate (ARCPAC), Stratosphere-Troposphere Analyses of Regional Transport in 2008 (START08), California Nexus 2010 (CalNex), Arctic Research of the Composition of the Troposphere from Aircraft and Satellites (ARCTAS), and CCN measurements in China (CCN_China). ARCPAC (Brock et al., 2011) was conducted during

March-April 2008 in the troposphere of the Alaskan Arctic, including particle size distributions, composition, and optical properties. START08 (Pan et al., 2010) was conducted during April-June 2008 to study the chemical and transport characteristics of the extratropical upper tropospheric and lower stratospheric region over central North America. CalNex (Ryerson et al., 2013) was conducted during May-July 2010 to provide improved scientific knowledge for emission control strategies to simultaneously address the interrelated issues of air quality and climate change. ARCTAS (Jacob et al., 2010) was conducted during April-June 2008 to investigate the chemistry of the Arctic's lower atmosphere. CCN_China (Zhang et al., 2011) was conducted over Beijing during July-September 2008, to investigate the impacts of aerosols on cloud formation.

4.3.3 Evaluation Protocol

The protocols for performance evaluation include spatial distributions and statistics, following the approach of Zhang et al. (2012b). The aircraft profile evaluation is based on the Atmospheric Model Working Group (AMWG) diagnostics package (Tilmes et al., 2015). Monthly-mean model results are compared for corresponding regions and seasons of the field campaign. The analysis of the performance statistics will focus on mean bias (MB), normalized mean bias (NMB), normalized mean error (NME), and root mean square error (RMSE). The radiative/cloud variables are evaluated annually, including outgoing longwave radiation (OLR) from NOAA/CDC; downwelling shortwave radiation (FSDS), downwelling longwave radiation (FLDS), shortwave cloud forcing (SWCF), and longwave cloud forcing (LWCF) from CERES; cloud fraction (CF), aerosol optical depth (AOD), cloud optical thickness (COT), precipitating water vapor (PWV), and CCN from MODIS, as well as

CDNC and LWP from Bennartz (2007). CDNC is calculated as an average value of layers between 850 and 960 hPa for comparison with the satellite-derived values. Chemical concentrations evaluated include CO, O_3, SO_2, ammonia (NH_3), NO_2, nitric acid (HNO_3), VOCs (i.e., formaldehyde, isoprene, and toluene), particulate matter (PM) with diameter less than and equal to 10 μm (PM_{10}) and 2.5 μm ($PM_{2.5}$), and $PM_{2.5}$ major components (e.g., SO_4^{2-}, NH_4^+, NO_3^-, black carbon (BC), organic carbon (OC), and total carbon (TC)) for CONUS and Europe. The chemical observations over East Asia are very limited, which only include surface observations of CO, SO_2, NO_2, and O_3 from Hong Kong, South Korea, and Japan, and PM_{10} over mainland China (derived from air pollution index), Hong Kong, South Korea, and Japan. Since $PM_{2.5}$ and PM_{10} are not explicit species simulated in MAM7, they are simply assumed to be the particles in the first 5 modes (i.e., Aitken, accumulation, primary carbon, fine sea-salt, and fine dust modes) and the total 7 modes (i.e., Aitken, accumulation, primary carbon, fine sea-salt, fine dust, coarse sea-salt, and coarse dust modes), respectively. Column concentrations of tropospheric CO, NO_2, HCHO, $C_2H_2O_2$, and tropospheric O_3 residual (TOR) are evaluated for globe. The CO column evaluation follows the AMWG diagnostics approach, which applies $1^o \times 1^o$ monthly mean Level 3 MOPITT a priori and averaging kernels to monthly mean model results to account for the a priori dependence and vertical resolution of the MOPITT data. The measured NO_2 and HCHO columns are derived from the satellite retrievals from SCIAMCHY, which are monthly mean gridded data on a $0.25^o \times 0.25^o$ horizontal grid resolution for the period of 2008-2010. The measured glyoxal column is derived from the satellite retrievals from SCIAMCHY, which are monthly mean gridded data on a $0.125^o \times 0.125^o$ horizontal grid resolution for the period

of 2008. The measured O_3 is derived from the combing retrievals from the Aura Ozone Monitoring Instrument and Microwave Limb Sounder observations, which are monthly mean gridded data on a $1.25^o \times 1.25^o$ horizontal grid resolution for the period of 2008-2010.

All surface observational data used for evaluating 2008-2010 simulations are available throughout 2008-2010 except for several variables with data during a limited time period of 2001-2010 including OC from EMEP, SOA from Lewandowski et al. (2013), and OA from Zhang et al. (2007) and Jimenez et al. (2009).

4.4 Results

4.4.1 Chemical Evaluations

Table 4.3 summarizes the performance statistics for major chemical species for CAM5-NCSU simulations with MOZART-4x and CB05_GE. Figure 4.1 shows the scatter plots between observations and model results. The statistical performance of MOZART-4x and CB05_GE are similar for most chemical species. As shown in Table 4.3, CO is underpredicted over East Asia by both MOZART-4x and CB05_GE, with NMBs of -65.6% and -65.7%, respectively. The underprediction of CO is mainly due to the underestimation of CO emissions from biomass burning (Tilmes et al., 2015). The underestimations in CO emissions lead to underpredictions of column CO concentrations, with NMBs of -25.8% and -24.4% for MOZART-4x and CB05_GE, respectively. Both MOZART-4x and CB05_GE largely overpredict the concentrations of SO_2 over CONUS (with NMBs of 580.2% and 561.6%, respectively), East Asia (with NMBs of 47.0% and 35.5% %, respectively), and Europe (with NMBs of 100.9% and 94.1%, respectively), likely due to the overestimation of SO_2 emissions, the uncertainties in the emission injection heights as well as the vertical

mixing scheme used. The overpredictions of surface SO_2 concentrations result in the overpredictions of the concentrations of SO_4^{2-} at the surface. Surface NH_3 concentrations from MOZART-4x and CB05_GE are overpredicted over Europe (with NMBs of 112.4% and 104.3%, respectively), likely due to the overestimation of NH_3 emissions. The overpredictions of the NH_3 concentrations result in the overpredictions of the NH_4^+ concentrations at the surface. The concentrations of NO_2 from MOZART-4x and CB05_GE are largely underpredicted over Europe (with NMBs of -61.4% and -62.1%, respectively) and East Asia (with NMBs of -74.1% and -74.8%, respectively), which is likely due to the uncertainties in estimating total NO_x emissions and emission injection heights as well. As shown in Figure 4.1, the concentrations of O_3 from MOZART-4x and CB05_GE are overpredicted over CONUS (with NMBs of 29.0% and 28.2% over the CASTNET sites, respectively), Europe (with NMBs of 19.3% and 22.2% over the EMEP sites, respectively) and East Asia (with NMBs of 68.8% and 65.7% over the KMOE sites, respectively). This is likely due to the less O_3 titration resulted from the underpredictions of NO_x, coarse resolution, as well as dilution of NO_x emissions. The overpredictions of SO_4^{2-} result in the underpredictions of NO_3^- and Cl^-, through thermodynamic equilibrium, and therefore overpredictions of HNO_3 over CONUS. However, HNO_3 is underpredicted over Europe, which is likely due to the underpredictions of NO_x. Cl^- is overpredicted over Europe, which is likely due to the uncertainties for the gas/particle partitioning over coarse modes (He and Zhang, 2014). Both MOZART-4x and CB05_GE predict $PM_{2.5}$ relatively well over CONUS, however, they underpredict PM_{10} over the AQS sites, with NMBs of -38.6% and -38.9%, respectively. The underpredictions of PM_{10} are likely due to the inaccurate predictions of

coarse particles. Both MOZART-4x and CB05_GE underpredict $PM_{2.5}$ and PM_{10} over Airbase and BDQA sites, however, they overpredict PM_{10} by 3.14 μg m^{-3} (or by 22.2%) and 3.43 μg m^{-3} (or by 24.2%) over the EMEP sites, respectively, which is likely due to the overpredictions of coarse particles (e.g., Cl^-) over these sites. Both MOZART-4x and CB05_GE underpredict PM_{10} by 33.61 μg m^{-3} (or by 33.4%) and 26.71 μg m^{-3} (or by 26.6%) over the MEPC sites in mainland China, respectively, which is mainly due to the uncertainties in the emissions in primary gases (e.g., SO_2, NO_x, NH_3, and VOCs) and particulate species (e.g., SO_4^{2-}, BC, and POA). Granier et al. (2011) compared the regional emissions among different inventories and indicated large uncertainties in the emissions over China. For example, the differences of BC biomass burning emissions over China among different inventories can be as large as a factor of 2.1, and the differences of SO_2 anthropogenic emissions can be as large as a factor of 1.8.

VOCs species such as HCHO, ISOP, and TOL are underpredicted over CONUS, likely due to the uncertainties in the biogenic emissions from MEGAN2.1, anthropogenic emissions (e.g., HCHO and TOL) and the chemical reactions as well as a coarse horizontal resolution used in this work. Both MOZART-4x and CB05_GE underpredict BC with NMBs of -29.3% and -29.3%, respectively. The underpredictions of BC are likely due to the underestimations of BC emissions, as well as uncertainties in the transport and wet removal by convection (Ma et al., 2013; Wang et al., 2013; Tilmes et al., 2015).

OC is slightly overpredicted with an NMB of 2.1% by MOZART-4x over CONUS, whereas it is moderately underpredicted with an NMB of -20.7% by CB05_GE. OC is evaluated against observations at the IMPROVE sites, and SOA dominates OC at these sites

for both simulations with MOZART4-x and CB05_GE, with SOA/OC ratios of 83.0% and 59.6%, respectively. Although no SOA measurements are available from IMPROVE for evaluation, the differences in OC predictions can be attributed to the differences in SOA predictions because of dominances of SOA in total OC. Compared to the SOA observations at the four sites in the U.S. from Lewandowski et al. (2013), MOZART-4x underpredicts SOA by 0.03 μg m^{-3} (or by 1.9%), whereas CB05_GE underpredicts SOA by 0.4 μg m^{-3} (or by 23.1%). Note that the SOA statistics are calculated using only four pairs of seasonal mean values at four sites in the U.S. where the observed SOA data are available during 2008-2010; they therefore may not be representative because of limited data used for calculation. Figure 4.2 compares simulated and observed SOA concentrations at the four sites. MOZART-4x predicts higher SOA than CB05_GE at all four sites, which reduces underpredictions at Cleveland and Medina, OH but increases overpredictions at Bakersfield and Pasadena, CA. This indicates a better capability of MOZART-4x to simulate SOA at these sites with relatively high SOA concentrations (≥ 1 μg m^{-3}) compared to CB05_GE despite its tendency of overpredictions at sites with lower SOA levels. The higher SOA concentrations predicted by MOZART-4x can be attributed to the higher OH levels and higher biogenic emissions in MOZART-4x. However, the concentration of OC is largely underpredicted by both MOZART-4x and CB05_GE over Europe, with NMBs of -74.2% and -75.1%, respectively, indicating the uncertainties in the emissions of SOA precursors and SOA formation treatment. For example, the aqueous-phase oxidation of VOCs in clouds is not taken into account in this work, which, however, can contribute several percentages of SOA in some areas and seasons over Europe (Couvidat et al., 2013). The hydrocarbon-like organic aerosol

(HOA) predicted by MOZART-4x and CB05_GE correlated well with the observations at 33 sites in the Northern Hemisphere (e.g., with correlation coefficients of 0.93 for both simulations) but the amount is largely underpredicted by both MOZART-4x and CB05_GE, with NMBs of -77.2% and -76.7%, respectively, indicating that the POA may be too volatile with the implementation currently in the model. Oxygenated organic aerosol (OOA), which is roughly equivalent to the sum of SOA and SVOA, is also largely underpredicted at the 33 sites by both MOZART-4x and CB05_GE, with NMBs of -56.5% and -62.3%, respectively. This is mainly due to the uncertainties in the oxidation rate and fragmentation rates as well as SOA formation treatment. The underpredictions of HOA and OOA result in an underprediction of total organic aerosol (TOA) by both MOZART-4x and CB05_GE, with NMBs of -67.8% and -71.2%, respectively.

Figure 4.3 shows the zonal mean of column concentrations of CO, HCHO, glyoxal, NO_2, and TOR for June, July, and August during 2008-2010. In general, MOZART-4x and CB05_GE predict similar zonal mean profiles of these species. Both MOZART-4x and CB05_GE underpredict column CO, due to a significant underestimation of CO emissions (Tilmes et al., 2015) and uncertainties in OH predictions. During summer, column HCHO is overpredicted over middle latitudes (30-60^o N) in the Northern Hemisphere and tropical regions (0-10^o S) in the Southern Hemisphere, while it is largely underpredicted over the rest of regions. The underprediction of column HCHO is likely due to the uncertainties in the emissions of HCHO and its precursors as well as pathways for secondary HCHO formation. Both MOZART-4x and CB05_GE underpredict column glyoxal, with more underpredictions in CB05_GE. The underpredictions of glyoxal are mainly due to the uncertainties in the

glyoxal chemical production and removal (Knote et al., 2014b). Several studies indicate that aromatics, isoprene, and ethyne are the major contributors to glyoxal formation (Washenfelder et al., 2011; Knote et al., 2014b). In MOZART-4x, glyoxal can be produced from photolysis of the oxidation products of toluene, and oxidation products of aromatics (e.g., benzene, toluene, and xylenes), isoprene, and ethyne. CB05_GE does not include pathways for glyoxal production through photolysis, but includes glyoxal production from oxidation of alkenes (e.g., OLE, IOLE, ethene, and ISOP) and aromatics (e.g., toluene and xylenes). Uncertainties in the emissions of these precursors and the production pathways can propagate into the predicted glyoxal concentrations. MOZART-4x includes additional pathways for glyoxal production through photolysis and improved treatments for glyoxal production from additional oxidized VOCs (e.g., benzene) products (Knote et al., 2014b), which can result in higher glyoxal than in CB05_GE. The major chemical loss of glyoxal includes photochemical loss and oxidation by OH. The uncertainties in OH levels can propagate into glyoxal predictions as well. In addition, CB05_GE includes an additional pathway for glyoxal loss through its uptake by aerosols, which is not included in MOZART-4x. This can explain in part the lower glyoxal concentrations predicted by CB05_GE than by MOZART-4x. An advanced treatment for glyoxal formation should be therefore developed in the future. Both MOZART-4x and CB05_GE overpredict column NO_2, likely due to the uncertainties in the NO_2 aircraft emissions and overpredictions of lightning NO_x. The lightning NO_x emissions are calculated online (i.e., 6.2 and 6.4 TgN yr^{-1} in CB05_GE and MOZART-4x, respectively), which is about 1.2-2.2 TgN yr^{-1} higher than that in Lamarque et al. (2012) and Tilmes et al. (2015). Tilmes et al. (2015) have shown that increased lightning

NO_x emissions in CAM-chem can lead to an increase in OH levels and therefore a decrease in the lifetime of methane and an underestimation of CO in the model. The higher zonal-mean concentrations of NO_2 in CB05_GE than those in MOZART-4x are likely due to additional NO_2 production from the reactions of VOCs with NO_3 radical in CB05_GE (e.g., reactions of NO_3 with OLE, IOLE, and ethene). The zonal-mean distribution of summer TOR from CB05_GE is similar to that from MOZART-4x. TOR is overpredicted over 40^o S-50^o N, and underpredicted over 40^o S-60^o S. The higher TOR from CB05_GE is mainly due to higher O_3 production from higher NO_2 and lower O_3 loss from lower OH in CB05_GE than in MOZART-4x.

Figure 4.4 compares the vertical profiles of major gases against the aircraft observations (i.e., ARCPAC, ARCTAS, START08, and CalNex). Compared with aircraft measurements, MOZART-4x and CB05_GE predict similar O_3 and CO profiles, whereas there are large differences in NO_x (above 9 km) and NO_y profiles (below 12 km). O_3 profiles from MOZART-4x and CB05_GE overall agree well with aircraft measurements, although O_3 is slightly overpredicted near the surface. As discussed previously, the significant underpredictions of CO profiles in both MOZART-4x and CB05_GE are mainly due to the underestimations of CO biomass burning emissions and uncertainties in OH predictions. Both MOZART-4x and CB05_GE underpredict the vertical concentrations of NO_x at higher altitudes (e.g., above 9 km in ARCTAS and STRAT08), with a slightly better agreement in CB05_GE than in MOZART-4x. The concentrations of NO_x near the surface are slightly overpredicted by both simulations. The underpredictions of the concentrations of NO_x at higher altitudes are likely due in part to the uncertainties in the NO_x emissions, the chemical

reactions of nitrogen cycles (e.g., heterogeneous reactions of NO_2, NO_3, and N_2O_5 over the surface of aerosol particles), the convection scheme, as well as the aircraft campaign data. Some field campaigns (e.g., ARCPAC) focus on the polluted regions with a significant contribution from biomass burning and local sources (Tilmes et al., 2015). The underestimations of emissions from these sources and uncertainties in the vertical mixing scheme can result in the underpredictions of their profiles. NO_y includes all the reactive nitrogen species. The simulated NO_y profiles from CB05_GE agree better with those observed during APCPAC, ARCTAS, and CalNex than those from MOZART-4x, whereas MOZART-4x predicts slightly better NO_y profile against START08 in the lower troposphere than CB05_GE. Figure 4.5 compares the vertical profile of simulated CCN against the aircraft observations from CCN_China. Both MOZART-4x and CB05_GE slightly overpredict CCN (at supersaturation of 0.2%) profile over Beijing area, with less overpredictions in MOZART-4x.

4.4.2 Column Comparisons

Figures 4.6a and b compare the column mass abundance of major gaseous and aerosol species simulated by MOZART-4x and CB05_GE. As shown in Figure 4.6a, column CO predicted by MOZART-4x is about 2.4×10^{20} m^{-2} (or by 2.3%) lower than that by CB05_GE in the global mean. The different column CO concentrations are due to different pathways for chemical production and loss of CO and different OH levels between MOZART-4x and CB05_GE. The chemical production of CO is mainly from photolysis and oxidation of VOCs species, and the chemical loss of CO is mainly from the oxidation by OH. Different concentrations of VOCs species can result in different chemical production of CO.

Meanwhile, the only chemical loss of CO in CB05_GE is the oxidation of CO by OH, which produces HO_2 and CO_2. Higher OH levels in MOZART-4x can result in more CO loss. MOZART-4x includes an additional loss pathway of CO oxidized by OH to produce CO_2 and H. As a result, the combined rate constant for both pathways of CO oxidation by OH in MOZART-4x is about 4% higher than in CB05_GE. All these differences result in 2301 and 2265 Tg yr^{-1} chemical loss of CO in MOZART-4x and CB05_GE, respectively.

The global mean differences in the simulated column concentrations of SO_2 and NH_3 between MOZART-4x and CB05_GE are 2.0×10^{18} m^{-2} (or by 12.5%) and 1.9×10^{17} m^{-2} (or by 3.1%), respectively. The lower column abundance of SO_2 in CB05_GE is mainly due the additional pathway for SO_2 loss through oxidation by O_3 over the surface of dust particles, which is not include in MOZART-4x. This pathway can produce more SO_4^{2-} and therefore, more NH_3 is partitioned into the particulate phase to form NH_4^+ which can neutralize additional SO_4^{2-}, resulting in lower column abundance of NH_3 in CB05_GE. Both column concentrations of NO_x and NO_y from MOZART-4x are about 9.4×10^{17} m^{-2} (or by 9.5%) and 3.6×10^{19} m^{-2} (or by 46.3%) lower than that from CB05_GE. The higher NO_x in CB05_GE is mainly due to the lower OH available for the chemical loss through the reaction of NO_2 with OH. NO_y in MOZART-4x includes NO_x, nitrate radical (NO_3), nitrogen pentoxide (N_2O_5), HNO_3, peroxynitric acid (HO_2NO_2), chlorine nitrate ($ClONO_2$), bromine nitrate ($BrONO_2$), peroxyacetyl nitrate (PAN), organic nitrate (ONIT), methacryloyl peroxynitrate (MPAN), peroxy radical from the reaction of NO_3 with ISOP (ISOPNO3), and lumped isoprene nitrate (ONITR), whereas NO_y in CB05_GE includes NO_x, NO_3, N_2O_5, HNO_3, HO_2NO_2, $ClONO_2$, $BrONO_2$, nitrous acid (HONO), PAN, higher peroxyacyl nitrates (PANX), and organic

nitrate (NTR). The reactions for reactive nitrogen species are different in MOZART-4x and CB05_GE, resulting in different NO_y predictions.

The tropospheric column O_3 from MOZART-4x is about 1.5 DU (or by 4.7%) lower than that from CB05_GE. Table 4.4 shows the tropospheric O_3 budget from MOZART-4x and CB05_GE. The burdens of tropospheric O_3 from MOZART-4x and CB05_GE are 325 Tg and 333 Tg, respectively, which is comparable to the previous studies using CAM (Lamarque et al., 2012; Young et al., 2013). The O_3 burden from MOZART-4x in this work is about 12 Tg (or 3.8%) higher than that in Tilmes et al. (2015), which is mainly due to the additional kinetic reactions included in this version of MOZART-4x. The dry deposition flux of O_3 from MOZART-4x is 679 Tg yr^{-1}, which is about 3.7% lower than that from CB05_GE (i.e., 705 Tg yr^{-1}). The lower O_3 dry deposition flux is mainly due to the lower O_3 concentration simulated by MOZART-4x. The O_3 chemical production and loss from CB05_GE and MOZART-4x are roughly within the range of Young et al. (2013). The O_3 chemical production from MOZART-4x is comparable to that of Lamarque et al. (2012), but the O_3 chemical production from CB05_GE is about 12.8% higher than Lamarque et al. (2012). In this table, chemical production is calculated mainly from reactions of NO with peroxy radicals and chemical loss is calculated mainly from the oxygen radical in the reaction of excited oxygen atom (O^1D) with water vapor (H_2O) and from the reactions of O_3 with the HO_2, OH, and alkenes. Different peroxy radicals and alkenes treated and different reaction rates used in the two mechanisms can contribute to the different chemical production and chemical loss of O_3. The O_3 lifetime is calculated based on the ratio of O_3 burden to the total O_3 loss (dry deposition + chemical loss). The O_3 lifetime from CB05_GE is comparable

to those reported by Young et al. (2013), and the O_3 lifetime from MOZART-4x is comparable to those reported by Lamarque et al. (2012) and Tilmes et al. (2015).

Column concentrations of OH, HCHO, and ISOP from MOZART-4x are higher than CB05_GE, with global mean values of 9.7×10^{13} m^{-2} (or by 0.8%), 3.5×10^{17} m^{-2} (or by 1.3%), and 1.1×10^{18} m^{-2} (or by 25.6%), respectively. The higher column concentrations of OH and HCHO are likely due to the photolysis of more peroxide species, better HO_x recycling, and higher precursors for secondary HCHO (e.g., ISOP) in MOZART-4x. MOZART-4x includes detailed organic peroxide species, whereas in CB05_GE, all the organic peroxide species are lumped into one species (i.e., ROOH). The uncertainties in HO_x recycling in CB05_GE can also result in uncertainties in OH predictions. The higher ISOP is mainly due to higher biogenic emissions and less chemical loss in MOZART-4x than that in CB05_GE. In MOZART-4x, the chemical loss of ISOP is mainly from the oxidation of ISOP by OH, O_3, and NO_3. However, in CB05_GE, the chemical loss of ISOP includes not only the oxidation of ISOP by OH, O_3, and NO_3, but also the consumption of ISOP by atomic oxygen (i.e., O), NO_2, and Cl.

As shown in Figure 4.6b, the differences in the domain average column mass abundances of most aerosol species (e.g., NH_4^+, BC, Cl^-, and POA) between MOZART-4x and CB05_GE are within ± 0.02 mg m^{-2}. The differences in the column SO_4^{2-} vary from -25.2 to 0.4 mg m^{-2}, with the global mean of -0.2 mg m^{-2}. The simulated column concentrations of SO_4^{2-} from MOZART-4x are much lower than those from CB05_GE over East Asia, west Europe, and Middle Africa. SO_2 can be oxidized by O_3 to form SO_4^{2-} on the surface of dust particles in CB05_GE, which explains additional formation of SO_4^{2-} by

CB05_GE over these regions. The differences of the spatial distributions and magnitudes in the column concentrations of NH_4^+ are similar to those of SO_4^{2-} over land areas, which is associated with thermodynamic equilibrium. The column concentrations of NO_3^- simulated by MOZART-4x are higher over East Asia, India, and Europe than those by CB05_GE, which is mainly due to its competition with SO_4^{2-} in forming ammonium salts in the particulate phase in those regions where the column NH_3 concentrations are high (Figure 4.6a). Dust emissions are very sensitive to the wind speed. Slightly changes in wind speeds can result in significant change in dust emissions, thus, dust concentrations.

The column concentrations of SOA predicted by MOZART-4x are about 0.18 mg m^{-2} (or by 8.4%) higher than those predicted by CB05_GE. The higher SOA column concentrations are mainly over most continental areas in the middle and low latitudes. The SOA mainly includes biogenic SOA, anthropogenic SOA, and semi-volatile SOA. The differences of SOA are mainly due to the higher BVOCs emissions and higher OH levels in MOZART-4x than in CB05_GE. Different branching ratios used in MOZART-4x and CB05_GE can also contribute to the different SOA predictions. MOZART-4x includes explicit species and more types of precursors for alkylperoxy radicals (RO_2), and different reaction rate constants for different reactions, whereas in CB05_GE, all oxidized VOCs are lumped as one species (i.e., RO_2) and branching ratios are estimated based on the only three reactions (i.e., reactions of RO_2 with NO, HO_2, and RO_2). These differences can contribute to the differences in the estimation of branching ratios, and therefore, affect the partitioning between organic gas and aerosols through the 1.5 D VBS treatment implemented in CAM5-NCSU.

4.4.3 SOA Comparisons

Figure 4.7 shows the contributions to total SOA (TSOA) concentrations from anthropogenic sources (ASOA), biogenic sources (BSOA), glyoxal (GLSOA), and semi-volatile organic aerosol (SVSOA) over Australia, Europe, North America, South Africa, South America, and East Asia over 2008-2010. The contributions of ASOA to TSOA predicted by MOZART-4x and CB05_GE are about 17-44%, and 10-47%, respectively, with South America the least and East Asia the most. The contributions of BSOA to TSOA predicted by MOZART-4x and CB05_GE are about 31-75%, and 26-76%, respectively, with East Asia the least and South America the most. The contribution of GLSOA to TSOA predicted by CB05_GE is about 2-6%. CB05_GE used in this work includes a simple conversion of glyoxal to condensable VOCs, which can be uptaken by preexisting particles to form SOA. However, this conversion is not included in MOZART-4x. Therefore, there is no GLSOA predicted by MOZART-4x despite it predicts higher glyoxal as shown in Figure 4.3. The contributions of SVSOA to TSOA predicted by MOZART-4x and CB05_GE are about 8-37%, and 8-41%, respectively, with South America the least and South Africa the most. Among four types of SOA, both MOZART-4x and CB05_GE predict BSOA as the main contributor over most regions (e.g., Australia, North America, South Africa, and South America) and ASOA as the main contributor over East Asia, which is mainly due to the much higher anthropogenic emissions over East Asia. Europe is a different example. MOZART-4x predicts BSOA as the top contributor (44%) and ASOA as the second largest contributor (40%), whereas CB05_GE predicts ASOA as the top contributor (45%) and BSOA as the second largest contributor (36%). Both MOZART-4x and CB05_GE predict

ASOA as the top contributor (46-59%) for spring, fall, and winter, and BSOA as the top contributor (57% and 47%, respectively) for summer over Europe. Since MOZART-4x predicts higher BSOA than CB05_GE, BSOA is dominant in MOZART-4x on the annual average. The higher BSOA from MOZART-4x than CB05_GE is mainly due to the higher BVOCs emissions in MOZART-4x and higher OH levels in MOZART-4x. The total BVOCs emission in MOZART-4x is about 2.5×10^{-3} kg m^{-2} yr^{-1}, which is about 7.2×10^{-5} kg m^{-2} yr^{-1} (or 2.9%) higher than CB05_GE. The higher BVOCs emissions in MOZART-4x are mainly due to the different species mapping for MEGAN emission calculations. The differences of SOA from biogenic alkenes between MOZART-4x and CB05_GE are MYRC and BCARY in MOZART-4x, and OCI, HUM, and TER in CB05_GE (as shown in Table 4.1). In CAM-chem that uses MOZART, MEGAN calculates all of the individual species and CAM-chem sums them up to map with the MOZART mechanism species. For example, MYRC emissions consist of myrcene and ocimene, BCARY emissions consist of beta-caryophyllene, alpha-bergamotene, beta-bisabolene, beta-farnescene, and alpha-humulene, and LIMON emissions consist of limonene, phellandrene, and terpinene. Therefore, the biogenic emissions for more types of VOCs in MOZART-4x are higher than those in CB05_GE, resulting in higher BSOA in MOZART-4x. The differences in SOA from aromatics between MOZART-4x and CB05_GE are BENZENE in MOZART-4x and PAH in CB05_GE (as shown in Table 4.1). The emissions of PAH are higher over Europe, East Asia, eastern U.S., and South Africa. The benzene emissions are about 1 order of magnitude higher than the emissions of PAH, and the rate constant of the oxidation of benzene by OH is temperature dependent whereas it is constant for oxidation of PAH by OH. In addition, OH levels are

higher in MOZART-4x than those in CB05_GE. These differences could result in different ASOA between two simulations. Both MOZART-4x and CB05_GE predict higher SVSOA contributions over South Africa than other regions, which is mainly due to the higher POA emissions (e.g., biomass burning) over this region.

Although the percentage contributions of different types of SOA predicted by MOZART-4x and CB05_GE are similar over most regions, the absolute mass concentrations of different types of SOA are different. For example, TSOA predicted by MOZART-4x is about 0.02-2.0 mg m^{-2} higher than by CB05_GE over these regions. ASOA predicted by MOZART-4x is about 0.068-1.017 mg m^{-2} higher than predicted by CB05_GE over most regions except Europe (0.054 mg m^{-2} lower) and East Asia (0.062 mg m^{-2} lower). BSOA predicted by MOZART-4x is about 0.162-1.365 mg m^{-2} higher than predicted by CB05_GE over most regions except Australia (0.003 mg m^{-2} lower). MOZART-4x includes SOA formation from benzene, which can predict higher ASOA formation. In addition, OH predicted by MOZART-4x is higher than CB05_GE (See Figure 4.6a), which can produce more condensable SOA gaseous precursors through oxidations of VOCs. The higher BVOCs emissions in MOZART-4x due to different mapping for MEGAN species can also contribute to the higher BSOA formation in MOZART-4x.

4.4.4 Cloud/Radiative Evaluations

Table 4.5 shows the statistical performance for major cloud/radiative variables for MOZART-4x and CB05_GE simulations. Radiative variables such as OLR, FSDS, and FLDS show excellent agreement with observations, with NMBs within ±8% for both simulations. However, SWCF is overpredicted by both MOZART-4x and CB05_GE, with

NMBs of 26.4% and 27.7%, respectively, and LWCF is underpredicted by both MOZART-4x and CB05_GE, with NMBs of -21.6% and -16.7%, respectively. All predicted radiative variables show high correlation with observations, with correlation coefficients of 0.9 to 0.99. CF is well predicted by MOZART-4x, with an NMB of 6.3%, whereas CCN5, CDNC, COT, and LWP are moderately overpredicted or underpredicted, with NMBs of -32.1%, 19.7%,-26.0%, and 2.8%, respectively. The performance of cloud variables is similar in CB05_GE, with NMBs of 6.0%, -29.0%, 20.8%, -26.0%, and 1.7% for CF, CCN5, CDNC, COT, and LWP, respectively. AOD is also underpredicted by both MOZART-4x and CB05_GE, with NMBs of -23.9% and -24.6%, respectively.

Figure 4.8 shows the Taylor diagram (Taylor, 2001) comparing the model performance of MOZART-4x with that of the CB05_GE for cloud and radiative predictions. The similarity between the two patterns is quantified in terms of their correlations (i.e., angle), their standard deviations (i.e., y axis), and the ratio of their variances (i.e., x axis). In general, the performance of major cloud/radiative variables between MOZART-4x and CB05_GE are similar. The major differences in the performance of cloud/radiative variables between MOZART-4x and CB05_GE are the variances of CCN5, CDNC, and SWCF, which is mainly due to the predicted aerosol distributions (see Figure 4.6b). The larger deviation of COT and LWP from observations (i.e., the two points located outside the diagram in Figure 4.8) suggests the uncertainties both in the model treatments for cloud dynamics and thermodynamics as well as in the satellite retrievals.

Due to the underpredictions of cloud variables (e.g., COT and CCN5), OLR is slightly overpredicted by 7.8 W m^{-2} (or by 3.6%), and LWCF is underpredicted by 4.8 W m^{-2}

(or by 21.6%) in MOZART-4x. Similarly, OLR is slightly overpredicted by 6.7 W m^{-2} (or by 3.1%) and LWCF is underpredicted by 3.7 W m^{-2} (or by 16.7%) in CB05_GE. Figure 4.9 shows the comparisons of satellite observations with model predictions for AOD, CCN5, CDNC, COT, and SWCF averaged during 2008-2010. The underpredictions of AOD over oceanic areas can be attributed to the uncertainties in the sea-salt emissions and inaccurate predictions of other PM components (e.g., marine organic aerosols) over the ocean and overestimation of oceanic AOD in the MODIS collection 5.1 (Levy et al., 2013). The underprediction of AOD over land (e.g., tropical islands) is mainly due to the significant underestimation of biomass burning emissions in the model (Tilmes et al., 2015). AOD is higher in MOZART-4x over most land areas (except East Asia and Europe) than in CB05_GE. The higher AOD in MOZART-4x is mainly due to higher SOA (e.g., over most land areas) and higher NO_3^- (e.g., over CONUS) in MOZART-4x. The lower AOD over East Asia and Europe in MOZART-4x is mainly due to the lower SO_4^{2-} as there is an additional pathway of SO_2 (oxidized by O_3) included in CB05_GE but it is not included in MOZART-4x and lower NH_4^+ to neutralize lower SO_4^{2-} through thermodynamic equilibrium. This additional pathway also results in higher H_2SO_4 predictions in CB05_GE and higher aerosol number concentration through homogeneous nucleation. Therefore, CCN5 is higher in CB05_GE than in MOZART-4x (see Figure 4.9). CDNC is moderately overpredicted for both cases. Cloud droplet formation is sensitive to both particle number concentrations and updraft velocity (Reutter et al., 2009). The overprediction of CDNC is due partly to high activation fractions (e.g., inclusion of adsorption activation from insoluble CCN and effective uptake coefficient of 0.06 used in this work) (Gantt et al., 2014) as well as the uncertainties

in the model treatments for cloud microphysics (e.g., resolved clouds and subgrid-scale cumulus clouds) and satellite retrievals (e.g., error propagation of the input variables to derive CDNC) (Bennartz, 2007). COT is largely overpredicted over Southeast Asia and South America and underpredicted over polar regions for both simulations. Overpredictions in CDNC and COT can increase cloud albedo and therefore, increase SWCF over the low and middle latitudes. The large underpredictions of COT over polar regions can be attributed to the uncertainties in plane-parallel visible-near-infrared retrievals with low solar zenith angle (Seethala and Horváth, 2010) and the influence of radiatively active snow on overlying cloud fraction (Kay et al., 2012). Due to the different gas-phase mechanisms, the predicted SWCF (Figure 4.9) and LWCF (Figure not shown) are different, with a global average difference of 0.5 W m^{-2} and 1.1 W m^{-2}, respectively. However, the absolute differences in simulated SWCF can be as large as 13.6 W m^{-2} as shown in Figure 4.9. The large differences of SWCF and LWCF between MOZART-4x and CB05_GE are mainly over subtropical regions (e.g., 20 ^{o}S-20 ^{o}N), which is mainly due to lower COT in MOZART-4x than in CB05_GE.

4.5 Conclusion

In this work, MOZART-4x and CB05_GE are coupled with CAM5-NCSU. MOZART-4x uses lumped species approach to represent organic chemistry whereas CB05_GE uses lumped structure approach. MOZART-4x and CB05_GE include different surrogates for SOA precursors, which can result in different SOA predictions. MOZART-4x includes HO_x recycling associated with improved isoprene chemistry whereas CB05_GE contains simpler isoprene chemistry, which can result in different OH and isoprene

predictions and thus, SOA predictions. CB05_GE includes additional oxidation of SO_2 by O_3 over the surface of dust particles to produce additional SO_4^{2-}, which is not included in MOZART-4x. These differences can result in different secondary gases and aerosols predictions.

The comparisons between the two gas-phase mechanisms are conducted in terms of chemical and cloud/radiative predictions. Predictions of major gases and inorganic aerosols predicted by MOZART-4x and CB05_GE are overall similar. Significant differences in some species (e.g., NO_y, glyoxal, and SOA) predictions are mainly due to the different reaction pathways treated in the two mechanisms. Large biases exist for surface SO_2, CO, and NH_3 predictions against available observations, which is likely due to the uncertainties in the emissions or emission injection heights. Several studies indicate that the uncertainties in regional emissions (e.g., BC and SO_2) can be expected to be as large as a factor of 2 or larger (Bond et al., 2007; Smith et al., 2011). Large discrepancies still remain for major species such as SO_2, NO_x, BC, and CO among different inventories (Granier et al., 2011). Both MOZART-4x and CB05_GE overpredict surface O_3 over CONUS, Europe, and East Asia, which is due in part to less O_3 titration resulted from underpredictions of NO_x, the use of a coarse grid resolution, as well as dilution of NO_x emissions. The overpredictions of SO_2 and NH_3 result in the overpredictions of SO_4^{2-} and NH_4^+ over CONUS and Europe. Both surface CO and column CO are underpredicted, which is mainly due to underestimations in the CO emissions from biomass burning and possible uncertainties in the OH production. Surface SO_2 is overpredicted whereas column SO_2 is underpredicted, indicating the uncertainties in the vertical mixing scheme or emission injection heights as reported in East Asia (Zhang et

al., 2015a, b). The large underpredictions of column glyoxal are mainly due to the uncertainties in the chemical production and loss for glyoxal. Tropospheric O_3 predicted by MOZART-4x is about 4.7% lower than CB05_GE, but agrees better with OMI/MLS. The lower column O_3 in MOZART-4x is mainly due to lower NO_2 and higher OH in MOZART-4x. The column SOA predicted by MOZART-4x is about 8.4% higher than CB05_GE, whereas there is not much difference for column POA. The difference in SOA column is mainly due to higher BVOCs emissions and higher OH levels in MOZART-4x than in CB05_GE. Chemical profiles (e.g., O_3, CO, and NO_x) predicted by CB05_GE and MOZART-4x are overall similar, whereas NO_y profile predicted by CB05_GE agree better with aircraft measurements than by MOZART-4x.

The concentrations of VOCs (e.g., formaldehyde, isoprene, and toluene) are moderately to largely underpredicted, which is likely due to the use of a coarse grid resolution, the uncertainties in the biogenic emissions, as well as chemical reactions (e.g., reaction rate coefficients for HCHO production and loss and isoprene chemistry). The concentration of OC over CONUS is well predicted by MOZART-4x, with an NMB of 2.1%, whereas it is moderately underpredicted by CB05_GE, with an NMB of -20.7%. Compared to the observations at the four sites in the U.S. from Lewandowski et al. (2013), SOA is well predicted by MOZART-4x, with an NMB of -1.9%, whereas it is moderately underpredicted by CB05_GE, with an NMB of -23.1%, indicating a better capability to predict SOA over these sites by MOZART-4x despite its tendency to overpredict SOA concentrations at sites with low SOA levels such as Bakersfield and Pasadena, CA. However, the concentrations of OC over Europe is largely underpredicted by both MOZART-4x and CB05_GE, with NMBs

of -74.2% and -75.1%, respectively, indicating the uncertainties in the emissions, chemical reactions, as well as SOA formation treatment. Both MOZART-4x and CB05_GE largely underpredict HOA in the Northern Hemisphere, with NMBs of -77.2% and -76.7%, respectively, indicating the uncertainties in the POA evaporation treatment as well as POA emissions. OOA is also underpredicted by both MOZART-4x and CB05_GE in the Northern Hemisphere, with NMBs of -56.5% and -62.3%, respectively, indicating the uncertainties in the emissions, fragmentation rates, as well as SOA formation treatment. $PM_{2.5}$ is well predicted over CONUS by both MOZART-4x and CB05_GE, with NMBs of 0.7% and -1.1%, respectively, whereas it is moderately underpredicted over Europe, with NMBs of -39.8% and -37.4%, respectively. The underpredictions of $PM_{2.5}$ over Europe are mainly due to the inaccurate predictions of OA over Europe. PM_{10} is underpredicted over CONUS, Europe, and East Asia by both MOZART-4x and CB05_GE, which is mainly due to the inaccurate predictions of coarse particles and uncertainties in the anthropogenic emissions (e.g., SO_2, BC, and OC) and online dust and sea-salt emissions. The different AOD predictions between CB05_GE and MOZART-4x are mainly due to the different predictions in SOA, SO_4^{2-}, NH_4^+, NO_3^-, and dust concentrations.

The cloud/radiative predictions from the two simulations are also similar, with slightly better domain average performance of CCN5, LWP, and LWCF in CB05_GE. But MOZART-4x predicts slightly better CCN profile over Beijing than CB05_GE compared to aircraft measurements. The different gas-phase mechanisms result in different predictions in aerosols and clouds, and therefore, a domain average difference of 0.5 W m^{-2} in simulated SWCF, which can be as large as 13.6 W m^{-2} over subtropical regions. Such differences are

caused by different aerosol and cloud predictions from both simulations. Radiative variables such as OLR, FSDS, and FLDS, show excellent agreement with observations, with NMBs within ±8% for both MOZART-4x and CB05_GE. However, there are large deviations for COT and LWP, indicating the uncertainties both in the model treatments for cloud dynamics and thermodynamics and in the satellite retrievals.

In summary, MOZART-4x and CB05_GE differ in their approaches to represent VOCs and surrogates for SOA precursors. MOZART-4x includes a more detailed representation of isoprene chemistry compared to CB05_GE. Based on the above comparisons of simulations using both mechanisms and evaluation against available measurements in this study, MOZART-4x with the 1.5 D VBS SOA module in CESM-NCSU generally gives a better agreement with observations for surface concentrations of O_3 over Europe, HNO_3, HCHO, ISOP over CONUS,, SOA, SO_4^{2-}, NO_3^-, and NH_4^+ over CONUS and Europe, , and column mass abundances of HCHO, CH_2O_2, SO_2,and O_3, whereas CB05_GE generally gives a better agreement for surface concentrations of SO_2, NH_3, O_3 over CONUS and East Asia, HNO_3 over Europe, $PM_{2.5}$ and PM_{10} over Europe, PM_{10} over East Asia, vertical profiles of NO_y, and column mass abundances of CO. Both simulations give predictions of cloud/radiative variables with slightly better domain average performance of CCN5, LWP, and LWCF in CB05_GE.

Table 4.1. Gas-phase organic aerosol precursors in the two mechanisms

Precursors	MOZART-4x[1]	CB05_GE[2]
Aromatics	TOLUENE, BENZENE , XYLENES, CRESOL	TOL, XYL, CRES, PAH
Alkanes	BIGALK	ALKH
Anthropogenic alkenes	C3H6, BIGENE	OLE, IOLE
Biogenic alkenes	APIN, BPIN, LIMON, MYRC, BCARY, ISOP	APIN, BPIN, LIM, OCI, HUM, TER, ISOP

[1] BIGALK: lumped alkanes C > 3; C_3H_6: propene; BIGENE: lumped alkenes C > 3; APIN: α-pinene + others; BPIN: β-pinene+others; LIMON: limonene + others; MYRC: myrcene + others; BCARY: beta-caryophyllene + other sesquiterpenes; ISOP: isoprene

[2] TOL: toluene and other monoalkyl aromatics; XYL: xylene and other polyalkyl aromatics; CRES: cresol and higher molecular weight phenols; PAH: polycyclic aromatic hydrocarbons; ALKH: long-chain alkanes, C >6; OLE: terminal olefin carbon bond (R-C=C); IOLE: internal olefin carbon bond (R-C=C-R); APIN: α-pinene; BPIN: β-pinene; LIM: limonene; OCI: ocimene; HUM: humulene; TER: terpinene; ISOP: isoprene

Table 4.2. Datasets for model evaluation

Species/Variables	Dataset (Number of sites)
Cloud fraction (CF), Cloud optical thickness (COT), Cloud liquid water path (LWP), Precipitating water vapor (PWV), Aerosol optical depth (AOD), Column cloud condensation nuclei (ocean) at S = 0.5% (CCN5)	MODIS
Cloud droplet number concentration (CDNC)	Bennartz (2007)
Shortwave cloud radiative forcing (SWCF) Longwave cloud radiative forcing (LWCF) Downwelling longwave radiation at surface (FLDS) Downwelling shortwave radiation at surface (FSDS)	CERES
Outgoing longwave radiation (OLR)	NOAA/CDC
Carbon monoxide (CO)	East Asia: NIESJ (2133), TAQMN (70), KMOE (258)
Ozone (O_3)	CONUS: CASTNET (141) Europe: Airbase (3846), BDQA (490), EMEP (317) East Asia: TAQMN (70), KMOE (258)
Sulfur dioxide (SO_2)	CONUS: CASTNET (141) Europe: Airbase (3846), BDQA (490), EMEP (317) East Asia: MEPC (84), NIESJ (2133), KMOE (258), TAQMN (70)
Nitric acid (HNO_3)	CONUS: CASTNET (141); Europe: EMEP (317)
Ammonia (NH_3)	Europe: Airbase (3846), EMEP (317)
Nitrogen dioxide (NO_2)	Europe: Airbase (3846), BDQA (490), EMEP (317) East Asia: NIESJ, TAQMN, KMOE
Sulfate (SO_4^{2-}), Ammonium (NH_4^+), Nitrate (NO_3^-)	CONUS: CASTNET (141), IMPROVE (199), STN (18129); Europe: Airbase (3846), EMEP (317)
Chloride (Cl^-)	CONUS: IMPROVE (199) Europe: Airbase (3846), EMEP (317)
Organic carbon (OC)	CONUS: IMPROVE (199); Europe: EMEP (317)
Black carbon (BC), Total carbon (TC)	CONUS: IMPROVE (199), STN(18129)
Formaldehyde (HCHO), Isoprene (ISOP), and Toluene (TOL)	CONUS: AQS (25877)
Hydrocarbon-like organic aerosol (HOA), Oxygenated organic aerosol (OOA), Total organic aerosol (TOA)	Northern Hemisphere: Zhang et al. (2007) and Jimenez et al. (2009) (Z07 & J09) (33)
Secondary organic aerosol (SOA)	CONUS: Ohio (2) and California (2) (Lewandowski et al., 2013)
Particulate matter with diameter less than and equal to 2.5 μm ($PM_{2.5}$)	CONUS: IMPROVE (199), STN (18129) Europe: BDQA (490), EMEP (317)
Particulate matter with diameter less than and equal to 10 μm (PM_{10})	CONUS: AQS (25877) Europe: Airbase (3846), BDQA (490), EMEP (317) East Asia: MEPC (84), NIESJ (2133), KMOE (258), TAQMN (70)
Column CO	Globe: MOPITT
Column NO_2, Column SO_2, Column HCHO, Column glyoxal ($C_2H_2O_2$)	Globe: SCIAMACHY
Tropospheric ozone residual (TOR)	Globe: OMI/MLS
O_3, CO, NO_x, and NO_y profiles	ARCPAC (Mar.-Apr., 2008), ARCTAS (Apr.-Jun., 2008), START08 (Apr.-Jun., 2008), and CalNex (May-Jun., 2010)
CCN_China	Beijing: Zhang et al. (2011) (Jul.-Sep., 2008)

NOAA/CDC: National Oceanic and Atmospheric Administration Climate Diagnostics Center; MODIS: Moderate Resolution Imaging Spectroradiometer; CERES: Clouds and Earth's Radiant Energy System; MOPITT: the Measurements Of Pollution In The Troposphere; OMI/MLS: the Aura Ozone Monitoring Instrument in combination with Aura Microwave Limb Sounder; SCIAMCHY: the SCanning Imaging Absorption spectroMeter for Atmospheric CHartographY; CASTNET: Clean Air Status and Trends Network; IMPROVE: Interagency Monitoring of Protected Visual Environments; STN: Speciation Trends Network; AQS: Air Quality System; EMEP: European Monitoring and Evaluation Program; BDQA: Base de Données sur la Qualité de l'Air; AirBase: European air quality database; MEPC: Ministry of Environmental Protection of China; TAQMN: Taiwan Air Quality Monitoring Network; NIESJ: National Institute for Environmental Studies of Japan; KMOE: Korean Ministry of Environment; ARCPAC: Aerosol, Radiation, and Cloud Processes affecting Arctic Climate in 2008 (Brock et al., 2011); ARCTAS: Arctic Research of the Composition of the Troposphere from Aircraft and Satellites (Jacob et al., 2010), START08: Stratosphere-Troposphere Analyses of Regional Transport in 2008 (Pan et al., 2010); CalNex: California Nexus 2010 (Ryerson et al., 2013)..

Table 4.3. Performance statistics of chemical species

Species	Domain	Obs	MOZART-4x			CB05_GE		
			Sim	NMB (%)[a]	NME (%)[a]	Sim	NMB (%)[a]	NME (%)[a]
CO (ppb)	East Asia	438.7	150.9	-65.6	65.7	150.4	-65.7	65.8
SO_2[b]	CONUS	1.7	11.6	580.2	580.2	11.2	561.6	561.6
	Europe	4.7	9.5	100.9	121.2	9.2	94.1	115.4
	East Asia	2.9	4.3	47.0	70.6	3.9	35.5	64.0
NH_3 ($\mu g\ m^{-3}$)	Europe	1.2	2.5	112.4	146.0	2.4	104.3	139.8
NO_2[c]	Europe	17.4	6.7	-61.4	65.5	6.6	-62.1	66.0
	East Asia	11.7	3.0	-74.1	75.2	3.0	-74.8	75.8
O_3[d]	CONUS	34.7	44.7	29.0	29.5	44.4	28.2	28.5
	Europe	56.2	78.6	39.9	40.8	80.6	43.5	44.2
	East Asia	29.8	48.3	62.4	62.4	47.7	60.3	60.3
HNO_3 ($\mu g\ m^{-3}$)	CONUS	0.9	2.1	145.0	145.2	2.2	154.7	154.7
	Europe	0.8	0.7	-15.6	65.4	0.8	-10.9	64.9
HCHO (ppb)	CONUS	2.3	1.6	-30.1	48.4	1.5	-36.3	49.0
ISOP (ppb)	CONUS	0.3	0.2	-27.3	63.2	0.2	-29.0	64.7
Toluene (ppb)	CONUS	0.5	0.2	-65.3	69.2	0.2	-65.1	69.1
Col. CO ($molec.cm^{-2}$)	Globe	1.6×10^{18}	1.2×10^{18}	-25.8	27.5	1.2×10^{18}	-24.4	26.1
Col. NO_2 ($molec.cm^{-2}$)	Globe	5.5×10^{14}	8.5×10^{14}	56.0	71.0	9.3×10^{14}	70.2	83.3
Col. HCHO ($molec.cm^{-2}$)	Globe	4.6×10^{15}	3.1×10^{15}	-31.2	39.2	3.1×10^{15}	-32.7	40.4
Col. C2H2O2 ($molec.cm^{-2}$)	Globe	2.8×10^{14}	3.9×10^{13}	-86.0	86.0	5.9×10^{12}	-97.9	-97.9
Col. SO_2(DU)	Globe	1.2	0.3	-70.1	90.1	0.3	-73.5	88.7
TOR (DU)	Globe	28.6	30.3	6.0	15.0	31.8	11.3	16.5
SO_4^{2-} ($\mu g\ m^{-3}$)	CONUS	1.8	3.0	72.9	72.9	3.3	89.7	89.7
	Europe	1.8	2.9	62.1	70.1	3.2	79.7	85.2
NH_4^+ ($\mu g\ m^{-3}$)	CONUS	0.9	1.3	37.8	49.9	1.3	44.3	55.6
	Europe	0.9	1.3	51.5	63.1	1.4	63.4	72.8
NO_3^- ($\mu g\ m^{-3}$)	CONUS	0.9	0.9	-6.0	44.4	0.7	-21.2	40.2
	Europe	1.7	1.2	-28.9	54.2	1.2	-30.5	53.4
Cl^- ($\mu g\ m^{-3}$)	CONUS	0.1	0.02	-78.1	84.3	0.02	-78.3	84.5
	Europe	1.1	4.1	273.4	274.7	4.2	273.7	274.8
BC ($\mu g\ m^{-3}$)	CONUS	0.3	0.2	-29.3	44.6	0.2	-29.3	44.6
OC ($\mu g\ m^{-3}$)	CONUS	0.9	1.0	2.1	33.2	0.7	-20.7	32.8
	Europe	2.9	0.7	-74.2	77.3	0.7	-75.1	78.0
TC ($\mu g\ m^{-3}$)	CONUS	1.8	1.3	-29.6	39.3	1.1	-42.1	45.8
SOA[e]	CONUS	1.8	1.8	-1.9	29.3	1.4	-23.1	35.8
HOA[e]	N.H.[f]	2.1	0.5	-77.2	81.5	0.5	-76.7	81.3
OOA[e]	N.H.[f]	4.8	2.1	-56.5	56.6	1.8	-62.3	62.3
TOA[e]	N.H.[f]	7.9	2.5	-67.8	68.2	2.3	-71.2	72.0
$PM_{2.5}$ ($\mu g\ m^{-3}$)	CONUS	7.4	7.5	0.7	27.6	7.4	-1.1	27.7
	Europe	14.4	8.9	-39.8	44.8	9.0	-37.4	42.9
PM_{10} ($\mu g\ m^{-3}$)	CONUS	20.6	12.6	-38.6	50.2	12.6	-38.9	50.7
	Europe	22.1	18.8	-14.9	39.9	19.2	-13.1	38.9
	East Asia	88.0	59.0	-32.9	41.1	64.8	-26.4	37.2

[a] NMB: normalized mean bias (%); NME: normalized mean error (%); [b] The unit is $\mu g\ m^{-3}$ for CONUS and ppb for East Asia. [c] The unit is $\mu g\ m^{-3}$ for Europe and ppb for East Asia. [d] The unit is ppb for CONUS and East Asia, and $\mu g\ m^{-3}$ for Europe. [e] SOA: secondary organic aerosol; HOA: hydrocarbon-like organic aerosol; OOA: oxygenated organic aerosol; TOA: total organic aerosol; [f] N.H.: northern hemisphere;

Table 4.4. Tropospheric ozone budget

Ozone	MOZART-4x	CB05_GE	Lamarque et al. (2012)	Young et al. (2013)
Burden (Tg)	325	333	328	337 ± 23
Dry Deposition ($Tg\ yr^{-1}$)	679	705	705	1003 ± 200
[a] Chemical Production ($Tg\ yr^{-1}$)	4974	5743	4897	5110 ± 606
[b] Chemical Loss ($Tg\ yr^{-1}$)	4259	5194	4604	4668 ± 727
Lifetime (days)	24	21	26	22.3 ± 2.0

[a] Chemical production is mainly contributed by reactions of NO with peroxy radicals;

[b] Chemical loss is mainly contributed by the oxygen radical in the $O(^1D)$ + water (H_2O) reaction and by the reactions of ozone with the hydroperoxyl radical (HO_2), OH, and alkenes;

Table 4.5. Performance statistics of meteorological/radiative variables

Variables[a]	Networks	Obs	MOZART-4x					CB05_GE				
			Sim	NMB (%)[b]	NME (%)[b]	RMSE[b]	Corr[b]	Sim	NMB (%)[b]	NME (%)[b]	RMSE[b]	Corr[b]
OLR ($W\ m^{-2}$)	NOAA/ CDC	217.0	224.8	3.6	4.1	10.0	0.99	223.7	3.1	3.9	9.6	0.98
FLDS ($W\ m^{-2}$)	CERES	306.7	307.3	0.2	3.1	11.6	0.99	307.3	0.2	3.1	11.5	0.99
FSDS ($W\ m^{-2}$)	CERES	163.4	150.9	-7.6	10.2	22.6	0.9	150.8	-7.7	10.2	22.7	0.9
SWCF ($W\ m^{-2}$)	CERES	-40.7	-51.5	26.4	33.4	19.0	0.9	-52.0	27.7	-34.4	19.6	0.9
LWCF ($W\ m^{-2}$)	CERES	22.4	17.6	-21.6	25.1	6.8	0.9	18.7	-16.7	23.8	6.6	0.9
CCN5 ($\#\ cm^{-2}$)	MODIS	2.2×10^{8}	1.5×10^{8}	-32.1	46.4	1.7×10^{8}	0.4	1.6×10^{8}	-29.0	46.6	1.7×10^{8}	0.4
CF (%)	MODIS	67.3	71.5	6.3	12.7	12.5	0.8	71.3	6.0	12.7	12.5	0.8
COT	MODIS	16.5	12.2	-26.0	61.6	14.0	-0.3	12.2	-26.0	61.3	14.0	-0.3
AOD	MODIS	0.15	0.11	-23.9	40.5	0.08	0.7	0.11	-24.6	40.5	0.08	0.7
PWV (cm)	MODIS	1.9	2.0	5.6	11.4	0.3	0.99	2.0	5.5	11.4	0.3	0.99
CDNC ($\#\ cm^{-3}$)	UM-W	105.8	126.6	19.7	38.7	56.5	0.5	127.8	20.8	39.1	58.1	0.6
LWP ($g\ m^{-2}$)	MODIS	142.0	65.2	-54.1	65.4	143.3	-0.4	64.7	-54.4	65.3	143.3	-0.4
	UM-W	84.6	87.0	2.8	38.3	42.3	0.4	86.0	1.7	37.7	41.7	0.4

[a] OLR: outgoing long wave radiation; FLDS: downwelling longwave radiation at the surface; FSDS: downwelling shortwave radiation at the surface; SWCF: shortwave cloud radiative forcing; LWCF: longwave cloud radiative forcing; CCN5: column CCN (ocean) at supersaturation of 0.5%; CF: cloud fraction; COT: clout optical thickness; AOD: aerosol optical depth; PWV: precipitable water vapor; CDNC: cloud droplet number concentration; LWP: liquid water path.

[b] NMB: normalized mean bias (%); NME: normalized mean error (%); RMSE: root mean squared error; Corr.: correlation coefficient

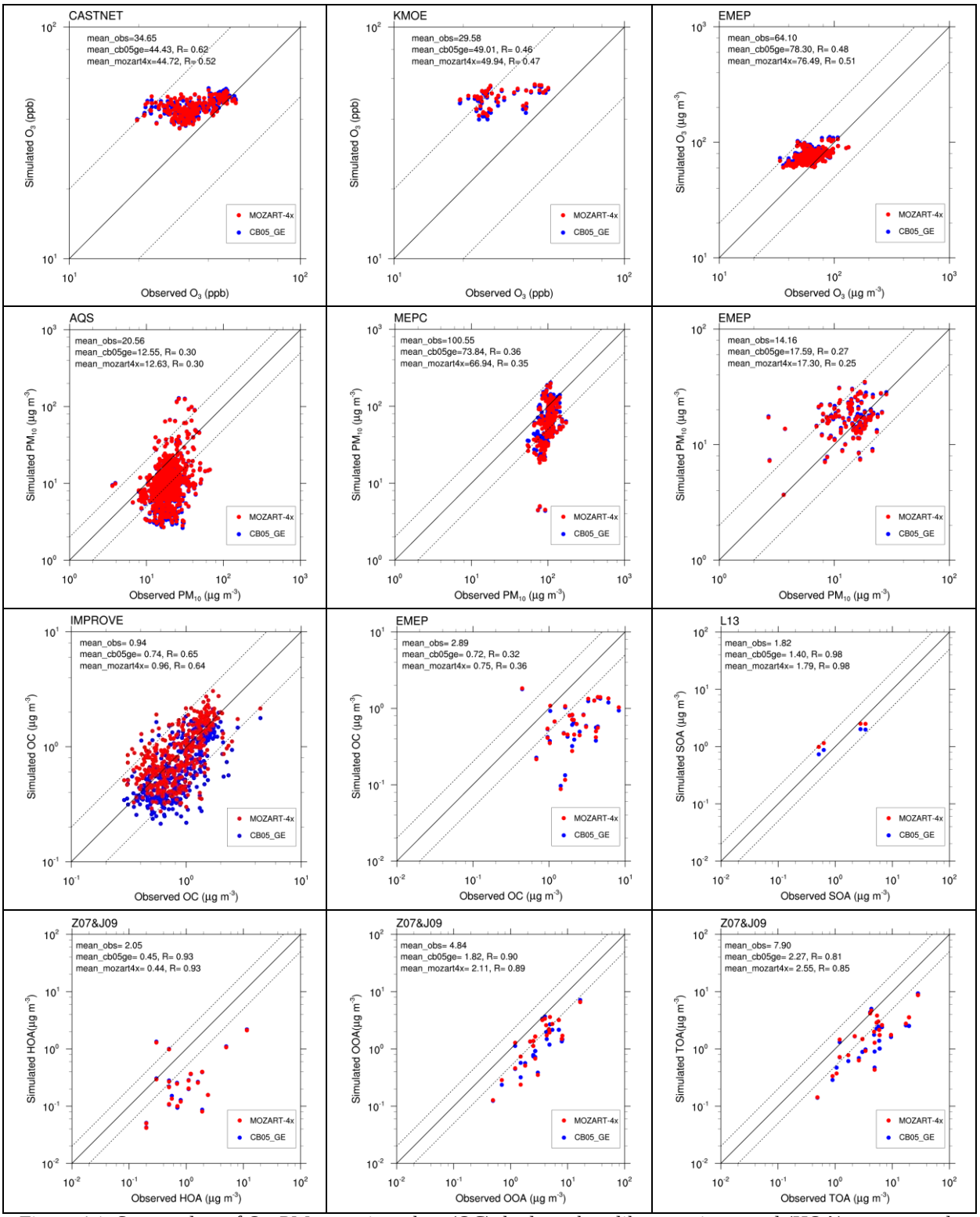

Figure 4.1. Scatter plots of O_3, PM, organic carbon (OC), hydrocarbon-like organic aerosol (HOA), oxygenated organic aerosol (OOA), total organic aerosol (TOA) over various sites during 2008-2010. The X (observations) and Y (simulations) axes are in log scale. Red dots represent MOZART-4x and blue dots represent CB05_GE. R is the correlation coefficient between simulated results and observational data. Z07: Zhang et al. (2007); J09: Jimenez et al. (2009); L13: Lewandowski et al. (2013).

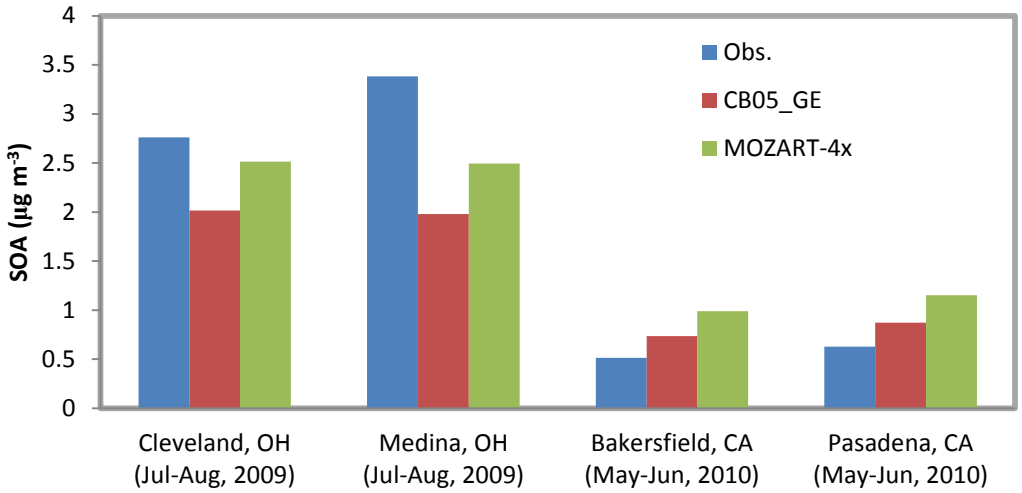

Figure 4.2. Comparisons of simulated and observed SOA concentrations at the four field study sites during 2009-2010. The observations are based on Lewandowski et al. (2013).

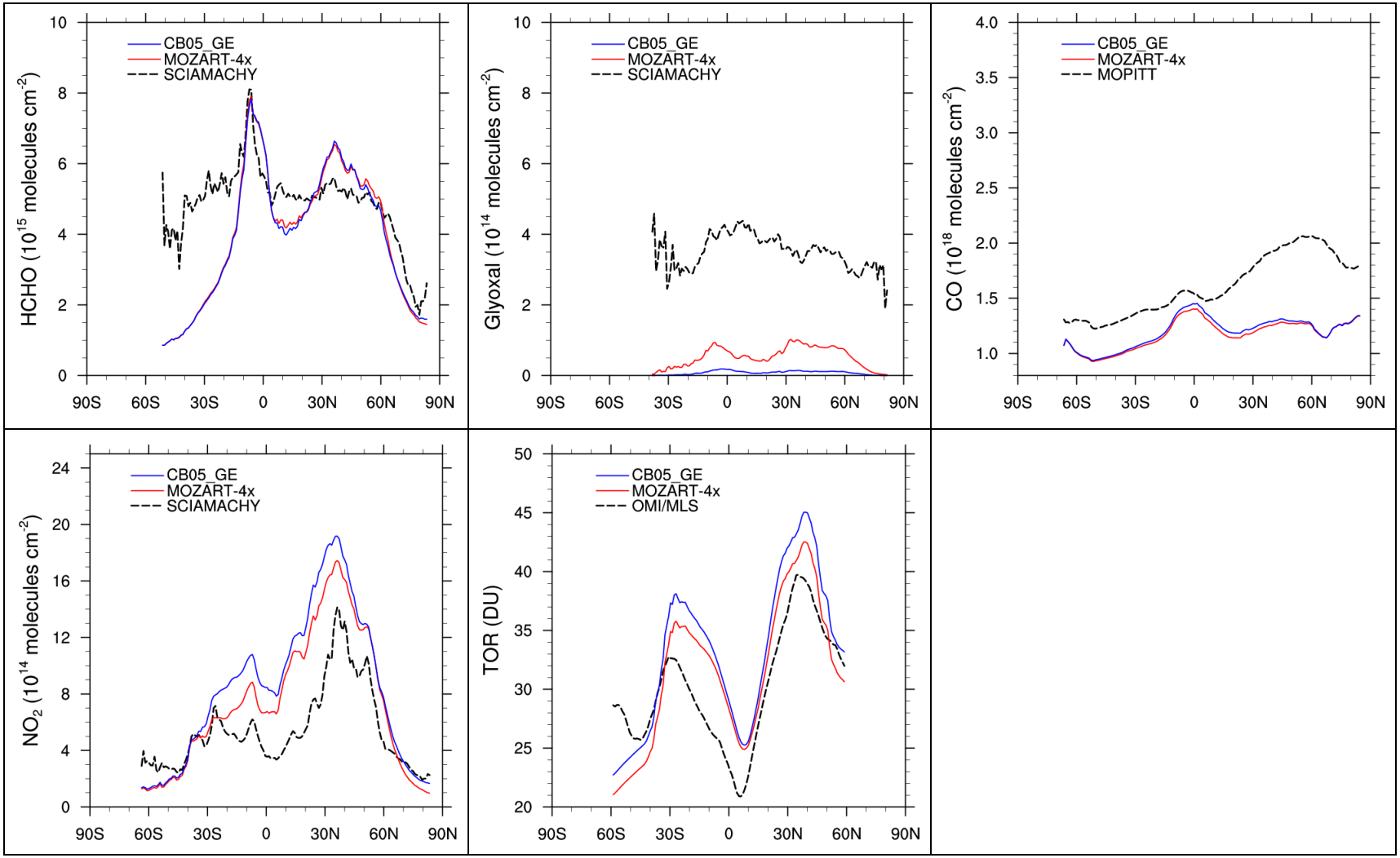

Figure 4.3. Zonal-mean profiles of HCHO, glyoxal, CO, NO_2, and TOR from CB05_GE and MOZART-4x simulations for June, July, and August during 2008-2010.

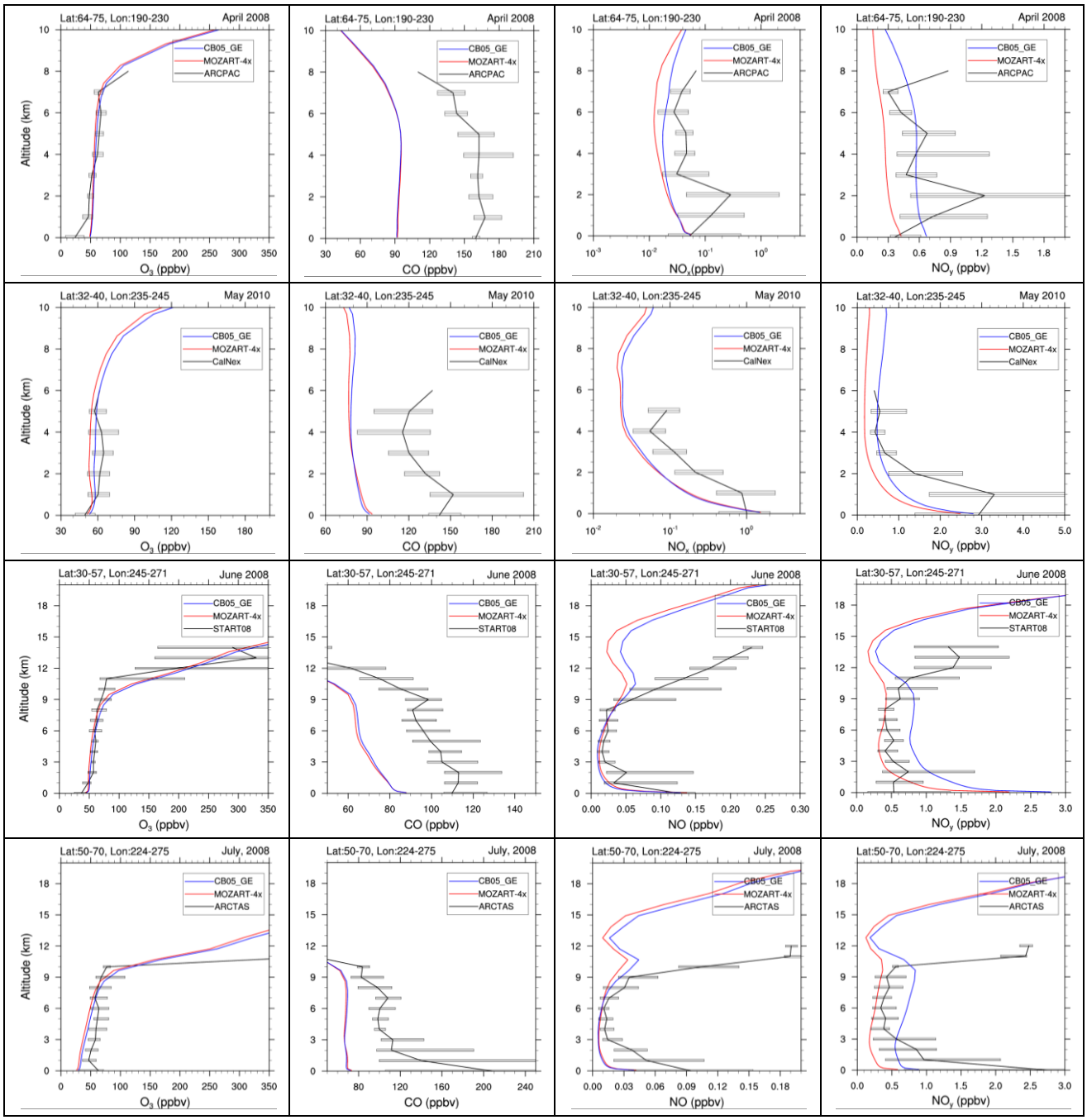

Figure 4.4. Simulated vertical profiles of O_3, CO, NO_x, and NO_y, against aircraft measurements. The black solid line represents observations from aircraft measurements (Pan et al., 2010; Brock et al., 2011; Ryerson et al., 2011; Jacob et al., 2010). The red solid and blue solid lines represent model output from MOZART-4x and CB05_GE, respectively.

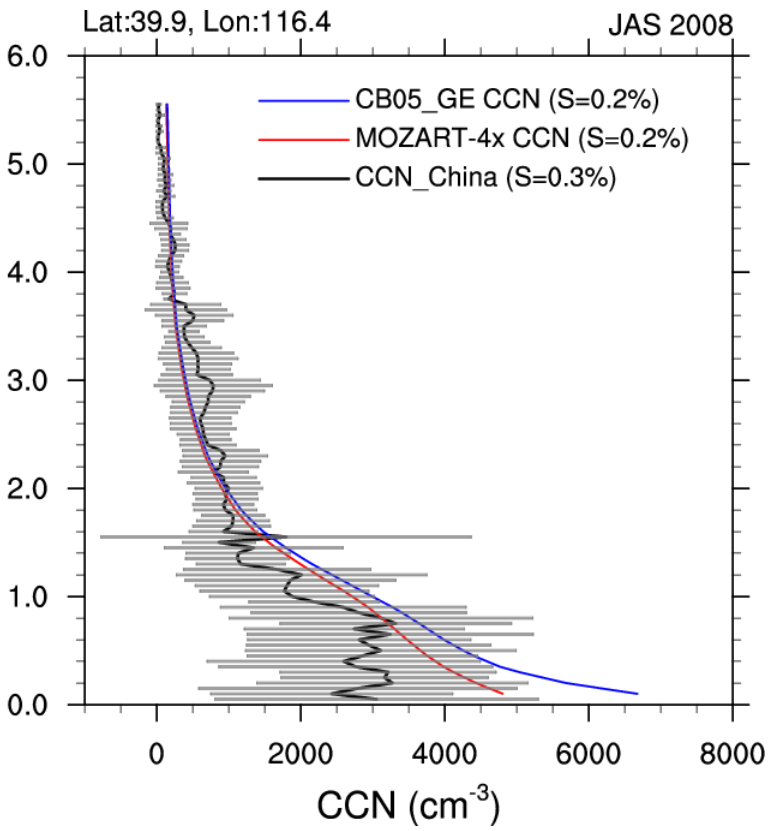

Figure 4.5. Simulated vertical profiles of CCN against aircraft measurements. The black solid line represents observations from aircraft measurements of Zhang et al. (2011). The red solid and blue solid lines represent model output from MOZART-4x and CB05_GE, respectively.

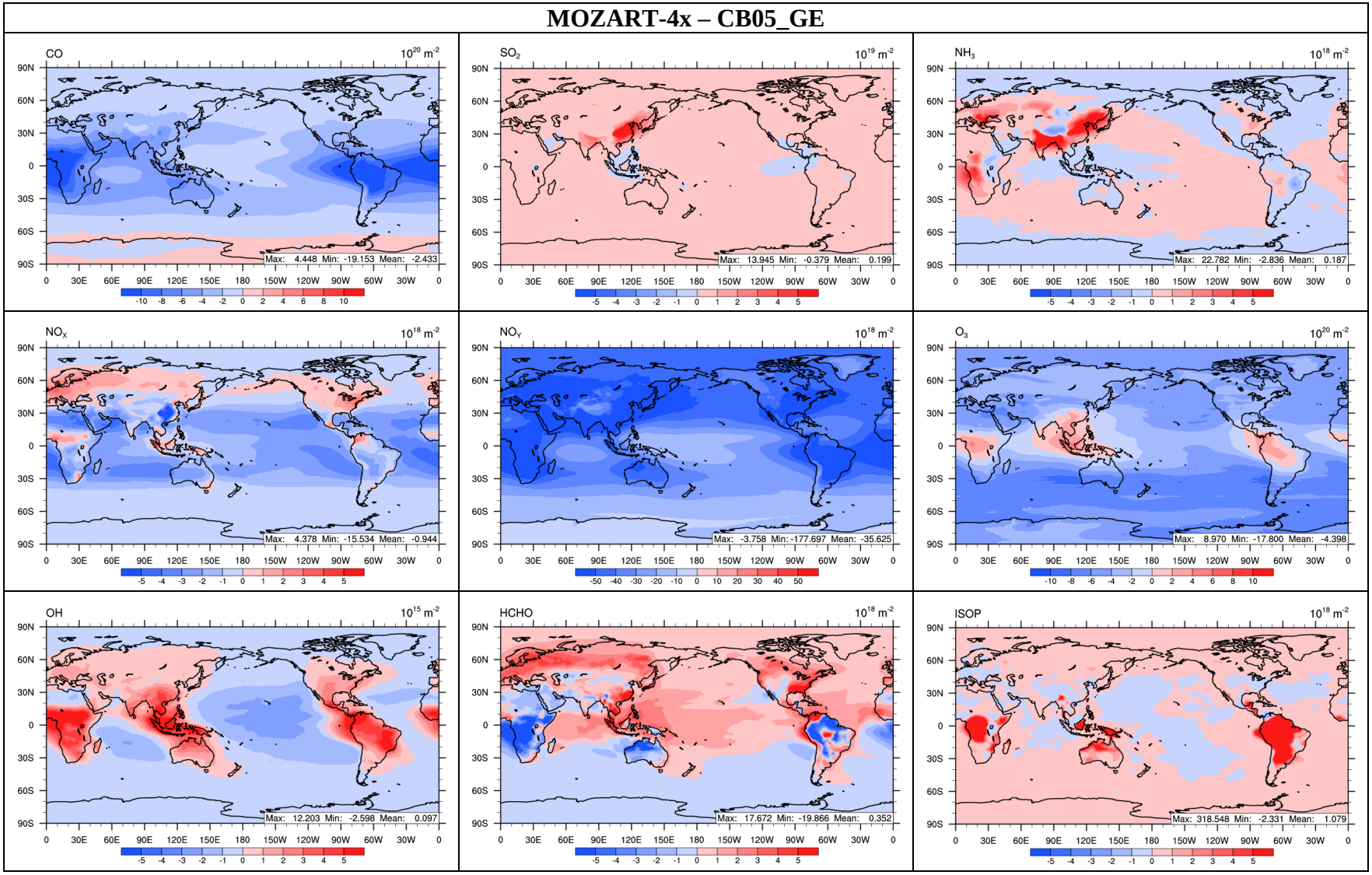

Figure 4.6a. Absolute differences averaged during 2008-2010 in tropospheric column concentrations of major gaseous species between MOZART-4x and CB05_GE.

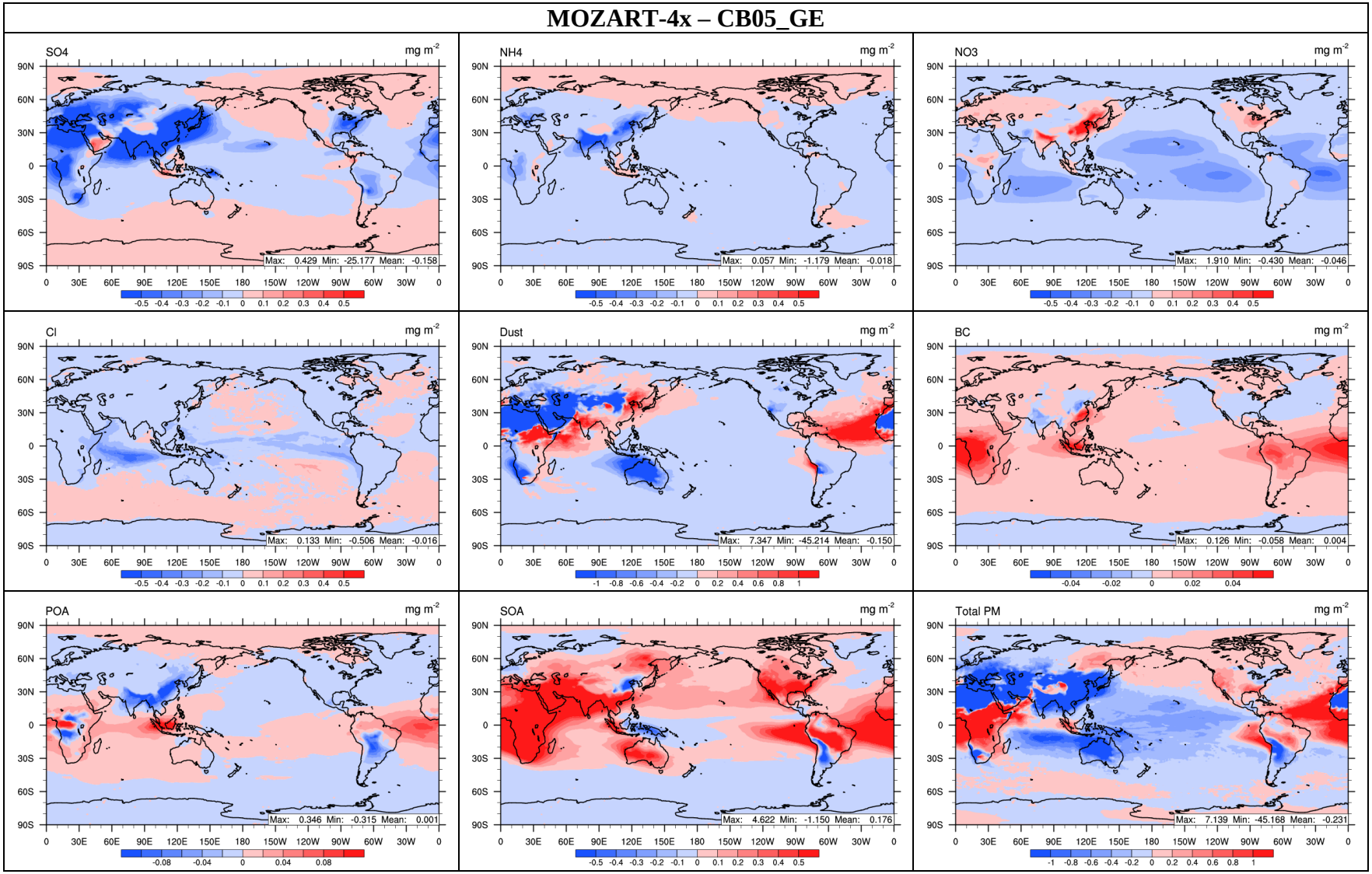

Figure 4.6b. Absolute differences averaged during 2008-2010 in tropospheric column concentrations of major aerosol species between MOZART-4x and CB05_GE.

Region	MOZART-4x	CB05_GE
Australia	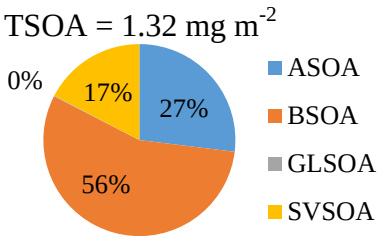	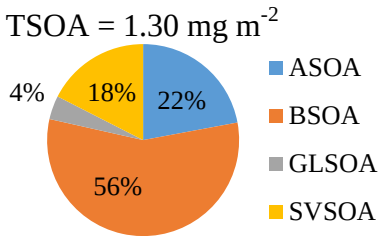
Europe	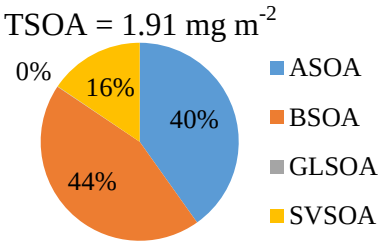	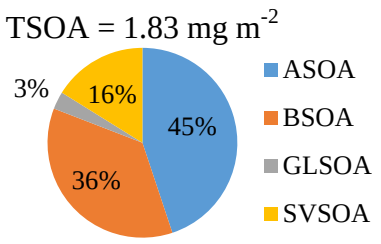
North America	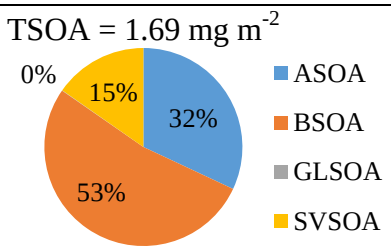	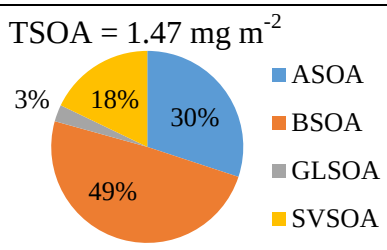
South Africa	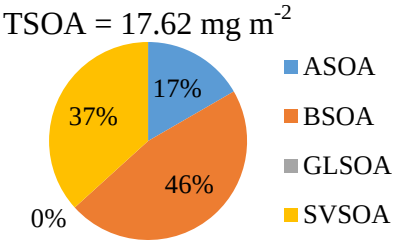	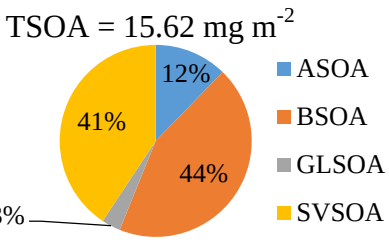
South America	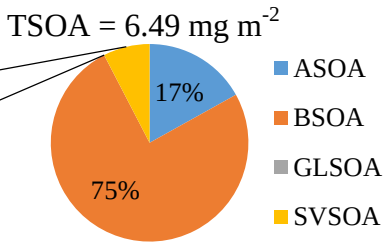	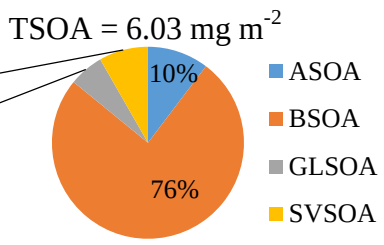
East Asia	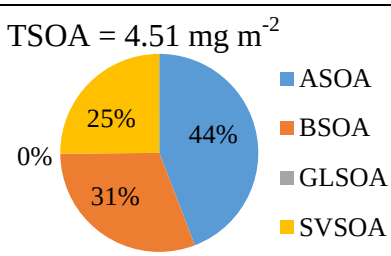	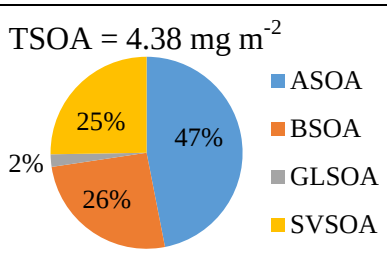

Figure 4.7. Column abundances (mg m^{-2}) averaged during 2008-2010 of secondary organic aerosols (SOA) from anthropogenic sources (ASOA), biogenic sources (BSOA), and glyoxal (GLSOA), and semi-volatile organic aerosol (SVSOA) over Australia, Europe, North America, South Africa, South America, and East Asia.

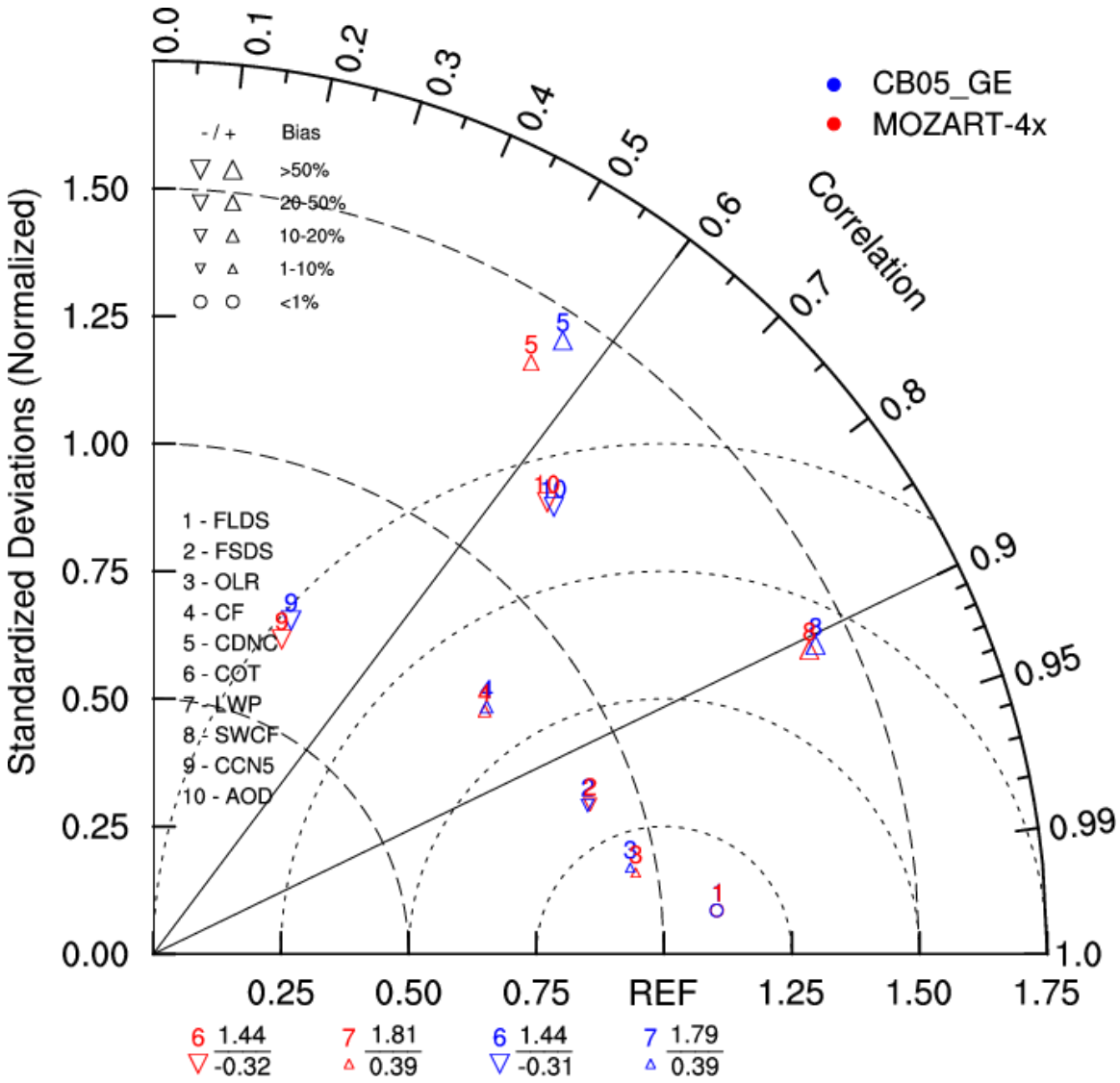

Figure 4.8. Taylor diagram of comparison of cloud and radiative predictions between MOZART-4x and CB05_GE. The results are based on 3-year average. This diagram represents the similarity between MOZART-4x and CB05_GE. X-axis represents the ratio of variances between observations and simulations (proportional to the reference point identified as "REF"), and Y-axis represents the normalized standard deviation between the two patterns (proportional to the radial distance from the origin). Two variables, COT and LWP, are located outside the diagram because the ratios of variance between simulated results and observations (the values of 1.81 from MOZART-4x and 1.79 from CB05_GE in the top) are larger than 1.75 for LWP and the correlation coefficients (the values of -0.32 from MOZART-4x and -0.31 from CB05_GE in the bottom) for COT are negative.

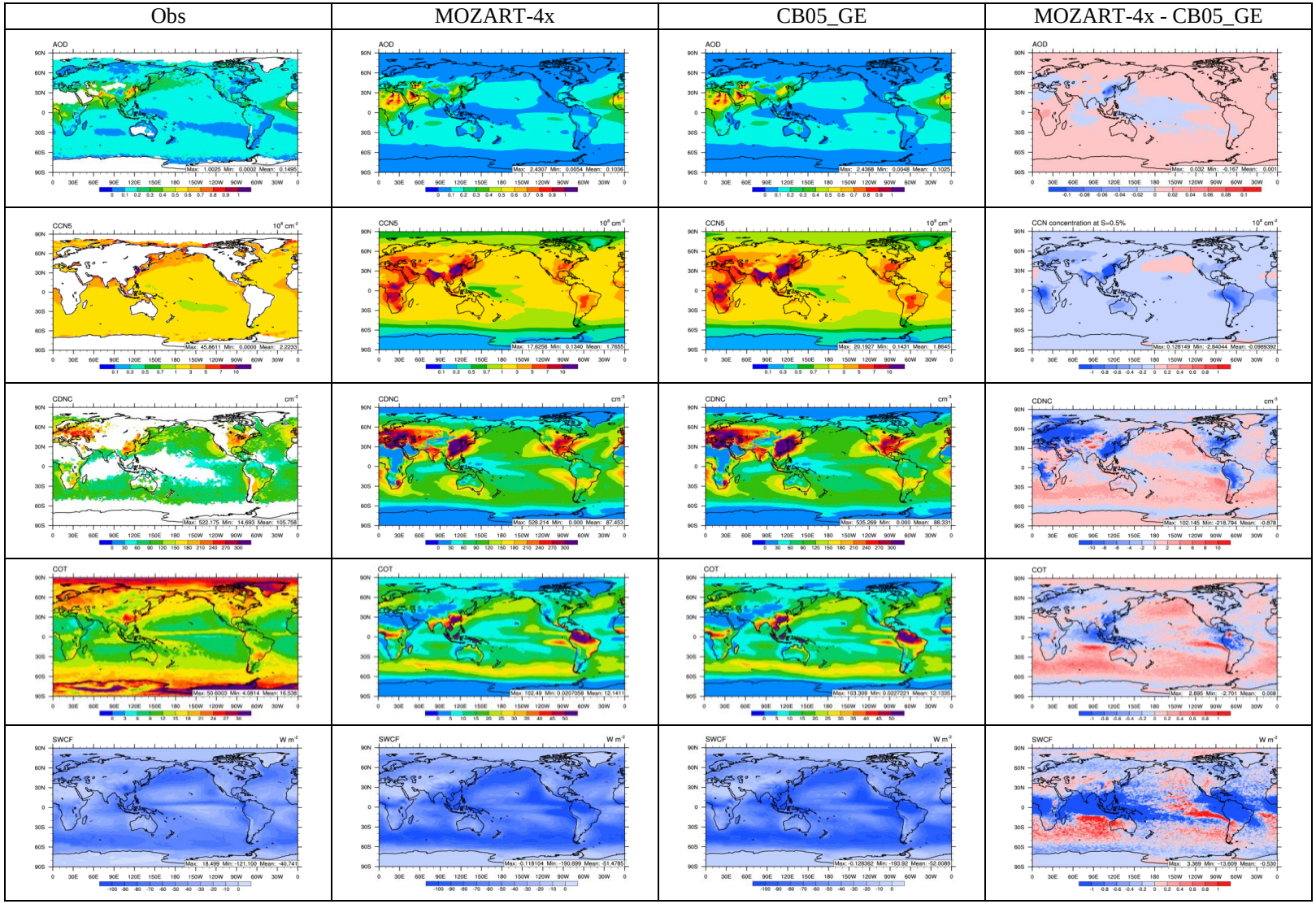

Figure 4.9. Comparison of satellite observations with predictions of for AOD, CCN5, CDNC, COT, and SWCF by MOZART-4x and CB05_GE.

CHAPTER 5. IMPACTS OFAIR-SEA INTERACTIONS ON REGIONAL AIR QUALITY PREDICTIONS: U.S. EAST COAST EXAMPLE

5.1. Introduction

Regional atmospheric models have been developed with higher grid resolution and allow more detailed treatments for gaseous and aerosol physical and chemical processes. 3-D regional atmospheric models, such as the Weather Research and Forecasting model with chemistry (WRF/Chem, Grell et al., 2005; Fast et al., 2006; Zhang et al., 2010b), the Community Multi-scale Air Quality (CMAQ, Binkowski and Roselle, 2003; Byun and Schere, 2006) model, and the Comprehensive Air Quality Model with Extensions (CAMx, ENVIRON, 1998, 2010), are often used for regional air quality studies. Most regional models consist of an atmospheric component coupled to a land surface scheme and forced by prescribed sea surface temperature (SST) over ocean. However, SST patterns can impact precipitation patterns and therefore affect atmospheric heating through latent heat flux. As a result, boundary layer conditions are impacted through air-sea interactions, resulting in changes in the planetary boundary height (PBLH), surface temperature, and surface wind. Most coastal areas contain dense population. The air pollutants such as ozone (O_3) and particulate matter (PM) trapped in the boundary layer of these regions can have adverse impacts on human health and environment. The changes in the horizontal SST gradients can impact the surface fluxes at atmosphere-ocean interface, which leads to changes in the surface winds and PBLH. Changes in surface wind can have significant impacts on dust and sea-salt emissions. Changes in PBLH can impact the vertical distribution of chemical species. Therefore, the feedbacks from the coupled ocean-atmosphere can impact the distribution and

concentration of chemical species, which can in turn affect human health, environment, and ecology. As such, it is also important to include the interactions among Earth components in the regional models based on geographical characteristics of the studying area, which makes regional earth system modeling important.

As a first step towards this goal, a regional atmospheric model (i.e., WRF) and the Regional Ocean Modeling System (ROMS) have been coupled for simulating the dynamic processes in the atmosphere and ocean. For example, the Coupled Ocean-Atmosphere-Wave-Sediment Transport (COAWST) Modeling System is designed to simulate the dynamic processes of coastal zones (Warner et al., 2010). In this coupled system, the atmosphere model, WRF, provides meteorology (e.g., temperature, humidity, pressure, and wind stresses), shortwave radiation, and surface heat fluxes to ROMS, and the resulting SST is fed back to WRF. The coupling of WRF-ROMS has been applied for a number of regional air-sea interaction studies (Nelson et al., 2014; Zambon et al., 2014). However, these studies focus on the effects of air-sea interactions on atmospheric dynamics and ocean circulation.

Meteorology and radiation are important for distribution and concentration of air pollutants (e.g., transport of air pollutants, photolysis, and chemical reactions). Chemical species can influence the meteorological and cloud/radiative variables by perturbating the atmospheric radiation budget and through cloud properties. While many of these coupled modeling systems include prescribed or constant chemistry (e.g., prescribed O_3 or AOD), little work has been done using coupled regional air quality model and regional ocean model. In this work, building on existing coupled WRF-ROMS in COAWST, WRF/Chem is coupled with ROMS in COAWST to study the effects of air-sea interactions on regional air quality

through better representation of air-sea interactions. The major objective in this work is to examine the impacts of air-sea interactions on model predictions of meteorology, chemistry, and cloud/radiation over coastal regions.

5.2 Model Configurations and Evaluation Protocols

5.2.1 Model Description and Setup

The WRF/Chem model is used in this work to represent the atmospheric conditions. It is based on WRF/Chem version 3.6.1 with additional modifications and updates by Wang et al. (2015a). The major updates include (1) the coupling of the 2005 Carbon Bond (CB05) gas-phase (Yarwood et al., 2005; Sarwar et al., 2008) with the existing Modal of Aerosol Dynamics in Europe with the Volatility Basis Set (MADE-VBS, Grell et al., 2005; Ahmadov et al., 2012) approach for simulating secondary organic aerosol (SOA); (2) incorporating the aqueous chemistry (AQChem) module of CMAQ version 5.0 (Sarwar et al., 2011) into WRF/Chem. This new chemistry-aerosol option of CB05-MADE/VBS has been coupled with existing model treatments and has been demonstrated its capability to simulate chemistry-aerosol-radiation-cloud feedbacks such as aerosol semi-direct effects on photolysis rates of major gases, aerosol indirect effects on cloud droplet numbers, and cloud effects on shortwave radiation (Wang et al., 2014a,b; Yahya, et al., 2014, 2015). In this work, this chemistry-aerosol option of CB05-MADE/VBS is applied for all the WRF/Chem simulations.

Table 5.1 shows the simulations conducted in this work. The WRF/Chem simulations are conducted over southeastern U.S. for July 2010, with 12-km horizontal resolution (i.e., 160 × 210 grid cells) and a vertical resolution of 35 layers from the surface to 100 hPa, with a

surface layer model height of 38 m. The emissions for WRF/Chem are from Wang et al. (2015b), which is based on the 2008 National Emission Inventory (NEI) (version 2, released April 10, 2012). The meteorological initial and boundary conditions (ICs and BCs) are generated from the National Center for Environmental Prediction Final Analysis (NCEP-FNL) and the chemical ICs and BCs are from the Community Earth System Model (CESM) every 6-hour output (He et al., 2015). The physics options used for baseline simulation (BASE) is summarized in Table 1 of Wang et al. (2015a). The cumulus parameterization scheme used in this work is based on Grell 3D ensemble scheme (referred to as G3D, Grell and Freitas, 2014), which allows for a series of different assumptions that are commonly used in convective parameterizations and includes options to spread subsidence to neighboring grid points. Besides for the options listed in Table 1 of Wang et al. (2015a), BASE also includes prescribed SST forcing from NCEP by updating every 6-hour. SEN1 is conducted with the same model configurations as BASE but with different cumulus parameterization scheme based on Grell and Freitas (2014) (referred to as GF scheme), which allows for subgrid scale convection representation. The differences in the model results between BASE and SEN1 can provide insights about the sensitivity of cumulus parameterization on model meteorological, cloud/radiative, and chemical predictions.

SEN2 is configured same as SEN1 but with 1-dimentional (1-D) ocean mixed layer (OML) treatment turned on. A simple OML module based on Pollard et al. (1973) is available in WRF/Chem, which includes wind driven ocean mixing and mixed layer deepening process. Surface wind stress generates currents in the ocean mixed layer (typically 30-100 m deep), which leads to mixing with cooler water below. The model does not

consider pressure gradients or horizontal advection, but does include Coriolis, which is important for the rotation of inertial currents and SST cooling. This process deepens and cools the mixed layer, which changes SST and hence surface fluxes. The initial mixed layer depth (i.e., 50 m) and temperature lapse rate (i.e., 0.14 K m^{-1}) are specified in the model for the entire domain, which is a significant source of uncertainty considering spatial variations. The OML model is called every model time step (i.e., 60 seconds) across every grid point and the SST is then fed back into the atmospheric model (i.e., WRF/Chem).

SEN3 is configured same as SEN1 for WRF/Chem, but with fully coupling with ROMS (updated through August 2014). ROMS is a 3-dimentional (3-D), free-surface, hydrostatic, and primitive equations ocean model, which uses vertically stretched terrain-following (σ) coordinates combined with advanced physics packages to allow simulation of advective processes, Coriolis, and viscosity in 3-dimensions. It includes high-order advection and time-stepping schemes, weighted temporal averaging of the barotropic mode, conservative parabolic splines for vertical discretization, and the barotropic pressure gradient term, which can be applied for estuarine, coastal and basin-scale oceanic processes (Marchesiello et al. 2003; He and Wilkin, 2006, He et al., 2008). The COAWST (Warner et al., 2010) modeling system is designed to enable the integration of oceanic, atmospheric, wave and morphological processes in the coastal ocean. It consists of three state-of-the-art numerical models representing the atmosphere (i.e., WRF), ocean (i.e., ROMS) and wave (i.e., Simulating WAves Nearshore, SWAN) conditions using the Model Coupling Toolkit (MCT). The COAWST model represents the latest in air-sea interaction and numerical model coupling. In this work, COAWST is configured for a two-way coupling only between WRF

and ROMS. NCSU's version of WRF/Chem replaces WRF and is coupled with ROMS within COAWST system to allow a better representation of air-sea interactions compared to standalone WRF/Chem, which can provide insights about the effects of air-sea interactions on coastal air quality.

ROMS is configured on the same grid resolution as WRF/Chem with 157 interior density (ρ) points in the Y direction and 207 interior ρ points in the X direction, and with 16 layers vertically in the ocean. The initial and boundary conditions are from the global HYbrid Coordinate Ocean Model (HYCOM) combined with the Navy Coupled Ocean Data Assimilation (NCODA). The coastline and bathymetry are extracted from the Global Self-consistent Hierarchical High-resolution Shorelines (GSHHS), and 5-Minute Gridded Global Relief Data Collection (ETOPO5), respectively. Figure 5.1 shows the diagram of the coupling WRF/Chem with ROMS within COAWST framework. ROMS is coupled with WRF through MCT. SST is computed in ROMS and then passed to WRF. Meanwhile, several variables are passed from WRF to ROMS, including the 10 m wind vectors, air temperature, atmospheric pressure, humidity, precipitation, downward shortwave and long wave radiations, and sensible and latent heat fluxes for use in a set of bulk flux formulas. Chemistry package is fully coupled with WRF within the COAWST framework. The time step for ROMS calculation is 30 seconds and the time frequency for the WRF/Chem-ROMS coupling is 10 minutes.

5.2.2 Available Measurements and Evaluation Protocol

A number of observational datasets from surface networks and satellites are used for model evaluation. They are summarized along with the variables to be evaluated in Table

5.2. The meteorological and radiative variables are evaluated, including temperature at 2-m (T2), relative humidity at 2-m (RH2), and wind speed at 10-m (WS10) observed from the National Climatic Data Center (NCDC); daily precipitation rate (Precip) derived from the Global Precipitation Climatology Project (GPCP) and the Multi-satellite Precipitation Analysis from the Tropical Rainfall Measuring Mission (TMAP); outgoing longwave radiation (OLR), downwelling shortwave radiation (SWD), downwelling longwave radiation (LWD), shortwave cloud forcing (SWCF), and longwave cloud forcing (LWCF) retrieved from the Clouds and Earth's Radiant Energy System (CERES) Energy Balanced And Filled data product (CERES-EBAF); cloud fraction (CF), cloud optical thickness (COT), and LWP retrieved from the CERES Synoptic product at 1^{o} spatial resolution (CERES-SYN1deg); aerosol optical depth (AOD), precipitating water vapor (PWV), and CCN retrieved from the Moderate Resolution Imaging Spectroradiometer (MODIS). Air-sea interaction related variables are evaluated including SST and WS10 from the National Data Buoy Center (NDBC); PBLH derived from the National Centers for Environmental Prediction (NCEP)/North American Regional Reanalysis (NARR); SST, sensible heat flux (SHFLX) and latent heat flux (LHFLX) derived from the Objectively Analyzed Air-Sea Fluxes (OAFlux). Surface chemical concentrations evaluated include O_3, sulfur dioxide (SO_2), nitric acid (HNO_3), particulate matter with diameter less and equal to 2.5 μm ($PM_{2.5}$) and 10 μm (PM_{10}), and $PM_{2.5}$ components such as sulfate (SO_4^{2-}), ammonium (NH_4^{+}), nitrate (NO_3^{-}), sodium (Na^{+}), chloride (Cl^{-}), elementary carbon (EC), and organic carbon (OC). These species are observed from various observational networks over southeastern U.S., such as the Clean Air Status and Trends Network (CASTNET), the Interagency Monitoring of Protected

Visual Environments (IMPROVE), the Speciation Trends Network (STN), and the Aerometric Information Retrieval System-Air Quality System (AIRS-AQS). The locations of these sites are plotted in Figure 5.2. Column concentrations are evaluated over southeastern U.S., including tropospheric carbon monoxide (CO) retrieved from the Measurements Of Pollution In The Troposphere (MOPITT), tropospheric nitrogen dioxide (NO_2) and formaldehyde (HCHO) retrieved from the SCanning Imaging Absorption spectroMeter for Atmospheric CHartographY (SCIAMACHY), and tropospheric O_3 residual (TOR) retrieved from the Aura Ozone Monitoring Instrument in combination with Aura Microwave Limb Sounder (OMI/MLS). The protocols for performance evaluation include spatial distributions and statistics, following the approach of Zhang et al. (2009). The analysis of the performance statistics focus on mean bias (MB), normalized mean bias (NMB), normalized mean error (NME), root mean square error (RMSE), and correlation coefficient (Corr.).

5.3 Impacts of Cumulus Parameterizations

5.3.1 Meteorological Predictions

Figures 5.3a and b show the absolute differences in meteorology, cloud/radiative variables, and chemical predictions between SEN1 and BASE. Compared to BASE, SEN1 predicts higher T2 over most land area, and lower T2 over part of oceanic area. The increases of T2 in SEN1 can be up to 0.76 ^{o}C and the decrease of T2 can be up to 0.4 ^{o}C, with a domain averaged increase of 0.06 ^{o}C. Q2 decreases in SEN1 over most of domain, with a domain averaged decrease of 0.3 g kg^{-1}, indicating much drier condition predicted in SEN1. GF scheme is designed to be less active as the grid size reduces to cloud resolving scales. As a result, precipitation decreases in SEN1 over most of domain, with a domain averaged

reduction of 3.6 mm day^{-1}. The reduction of the precipitation is mainly from the combined changes of increase in convective precipitation and decrease in non-convective precipitation. Due to the more convection in SEN1, PBLH predicted by SEN1 also increases up to 185 m, with a domain averaged increase of 50.6 m.

Due to higher T2 and lower Q2 predicted by SEN1, less water vapor can condense onto the CCN surface. As a result, cloud droplets are smaller predicted by SEN1 than BASE. CDNC predicted by SEN1 varies throughout the domain, with increase up to 993 cm^{-3} and decrease up to 749 cm^{-3}, with a domain averaged increase of 3 cm^{-3}. Small cloud droplets in SEN1 can deplete the available liquid water to grow, which leads to reduction in LWP and CF. As a result, SEN1 predicts lower CF and LWP, with a domain averaged decrease of 6.6% and 17.7 g m^{-2}, respectively. However, COT increases in SEN1, with a domain averaged increase of 16.0. The increase of COT is likely due to the decrease of cloud effective radius from smaller cloud droplets and lower LWP in SEN1. The decrease of SWCF over land and near coast areas and increase of SWCF over remote ocean are mainly due to the combined changes in CDNC and increase of COT over these regions. As a result, compared to BASE, SEN1 predicts higher SWCF up to 49 W m^{-2} and lower SWCF up to 45.3 W m^{-2}, with a domain averaged decrease of 1.7 W m^{-2}. The decrease or increase in SWCF can result in an increase or a decrease in SWD. Compared to BASE, SEN1 predicts higher SWD by up to 52.71 W m^{-2} and lower SWD by up to 51.8 W m^{-2}, with a domain averaged of 1.4 W m^{-2}.

Table 5.3a and Figure 5.4 shows the model performance of BASE and SEN1. Meteorological variables such as T2, RH2, and SST are well predicted in both BASE and

SEN1, with absolute NMBs within ±5%, and with slightly better performance in SEN1. WS10 is moderately underpredicted against NCDC sites in both BASE and SEN1, with NMBs of -58.3% and -61.3%, respectively, whereas it is well predicted against CASTNET sites, with NMBs of 5.4% and 4.9%, respectively. With GF in SEN1, PBLH are impacted significantly over ocean, with increasing NMBs from 0.2% in BASE to 16.2% in SEN1. Both LHFLX and SHFLX are overpredicted in BASE and SEN1, which is mainly due to the inaccurate representing the air-sea interactions. Compared to BASE, SEN1 improves the predictions of Precip over land (ocean) significantly, by reducing NMB of 95.9% (335.2%) to 31.7% (211.5%) against GPCP and reducing NMB of 111.5% (42.2%) to 218.8% (128.2%) against TMAP. CF is also improved by reducing NMB from 23.7% in BASE to -1.0% in SEN1 over land, and from 48.7% in BASE to 42.3% in SEN1 over ocean, compared to CERES SYN1deg observations. LWP is more underpredicted with NMBs from -35.0% in BASE to -80.7% in SEN1 over land but improved significantly with NMBs from 304.6% in BASE to 35.1% in SEN1 over ocean. The performance of COT is improved over land with NMBs reducing from -70.3% in BASE to -39.5% in SEN1 whereas it is degraded over ocean, with NMBs increasing from -21.8% in BASE to 64.6% in SEN1. The large overpredictions of COT over ocean are likely due to the smaller cloud effective radius in SEN1, which indicates the uncertainties in the treatments of cloud dynamics and thermodynamics. Compared to MODIS data, PWV over land is more underpredicted, with NMBs from -0.7% in BASE to -5.8% in SEN1 and PWV is improved over ocean with NMBs from 12.1% in BASE to 4.1% in SEN1. AOD over land is slightly improved with NMBs from 2.4% in BASE to 1.5% in SEN1 and AOD over ocean is slightly improved with NMBs from -35.0 in

BASE to -34.6% in SEN1. CCN5 is improved in SEN1, with NMBs from 21.1% in BASE to -0.8% in SEN1. The decreases of CCN5 in SEN1 are likely due to the lower aerosol number concentrations in SEN1.

Radiative variables such as LWD, SWD, and OLR are comparable in BASE and SEN1, with slightly better performance of LWD over ocean (NMBs from 0.8% to 0.3%), SWD over land (NMBs from -2.4% to -0.5%), and OLR over land (NMBs from -13.9% to -7.0%) and ocean (NMBs from -22.9% to -20.7%) in SEN1. On the other hand, there are significant changes in SWCF and LWCF. Compared to BASE, the domain averaged SWCF predicted by SEN1 decreases from -72.1 W m^{-2} to -66.5 W m^{-2} over land, with NMBs from 57.2% to 45.1%, and increases from -118.1 W m^{-2} to -120.2 W m^{-2} over ocean, with NMBs from 108.9% to 112.5%. The domain averaged LWCF predicted by SEN1 decreases from 53.2 W m^{-2} to 37.7 W m^{-2} over land, with NMBs from 67.7% to 18.9%, and decreases from 77.8 W m^{-2} to 74.5 W m^{-2} over ocean, with NMBs from 152.1% to 141.4%. The improvements of SWCF and LWCF over land are attributed to the improvement of cloud variables (e.g., CF and COT) over land. The large overpredictions of SWCF and LWCF over ocean are attributed to the inaccurate predictions clouds over ocean, indicating the model uncertainties in the cloud dynamics and thermodynamics.

5.3.2 Chemical Predictions

As shown in Figure 5.3b, compared to BASE, SEN1 predicts higher surface CO and SO_2, with domain averaged of 5.6 ppb and 0.05 ppb, respectively. The increase of CO and SO_2 are likely due to the lower chemical loss through oxidation by lower OH levels and less wet deposition in SEN1. The increase of surface NO_2 over land is likely due to less wet

deposition, and the decrease of surface NO_2 over ocean is likely due to the increase of more convection over ocean (e.g., higher PBLH). The increase of surface O_3 in SEN1 is likely due to the increase of NO_2 and the decrease of O_3 is likely due to the more vertical mixing. The decrease of O_3 over southwestern land is likely due to the more chemical loss through oxidation with alkenes under more stable and warmer conditions over these regions. Compared to BASE, SEN1 predicts higher SO_4^{2-} by up to 1.0 μg m^{-3} and lower SO_4^{2-} by up to 1.6 μg m^{-3}. The increase of SO_4^{2-} is mainly due to the increase of SO_2 and decrease of wet deposition. The decrease of SO_4^{2-} is mainly due to the decrease of chemical production from lower OH levels over these regions. The increase of SOA is mainly due to the increase of ASOA (by 0.21 μg m^{-3}) and increase of BSOA (by 0.34 μg m^{-3}). The increase of ASOA can be attributed to the less wet deposition. The increase of BSOA can be attributed to less wet deposition and higher biogenic emissions from higher SWD and T2. Compared to BASE, SEN1 predicts higher $PM_{2.5}$ up to 4.9 μg m^{-3}, with a domain averaged of 0.68 μg m^{-3}, and higher PM_{10} up to 4.9 μg m^{-3}, with a domain averaged of 0.17 μg m^{-3}. The decrease of PM_{10} over remote ocean is mainly due to the decrease of sea-salt from lower WS10 in SEN1.

Table 5.3b shows the statistical performance for chemical predictions. As precipitation is reduced in SEN1, gases and aerosols are less underpredicted or more overpredicted, with better performance of surface TC (with NMBs from -16.2% to 1.0% against STN), $PM_{2.5}$ (with NMBs from -22.2% to -12.0% against IMPROVE, and from -29.3% to -25.1% against STN), PM_{10} (with NMBs from -65.4% to -62.1% against AIRS-AQS), and column SO_2 (with NMBs from -66.6% to -61.2% against SCIAMACHY).

5.4 Impacts of Ocean Treatment

5.4.1 Impacts on Meteorology

Figures 5.5a and b show the comparison of satellite observations/reanalysis data with model predictions by SEN1, SEN2, and SEN3. With 1-D OML treatment, most meteorological, cloud, and radiative variables are comparable in SEN1 and SEN2. For example, SST and PBLH slightly decrease by 0.1 ^{o}C and 1.2 m over ocean in SEN2 compared to SEN1. The 1-D OML treatment represents cooling of SST due to deep mixing of the ocean layers below with stably stratified cooler water. This cools the mixed layer, which reduces the SST and hence surface fluxes. In SEN2, LHFLX increases by 0.7 W m^{-2} and SHFLX increases by 0.1 W m^{-2} over ocean compared to SEN1. The negative correlation between LHFLX and SST indicates the dominance of atmospheric forcing of the ocean in western Atlantic Ocean and the contribution of atmospheric forcing to SST variations in these regions. However, due to the simplified assumptions and treatment in 1-D OML, the impacts of 1-D ocean mixed layer are small, with domain averaged increase of SWD and LHFLX by 0.5 W m^{-2} and 0.4 W m^{-2}, respectively.

With coupling of 3-D ROMS in SEN3, boundary layer properties are affected significantly. For example, SEN3 predicts lower SST by up to 1.9 ^{o}C, with a domain averaged decrease of 0.9 ^{o}C. SST is prescribed in SEN1, whereas it is prognostic in ROMS. The decrease of SST in SEN3 is mainly due to the lower SST from initial conditions from global HYCOM. SEN3 also predicts lower PBLH over ocean, with domain averaged decrease of 56.5 m, indicating a more stable condition in SEN3. The decrease of PBLH is mainly due to the decrease of heat fluxes through interactions with ocean. T2 and SST decrease in SEN3, resulting less evaporation and LHFLX. As a result, SEN3 predicts lower

LHFLX by up to 128.6 W m^{-2}, with a domain averaged decrease of 27.6 W m^{-2}. Comparing SEN3 to SEN1, the LHFLX-SST correlation is positive, suggesting the dominance of oceanic forcing of atmosphere in the western Atlantic Ocean. Due to the less evaporation in SEN3, precipitation and cloud are also reduced, resulting in higher SWD, with a domain average of 9.7 W m^{-2}.

As shown in Figure 5.4, the prescribed SST in SEN1 agrees well with observations from OAFlux, with NMB of 0.6%. SST is well predicted in SEN2, with NMB of 0.4%, whereas it is slightly underpredicted in SEN3, with NMBs of -2.8%. SEN1 and SEN2 are driven by prescribed SST from NCEP, with SST changes due to OML treatment in SEN2, whereas SST is prognostic in SEN3. Both SEN1 and SEN2 give warm SST bias for Gulf Stream (see Figure 5.5a), whereas SEN3 gives cold bias for SST. In SEN1 and SEN2, warm SST can increase evaporation and convective instability. As a result, an atmospheric circulation that produces moisture convergence and convection can occur to respond to SST gradients. Compared to NCEP/NARR data, both SEN1 and SEN2 overpredict PBLH over ocean, with NMBs of 16.2%, and 16.0%, respectively, whereas SEN3 predicts PBLH well, with an NMB of -3.1%. Compared to GPCP data, precipitation is largely overpredicted over ocean in both SEN1, and SEN2, with NMBs of 211.5% and 210.3%, respectively, whereas it is significantly improved in SEN3, with an NMB of 119.2%. LHFLX/SHFLX are largely overpredicted in SEN1 and SEN2, with NMBs of 60.1%/138.2%, and 60.7%/ 140.7%, respectively, whereas they are improved in SEN3 significantly, with NMBs of 18.9%/50.2%. Compared to OML treatment, SST reanalysis data is dominant for SST predictions in SEN2, which can drive atmospheric anomalies, and therefore generate larger monthly mean

precipitation and LHFLX anomalies compared to the coupled simulation SEN3, especially over the regions with warm SST and high precipitation (e.g., Gulf Stream). In SEN3, atmospheric wind and heat fluxes are computed by WRF and passed to ROMS for SST calculation. The changes in wind and heat fluxes can contribute to the SST anomalies in these regions, and SST anomalies can induce opposite atmospheric changes in coupled simulation SEN3 (Wu and Kirtman 2005, 2007). As a result, the biases in the atmospheric predictions (e.g., WS10, PBLH, Precip, LHFLX, and SHFLX) are smaller in SEN3 than in SEN1 and SEN2.

Most cloud variables are comparable in SEN1 and SEN2 but are improved in SEN3 especially over ocean. Figure 5.5b shows the comparison of satellite observations with predictions of AOD, CCN5, COT, and SWCF by SEN1 and SEN3. As shown in Figure 5.5b, SEN3 predicts higher AOD up to 0.038, and lower AOD up to 0.048, with a domain averaged of 0.0002. The higher AOD can be attributed to the higher aerosol concentrations from less wet deposition in SEN3. Compared to MODIS data, both SEN1 and SEN3 overpredict AOD over land by 1.5% and 3.5%, respectively, and underpredict AOD over ocean by 34.6% and 31.5%, respectively. The underpredictions of AOD over ocean are likely due to the inaccurate predictions of marine aerosols (e.g., sea-salt). Column CCN5 is lower in SEN3 over most domain, with a domain averaged of 3.1×10^{-7} cm^{-2}. Compared to MODIS data, column CCN5 over ocean is underpredicted by both SEN1 and SEN3. The underpredictions of CCN5 are likely due to the inaccurate predictions of aerosol number concentrations, and uncertainties in the cloud thermodynamics. Compared to SEN1, SEN3 predicts higher COT up to 62.2, and lower COT up to 87.4, with a domain averaged decrease

of 3.9. Compared to satellite data, both SEN1 and SEN3 underpredict COT over land, with NMBs of -39.5% and -39.8%, respectively, and overpredict COT over ocean, with NMBs of 64.6% and 37.5% respectively. The biases in COT predictions are likely due to the model uncertainties in cloud dynamics and thermodynamics. Compared to SEN1, SEN3 predicts higher SWCF up to 21.0 W m^{-2}, and lower SWCF up to 77.9 W m^{-2}, with a domain averaged decrease of 10.9 W m^{-2}. The decrease of SWCF in SEN3 is mainly due to the decrease of COT and CDNC in SEN3. Compared to satellite data, SWCF is improved over ocean significantly, with NMBs from 112.5% in SEN1 to 78.5% in SEN3. Other cloud/radiative variables are also improved over ocean. For example, CF is improved over ocean, with NMBs from 42.3% in SEN1 to 36.7% in SEN3. LWP is improved over ocean, with NMBs from 35.1% in SEN1 to -29.2% in SEN3. Due to the improved cloud predictions, most radiative variables are also improved over ocean. For example, SWD is improved over ocean with NMBs from -20.6% to -13.7%. OLR and LWCF are improved over ocean as well, with NMBs of -20.7% to -16.8%, and from 141.4% to 107.7%, respectively.

5.4.2 Impacts on Chemistry

Figures 5.6a and b show the absolute differences between SEN2 and SEN1, and SEN3 and SEN1 for surface chemical predictions. With 1-D OML treatment, the changes of most surface chemical species are small. For example, the differences in surface CO between SEN1 and SEN2 are within 11 ppb (or within 3%). The absolute differences in surface SO_2, NO_2, O_3, and OH are within 2 ppb, and the percentage differences can be as large as 29.8%, 14.4%, 6.5%, and 9.8%, respectively. Although the absolute differences in surface SO_4^{2-}, SOA, $PM_{2.5}$ and PM_{10} are within 1.5 μg m^{-3}, the percentage differences can be as large as

20.2%, 757.5%, 9.0%, and 11.7% respectively. The significant change of SOA (i.e., increase up to 757.5%) in SEN2 is likely due to higher OH levels and lower PBLH over southeastern domain (e.g. 31–34^{o} N). With coupling of 3-D ROMS, the changes of most surface chemical species between SEN1 and SEN3 are much larger than those between SEN1 and SEN2. For example, surface CO can increase as large as 196.5 ppb and decrease as large as 304.9 ppb. Although the absolute differences in surface SO_2 and OH between SEN1 and SEN3 are with 1.5 ppb, the percentage differences in surface SO_2 and OH can be as large as 134.4% and 83.6%, respectively. The changes of surface NO_2 and O_3 are also significant, which can be as large as 18.0 ppb (or 189.2%) and 17.3 ppb (or 44.8%), respectively. The decreases of CO, SO_2, and NO_2 are likely due in part to the oxidation with higher OH concentrations in SEN3. The increase in OH concentrations can be attributed to the decrease of precipitation and PBLH, and the increase of SWD in SEN3. Compared to SEN1, surface SO_4^{2-} predicted by SEN3 can increase as large as 0.9 μg m^{-3} and decrease as large as 1.2 μg m^{-3}. The changes in surface SO_4^{2-} predictions are mainly due in part to changes in SO_2 and OH concentrations through gas-phase oxidation, and changes in cloud fraction through aqueous phase chemistry. Surface SOA predicted by SEN3 can increase as large as 0.7 μg m^{-3} and decrease as large as 1.5 μg m^{-3}. The changes in SOA predictions are likely due to the combined changes in OH concentrations, precipitation, SWD, and PBLH. There are similar patterns in surface $PM_{2.5}$ and PM_{10} changes over land. Both $PM_{2.5}$ and PM_{10} increase over 30-33^{o}N, and decrease over 33-40^{o}N. The increase of $PM_{2.5}$ can be as large as 3.0 μg m^{-3} and the decrease of $PM_{2.5}$ can be as large as 7.9 μg m^{-3}. The increase of $PM_{2.5}$ can be attributed to the decrease in precipitation and PBLH over these regions and the decrease of $PM_{2.5}$ can be attributed to the

combined effects of increase in precipitation and PBLH. The decreases of PM_{10} over remote ocean are mainly due the decreases in sea-salt predictions from lower WS10 in SEN3 than SEN1. As shown in Figure 5.6b, most significant changes in surface chemical predictions are along coast, over remote ocean, and part of inland regions, indicating the significant impacts of air-sea interactions on air quality.

Figure 5.7a and b show the time series observations and model predictions over coastal sites from CASTNET, IMPROVE, and AIRS-AQS for surface max 8-h O_3 and $PM_{2.5}$. Compared to SEN1, the differences in Max 8-h O_3 can be as large as about 15 ppb over CASTNET sites. Max 8-h O_3 predicted by SEN1, SEN2, and SEN3 overall correlated well over CASTNET sites, with a better performance by SEN3 over BFT142 and IRL141. Compared to SEN1, the differences in Max 8-h O_3 can be as large as about 20 ppb over AQS sites. Max 8-h O_3 concentrations are large overpredicted by three simulations over AQS sites such as site 121012001 and site 280470008. As shown in Figure 5.7b, $PM_{2.5}$ is overall well predicted over IMPROVE and AQS sites. Compared to SEN1, the differences in surface $PM_{2.5}$ predictions can be as large as about 15 μg m^{-3} over IMPROVE sites and as large as about 6 μg m^{-3} over AQS sites, with a better performance by SEN3 over CHAS1, ROMA1, EVER1, and SWAN1.

Figure 5.8 shows the scatter plots for major chemical species over various observational networks. Compared to SEN1, SEN3 overall predicts better chemical concentrations. For example, surface gas species such as SO_2 and HNO_3 are improved by reducing NMBs from 204.5% to 192.1%, and 92.4% to 85.1%, respectively. Hourly O_3 is also improved by reducing NMBs from 27.3% to 26.4% against AIRS-AQS sites. Max 1-h

and 8-h O_3 are also improved by reducing NMBs from 3.0 % to 2.1% against CASTNET (15.6% to 14.8% against AIRS-AQS), and 13.2% to 12.2% against CASTNET (20.0 to 19.2% against AIRS-AQS), respectively. Aerosol species such as SO_4^{2-}, NH_4^+, and NO_3^- are slightly or moderately improved against STN observations. Na^+ and Cl^- are largely underpredicted in both SEN1 and SEN3, indicating the uncertainties in the online sea-salt emission modules. EC is slightly improved in SEN3, whereas OC and TC are slightly degraded in SEN3. $PM_{2.5}$ is slightly improved in SEN3 over IMPROVE sites, but degraded against STN sites. PM_{10} is also slightly improved in SEN3, with reducing NMB from -62.1% to -61.7%. The large underpredictions of PM_{10} are likely due to the inaccurate predictions of sea-salt concentrations. The column concentrations are comparable in SEN1 and SEN3, with slightly better performance of column SO_2.

5.5 Conclusions

In this section, different cumulus parameterization schemes are tested in WRF/Chem to study the sensitivity of cumulus schemes on model predictions. In addition, WRF/Chem simulations with 1-D OML treatments and 3-D ROMS coupling are conducted to study the impacts of air-sea interactions on air quality predictions. Due to the consideration of resolving subgrid-scale clouds, SEN1 with GF scheme can predict much better precipitation compared to BASE with G3D scheme, with NMBs reducing from 95.9% to 31.7% over land, and from 335.2% to 211.5% over ocean against GPCP. Compared to BASE, SEN1 improves most cloud and radiative variables, such as CF, COT, LWD, SWD, and OLR, mainly over ocean. Due to the improvement in cloud predictions, SWCF and LWCF are also improved. However, large overpredictions of clouds and radiative forcing over ocean indicate the model

uncertainties in the cloud dynamics and thermodynamics. The changes in meteorology, clouds, and radiation in SEN1 can impact chemical predictions. As precipitation is reduced in SEN1, gases and aerosols are less underpredicted or more overpredicted, with better performance of surface TC, $PM_{2.5}$, PM_{10}, and column SO_2 in SEN1 than BASE.

With inclusion of ocean treatments in SEN2 and SEN3, boundary layer properties are changed. As OML is a simplified 1-D treatment with large uncertainty, the impacts on boundary layer are not as significant as 3-D ROMS coupling, which consists of detailed primitive equations for 3-D ocean circulation and dynamics. SEN2 is forced by prescribed SST. The warm bias of SST over Gulf Stream can generate larger monthly mean rainfall and surface latent heat flux anomalies compared to SEN3, of which SST is prognostic in ROMS. As a result, precipitation, LHFXL and SHFLX are improved significantly in SEN3, with NMBs reducing from 211.5% in SEN1 to 119.2% in SEN3, 60.1% in SEN1 to 18.9% in SEN3, and 138.2% in SEN1 to 50.2% in SEN3, respectively. However, compared to OAflux, SST predicted in SEN3 is underpredicted with NMB of -2.8%, which is mainly due to the lower initial conditions from global HYCOM data. Due to the improvement in surface heat fluxes, PBLH is also improved in SEN3, with NMBs reducing from 16.2% in SEN1 to -3.1% in SEN3 over ocean. Due to more stable boundary layer and less evaporation over ocean in SEN3, most cloud variables over ocean are also improved in SEN3, such as CF, COT, and LWP. As a result, radiative variables over ocean are also improved, such as SWD, OLR, SWCF, and LWCF.

Due to the changes in the boundary layer properties, surface chemical predictions are affected significantly in SEN3. For example, With 1-D OML treatment, surface O_3 and $PM_{2.5}$

can increase as large as 1.8 ppb and 1.0 μg m^{-3}, and decreases as large as 1.4 ppb and 1.1 μg m^{-3}, with a domain averaged increase of 0.03 ppb and 0.02 μg m^{-3}, respectively. With coupling of 3-D ROMS, surface O_3 and $PM_{2.5}$ can increase as large as 12.0 ppb and 3.0 μg m^{-3}, and decreases as large as 17.3 ppb and 7.9 μg m^{-3}, with a domain averaged decrease of 0.67 ppb and 0.08 μg m^{-3}, respectively. The largest differences in surface O_3 predictions are along the coastal areas and remote ocean, whereas the largest differences in surface $PM_{2.5}$ predictions are not only along the coastal areas and remote ocean, but also over inland areas, indicating the significant impacts of air-sea treatments on chemical predictions. Compared to SEN1, SEN3 shows overall better performance for chemical concentrations, such as SO_2, HNO_3, Max 1-h and 8-h O_3, SO_4^{2-}, NH_4^+, and NO_3^-, and PM_{10}. The simulated column concentrations are comparable in SEN1 and SEN3, with slightly better performance of column SO_2 in SEN3.

Table 5.1 Simulation design

Run Index	Description	Purpose
BASE	Baseline, NCSU's version of WRF/Chem with G3 cumulus parameterization (cu_physics = 5)	Severed as baseline
SEN1	Same as BASE, but with GF cumulus parameterization (cu_physics = 3)	The differences between SEN1 and BASE indicate the impacts of cumulus parameterization on model predictions; Severed as basedline2 to investigate the impacts from ocean treatments.
SEN2	Same as SEN1, but with 1-D ocean mixed layer treatment (sf_ocean_physics = 1)	The differences between SEN2 and SEN1 indicate the impacts of 1-D ocean mixed layer treatment on model predictions
SEN3	Same as SEN1, but with coupling of ROMS within COAWST frame work	The differences between SEN3 and SEN1 indicate the impacts of air-sea coupling on model predictions

Table 5.2. Datasets for model evaluation

Species/Variables	**Dataset**	**Spatial (Temporal) Resolution**
Temperature at 2-m (T2), Relative humidity at 2-m (RH2), Wind speed at 10-m (WS10)	Land: NCDC; Ocean: NDBC	400 sites (hourly); 15 sites (hourly)
Planetary boundary layer height (PBLH)	NCEP/NARR	32-km (monthly)
Sea surface temperate (SST), sensible heat flux (SHFLX), latent heat flux (LHFLX)	OAFlux	1^o (monthly)
Precipitation (Precip)	GPCP, TMAP	2.5^o (monthly), 0.25^o (daily)
Outgoing longwave radiation (OLR), Downwelling longwave radiation (LWD), Downwelling shortwave radiation (SWD), Shortwave cloud radiative forcing (SWCF), Longwave cloud radiative forcing (LWCF)	CERES-EBAF	1^o (monthly)
Cloud fraction (CF), Cloud optical thickness (COT), Cloud liquid water path (LWP)	CERES-SYN1deg	1^o (monthly)
Precipitating water vapor (PWV), Aerosol optical depth (AOD), Column cloud condensation nuclei (ocean) at S = 0.5% (CCN5),	MODIS	1^o (monthly)
Max 1-h Ozone (O_3), Max 8-h O_3	CASTNET, AIRS-AQS	38 sites (hourly), 420 (hourly)
Hourly O_3	AIRS-AQS	420 (hourly)
Sulfur dioxide (SO_2), Nitric acid (HNO_3)	CASTNET	38 sites (weekly)
Sulfate (SO_4^{2-}), Ammonium (NH_4^+), Nitrate (NO_3^-)	CASTNET, IMPROVE, STN	38 sites (weekly), 29 sites (3-day), 74 sites (3-day to weekly)
Organic carbon (OC)	IMPROVE	29 sites (3-day)
Elementary carbon (EC), Total carbon (TC)	IMPROVE, STN	29 sites (3-day), 74 sites (3-day to weekly)
Particulate matter with diameter less than and equal to 2.5 μm ($PM_{2.5}$)	IMPROVE, STN	29 sites (3-day), 74 sites (3-day to weekly)
Particulate matter with diameter less than and equal to 10 μm (PM_{10})	AIRS-AQS	53 sites (hourly)
Tropospheric carbon monoxide (CO)	MOPITT	1^o (monthly)
Tropospheric SO_2, nitrogen dioxide (NO_2), formaldehyde (HCHO)	SCIAMCHY	0.25^o (monthly)
Tropospheric ozone residual (TOR)	OMI/MLS	1.25^o (monthly)

NCDC: National Climatic Data Center; NDBC: National Data Buoy Center; NCEP/NAAR: National Centers for Environmental Prediction and North American Regional Reanalysis; OAFlux: Objectively Analyzed Air-Sea Fluxes; GPCP: the Global Precipitation Climatology Project; TMAP: Multi-satellite Precipitation Analysis from the Tropical Rainfall Measuring Mission; CERES-EBAF: Clouds and Earth's Radiant Energy System Energy Balanced And Filled data product; CERES-SYN1deg: CERES Synoptic product at 1^o spatial resolution; MODIS: Moderate Resolution Imaging Spectroradiometer; OMI/MLS: the Aura Ozone Monitoring Instrument in combination with Aura Microwave Limb Sounder; MOPITT: the Measurements Of Pollution In The Troposphere; the Global Ozone Monitoring Experiment; SCIAMCHY: the SCanning Imaging Absorption spectroMeter for Atmospheric CHartographY; CASTNET: Clean Air Status and Trends Network; IMPROVE: Interagency Monitoring of Protected Visual Environments; STN: Speciation Trends Network; AIRS-AQS: the Aerometric Information Retrieval System-Air Quality System.

Table 5.3a. Statistical performance of meteorological, cloud, and radiative variables

Species/ Variables	Datesets		BASE				SEN1				SEN2				SEN3			
		obs	sim	NMB (%)	NME (%)	Corr	sim	NMB (%)	NME (%)	Corr	sim	NMB (%)	NME (%)	Corr	sim	NMB (%)	NME (%)	Corr
T2 (^{o}C)	NCDC	26.6	25.3	-4.9	8.8	0.82	25.4	-4.3	8.4	0.83	25.4	-4.3	8.4	0.83	25.4	-4.4	8.4	0.83
	NDBC	27.8	27.3	-1.8	3.6	0.87	27.4	-1.4	3.4	0.89	27.4	-1.4	3.5	0.89	26.7	-3.7	6.0	0.74
RH2 (%)	NCDC	73.9	74.6	1.0	14.8	0.67	73.6	-0.4	14.3	0.69	73.6	-0.4	14.3	0.68	73.7	-0.2	14.3	0.69
WS10 ($m\ s^{-1}$)[1]	NCDC	6.8	2.8	-58.3	62.3	0.16	2.6	-61.3	63.6	0.20	2.6	-61.5	63.7	0.20	2.7	-60.6	63.1	0.21
	NDBC	5.5	6.9	25.1	48.2	0.28	6.1	10.6	34.4	0.47	6.1	10.1	34.5	0.47	5.9	7.1	30.6	0.56
Precip ($mm\ day^{-1}$)	GPCP (land)	4.1	8.1	95.9	110.0	0.14	5.4	31.7	46.1	0.36	5.4	31.9	44.9	0.38	5.3	29.5	40.6	0.35
	GPCP (ocean)	3.9	16.8	335.2	339.7	0.18	12.0	211.5	215.5	0.24	12.0	210.3	214.7	0.25	8.5	119.2	124.5	0.37
	TMPA (land)	3.8	8.1	111.5	127.6	0.15	5.4	42.2	58.8	0.27	5.4	42.4	57.6	0.28	5.3	39.8	53.2	0.23
	TMPA (ocean)	5.3	16.8	218.8	223.8	0.30	12.0	128.2	133.4	0.38	12.0	127.3	132.4	0.40	8.5	60.6	73.4	0.46
LWD ($W\ m^{-2}$)[2]	CERES (land)	415.0	401.6	-3.2	3.2	0.96	400.5	-3.5	3.5	0.95	399.6	-3.7	3.7	0.95	399.7	-3.7	3.7	0.96
	CERES (ocean)	416.9	420.4	0.8	1.4	0.83	418.1	0.3	1.1	0.84	416.9	0.01	1.0	0.83	412.4	-1.1	1.2	0.83
SWD ($W\ m^{-2}$)[3]	CERES (land)	263.7	257.3	-2.4	8.8	0.36	262.5	-0.5	8.5	0.40	261.6	-0.8	8.4	0.35	261.2	-0.9	7.7	0.35
	CERES (ocean)	266.1	213.9	-19.6	19.8	0.51	211.4	-20.6	21.2	0.48	211.3	-20.6	21.3	0.48	229.6	-13.7	14.2	0.49
	CASTNET	272.4	295.3	8.4	34.7	0.88	299.7	10.0	34.6	0.88	298.8	9.7	35.1	0.88	299.3	9.9	34.3	0.88
OLR ($W\ m^{-2}$)	CERES (land)	259.9	223.8	-13.9	14.0	0.48	241.7	-7.0	7.2	0.64	240.8	-7.3	7.5	0.64	241.7	-7.0	7.1	0.61
	CERES (ocean)	253.7	195.6	-22.9	22.9	0.33	201.1	-20.7	20.7	0.51	200.7	-20.9	20.9	0.51	211.1	-16.8	16.8	0.56
SWCF ($W\ m^{-2}$)	CERES (land)	-45.9	-72.1	57.2	61.8	0.32	-66.5	45.1	50.8	0.42	-66.5	45.1	50.9	0.39	-66.5	45.0	49.4	0.33
	CERES (ocean)	-56.6	-118.1	108.9	109.3	0.50	-120.2	112.5	113.7	0.47	-119.4	111.2	112.4	0.46	-100.9	78.5	79.3	0.54
LWCF ($W\ m^{-2}$)	CERES (land)	31.7	53.2	67.7	71.7	0.34	37.7	18.9	37.3	0.49	37.7	19.1	37.1	0.49	37.1	17.2	34.4	0.46
	CERES (ocean)	30.9	77.8	152.1	152.1	0.25	74.5	141.4	141.9	0.42	74.2	140.3	140.9	0.42	64.1	107.7	108.1	0.49
CF (%)	CERES(land)	46.3	57.3	23.7	32.8	0.26	45.8	-1.0	27.1	0.32	45.7	-1.2	27.4	0.29	45.9	-0.9	26.7	0.29
	CERES (ocean)	53.3	79.8	48.7	50.2	0.16	75.9	42.3	46.1	0.14	75.9	42.3	46.2	0.14	72.9	36.7	39.3	0.20
COT	CERES (land)	34.8	10.3	-70.3	70.4	-0.38	21.1	-39.5	53.0	-0.39	21.0	-39.8	52.2	-0.44	21.0	-39.8	49.9	-0.35
	CERES (ocean)	26.2	20.5	-21.8	35.0	0.36	43.2	64.6	77.5	0.28	42.6	62.5	75.4	0.28	36.0	37.5	58.3	0.27
LWP ($g\ m^{-2}$)	CERES (land)	119.5	76.3	-35.0	87.2	-0.41	22.7	-80.7	87.0	-0.25	21.0	-82.2	87.6	-0.24	16.1	-86.3	88.1	-0.02
	CERES (ocean)	81.8	331.0	304.6	323.4	0.07	110.5	35.1	110.8	0.01	112.6	37.6	112.0	-0.00	57.9	-29.2	83.7	0.14
PWV (cm)	MODIS (land)	4.4	4.3	-0.7	4.4	0.96	4.1	-5.8	6.2	0.96	4.1	-5.8	6.1	0.96	4.1	-6.3	6.5	0.97
	MODIS (ocean)	4.5	5.0	12.1	12.5	0.79	4.7	4.1	6.3	0.82	4.7	4.0	6.3	0.82	4.5	0.6	4.5	0.84
AOD	MODIS (land)	0.15	0.16	2.4	23.6	0.47	0.16	1.5	22.4	0.53	0.16	1.5	22.9	0.51	0.16	3.5	22.7	0.54
	MODIS (ocean)	0.21	0.14	-35.0	35.0	0.44	0.14	-34.6	34.9	0.34	0.14	-34.5	34.6	0.35	0.14	-31.5	32.2	0.29
CCN5 ($10^8\ cm^{-2}$)	MODIS (ocean)	2.8	3.4	21.1	45.8	0.25	2.8	-0.8	42.5	-0.03	2.8	-0.7	42.7	-0.01	2.5	-12.7	40.3	0.07
PBLH (m)	NARR (land)	872.6	544.1	-37.6	37.6	0.32	556.4	-36.2	36.2	0.40	553.4	-36.6	36.6	0.42	557.1	-36.2	36.2	0.41
	NARR (ocean)	530.0	531.3	0.2	20.6	0.24	615.9	16.2	26.0	0.24	614.7	16.0	25.8	0.25	513.4	-3.1	22.0	0.12
SST (^{o}C)	OAflux (ocean)	28.3	28.5	0.6	1.2	0.76	28.5	0.6	1.2	0.76	28.4	0.4	1.2	0.76	27.5	-2.8	3.8	0.63
	NDBC	27.8	27.9	0.3	1.8	0.96	27.9	0.3	1.8	0.96	27.8	0.2	2.4	0.93	27.0	-2.9	4.8	0.78
LHFLX ($W\ m^{-2}$)	OAflux (ocean)	111.6	177.8	59.3	59.3	0.61	178.7	60.1	60.2	0.72	179.4	60.7	60.8	0.71	132.7	18.9	26.9	0.47
SHFLX ($W\ m^{-2}$)	OAflux (ocean)	5.2	15.2	195.4	196.6	0.62	12.3	138.2	139.8	0.67	12.4	140.7	142.4	0.66	7.7	50.2	76.9	0.36

Table 5.3b. Statistical performance of chemical species

Species/ Variables*	Datasets		Simulations															
			BASE				SEN1				SEN2				SEN3			
		obs	sim	NMB (%)	NME (%)	Corr	sim	NMB (%)	NME (%)	Corr	sim	NMB (%)	NME (%)	Corr	sim	NMB (%)	NME (%)	Corr
SO_2	CASTNET	1.2	3.3	181.8	199.2	0.36	3.6	204.5	219.4	0.31	3.6	201.1	205.6	0.33	3.4	192.1	207.1	0.33
HNO_3	CASTNET	1.1	2.0	81.0	82.3	0.70	2.1	92.4	93.0	0.58	2.1	91.9	92.5	0.57	2.0	85.1	85.6	0.62
Max 1-h O_3	CASTNET	51.6	52.5	1.8	19.9	0.52	53.1	3.0	19.4	0.55	52.8	2.4	20.0	0.53	52.6	2.1	19.7	0.54
	AIRS-AQS	52.4	59.5	13.6	23.3	0.58	60.6	15.6	24.2	0.57	60.5	15.4	23.5	0.57	60.2	14.8	23.7	0.58
Max 8-h O_3	CASTNET	46.8	52.3	11.6	21.4	0.58	53.0	13.2	21.5	0.61	52.8	12.7	21.8	0.59	52.5	12.2	21.5	0.59
	AIRS-AQS	47.3	55.6	17.4	24.0	0.99	56.8	20.0	25.5	0.99	56.7	19.8	25.7	0.99	56.6	19.2	25.1	0.99
Hourly O_3	AIRS-AQS	31.7	39.8	25.5	40.2	0.68	40.3	27.3	41.4	0.68	40.2	27.1	41.4	0.68	40.0	26.4	40.7	0.69
NH_4^+	STN	1.0	1.2	19.5	64.4	0.44	1.2	19.6	62.3	0.45	1.2	20.0	63.3	0.44	1.2	17.0	63.0	0.46
	CASTNET	1.2	1.2	-1.4	37.0	0.49	1.2	1.3	35.2	0.50	1.2	0.4	35.1	0.47	1.2	-1.6	34.0	0.51
SO_4^{2-}	IMPROVE	3.1	2.9	-5.4	57.4	0.35	2.9	-5.1	53.6	0.40	2.9	-5.1	52.3	0.41	2.9	-4.0	50.7	0.41
	STN	3.6	3.4	-4.1	57.1	0.30	3.1	-13.9	51.5	0.38	3.1	-13.7	51.1	0.38	3.1	-13.6	52.3	0.34
	CASTNET	4.1	3.6	-10.9	32.2	0.39	3.4	-15.6	31.1	0.43	3.4	-16.1	32.6	0.39	3.4	-17.2	31.5	0.42
NO_3^-	IMPROVE	0.3	0.4	46.7	122.3	0.34	0.4	63.3	138.8	0.23	0.4	62.3	140.1	0.19	0.4	48.6	124.7	0.31
	STN	0.4	0.6	33.3	106.2	0.28	0.7	61.6	128.3	0.26	0.7	63.5	131.7	0.21	0.6	51.0	120.7	0.22
	CASTNET	0.4	0.6	38.7	122.0	0.10	0.6	50.9	130.8	0.10	0.6	48.5	129.3	0.11	0.6	42.4	124.4	0.13
Na^+	IMPROVE	0.4	0.1	-64.6	71.1	0.40	0.1	-68.8	73.8	0.39	0.1	-69.2	73.9	0.39	0.1	-69.0	73.4	0.40
Cl^-	IMPROVE	0.2	0.03	-77.6	82.9	0.52	0.02	-86.0	88.0	0.57	0.02	-85.2	88.2	0.57	0.03	-83.7	85.4	0.66
EC	IMPROVE	0.3	0.3	18.0	63.8	0.45	0.4	43.0	81.1	0.29	0.4	42.2	80.6	0.28	0.4	40.4	79.1	0.27
OC	IMPROVE	1.5	1.4	-2.5	54.3	0.41	1.9	30.0	66.4	0.40	1.9	28.9	66.0	0.38	1.9	30.3	63.2	0.41
TC	STN	2.9	2.4	-16.2	46.3	0.50	2.9	1.0	46.3	0.46	2.9	1.2	47.5	0.45	2.8	-2.6	46.1	0.45
$PM_{2.5}$	IMPROVE	10.2	7.9	-22.2	44.7	0.30	9.0	-12.0	40.5	0.31	9.0	-12.0	40.3	0.31	9.0	-11.8	39.0	0.33
	STN	14.1	10.0	-29.3	42.2	0.38	10.6	-25.1	41.5	0.36	10.6	-25.0	41.3	0.36	10.3	-27.1	41.8	0.36
PM_{10}	AIRS-AQS	27.4	9.5	-65.4	69.9	0.11	10.4	-62.1	66.8	0.13	10.4	-62.0	66.5	0.14	10.5	-61.7	66.3	0.13
Col.CO	MOPITT	1.8×10^{18}	2.6×10^{18}	50.2	50.2	0.78	2.6×10^{18}	50.7	50.7	0.81	2.6×10^{18}	50.8	50.8	0.80	2.6×10^{18}	50.8	50.8	0.80
Col. SO_2	SCIMACHY	0.27	0.09	-66.6	73.9	0.31	0.10	-61.2	69.7	0.33	0.10	-61.4	69.8	0.33	0.10	-61.1	69.3	0.33
Col.NO_2	SCIMACHY	1.3×10^{15}	2.8×10^{15}	116.3	116.7	0.79	3.0×10^{15}	129.0	129.2	0.79	3.0×10^{15}	129.0	129.3	0.79	3.0×10^{15}	132.2	132.4	0.78
TOR	SCIMACHY	40.1	44.7	11.6	13.0	0.68	46.3	15.6	16.4	0.64	46.4	15.8	16.6	0.64	47.1	17.5	17.8	0.64

* The units for all surface gaseous and aerosol species are μg m^{-3} except for O_3 (ppb). The units for column CO and NO_2 are molecules cm^{-2} and for column SO_2 and TOR are DU.

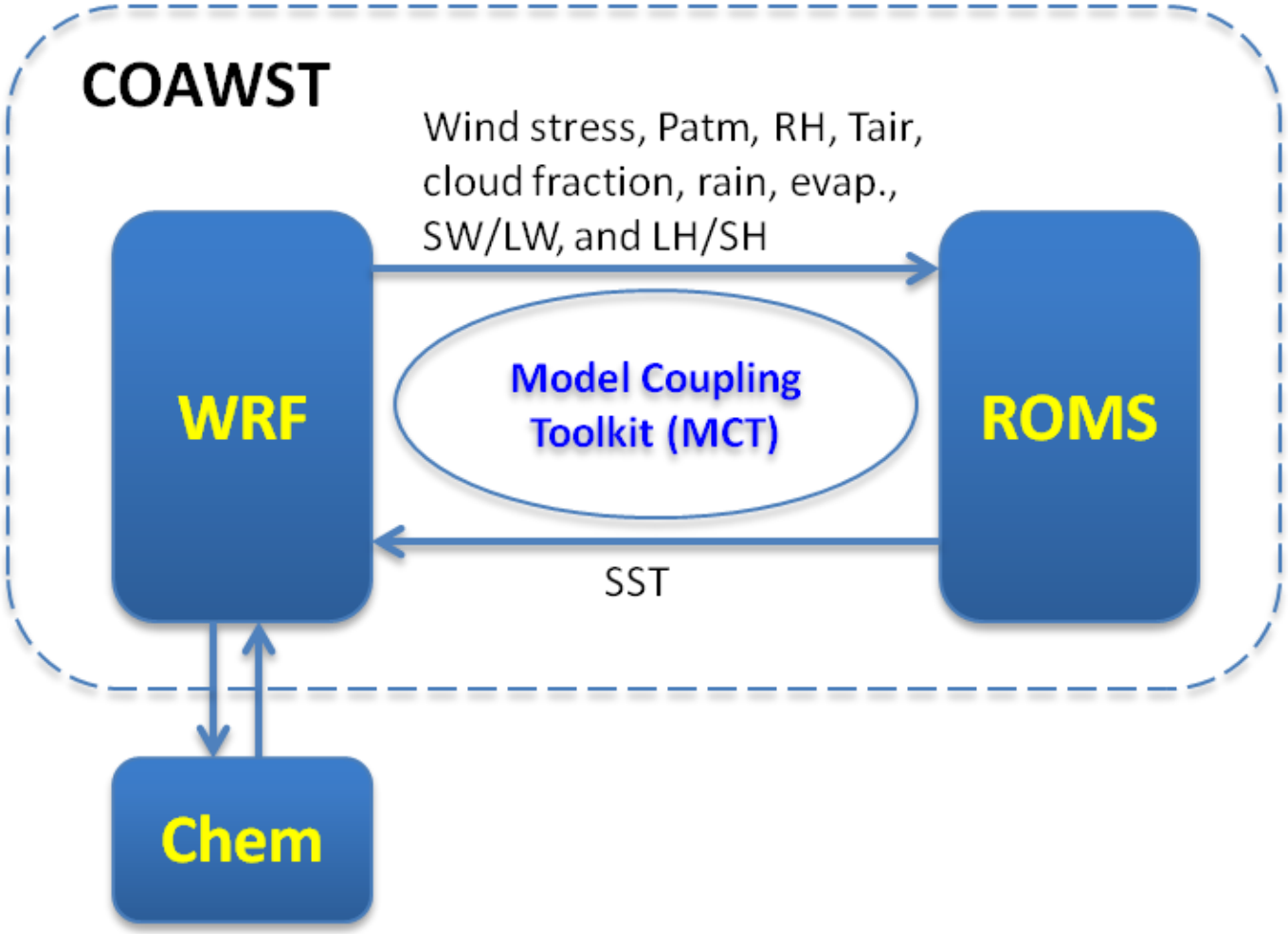

Figure 5.1. Diagram of WRF/Chem-ROMS coupling within COAWST. Patm, atmospheric pressure; RH, relative humidity; Tair, air temperature; evap., evaporation; SW/LW, net shortwave and longwave radiation at surface; LH/SH, latent and sensible heat fluxes at surface; SST, sea surface temperature.

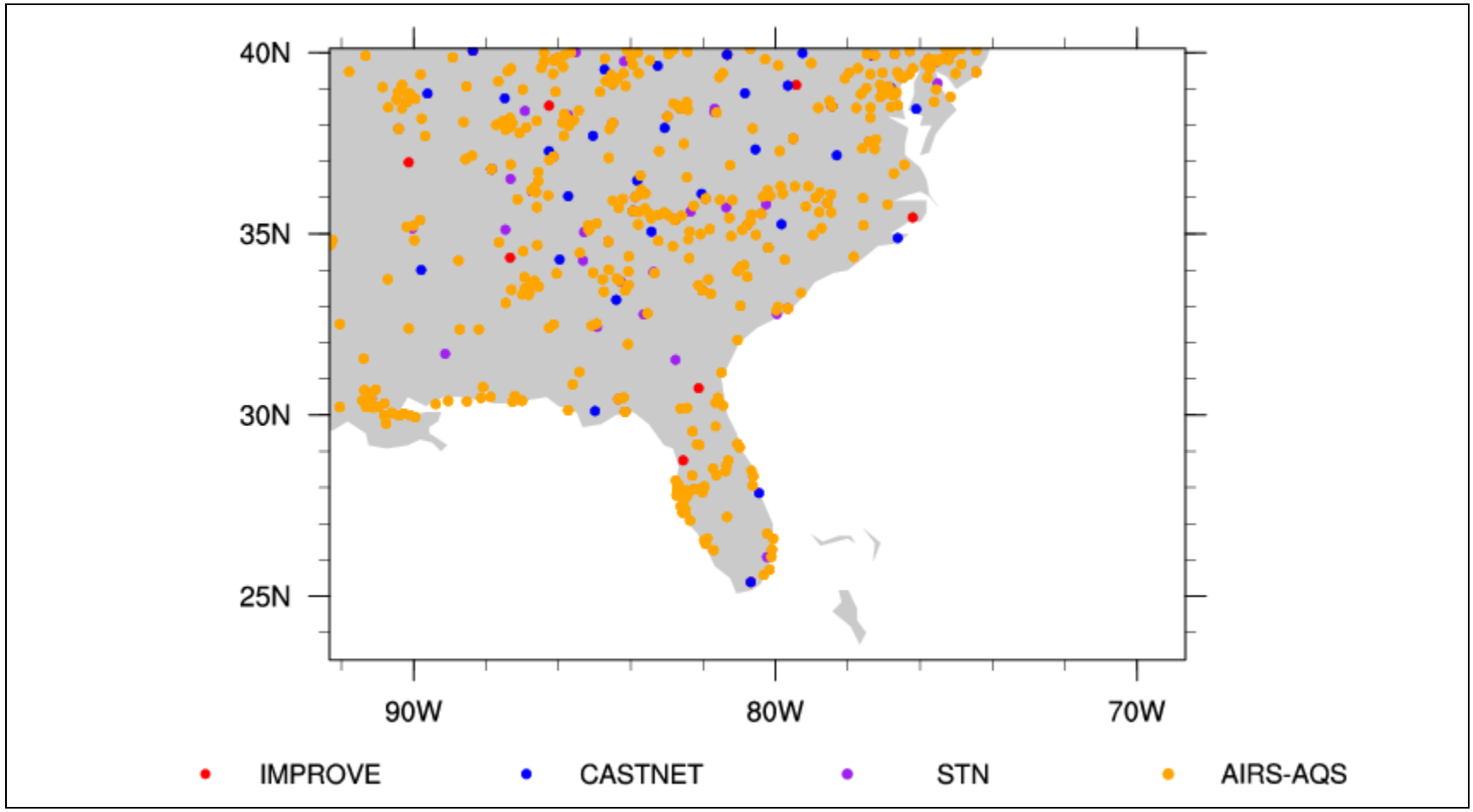

Figure 5.2. Chemical observational sites including IMPROVE, CASTNET, STN, and AIRS-AQS over the study domain.

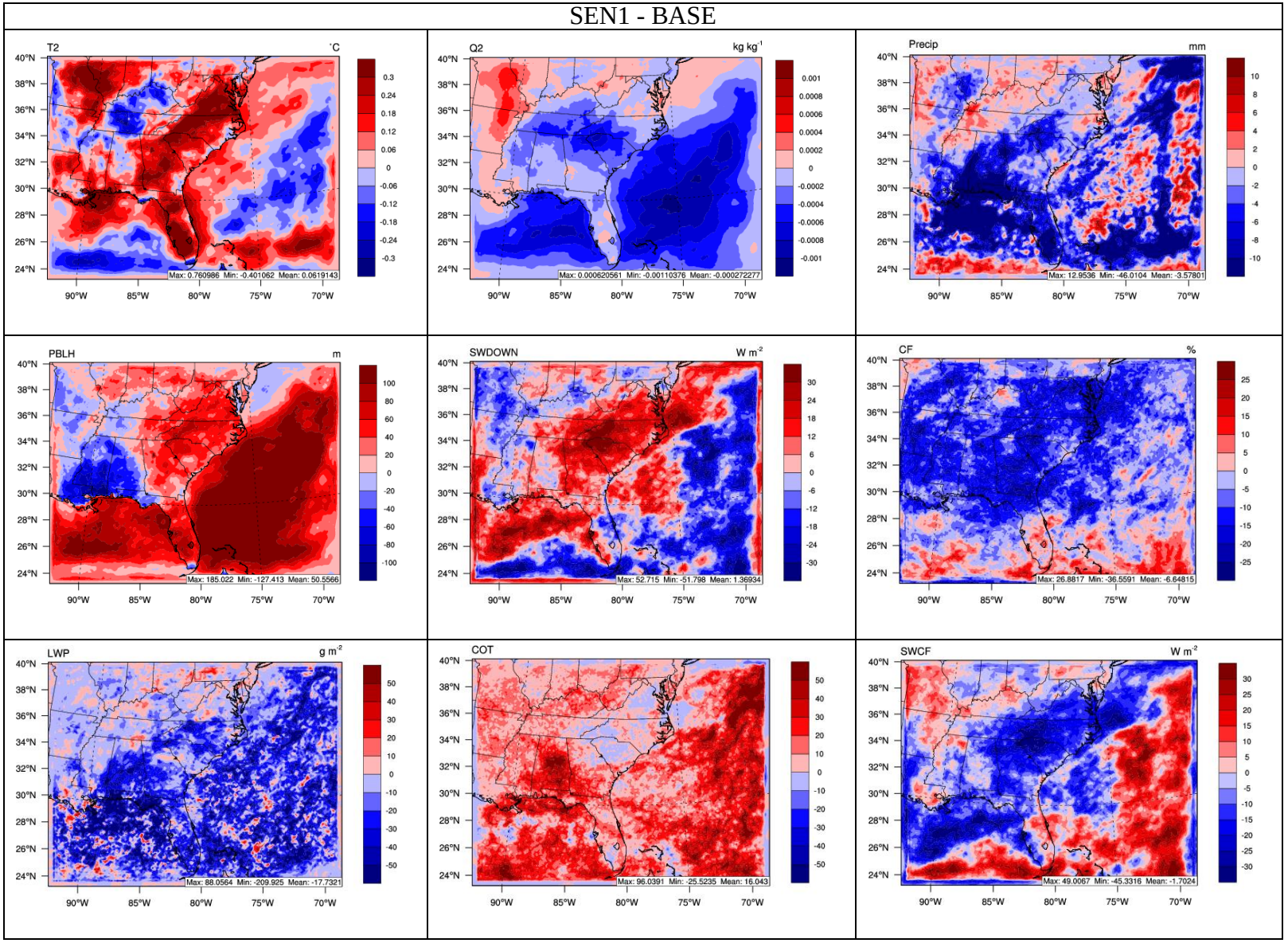

Figure 5.3a. Absolute differences in predictions of major meteorological and cloud/radiative variables between BASE and SEN1.

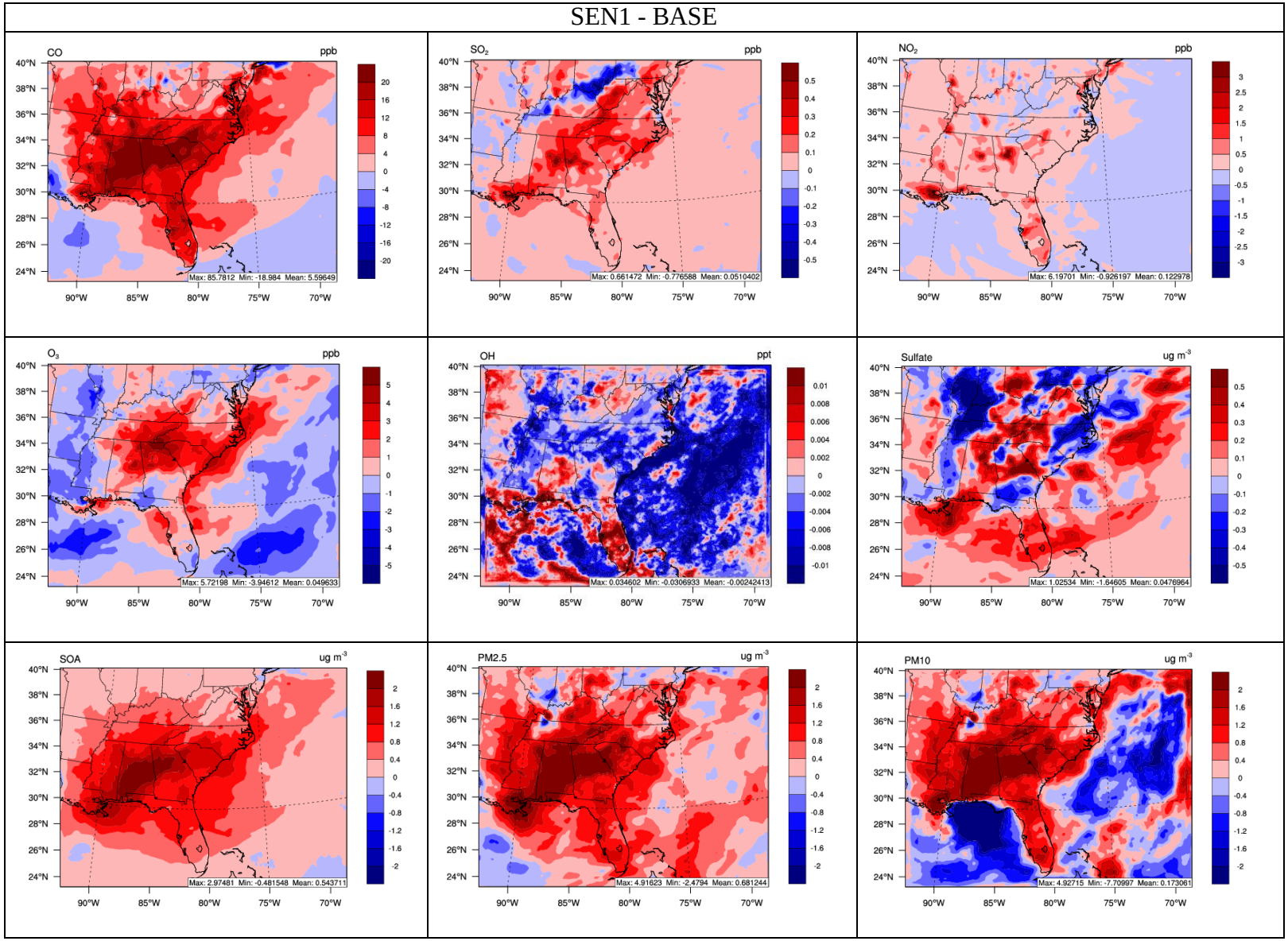

Figure 5.3b. Absolute differences in predictions of surface chemical species between BASE and SEN1.

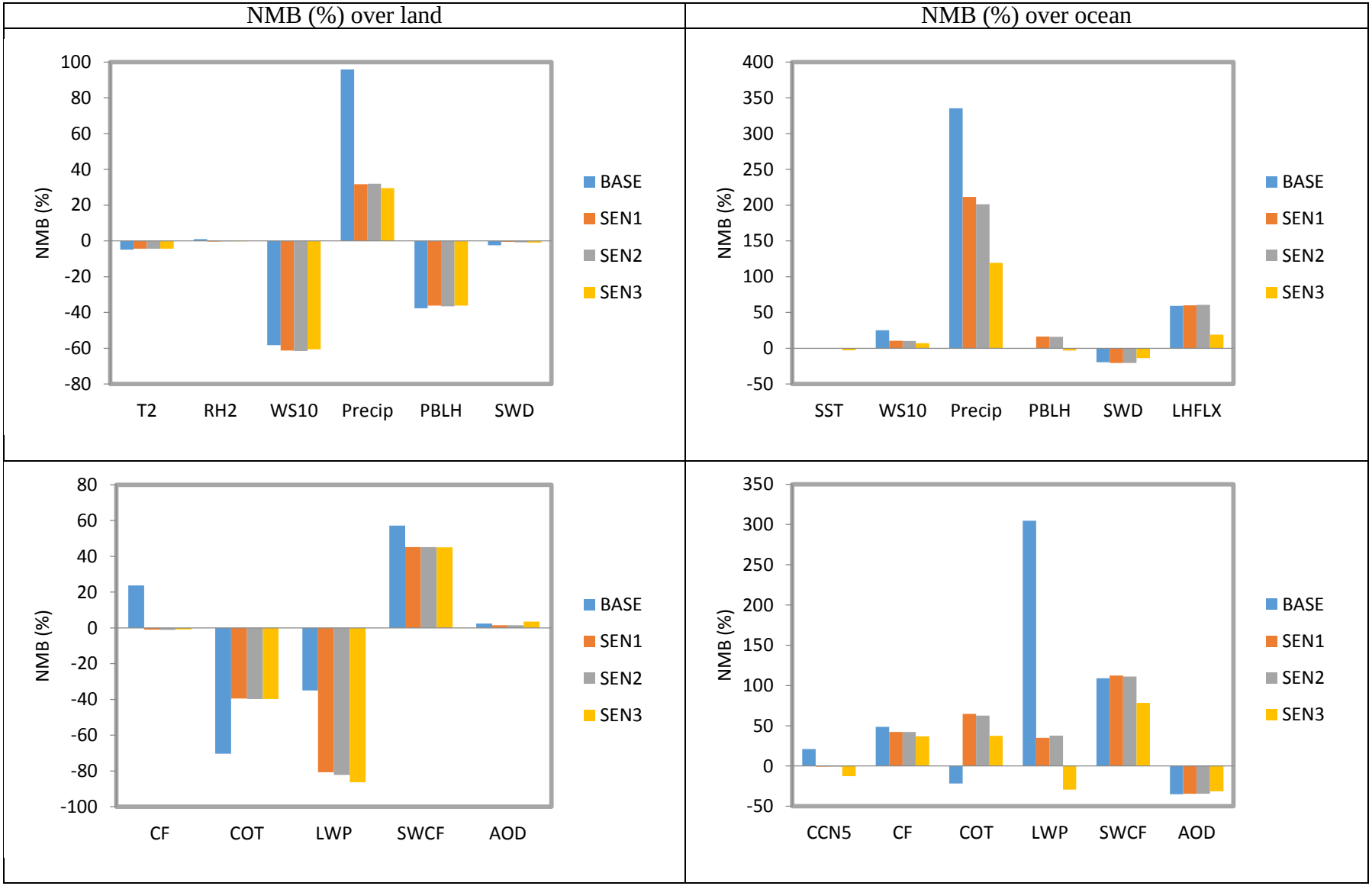

Figure 5.4. Bar plots of normalized mean bias (NMB, %) for major meteorological, and cloud/radiative variables over land and ocean.

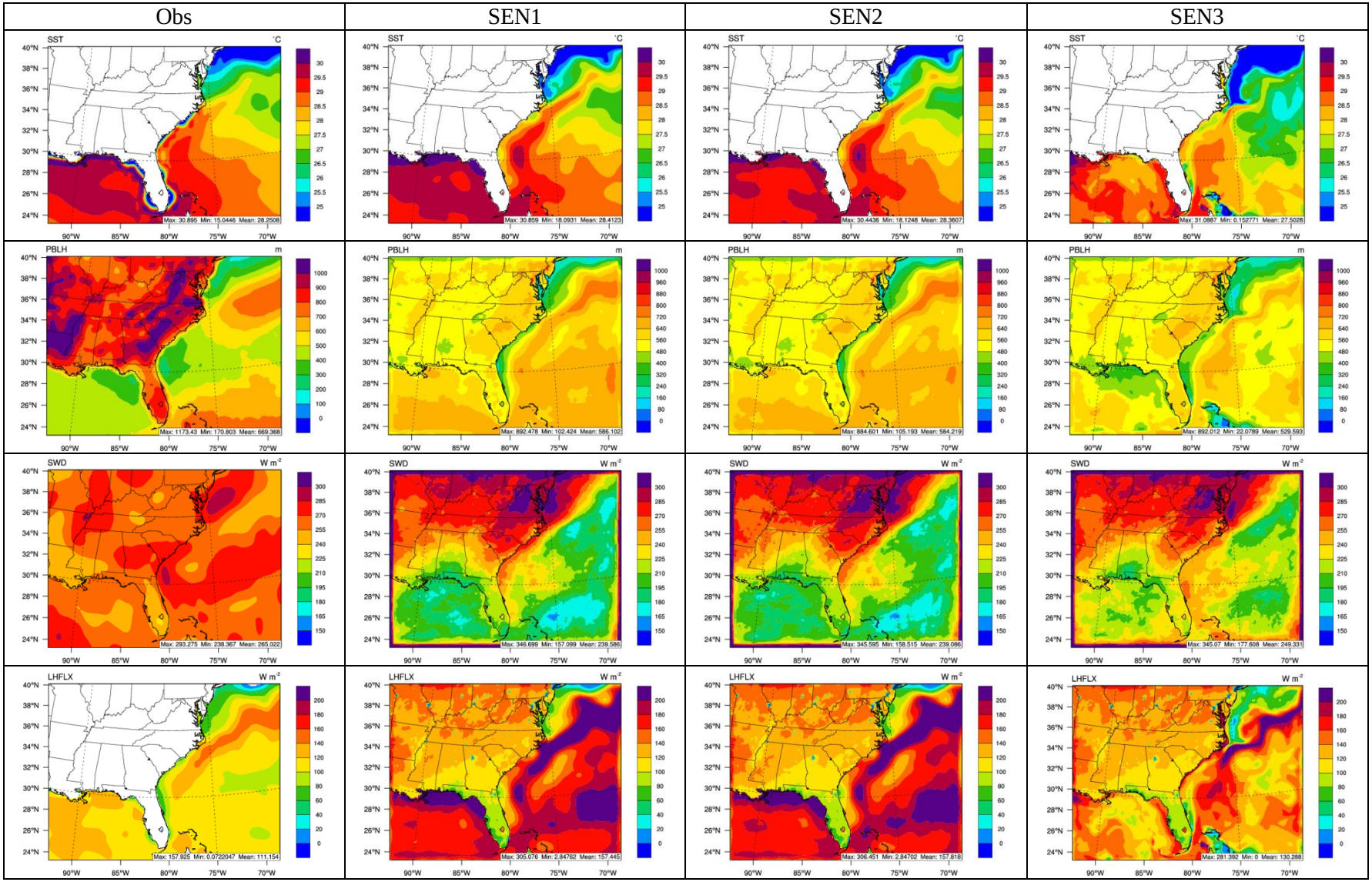

Figure 5.5a. Comparison of satellite observations/reanalysis data with predictions of for SST, PBLH, SWD, and LHFLX by SEN1, SEN2, and SEN3.

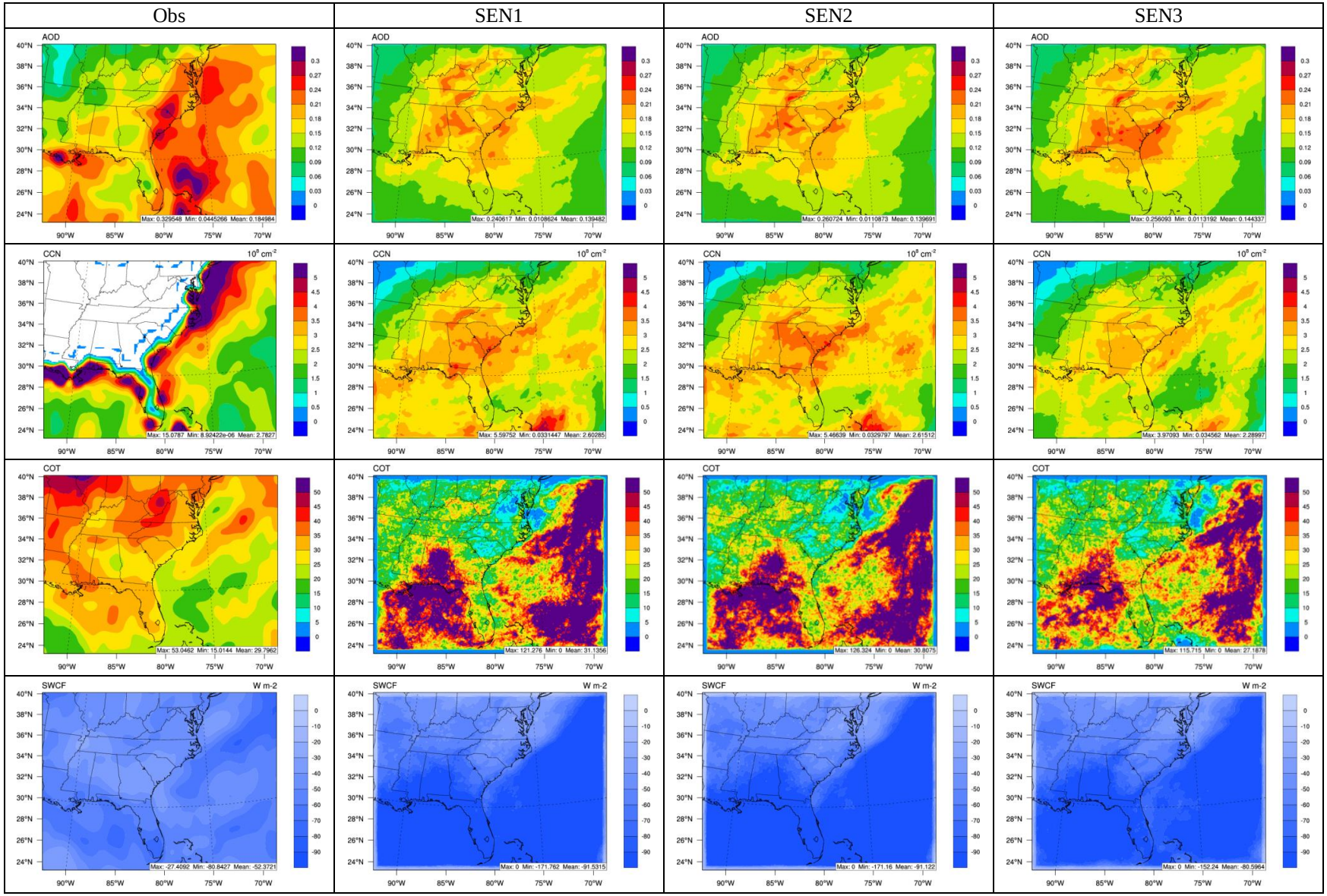

Figure 5.5b. Comparison of satellite observations with predictions of for AOD, CCN5, COT, and SWCF by SEN1 and SEN3.

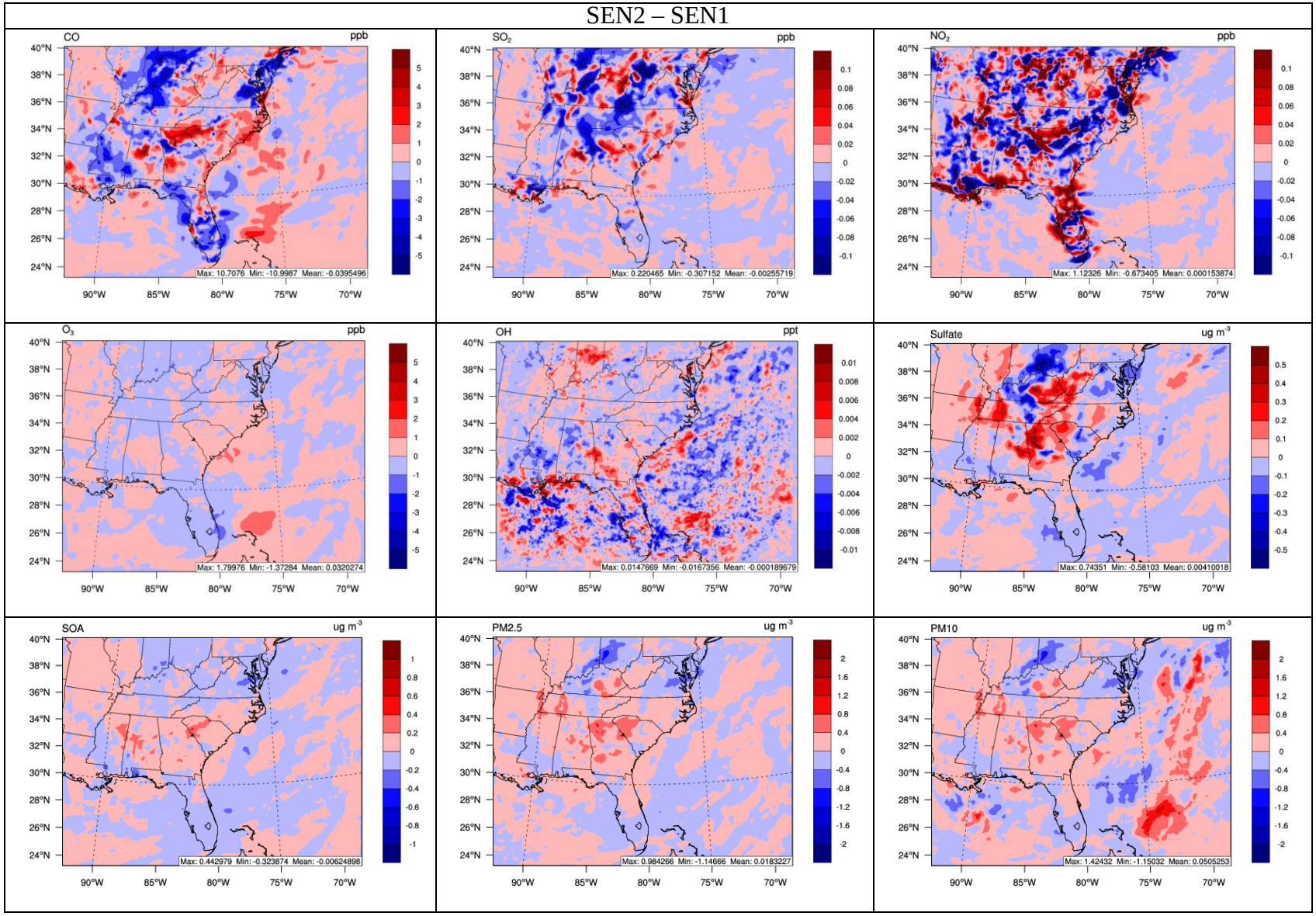

Figure 5.6a. Absolute differences in predictions of surface chemical species between SEN1 and SEN2.

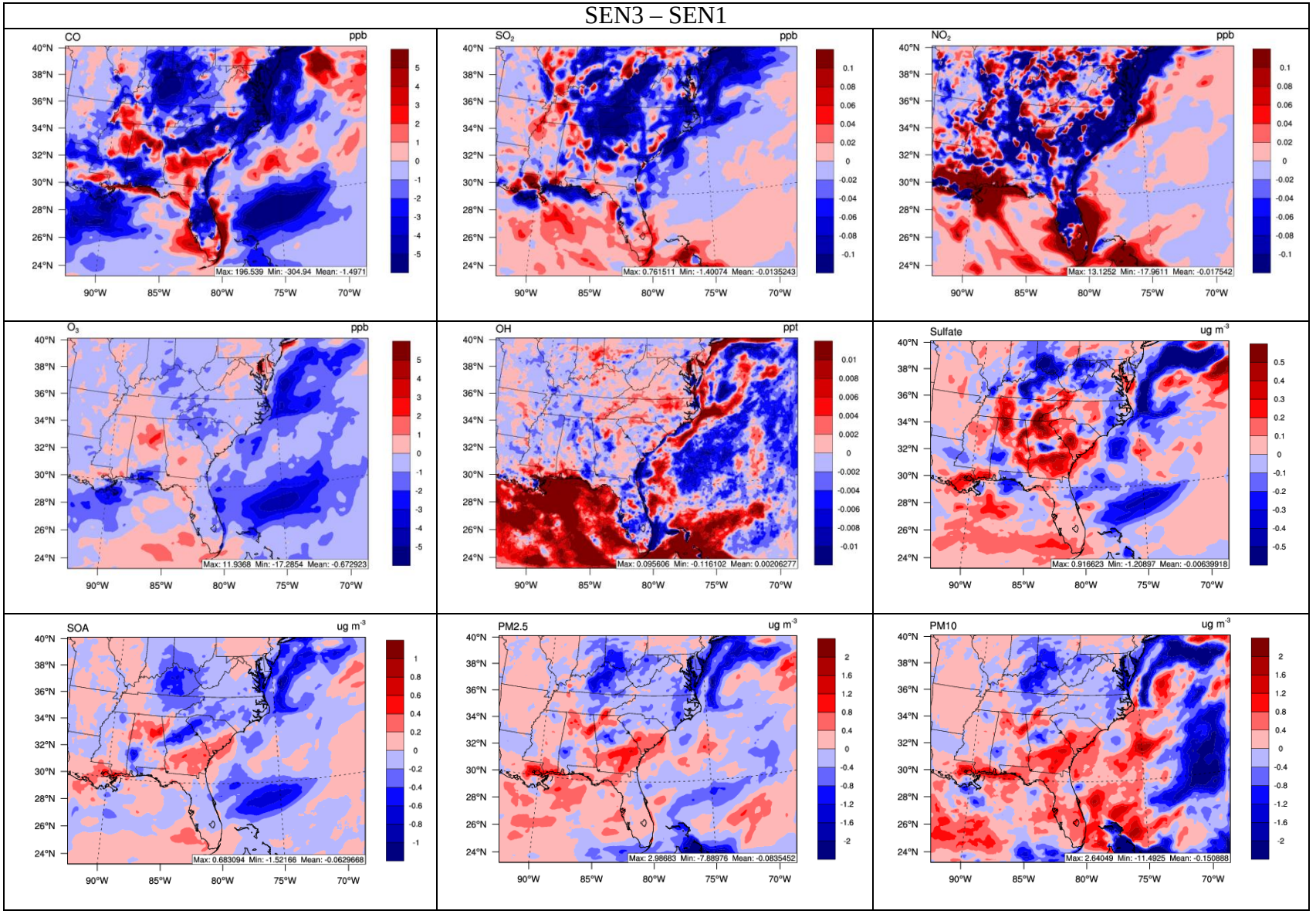

Figure 5.6b. Absolute differences in predictions of surface chemical species between SEN1 and SEN3.

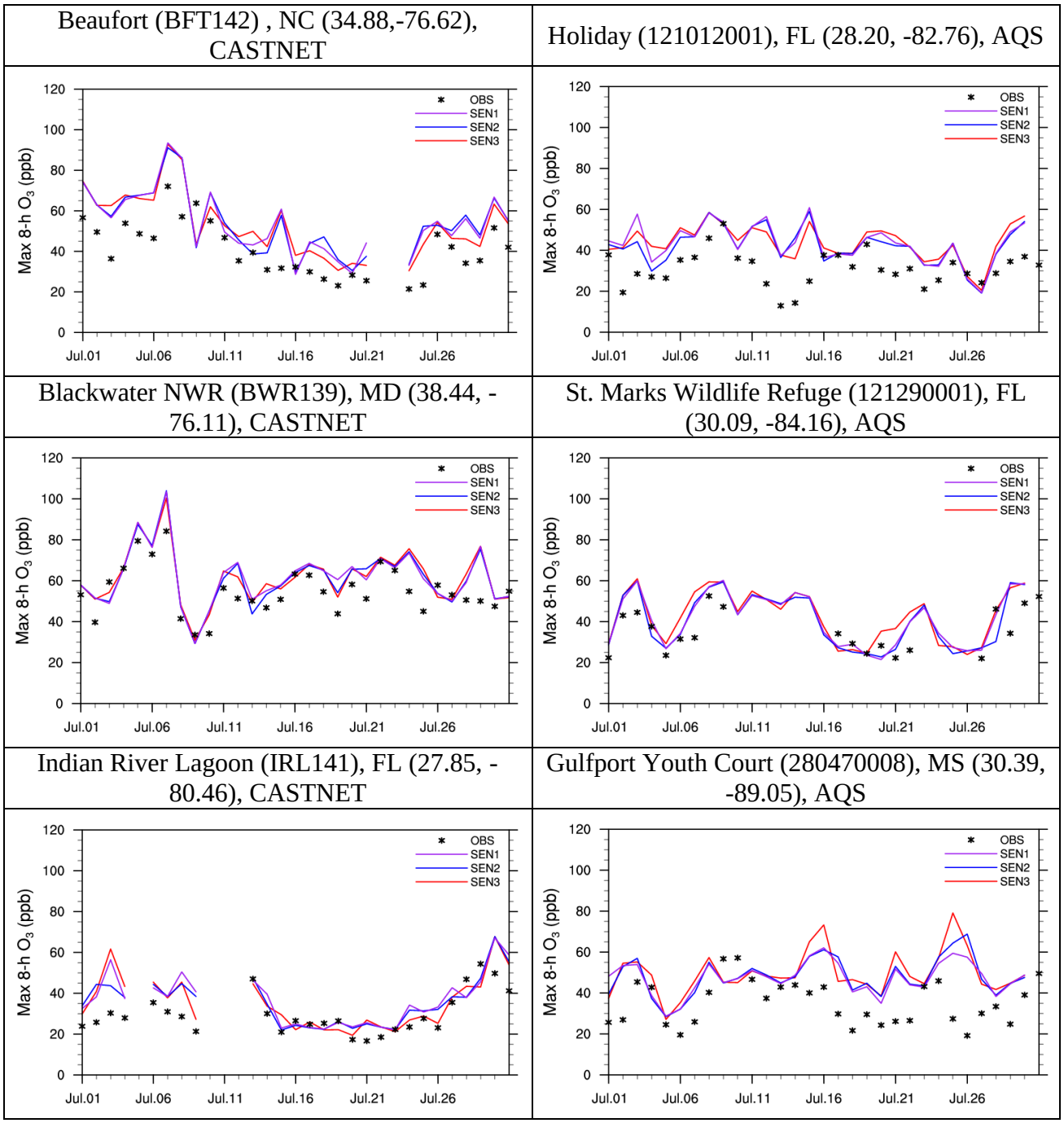

Figure 5.7a. Maximum 8-h ozone at 6 sites, 3 from CASTNET, and 3 from AIRS-AQS. The black markers represent observations. The purple, blue, and red lines represent simulated results from SEN1, SEN2, and SEN3, respectively.

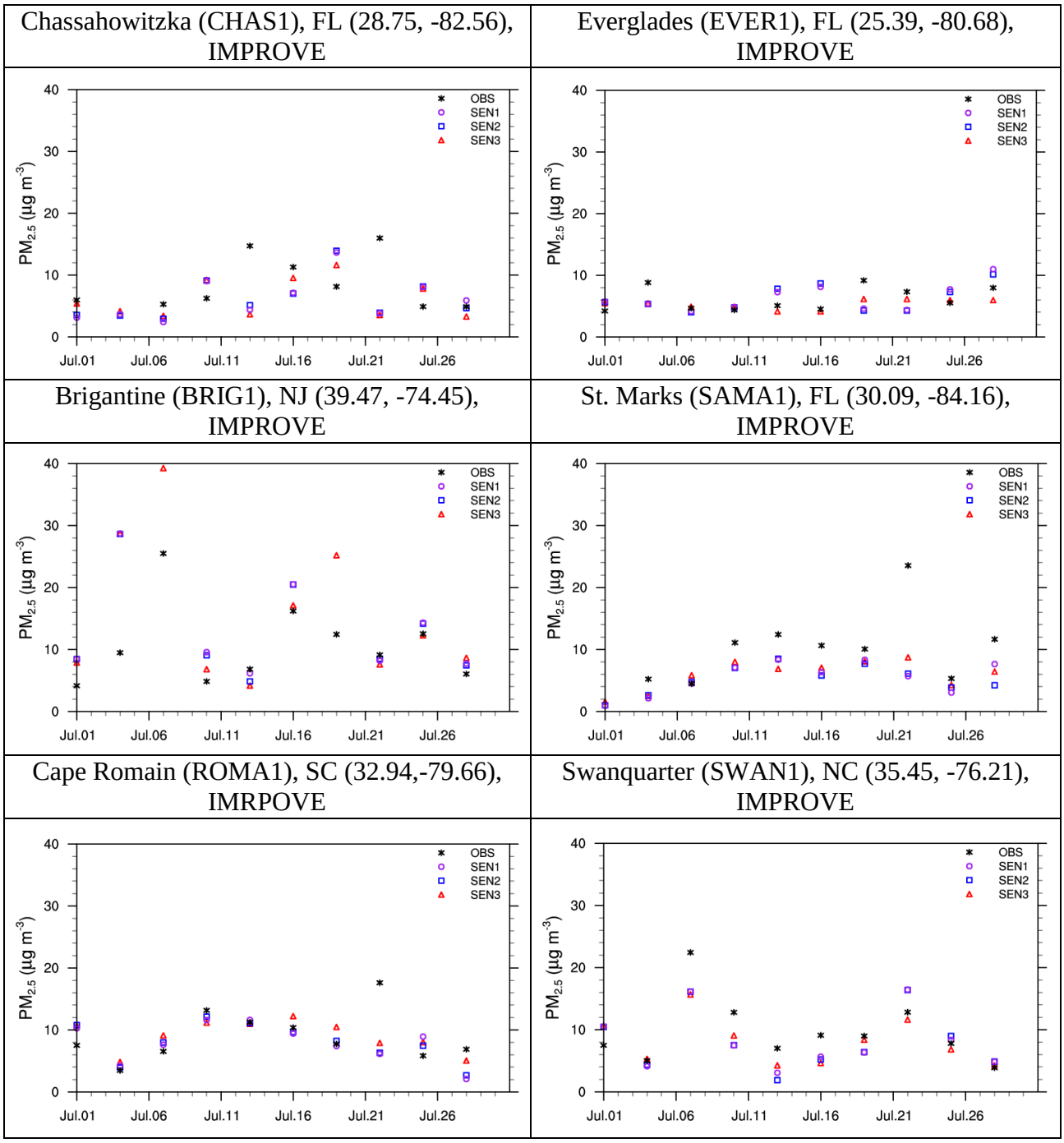

Figure 5.7b. Surface $PM_{2.5}$ concentrations at 6 sites from IMRPOVE. The black markers represent observations. The purple, blue, and red markers represent simulated results from SEN1, SEN2, and SEN3, respectively.

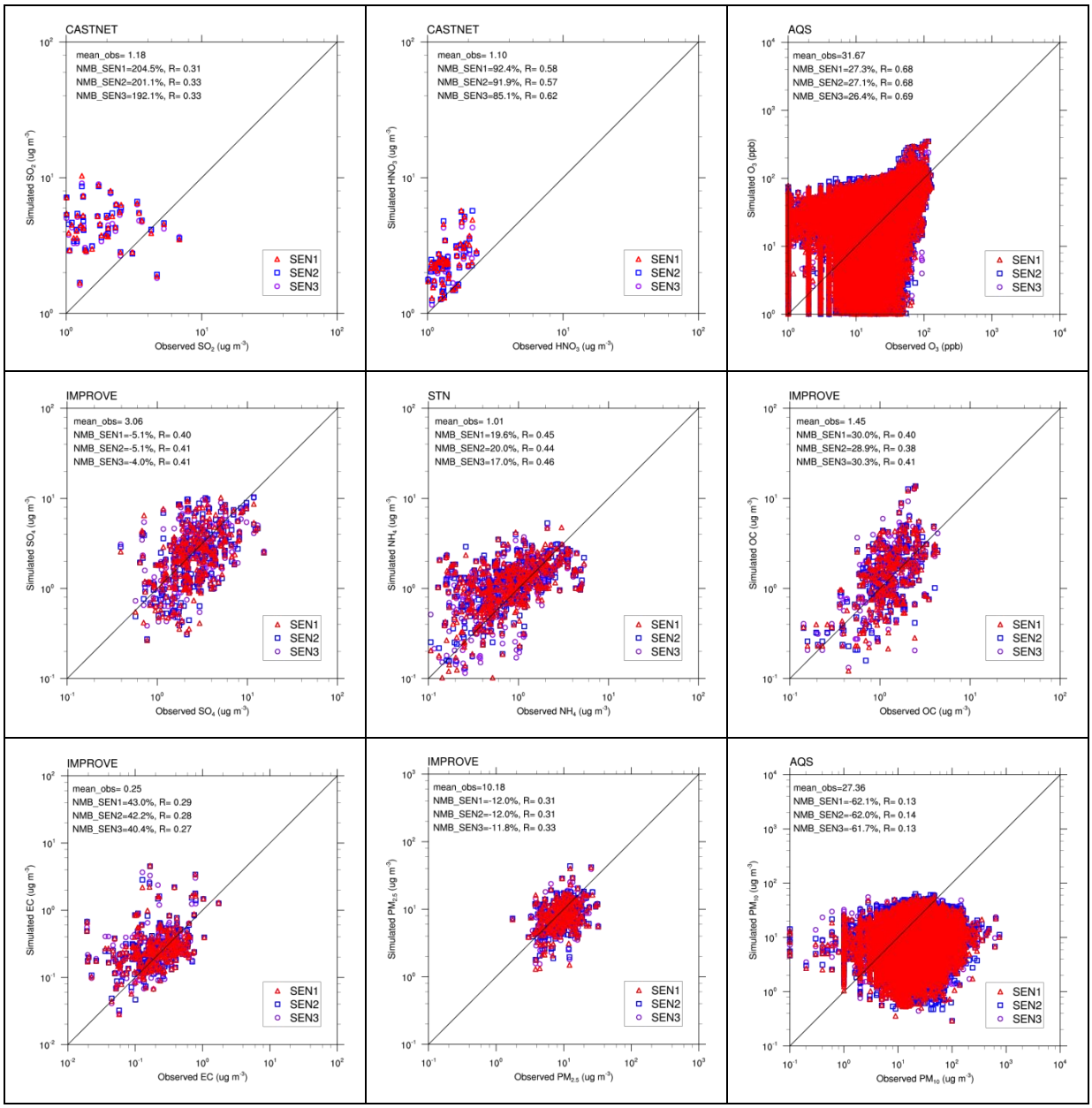

Figure 5.8. Scatter plots of major chemical species over different networks.

CHAPTER 6. CONCLUSIONS

6.1 Conclusions

The uncertainties associated with cloud, aerosol, and their feedbacks, as well as uncertainties in near- and long-term projections from earth system models are emerging issues to be addressed by the scientific community. CESM is a global Earth system model that has been developed to simulate the entire Earth system by coupling physical climate system with chemistry, biogeochemistry, biology, and human systems, and it has been applied to simulate global climate change as part of IPCC-AR5. In this work, to reduce the uncertainties associated with predicted aerosol impacts on climate, several advanced chemistry and aerosol treatments are implemented to CESM/CAM5.

The gas-phase chemistry and subsequent gas-to-particle conversion processes such as new particle formation, condensation, and thermodynamic partitioning have large impacts on air quality, climate, and public health through influencing the amounts and distributions of gaseous precursors and secondary aerosols. Their roles in global air quality and climate are examined in CESM/CAM5. In this work, CESM/CAM5 is first improved and developed through incorporating a new gas-phase chemistry mechanism based on CB05_GE and several advanced inorganic aerosol treatments for condensation of volatile species, ion-mediated nucleation, and explicit inorganic aerosol thermodynamics for sulfate, ammonium, nitrate, sodium, and chloride. Comparing to the simple gas-phase chemistry, CB05_GE can predict many more gaseous species, and thus could improve model performance for $PM_{2.5}$, PM_{10}, PM components, and some PM gaseous precursors such as SO_2 and NH_3 in several regions, as well as AOD and cloud properties (e.g., CF and CDNC), and SWCF on globe.

The modified condensation and aqueous-phase chemistry could further improve the predictions of additional variables such as HNO_3, NO_2, and O_3 in some regions, and new particle formation rate and AOD over globe. IMN can improve the predictions of secondary $PM_{2.5}$ components, $PM_{2.5}$, and PM_{10} over Europe, as well as AOD and CDNC over globe. The explicit inorganic aerosol thermodynamics using ISORROPIA II improves the predictions of all major $PM_{2.5}$ components and their gaseous precursors in some regions, as well as downwelling shortwave radiation, SWCF, and cloud condensation nuclei at a supersaturation of 0.5% over globe. For simulations of 2001-2005 with all the modified and new treatments, the improved model predicts that on a global average, SWCF increases by 2.7 W m^{-2}, reducing NMBs of SWCF from -5.4% to 1.2%. Uncertainties in emissions can explain largely the inaccurate predictions of precursor gases (e.g., SO_2, NH_3, and NO) and primary aerosols (e.g., BC and POM). Additional factors leading to discrepancies between model predictions and observations include assumptions associated with equilibrium partitioning for fine particles assumed in ISORROPIA II, irreversible gas/particle mass transfer treatments for coarse particles, uncertainties in model treatments such as dust emissions, secondary organic aerosol formation, multiple-phase chemistry, cloud microphysics, aerosol-cloud interaction, dry and wet deposition, and model parameters (e.g., accommodation coefficients and prefactors of the nucleation power law), as well as uncertainties in model configurations such as the use of a coarse grid resolution.

The CESM with advanced chemistry and aerosol treatments (referred to as CESM-NCSU) is then applied for decadal (2001-2010) global climate predictions. A comprehensive evaluation is performed focusing on the CAM5 by comparing simulation results with

observations/reanalysis data and CESM ensemble simulations from CMIP5. The improved model can predict most meteorological and radiative variables relatively well with NMBs of -14.1% to -9.7% and 0.7% to 10.8%, respectively, although T2 is slightly underpredicted. Cloud variables such as CF and PWV are well predicted, with NMBs of -10.5% to 0.4%, whereas CCN, LWP, and COT are moderately-to-largely underpredicted, with NMBs of -82.2% to -31.2%, and CDNC is overpredicted by 26.7%. These biases indicate the limitations and uncertainties associated with cloud dynamics and thermodynamics (e.g., resolved clouds and subgrid-scale cumulus clouds). Chemical concentrations over the continental CONUS (e.g., SO_4^{2-}, Cl^-, OC, and $PM_{2.5}$) are reasonably well predicted with NMBs of -12.8% to -1.18%. Concentrations of SO_2, SO_4^{2-}, and PM_{10} are also reasonably well predicted over Europe with NMBs of -20.8% to -5.2%, so are predictions of SO_2 concentrations over the East Asia with an NMB of -18.2%, and TOR over the globe with an NMB of -3.5%. Most meteorological and radiative variables predicted by CESM-NCSU agree well overall with those predicted by CESM-CMIP5. The performance of LWP and AOD predicted by CESM-NCSU is better than that of CESM-CMIP5 in terms of model bias and correlation coefficients. Large biases for some chemical predictions can be attributed to uncertainties in the emissions of precursor gases (e.g., SO_2, NH_3, and NO_x) and primary aerosols (e.g., BC and POM) as well as uncertainties in formulations of some model components (e.g., online dust and sea-salt emissions, secondary organic aerosol formation, and cloud dynamics). Comparisons of CESM simulation with baseline emissions and 20% of anthropogenic emissions from the baseline emissions indicate that anthropogenic gas and aerosol species

can decrease FSDS by 4.7 W m^{-2} (or by 2.9%) and increase SWCF by 3.2 W m^{-2} (or by 3.1%) in the global mean.

Atmospheric chemistry plays a key role in determining the amounts and distributions of oxidants and gaseous precursors that control the formation of secondary gaseous and aerosol pollutants; all of those species can interact with the climate system. To understand the impacts of different gas-phase mechanisms on global air quality and climate predictions, a comprehensive comparative evaluation is performed in CESM/CAM5-chem with two most commonly-used gas-phase chemical mechanisms: CB05_GE and MOZART-4x. MOZART-4x and CB05_GE use different approaches to represent VOCs and different surrogates for SOA precursors. MOZART-4x includes a more detailed representation of isoprene chemistry compared to CB05_GE. CB05_GE includes additional oxidation of SO_2 by O_3 over the surface of dust particles, which is not included in MOZART-4x. The results show that the two CAM5-chem simulations with CB05_GE and MOZART-4x predict similar chemical profiles for major gases (e.g., O_3, CO, and NO_x) compared to the aircraft measurements, with generally better agreement for NO_y profile by CB05_GE than MOZART-4x. The concentrations of SOA at four sites in CONUS and OC over the IMPROVE sites are well predicted by MOZART-4x (with NMBs of -1.9% and 2.1%, respectively) but moderately underpredicted by CB05_GE (with NMBs of -23.1% and -20.7%, respectively). This is mainly due to the higher biogenic emissions and OH levels simulated with MOZART-4x than with CB05_GE. The concentrations of OC over Europe are largely underpredicted by both MOZART-4x and CB05_GE, with NMBs of -73.0% and -75.1%, respectively, indicating the uncertainties in the emissions of precursors and primary OC and relevant

model treatments such as the oxidations of VOCs and SOA formation. Uncertainties in the emissions and convection scheme can contribute to the large bias in the model predictions (e.g., SO_2, CO, BC, and AOD). The two simulations also have similar cloud/radiative predictions, with slightly better performance of domain averaged CCN5 by CB05_GE, but slightly better agreement with observed CCN (at supersaturation of 0.2%) profile over Beijing by MOZART-4x. The CESM simulations with two gas-phase mechanisms result in a global average difference of 0.5 W m^{-2} in simulated SWCF, with significant differences (e.g., up to 13.6 W m^{-2}) over subtropical regions.

Finally, as a first step towards a goal of developing a regional Earth System Model, WRF/Chem is coupled with ROMS within COAWST framework to understand the impacts of air-sea interactions on coastal air quality predictions. Sensitivity simulations with different cumulus parameterization schemes and ocean treatments are conducted over southeastern U.S. for July 2010 using WRF/Chem. The results show that two cumulus parameterization schemes can result in an 85-m difference in the domain averaged PBLH, and 4.8-mm for daily precipitation. With 1-D OML treatment in WRF/Chem and 3-D ROMS coupling with WRF/Chem, the changes in the SST are 0.1 ^oC and 1.0 ^oC, respectively, and the differences in surface O_3 and $PM_{2.5}$ can be as large as 17.3 ppb and 7.9 μg m^{-3}, respectively. The largest changes in surface O_3 and $PM_{2.5}$ occur not only along coast and remote ocean, but also over inland area, indicating the significant impacts of air-sea interactions on chemical predictions. With coupling of 3-D ROMS, WRF/Chem-ROMS predictions of most cloud and radiative variables are improved, especially over ocean. WRF/Chem-ROMS predictions of surface

chemical species such as SO_2, HNO_3, Max 1-h and 8-h O_3, SO_4^{2-}, NH_4^+, NO_3^-, and PM_{10} are also improved.

In conclusion, more comprehensive gas-phase mechanism can affect secondary gases and aerosol predictions and affect climate through chemistry feedbacks to climate system, demonstrating the importance of simulating chemistry-climate interactions in global Earth system models. The comparisons of CB05_GE and MOZART-4x indicate the impacts of different gas-phase mechanisms on SOA and climate predictions. IMN can increases nucleation rate and aerosol number concentrations in the upper troposphere and stratosphere and therefore improve the predictions of clouds, demonstrating ions are major sources for new particle formation in the upper layer. ISORROPIA II can improve the predictions of major inorganic gases and aerosols, demonstrating the importance of simulating gas-particle partitioning in the model. The coupling of WRF/Chem with ROMS demonstrate the importance of air-sea interaction treatments on regional air quality predictions. The comprehensive evaluation in this work indicate the benefits from new model treatments for climate and air quality predictions in global and regional scales and also identify the model uncertainties in the model treatments which can be reduced in the future.

6.2 Limitations and Future Work

This work demonstrates the capability of improved CESM/CAM5 in representing interactions among atmospheric chemistry, aerosols, cloud, and climate by implementing new gas-phase mechanisms and advanced aerosol treatments for aerosol nucleation and aerosol thermodynamics. Comprehensive evaluations are conducted in this work and reveal several model uncertainties that need to be addressed to further improve CESM/CAM5's

skills in represent present atmosphere. The model biases associated with uncertainties in gas-phase mechanisms, aerosol chemical/physical treatments, cloud dynamics and thermodynamics, and emission inventories are identified. The sensitivity simulations with different gas-phase mechanisms, aerosol treatments, and emissions indicate the significant impacts of these treatments/inputs on model predictions.

Other limitations of this work lie in the model treatments for atmospheric chemistry and aerosol. For example, uncertainties in the HO_x recycling associated with isoprene chemistry in CB05_GE can result in uncertainties in predicting SOA concentrations. Uncertainties in the glyoxal mechanism can also contribute to the uncertainties in predicting SOA concentrations. These uncertainties in the gas-phase chemical mechanism can be reduced in the future. Aerosol thermodynamics involving coarse particles (in coarse sea-salt and dust modes) is currently not treated explicitly in this work, given the high computational cost (by at least a factor of 3) for solving the non-equilibrium system involving coarse particles. Instead, the simple kinetic approach used in the default CAM5 is used to simulate the condensation of inorganic gases onto coarse modes. An explicit treatment for coarse particles thermodynamics can be implemented in the future. Aqueous phase oxidation of VOCs in cloud is not currently treated in the model, which could partly explain the underpredictions of OC over Europe. This missing pathway can be implemented in the future to accounts for the SOA formation in aqueous phase chemistry.

This work also demonstrates the significant impacts of air-sea interactions on regional air quality predictions by conducting WRF/Chem simulations with different ocean treatments (i.e., 1-D OML and 3-D ROMS). Comprehensive evaluations are conducted in this work and

reveal several model uncertainties associated with initial conditions for ROMS and relatively coarse vertical resolution for ocean layers, which can partly explain the underpredictions of SST in WRF/Chem-ROMS. Sensitivity simulations with improved initial conditions for ROMS and increase of vertical resolution for ROMS can be conducted in the future to estimate the impacts from model input and model setup, which can provide insights to further reduce model uncertainties in the future.

To take advantage of existing coupling system of COAWST, the coupling of WRF/Chem with ROMS can extend to interact with wave model to enable the impacts from wave breaking, which can affect sea-salt emissions and aerosol concentrations over remote ocean. In current WRF/Chem-ROMS coupling, there are no directly exchanged fields between atmospheric chemistry and ocean model, which could be improved in the future. For example, atmospheric chemistry and marine chemistry can be linked together to address inaccurate predictions of O_3 over ocean. Marine chemistry can not only impact the chemical predictions in ocean but also impact marine ecosystem. Biogeochemical cycle can also be linked among land, atmosphere, and ocean to enable the interactions among these components in regional scales. These linkages can be built in the future to develop a fully coupled regional Earth system model and thus can be applied for regional climate simulations. If there are enough computational resources, the model can be applied for finer grid resolution to resolve fine scale processes such as convective clouds and coastal processes.

Although the comprehensive evaluation are conducted in this work to provide insights into the model uncertainties associated with the model treatments, the quantifications

of model uncertainties are not included in this work, which could be included in the future. Ensemble simulation is a useful method to quantify uncertainty and variability. Perturbed-Parameter Ensembles (PPE) can be applied to assess climate uncertainty using same climate model but different combinations of several key input parameters (Murphy et al., 2004; Jackson et al., 2008; Collins et al., 2011b). Statistical techniques (e.g. probability distribution functions) can then be applied to PPE to make uncertainty and variability in quantitative form. At this point, due to the limited computational sources and time, this work focuses more on the sensitivity studies to identify key controlling parameters (e.g., sensitivity ranking), model improvement (e.g., to develop more accurate and representative treatments or parameterizations), and model evaluation against observations than applying statistical techniques to quantify uncertainty. However, this method could be included in the future to quantify model uncertainty.

REFERENCES

Abdul-Razzak, H. and Ghan, S. J.: A parameterization of aerosol activation, Part 2: Multiple aerosol types, J. Geophys. Res., 105, 6837-6844, 2000.

Adams, P. J. and Seinfeld, J. H.: Predicting global aerosol size distributions in general circulation models, J. Geophys. Res., 107(D19), 4370, doi:10.1029/2001JD001010, 2002.

Aghedo, A. M., Bowman, K. W., Worden, H. M., Kulawik, S. S., Shindell, D. T., Lamarque, J.-F., Faluvegi, G., Parrington, M., Jones, D. B. A., and Rast, S.: The vertical distribution of ozone instantaneous radiative forcing from satellite and chemistry climate models, J. Geophys. Res., 116, D01305, doi:10.1029/2010JD014243, 2011.

Ahmadov, R., McKeen, S., Robinson, A., Bahreini, R., Middlebrook, A., de Gouw, J., Meagher, J., Hsie, E., Edgerton, E., Shaw, S., and Trainer, M.: A volatility basis set model for summertime secondary organic aerosols over the eastern United States in 2006, J. Geophys. Res., 117, D06301, doi:10.1029/2011JD016831, 2012.

Andreae, M. O.: A new look at aging aerosols, Science, 326, 1493-1494, doi: 10.1126/science.1183158, 2009.

Appel, K. W., Pouliot, G. A., Simon, H., Sarwar, G., Pye, H. O. T., Napelenok, S. L., Akhtar, F., and Roselle, S. J.: Evaluation of dust and trace metal estimates from the Community Multiscale Air Quality (CMAQ) model version 5.0, Geosci. Model Dev., 6, 883-899, 2013.

Arstila, H., Korhonen, P., and Kulmala, M.: Ternary nucleation: Kinetics and application to water-ammonia-hydrochloric acid system, J. Aerosol Sci., 30, 131-138, doi:10.1016/S0021-8502(98)00033-0, 1999.

Barahona, D. and Nenes, A.: Parameterization of cloud droplet formation in large-scale models: Including effects of entrainment, J. Geophys. Res., 112, D16206, doi:10.1029/2007JD008473, 2007.

Barahona, D., West, R. E. L., Stier, P., Romakkaniemi, S., Kokkola, H., and Nenes, A.: Comprehensively accounting for the effect of giant CCN in cloud activation parameterizations, Atmos. Chem. Phys., 10(5), 2467-2473, doi:10.5194/acp-10-2467-2010, 2010.

Barth, M. C., Rasch, P. J., Kiehl, J. T., Benkovitz, C. M., and Schwartz, S. E.: Sulfur chemistry in the National Center for Atmospheric Research Community Climate Model: Description, evaluation, features and sensitivity to aqueous chemistry, J. Geophys. Res., 105, 1387-1415, 2000.

Bellouin, N., Rae, J., Jones, A., Johnson, C., Haywood, J., and Boucher, O.: Aerosol forcing in the Climate Model Intercomparison Project (CMIP5) simulations by HadGEM2-ES and the role of ammonium nitrate, J. Geophys. Res., 116, D20206, doi:10.1029/2011JD016074, 2011.

Berndt, T., Sipilä, M., Stratmann, F., Petäjä, T., Vanhanen, J., Mikkilä, J., Patokoski, J., Taipale, R., Lee Mauldin III, R., and Kulmala, M.: Enhancement of atmospheric H2SO4/H2O nucleation: organic oxidation products versus amines, Atmos. Chem. Phys., 14, 751-764, 2014.

Bennartz, R.: Global assessment of marine boundary layer cloud droplet number concentration from satellite, J. Geophys. Res., 112, D02201, doi: 10.1029/2006JD007547, 2007.

Bey, I., Jacob, D. J., Yantosca, R. M., Logan, J. A., Field, B. D., Fiore, A. M., Li, Q., Lui, H. Y., Mickley, L. J., and Schultz, M. G.: Global modeling of tropospheric chemistry with assimilated meteorology: Model description and evaluation, J. Geophys. Res., 106(D19), 23073-23095, 2001.

Binkowski, F. S. and Roselle, S. J.: Models-3 Community multiscale air quality (CMAQ) model aerosol component, 1 Model description, J. Geophys. Res., 108(D6) 4183, doi:10.1029/2001JD001409, 2003.

Bond, T. C., Bhardwaj, E., Dong, R., Jogani, R., Jung, S., Roden, C., Streets, D. G., and Trautmann, N. M.: Historical emissions of black and organic carbon aerosol from energy-

related combustion, 1850-2000, Global Biogeochem. Cy., 21, GB2018, doi:10.1029/2006GB002840, 2007.

Bretherton, C. S. and Park, S.: A new moist turbulence parameterization in the community atmosphere model, J. Climate, 22, 3422-3448, 2009.

Brock, C. A., Cozic, J., Bahreini, R., Froyd, K. D., Middlebrook, A. M., McComiskey, A., Brioude, J., Cooper, O. R., Stohl, A., Aikin, K. C., de Gouw, J. A., Fahey, D. W., Ferrare, R. A., Gao, R.-S., Gore, W., Holloway, J. S., Hübler, G., Jefferson, A., Lack, D. A., Lance, S., Moore, R. H., Murpphy, D. M., Nenes, A., Novelli, P. C., Nowak, J. B., Ogren, J. A., Peischl, J., Pierce, R. B., Pilewskie, P., Quinn, P. K., Ryerson, T. B., Schmidt, K. S., Schwarz, J. P., Sodemann, H., Spackman, J. R., Stark, H., Thomson, D. S., Thornberry, T., Veres, P., Watts, L. A., Warneke, C., and Wollny, A. G.: Characteristics, sources, and transport of aerosols measured in spring 2008 during the aerosol, radiation, and cloud processes affecting Arctic Climate (ARCPAC) Project, Atmos. Chem. Phys., 11, 2423-2453, doi:10.5194/acp-11-2423-2011, 2011.

Byun, D. W. and Schere, K. L.: Review of the governing equations, computational algorithms, and other components of the Models-3 Community Multiscale Air Quality (CMAQ) Modeling System, Appl. Mech. Rev., 59, 51-77, 2006.

Capaldo, K. P., C. Pilinis, and S. N. Pandis: A computationally efficient hybrid approach for dynamic gas/aerosol transfer in air quality models, Atmos. Environ., 34, 3617-3627, 2000.

Cappa, C. D. and Jimenez, J. L.: Quantitative estimates of the volatility of ambient organic aerosol, Atmos. Chem. Phys., 10, 5409-5424, doi:10.5194/acp-10-5409-2010, 2010.

Chan, A. W. H., Kautzman, K. E., Chhabra, P. S., Surratt, J. D., Chan, M. N., Crounse, J. D., Kürten, A., Wennberg, P. O., Flagan, R. C., and Seinfeld, J. H.: Secondary organic aerosol formation from photooxidation of naphthalene and alkylnaphthalens: implications for oxidation of intermediate volatility organic compounds (IVOCs), Atmos. Chem. Phys., 9, 3049-3060, 2009.

Chuang, P. Y.: Measurement of the timescale of hygroscopic growth for atmospheric aerosols, J.Geophys. Res., 108(D9), 4282., doi: 10.1029/2002JD002757, 2003.

Collins, W. D., Bitz, C. M., Blackmon, M. L., Bonan, G. B., Bretherton, C. S., Carton, J. A., Chang, P., Doney, S. C., Hack, J. J., Henderson, T. B., Kiehl, J. T., Large, W. G., McKenna, D. S., Santer, B. D., and Smith, R. D.: The Community Climate System Model version3 (CCSM3), J. Clim., 19, 2122-2143, doi:10.1175/JCLI3761.1, 2006.

Collins, W. J., Bellouin, N., Doutriauz-Boucher, M., Gedney, N., Halloran, P., Hinton, T., Hughes, J., Jones, C. D., Joshi, M., Liddicoat, S., Martin, G., O'Connor, F., Rae, J., Senior, C., Sitch, S., Totterdell, I., Wiltshire, A., and Woodward, S.: Development and evaluation of an Earth-System model – HadGEM2, Geosci. Model Dev., 4, 1-51-1075, 2011a.

Collins, M., Booth, B. B. B., Bhaskaran, B., Harris, G. R., Murphy, J. M., Sexton, D. M. H., and Webb, M. J.: Climate model errors, feedbacks and forcings: a comparison of perturbed physics and multi-model ensembles, Climate Dyn., 36, 1737-1766, doi:10.1007/s00382-010-0808-0, 2011b.

Collins, W. D., Rasch, P. J., Boville, B. A., Hack, J. J., McCaa, J. R., Williamson, D. L., Kiehl, J. T., Briegleb, B., Bitz, C., Lin, S. J., Zhang, M., and Dai, Y.: Description of the NCAR Community Atmosphere Model (CAM 3.0), NCAR Tech. Note, NCAR/TN-464+STR, Natl. Cent. for Atmos. Res, 2004.

Couvidat, F., Debry, é., Sartelet, K., and Seigneur, C.: A hydrophilic/hydrophobic organic (H^2O) model: Development, evaluation and sensitivity analysis, J. Geophys. Res., 117, D10304, doi:10.1029/2011JD017214, 2012.

Couvidat, F., Sartelet, K., and Seigneur, C.: Investigating the impact of aqueous-phase chemistry and wet deposition on organic aerosol formation using a molecular surrogate modeling approach, Environ. Sci. Technol., 47, 914-922, 2013a.

Couvidat, F., Kim, Y., Sartelet, K., Seigneur, C., Marchand, N., and Sciare, J.: Modeling secondary organic aerosol in an urban area: application to Paris, France, Atmos. Chem. Phys., 13, 983-996, 2013b.

Donahue, N. M., Robinson, A. L., Stanier, C. O., and Pandis, S. N.: Coupled partitioning, dilution, and chemical aging of semivolatile organics, Environ. Sci. Technol., 40, 2635-2643, 2006.

Donahue, N. M., Epstein, S. A., Pandis, S. N., and Robinson, A. L.: A two-dimensional volatility basis set: 1. organic-aerosol mixing thermodynamics, Atmos. Chem. Phys., 11, 3303-3318, 2011.

Donahue, N. M., Kroll, J. H., Pandis, S. N., and Robinson, A. L.: A two-dimensional volatility basis set: 2. Diagnostics of organic-aerosol evolution, Atmos. Chem. Phys., 11, 615-634, 2012.

Dunne, J. P., John, J. G., Adcroft, A. J., Griffies, S. M., Hallberg, R. W., Shevliakova, E., Stouffer, R. J., Cooke, W., Dunne, K. A., Harrison, M. J., Krasting, J. P., Malyshev, S. L., Milly, P. C. D., Phillipps, P. J., Sentman, L. T., Samuels, B. L., Spelman, M. J., Winton, M., Wittenberg, A. T., and Zadeh, N.: GFDL's ESM2 global coupled climate-carbon earth system models. Part I: Physical formulation and baseline simulation characteristics, J. Climate, 25, 6646-6665, 2012.

Dunne, J. P., John, J. G., Shevliakova, E., Stouffer, R. J., Krasting, J. P., Malyshev, S. L., Milly, P. C. D., Sentman, L. T., Adcroft, A. J., Cooke, W., Dunne, K. A., Griffies, S. M., Hallberg, R. W., Harrison, M. J., Levy, H., Wittenberg, A. T., Phillips, P. J., and Zadeh, N.: GFDL's ESM2 global coupled climate-carbon earth system models. Part II: Carbon system formulation and baseline simulation characteristics, J. Climate, 26, 2247-2267, 2013.

Dutkiewicz, S., Sokolov, A. P., Scott, J., and Stone, P. H.: A three-dimensional ocean-seaice-carbon cycle model and its coupling to a two-dimensional atmospheric model: Uses in climate change studies, Rep. 122, Joint Program on the Sci. and Policy of Global Change, 51 pp., Mass. Inst. of Technol., Cambridge, May 2005.

Emmons, L. K., Walters, S., Hess, P. G., Lamarque, J.-F., Pfister, G. G., Fillmore, D., Granier, C., Guenther, A., Kinnison, D., Laepple, T., Orlando, J., Tie, X., Tyndall, G., Wiedinmyer, C., Baughcum, S. L., and Kloster, S.: Description and evaluation of the Model for Ozone and Related chemical Tracers, version 4 (MOZART-4), Geosci. Model Dev., 3, 43-67, doi:10.5194/gmd-3-43-2010, 2010.

ENVIRON: User's Guide to the Comprehensive Air Quality Model with Extensions (CAMx) Version 2.0, Available at: http://www.camx.com, 1998.

ENVIRON: User's guide to the Comprehensive Air Quality Model with Extensions (CAMx). Version 5.2, Available at: http://www.camx.com, 2010.

Faraji, M., Kimura, Y., McDonald-Buller, E., and Allen, D.: Comparison of the carbon bond and SAPRC photochemical mechanisms under conditions relevant to southeast Texas, Atmos. Environ., 42, 5821–5836, doi:10.1016/j.atmosenv.2007.07.048, 2008.

Fast, J. D., Gustafson Jr., W. I., Easter, R. C., Zaveri, R. A., Barnard, J. C., Chapman, E. G., Grell, G. A., and Peckham, S. E.: Evolution of ozone, particulates, and aerosol direct radiative forcing in the vicinity of Houston using a fully coupled meteorology-chemistry-aerosol model, J. Geophys. Res., 111, D21305, doi:10.1029/2005JD006721, 2006.

Fountoukis, C. and Nenes, A.: Continued development of a cloud droplet formation parameterization for global climate models, J. Geophys. Res., 110, D11212, doi:10.1029/2004 JD005591, 2005.

Fountoukis, C and Nenes, A.: ISORROPIA II: a computationally efficient thermodynamic equilibrium model for K^+- Ca^{2+} -Mg^{2+} -NH^{4+} -Na^+-SO_4^{2-}-NO_3^--Cl^--H_2O aerosols, Atmos. Chem. Phys., 7, 4639–4659, doi:10.5194/acp-7-4639-2007, 2007.

Frost, G. J., McKeen, S. A., Trainer, M., Ryerson, T. B., Neuman, J. A., Roberts, J. M., Swanson, A., Holloway, J. S., Sueper, D. T., Fortin, T., Parrish, D. D., Fehsenfeld, F. C., Flocke, F., Peckham, S. E., Grell, G. A., Kowal, D., Cartwright, J., Auerbach, N., and Habermann, T.: Effects of changing power plant NOx emissions on ozone in the eastern

United States: Proof of concept, J. Geophys. Res., 111, D12306, doi:10.1029/2005JD006354, 2006.

Gantt, B., He, J., Zhang, X., Zhang, Y., and Nenes, A.: Incorporation of advanced aerosol activation treatments into CESM/CAM5: model evaluation and impacts on aerosol indirect effects, Atmos. Chem. Phys., 14, 7485-7497, 2014.

Gery, M. W., Whitten, G. Z., Killus, J. P., and Dodge, M. C.: A photochemical kinetics mechanism for urban and regional scale computer modeling, J. Geophys. Res., 94(D10), 12,925-12,956, doi:10.1029/JD094iD10p12925, 1989.

Gettelman, A., Morrison, H., and Ghan, S. J.: A new two-moment bulk stratiform cloud microphysics scheme in the community atmosphere model, version 3 (CAM3). Part II: Single-column and global results, J. Climate, 21(15), 3660-3679, 2008.

GFDL Global Atmospheric Model Development Team: The new GFDL Global Atmosphere and Land Model AM2-LM2: Evaluation with prescribed SST simulations, J. Clim., 17, 4641-4673, 2004.

Ghan, S. J., Abdul-Razzak, H., Nenes, A., Ming, Y., Liu, X., Ovchinnikov, M., Shipway, B., Meskhidze, N., Xu, J., and Shi, X.: Droplet nucleation: physically-based parameterizations and comparative evaluation, J. Adv. Model. Earth Syst., 3, M10001, doi:10.1029/2011MS000074, 2011.

Ghan, S. J., Liu, X., Easter, R. C., Zaveri, R., Rasch, P. J., and Yoon, J.-H.: Toward a minimal representation of aerosols in climate models: comparative decomposition of aerosol direct, semidirect, and indirect radiative forcing, J. Climate, 25, 6461-6476, 2012.

Ghan, S. J. and Zaveri, R. A.: Parameterization of optical properties for hydrated internally mixed aerosol, J. Geophys. Res., 112, D10201, doi:10.1029/2006JD007927, 2007.

Giorgetta, A. Jungclaus, M, J., Reick, C. H., Legutke, S., Bader, J., Bottinger, M., Brovkin, V., Crueger, T., Esch, M., Fieg, K., Glushak, K., Gayler, V., Haak, H., Hollweg, H.-D., Ilyina, T., Kinne, S., Kornblueh, L., Matei, D., Mauritsen, T., Mikolajewicz, U., Mueller, W., Notz, D., Pithan, F., Raddatz, T., Rast, S., Redler, R., Roeckner, E., Schmidt, H.,

Schnur, R., Segschneider, J., Six, K. D., Stockhause, M., Timmreck, C., Wegner, J., Widmann, H., Wieners, K.-H., Claussen, M., Marotzke, J., and Stevens, B.: Climate and carbon cycle changes from 1850 to 2100 in MPI-ESM simulations for the Coupled Model Intercomparison Project phase 5, J. Adv. Model. Earth Syst., 5, 572-597, doi:10.1002/jame.20038, 2013.

Glotfelty, T., He, J., Gantt, B., and Zhang, Y.: Implementing a Volatility Basis Set Approach for Simulation of Secondary Organic Aerosol and its Climatic Impacts in CESM-CAM5, Abstract A31D-0107 presented at 2013 Fall Meeting, AGU, San Francisco, CA, December 9-13, 2013.

Glotfelty, T., He, J., and Zhang, Y.: Updated organic aerosol treatments in CESM/CAM5: development and initial application, in preparation, 2015.

Granier, C., Bessagnet, B., Bond, T., D'Angiola, A., Denier van der Gon, H., Frost, G. J., Heil, A., Kaiser, J. W., Kinne, S., Klimont, Z., Kloster, S., Lamarque, J.-F., Liousse, C., Masui, T., Meleux, F., Mieville, A., Ohara, T., Raut, J.-C., Riahi, K., Schultz, M. G., Smith, S. J., Thompson, A., van Aardenne, J., van der Werf, G. R., and van Vuuren, D. P.: Evolution of anthropogenic and biomass burning emissions of air pollutants at global and regional scales during the 1980-2010 period, Climatic Change, 109, 163-190, doi:10.1007/s10584-011-0154-1, 2011.

Grell, G. A., Peckham, S. E., Schmitz, R., McKeen, S. A., Frost, G., Skamarock, W. C., and Eder, B.: Fully coupled "online" chemistry within the WRF model, Atmos. Environ., 39 (37), 6957-6975. http://dx.doi.org/10.1016/j.atmosenv.2005.04.027, 2005.

Grell, G. A. and Freitas, S. R.: A scale and aerosol aware stochastic convective parameterization for weather and air quality modeling, Atmos. Chem. Phys., 14, 5233-5250, doi:10.5194/acp-14-5233-2014, 2014.

Guenther, A. B., Jiang, X., Heald, C. L., Sakulyanontvittaya, T., Duhl, T., Emmons, L. K., and Wang, X.: The Model of Emissions of Gases and Aerosols from Nature version 2.1 (MEGAN2.1): an extended and updated framework for modeling biogenic emissions, Geosci. Model Dev., 5, 1471-1492, doi:10.5194/gmd-5-1471-2012, 2012.

Guenther A., Karl, T., Harley, P., Wiedinmyer, C., Palmer, P. I., and Geron, C.: Estimates of global terrestrial isoprene emissions using MEGAN (Model of Emissions of Gases and Aerosols from Nature), Atmos. Chem. Phys., 6, 3181-3210, 2006.

He, J. and Zhang, Y.: Improvement and further development in CESM/CAM5: gas-phase chemistry and inorganic aerosol treatments, Atmos. Chem. Phys., 14, 9171-9200, doi:10.5194/acp-14-9171-2014, 2014.

He, J., Zhang, Y., Glotfelty, T., He, R., Bennartz, R., Rausch, J., and Sartelet, K.: Decadal simulation and comprehensive evaluation of CESM/CAM5.1 and advanced chemistry, aerosol microphysics, and aerosol-cloud interactions, J. Adv. Model. Earth Syst., 7, 110-141, doi: 10.1002/2014MS000360, 2015.

He, R. and Wilkin, J. L.: Barotropic tides on the southeast New England shelf: A view from a hybrid data assimilative modeling approach, J. Geophys. Res., 111, C08002, doi:10.1029/2005JC003254, 2006.

He, R., McGillicuddy Jr., D. J., Keafer, B. A., and Anderson, D. M.: Historic 2005 toxic bloom of Alexandrium fundyense in the western Gulf of Maine: 2. Coupled biological numerical modeling, 113, C07040, doi:10.1029/2007JC004602, 2008.

Heald, C. L., Henze, D. K., Horowitz, L. W., Feddema, J., Lamarque, J.-F., Guenther, A., Hess, P. G., Vitt, F., Seinfeld, J. H., Goldstein, A. H., and Fung, I.: Predicted change in global secondary organic aerosol concentrations in response to future climate, emissions, and land use change, J. Geophys. Res., 113, D05211, doi:10.1029/2007JD009092, 2008.

Heintzenberg, J.: Fine particles in the global troposphere, A review. Tellus, 41B, 149-160, 1989.

Hoffmann, T., O'Dowd, C. D., and Seinfeld, J. H.: Iodine oxide homogeneous nucleation: An explanation for coastal new particle production, Geophys. Res. Lett., 28(10), 1949-1952, 2001.

Horowitz, L. W.: Past, present, and future concentrations of tropospheric ozone and aerosols: methodology, ozone evaluation, and sensitivity to aerosol wet removal, J. Geophys. Res., 111, D22211, doi:10.1029/2005JD006937, 2006.

Hodzic, A., Jimenez, J. L., Madronich, S., Canagaratna, M. R., DeCarlo, P. F., Kleinman, L., and Fast, J.: Modeling organic aerosols in a mega-city: Potential contribution of semi-volatile and intermediate volatility primary organic compounds to secondary organic aerosol formation, Atmos. Chem. Phys., 10(12), 5491-5514, doi:10.5194/acp-10-5491-2010, 2010.

Hu, X.-M., Y. Zhang, M. Z. Jacobson, and C. K. Chan: Coupling and evaluating gas/particle mass transfer treatments for aerosol simulation and forecast, J. Geophys. Res., 113, D11208, doi:10.1029/2007JD009588, 2008.

Hudman, R. C., Jacob, D. J., Turquety, S., Leibensperger, E. M., Murray, L. T., Wu, S., Gilliland, A. B., Avery, M., Bertram, T. H., Brune, W., Cohen, R. C., Dibb, J. E., Flocke, F. M., Fried, A., Holloway, J., Neuman, J. A., Orville, R., Perring, A., Ren, X., Sachse, G. W., Singh, H. B., Swanson, A., and Wooldridge, P. J.: Surface and lightning sources of nitrogen oxides over the United States: Magnitudes, chemical evolution, and outflow, J. Geophys. Res., 112, D12S05, doi:10.1029/2006JD007912, 2007.

Hurrell, J. W., Holland, M. M., Gent, P. R., Ghan, S., Kay, J. E., Kushner, P. J., Lamarque, J.-F., Large, W. G., Lawrence, D., Lindsay, K., Lipscomb, W. H., Long, M. C., Mahowald, N., Marsh, D. R., Neale, R. B., Rasch, P., Vavrus, S., Vertenstein, M., Bader, D., Collins, W. D., Hack, J. J., Kiehl, J., and Marshall, S.: The Community Earth System Model: A framework for collaborative research, Bull. Amer. Meteor. Soc., 94, 1339-1360, 2013.

Iacono, M. J., Delamere, J. S., Mlawer, E. J., and Clough, S. A.: Evaluation of upper tropospheric water vapor in the NCAR Community Climate Model (CCM3) using modeled and observed HIRS radiances, J. Geophys. Res., 108(D2), 4037, doi:10.1029/2002jd002539, 2003.

Iacono, M. J., Delamere, J. S., Mlawer, E. J., Shephard, M. W., Clough S. A., and Collins, W. D.: Radiative forcing by long-lived greenhouse gases: Calculations with the AER radiative transfer models, J. Geophys. Res., 113(D13), D13103, doi:10.1029/2008jd009944, 2008.

Jackson, C. S., Sen, M. K., Huerta, G., Deng, Y., and Bowman, K. P.: Error Reduction and Convergence in Climate Prediction, J. Climate, 21, 6698-6709, doi:10.1175/2008jcli2112.1, 2008.

Jacob, D. J., Crawford, J. H., Maring, H., Clarke, A. D., Dibb, J. E., Emmons, L. K., Ferrare, R. A., Hostetler, C. A., Russell, P. B., Singh, H. B., Thompson, A. M., Shaw, G. E., McCauley, E., Pederson, J. R., and Fisher, J. A.: The Arctic Research of the Composition of the Troposphere from Aircraft and Satellites (ARCTAS) mission: design, execution, and first results, Atmos. Chem. Phys., 10, 5191-5212, doi:10.5194/acp-10-5191-2010, 2010.

Jacob, D. J. and Winner, D. A.: Effect of climate change on air quality, Atmos. Environ., 43, 51-63, 2009.

Jacobson, M. Z.: Studying the effect of calcium and magnesium on size-distributed nitrate and ammonium with EQUISOLV II, Atmos. Environ., 33, 3635-3649, 1999.

Jacobson, M. Z.: Short-term effects of controlling fossil-fuel soot, biofuel soot and gases, and methane on climate, Arctic ice, and air pollution health, J. Geophys. Res., 115, D14209, doi:10.1029/2009JD013795, 2010.

Jacobson, M. Z. (2005), A solution to the problem of nonequilibrium acid/base gas-particle transfer at long time step, Aerosol Sci. Technol., 39, 92-103.

Jathar, S. H., Farina, S. C., Robinson, A. L., and Adams, P. J.: The influence of semi-volatile and reactive primary emissions on the abundance and properties of global organic aerosol, Atmos. Chem. Phys., 11, 7727-7746, doi:10.5194/acp-11-7727-2011, 2011.

Jimenez, J. L., Canagaratna, M. R., Donahue, N. M., Prevot, A. S. H., Zhang, Q., Kroll, J. H., DeCarlo, P. F., Allan, J. D., Coe, H., Ng, N. L., Aiken, A. C., Docherty, K. S., Ulbrich, I. M., Grieshop, A. P., Robinson, A. L., Duplissy, J., Smith, J. D., Wilson, K. R., Lanz, V. A., Hueglin, C., Sunn, Y. L., Tian, J., Laaksonen, A., Raatikainen, T., Rautiainen, J., Vaattovaara, P., Ehn, M., Kulmala, M., Tomlinson, J. M., Collins, D. R., Cubison, M. J., Dunlea, E., J., Huffman, J. A., Onaasch, T. B., Alfarra, M. R., Williams, P. I., Bower, K.,

Kondo, Y., Schneider, J., Drewnick, F., Borrmann, S., Weimer, S., Demerjian, K., Salcedo, D., Cottrell, L., Griffin, R., Takami, A., Miyoshi, T., Hatakeyama, S., Shimono, A., Sun, J. Y., Zhang, Y. M., Dzepina, K., Kimmel, J. R., Sueper, D., Jayne, J. T., Herndon, S. C., Trimborn, A. M., Williams, L. R., Wood, E. C., Middlebrook, A. M., Kolb, C. E., Baltensperger, U., Worsnop, D. R.: Evolution of organic aerosols in the atmosphere, Science, 326, 1525-1529, doi:10.1126/science.1180353, 2009.

Karamchandani, P., Zhang, Y., Chen, S.-Y., and Balmori-Bronson, R.: Development of an extended chemical mechanism for global-through-urban applications, Atmos. Pollut. Res., 3, 1-24, doi: 10.5094/APR.2011.047, 2012.

Kay, J. E., Hillman, B. R., Klein, S. A., Zhang, Y., Medeiros, B., Pincus, R., Gettelman, A., Eaton, B., Boyle, J., Marchand, R., and Ackerman, T. P.: Exposing global cloud biases in the Community Atmosphere Model (CAM) using satellite observations and their corresponding instrument simulators, J. Climate, 25, 5190-5207, doi:10.1175/JCLI-D-11-00469.1, 2012.

Kelly, J. T., P. V. Bhave, C. G. Nolte, U. Shankar, and K. M. Foley: Simulating emission and chemical evolution of coarse sea-salt particles in the Community Multiscale Air Quality (CMAQ) model, Geosci. Model Dev., 3, 257-273, 2010.

Keppel-Aleks, G., Randerson, J. T., Lindsay, K., Stephens, B. B., Moore, J. K., Doney, S. C., Thornton, P. E., Mahowald, N. M., Hoffman, F. M., Sweeney, C., Tans, P. P., Wennberg, P. O., and Wofsy, S. C.: Atmospheric carbon dioxide variability in the Community Earth System Model: Evaluation and transient dynamics during the twentieth and twenty-first centuries, J. Climate, 26, 4447-4475, 2013.

Kim Y., Sartelet, K., and Seigneur C.: Comparison of two gas-phase chemical kinetic mechanisms of ozone formation over Europe, J. Atmo. Chem., 62, 89-119, DOI10.1007/s10874-009-9142-5, 2009.

Kim, Y., Sartelet, K., and Seigneur, C.: Formation of secondary aerosols: impact of the gas-phase chemical mechanism, Atmos. Chem. Phys. 11, 583-598, doi:10.5194/acp-11-583-2011, 2011a.

Kim, Y., Couvidat, F., Sartelet, K., and Seigneur, C.: Comparison of different gas-phase mechanisms and aerosol modules for simulating particulate matter formation, J. Air Waste Manage. Assoc., 61, 1218-1226, doi:10.1080/10473289.2011.603999, 2011b.

Kinnison, D. E., Brasseur, G. P., Walters, S., Garcia, R. R., Marsh, D. A., Sassi, F., Boville, B. A., Harvey, L., Randall, C., Emmons, L., Lamarque, J.-F., Hess, P., Orlando, J., Tyndall, G., Tie, X. X., Randel, W., Pan, L., Gettelman, A., Granier, C., Diehl, T., Niemeier, U., and Simmons, A. J.: Sensitivity of chemical tracers to meteorological parameters in the MOZART-3 chemical transport model, J. Geophys. Res., 112, D20302, doi:10.1029/2006JD007879, 2007.

Knote, C., Tuccella, P., Curci, G., Emmons, L., Orlando, J. J., Madronich, S., Baró, R., Jiménez-Guerrero, P., Luecken, D., Hogrefe, C., Forkel, R., Werhahn, J., Hirtl, M., Pérez, J. L., San José, R., Giordano, L., Brunner, D., Khairunnisa, Y., and Zhang, Y.: Influence of the choice of gas-phase mechanism on predictions of key gaseous pollutants during the AQMEII phase-2 intercomparison, Atmos. Environ., 115, 553-568, doi: 10.1016/j.atmosenv.2014.11.066, 2014a.

Knote, C., Hodzic, A., Jimenez, J. L., Volkamer, R., Orlando, J. J., Baidar, S., Brioude, J., Fast, J. Gentner, D. R., Goldstein, A. H., Hayes, P. L., Knighton, W. B., Oetjen, H., Setyan, A., Stark, H., Thalman, R., Tyndall, G., Washenfelder, R., Waxman, E., and Zhang, Q.: Simulation of semi-explicit mechanisms of SOA formation from glyoxal in aerosol in a 3-D model, Atmos. Chem. Phys., 14, 6213-6239, doi:10.5194/acp-14-6213-2014, 2014b.

Koloutsou-Vakakis S., Rood, M. J., Nenes, A., and Pilinis, C.: Modeling of aerosol properties related to direct climate forcing, J. Geophys. Res., 103(D14), 17009-17032, doi: 10.1029/98JD00068, 1998.

Kumar, P., Sokolik, I. N., and Nenes, A.: Parameterization of cloud droplet formation for global and regional models: including adsorption activation from insoluble CCN, Atmos. Chem. Phys., 9, 2517-2532, doi:10.5194/acp-9-2517-2009, 2009.

Kulmala, M., Vehkamaki, H., Petaja, T., Dal Maso, M., Lauri, A., Kerminen, V.-M., Birmili, W., and McMurry, P.: Formation and growth rates of ultrafine atmospheric particles: A review of observations, J. Aerosol Sci., 35, 143-176, 2004.

Lamarque, J.-F., Bond, T. C., Eyring, V., Granier, C., Heil, A., Klimont, Z., Lee, D., Liousse, C., Mieville, A., Owen, B., Schultz, M. G., Shindell, D., Smith, S. J., Stehfest, E., Van Aardenne, J., Cooper, O. R., Kainuma, M., Mahowald, N., Mc- Connell, J. R., Naik, V., Riahi, K., and van Vuuren, D. P.: Historical (1850-2000) gridded anthropogenic and biomass burning emissions of reactive gases and aerosols: methodology and application, Atmos. Chem. Phys., 10, 7017-7039, doi:10.5194/acp- 10-7017-2010, 2010.

Lamarque, J. F., Emmons, L. K., Hess, P. G., Kinnison, D. E., Tilmes, S., Vitt, F., Heald, C. L., Holland, E. A., Lauritzen, P. H., Neu, J., Orlando, J. J., Rasch, P. J., and Tyndall, G. K.:CAM-chem: description and evaluation of interactive atmospheric chemistry in CESM, Geosci. Model Dev., 5, 369-411, doi:10.5194/gmd-5-369-2012, 2012.

Lamarque, J.-F., Kiehl, J. T., Hess, P. G., Collins, W. D., Emmons, L. K., Ginoux, P., Luo, C., and Tie, X. X.: Response of a coupled chemistry-climate model to changes in aerosol emissions: global impact on the hydrological cycle and the tropospheric burdens of OH, ozone, and NOx, J. Geophys. Res., 32, L16809, doi:10.1029/2005GL023419, 2005.

Lamarque, J.-F., McConnell, J. R., Shindell, D. T., Orlando, J. J., and Tyndall, G. S.: Understanding the drivers for the 20th century change of hydrogen peroxide in Antarctic ice-cores, Geophys. Res. Lett., 38, L04810, doi:10.1029/2010GL045992, 2011a.

Lamarque, J.-F., Kyle, G. P., Meinshausen, M., Riahi, K., Smith, S. J., van Vuuren, D. P., Conley, A., and Vitt, F.: Global and regional evolution of short-lived radiatively-active gases and aerosols in the Representative Concentration Pathways, Climatic Change, 109, 191-212, 2011b.

Lamarque, J.-F., Kinnison, D. E., Hess, P. G., and Vitt, F.: Simulated lower stratospheric trends between 1970 and 2005: identifying the role of climate and composition changes, J. Geophys. Res., 113, D12301, doi:10.1029/2007JD009277, 2008.

Lamarque, J. F., Shinedell, D. T., Josse, B., Young, P. J., Cionni, I., Eyring, V., Bergmann, D., Cameron-Smith, P., Collins, W. J., Doherty, R., Dalsoren, S., Faluvegi, G., Folberth, G., Ghan, S. J., Hiriwutz, L. W., Lee, Y. H., MacKenzie, I. A., Nagashima, T., Naik, V., Plummer, D., Righi, M., Rumbold, S. T., Schulz, M., Skeie, R. B., Stevenson, D. S., Strode, S., Sudo, K., Szopa, S., Voulgarakis, A., and Zeng, G.: The atmospheric chemistry and climate model intercomparison project: overview and description of models, simulations and climate diagnostics, Geosci. Model Dev., 6, 179-206, doi:10.5194/gmd-6-179-2013, 2013.

Lamarque, J.-F. and Solomon, S.: Impact of Changes in Climate and Halocarbons on Recent Lower Stratosphere Ozone and Temperature Trends, J. Climate, 23, 2599-2611, 2010.

Lane, T. E., Donahue, N. M., and Pandis, S. N.: Simulating secondary organic aerosol formation using the volatility basis-set approach in a chemical transport model, Atmos. Environ., 42(32), 7439–7451, doi:10.1016/j.atmosenv.2008.06.026, 2008.

Lawrence, D. M., Oleson, K. W., Flanner, M. G., Thornton, P. E., Swenson, S. C., Lawrence, P. J., Zeng, X., Yang, Z.-L., Levis, S., Sakaguchi, K., Bonan, G. B., and Slater, A. G.: Parameterization improvements and functional and structural advances in version 4 of the Community Land Model, J. Adv. Model. Earth Syst., 3, Art. 2011MS000045, 27 pp, doi: 10.1029/2011MS000045, 2011.

Langmann, B., Varghese, S., Marmer, E., Vignati, E., Wilson, J., Stier, P., and O'Dowd, C.: Aerosol distribution over Europe: a model evaluation study with detailed aerosol microphysics, Atmos. Chem. Phys., 8, 1591-1607, 2008.

Lawrence, D. M., Oleson, K. W., Flanner, M. G., Thornton, P. E., Swenson, S. C., Lawrence, P. J., Zeng, X., Yang, Z.-L., Levis, S., Sakaguchi, K., Bonan, G. B., and Slater, A. G.: Parameterization improvements and functional and structural advances in version 4 of the Community Land Model, J. Adv. Model. Earth Syst., 3, Art. 2011MS000045, 27 pp, doi: 10.1029/2011MS000045, 2011.

Levy, R. C., Mattoo, S., Munchak, L. A., Remer, L. A., Sayer, A. M., Patadia, F., and Hsu, N. C.: The Collection 6 MODIS aerosol products over land and ocean, Atmos. Meas. Tech., 6, 2989–3034, doi:10.5194/amt-6-2989-2013, 2013.

Lewandowski, M., Piletic, I. R., Kleindienst, T. E., Offenberg, J. H., Beaver, M. R., Jaoui, M., Docherty, K. S., and Edney, E. O.: Secondary organic aerosol characterization at field sites across the United States during the spring-summer period, Int. J. Environ. An. Ch., 93, 1084-1103, 2013.

Liao, H., Adams, P. J., Chung, S. H., Seinfeld, J. H., Mickley, L. J., and Jacob, D. J.: Interactions between tropospheric chemistry and aerosols in a unified general circulation model, J. Geophys. Res., 108(D1), 4001, doi:10.1029/2001JD001260, 2003.

Lipscomb, W. H., Fyke, J. G., Vizcaino, M., Sacks, W. J., Wolfe, J., Vertenstein, M., Craig, A., Kluzek, E., and Lawrence, D. M.: Implementation and initial evaluation of the Glimmer Community Ice Sheet Model in the Community Earth System Model, J. Climate, 26, 7352-7371, 2013.

Liu, X., Easter, R. C., Ghan, S. J., Zaveri, R., Rasch, P., Shi, X., Lamarque, J.-F., Gettleman, A., Morrison, H., Vitt, F., Conley, A., Park, S., Neale, R., Hannay, C., Ekman, A. M. L., Hess, P., Mahowald, N., Collins, W., Iacono, M.J., Bretherton, C. S., Flanner, M. G., and Mitchell, D.L.: Toward a minimal representation of aerosols in climate models: description and evaluation in the Community Atmosphere Model CAM5, Geosci. Model Dev., 5, 709-739, 2012.

Luecken, D. J., Phillips, S., Sarwar, G., and Jang, C.: Effects of using the CB05 vs. SAPRC99 vs. CB4 chemical mechanism on model predictions: Ozone and gas-phase photochemical precursor concentrations, Atmos. Environ., 42, 5805-5820, doi:10.1016/j.atmosenv.2007.08.056, 2008.

Ma, P.-L., Rasch, P. J., Wang, H., Zhang, K., Easter, R. C., Tilmes, S., Fast, J. D., Liu, X., Yoon, J.-H., and Lamarque, J.-F.: The role of circulation features on black carbon transport into the Arctic in the Community Atmosphere Model version 5 (CAM5), J. Geophys. Res. Atmos., 118, 4657-4669, doi:10.1002/jgrd.50411, 2013.

Marchesiello, McWilliams, P. J. C., and Shchepetkin, A.: Equilibrium structure and dynamics of the California current system, J. Phys. Oceanogr., 33, 753-783, 2003.

Marsh, A. R. W., and McElory, W. J.: The dissociation constant and Henry's law constant of HCl in aqueous solution, Atmos. Environ., 19, 1075-1080, 1985.

Martensson, E. M., Nilsson, E. D., deLeeuw, G., Cohen, L. H., and Hansson, H. C.: Laboratory simulations and parameterization of the primary marine aerosol production, J. Geophys. Res., 108(D9), 4297, doi:10.1029/2002JD002263, 2003.

Martin, G. M., Bellouin, N., Collins, W. J., Culverwell, I. D., Halloran, P. R., Hardiman, S. C., Hinton, T. J., Jones, C. D., McDonald, R. E., McLaren, A. J., O'Connor, F. M., Roberts, M. J., Rodriguez, J. M., Woodward, S., Best, M. J., Brooks, M. E., Brown, A. R., Butchart, N., Dearden, C., Derbyshire, S. H., Dharssi, I., Doutriaux-Boucher, M., Edwards, J. M., Falloon, P. D., Gedney, N., Gray, L. J., Hewitt, H. T., Hobson, M., Huddleston, M. R., Hughes, J., Ineson, S., Ingram, W. J., James, P. M., Johns, T. C., Johnson, C. E., Jones, A., Jones, C. P., Joshi, M. M., Keen, A. B., Liddicoat, S., Lock, A. P., Maidens, A. V., Manners, J. C., Milton, S. F., Rae, J. G. L., Ridley, J. K., Sellar, A., Senior, C. A., Totterdell, I. J., Verhoef, A., Vidale, P. L., and Wiltshire, A.: The HadGEM2 family of Met Office Unified Model climate configurations, Geosci. Model Dev., 4, 723-757, doi:10.5194/gmd-4-723-2011, 2011.

May, A. A., Presto, A. A., Hennigan, C. J., Nguyen, N. T., Gordon, T. D., and Robinson, A. I.: Gas-particle partitioning of primary organic aerosol emissions: (1), gasoline vehicle exhaust, Atmos. Environ., 77, 128-139, doi:10.1016/j.atmosenv.2013.04.060, 2013a.

May, A. A., Levin, E. J. T., Hennigan, C. J., Riipinen, I., Lee, T., Collett Jr., J. L., Jimenez, J. L., Kreidenweis, S. M., and Robinson, A. L.: Gas-particle partitioning of primary organic aerosol emissions: 3. Biomass burning, J. Geophys. Res. Atmos., 118, 11,327-11,338, doi:10.1002/jgrd.50828, 2013b.

Meng, Z. and Seinfeld, J. H.: Time scales to achieve atmospheric gas-aerosol equilibrium for volatile species, Atmos. Environ., 30, 2889-2900, 1996.

Meng, Z, Dabdub, D., and Seinfeld, J.H.: Size- and chemically-resolved model of atmospheric aerosol dynamics. J. Geophys. Res., 103, 3419-3435, 1998.

Merikanto, J., Napari, I., Vehkamaki, H., Anttila, T., and Kulmala, M.: New parameterization of sulfuric acid-ammonia-water ternary nucleation rates at tropospheric conditions, J. Geophys. Res., 112, D15207, doi: 10.1029/2006JD007977, 2007.

Mlawer, E. J., Taubman, S. J., Brown, P. D., Iacono, M. J., and Clough, S. A.: Radiative transfer for inhomogeneous atmospheres: RRTM, a validated correlated-k model for the longwave, J. Geophys. Res., 102(D14), 16663-16682, 1997.

Michoud, V., Kukui, A., Camredon, M., Colomb, A., Borbon, A., Miet, K., Aumont, B., Beekmann, M., Durand-Jolibois, R., Perrier, S., Zapf, P., Siour, G., Ait-Helal, W., Locoge, N., Sauvage, S., Afif, C., Gros, V., Furger, M., Ancellet, G., and. Doussin, J. F.: Radical budget analysis in a suburban European site during the MEGAPOLI summer field campaign, Atmos. Chem. Phys., 12, 11951-11974, doi:10.5194/acp-12-11951-2012, 2012.

Monier, E., Scott, J. R., Sokolov, A. P., Forest, C. E., and Schlosser, C. A.: An integrated assessment modeling framework for uncertainty studies in global and regional climate change: the MIT IGSM-CAM (version 1.0), Geosci. Model Dev., 6, 2063-2085, 2013.

Morrison, H. and Gettelman, A.: A new two-moment bulk stratiform cloud microphysics scheme in the community atmosphere model, version 3 (CAM3). Part I: Description and numerical tests, J. Climate, 21(15), 3642-3659, 2008.

Murphy, J. M., Sexton, D. M. H., Barnett, D. N., Jones, G. S., Webb, M. J., and Collins, M.: Quantification of modeling uncertainties in a large ensemble of climate change simulations, Nature, 430, 768-772, doi:10.1038/nature02771, 2004.

Nakajima, T. Y., Suzuki, K., and Stephens, G. L.: Droplet Growth in Warm Water Clouds Observed by the A-Train. Part I: Sensitivity Analysis of the MODIS-Derived Cloud Droplet Sizes, Journal of the Atmospheric Sciences, 67(6), 1884-189610.1175/2009jas3280.1, 2010.

Neale, R. B., Chen, C. C., Gettelman, A., Lauritzen, P. H., Park, S., Williamson, D. L., Conley, A. J., Garcia, R., Kinnison, D., Lamarque, J. F., Marsh, D., Mills, M., Smith, A. K., Tilmes, S., Vitt, F., Morrison, H., Cameron-Smith, P., Collins, W. D., Iacono, M. J., Easter, R. C., Ghan, S. J., Liu, X. H., Rasch, P. J., and Taylor, M. A.: Description of the NCAR Community Atmosphere Model (CAM5.0), NCAR Tech. Note, NCAR/TN-486+STR, Natl. Center. for Atmos. Res., 2012.

Nelson, J., He, R., Warner, J. C., and Bane, J.: Air-sea interactions during strong winter extratropical storms, Ocean Dynamics, doi:10.1007/s10236-014-0745-2, 2014.

Nenes, A., Pandis, S. N., and Pilinis, C.: ISORROPIA: A new thermodynamic equilibrium model for multiphase multicomponent inorganic aerosols, Aquatic Geochemistry, 4, 123-152, 1998.

Nenes, A. and Seinfeld, J. H.: Parameterization of cloud droplet formation in global climate models, J. Geophys. Res., 108(D14), 4415, doi:10.1029/2002JD002911, 2003.

O'Connor, F. M., Johnson, C. E., Morgenstern, O., Abraham, N. L., Braesicke, P., Dalvi, M., Folberth, G. A., Sanderson, M. G., Telford, P. J., Voulgarakis, A., Young, P. J., Zeng, G., Collins, W. J., and Pyle, J. A.: Evaluation of the new UKCA climate-composition model-Part 2: The troposphere, Geosci. Model Develop., 7, 41-91, doi:10.5194/gmd-7-41-2014, 2014.

Pan, L. L., Bowman, K. P., Atlas, E. L., Wofsy, S. C., Zhang, F., Bresch, J. F., Ridley, B. A., Pittman, J. V., Homeyer, C. R., Romashkin, P., and Cooper, W. A.: The stratosphere-troposphere analyses of regional transport 2008 (START08) experiment, Bull. Am. Meteorol. Soc., 91, 327-342, 2010.

Park, S. and Bretherton, C. S.: The university of Washington shallow convection and moist turbulence schemes and their impact on climate simulations with the community atmosphere model, J. Climate, 22, 3449-3469, 2009.

Pollard, R. T., Rhines, P. B., and Thompson, R. O. R. Y.: The deepening of the wind mixed layer, Geophys. Fluid Dyn., 3, 381-404, 1973.

Price, C. and Rind, D.: A simple lightning parameterization for calculating global lightning distributions, J. Geophys. Res., 97, 9919-9933, doi:10.1029/92JD00719, 1992.

Price, C., Penner, J., and Prather, M.: NO_x from lightning 1, Global distribution based on lightning physics, J. Geophys. Res., 102, 5929-5941, 1997.

Raes, F., Augustin, J., and Vandingenen, R.: The role of ion-induced aerosol formation in the lower atmosphere, J. Aerosol Sci., 17, 466-470, doi: 10.1016/0021-8502(86)90135-7, 1986.

Rausch, J., Heidinger, A., and Bennartz, R.: Regional assessment of microphysical properties of marine boundary layer cloud using the PATMOS-x dataset, J. Geophys. Res., 115, D23212, doi:10.1029/2010JD014468, 2010.

Reiter, R.: Phenomena in atmospheric and environmental electricity, Elsevier, New York, 1992.

Reutter, P., Su, H., Trentmann, J., Simmel, M., Rose, D., Gunthe, S. S., Wernli, H., Andreae, M. O., and Pöschl, U.: Aerosol- and updraft-limited regimes of cloud droplet formation: influence of particle number, size and hygroscopicity on the activation of cloud condensation nuclei (CCN), Atmos. Chem. Phys., 9, 7067-7080, doi:10.5194/acp-9-7067-2009, 2009.

Robinson, A. L., Donahue, N. M., Shrivastava, M. K., Weitkamp, E. A., Sage, A. M., Grieshop, A. P., Lane, T. E., Pierce, J. R., and Pandis, S. N.: Rethinking organic aerosols: Semivolatile emissions and photochemical aging, Science, 315, 1259-1262, doi:10.1126/science.1133061, 2007.

Ryerson, T. B., Andrews, A. E., Angevine, W. M., Bates, T. S., Brock, C. A., Cairns, B., Cohen, R. C., Cooper, O. R., de Gouw, J. A., Fehsenfeld, F. C., Ferrare, R. A., Fischer, M. L., Flagan, R. C., Goldstein, A. H., Hair, J. W., Hardesty, R. M., Hostetler, C. A., Jimenez, J. L., Langford, A. O., McCauley, E., McKeen, S. A., Molina, L. T., Nenes, A., Oltmans, S. J., Parrish, D. D., Pederson, J. R., Pierce, R. B., Prather, K., Quinn, P. K., Seinfeld, J. H., Senff, C. J., Sorooshian, A., Stutz, J., Surratt, J. D., Trainer, M., Volkamer, R., Williams, E. J., and Wofsy, S. C.: The 2010 California Research at the Nexus of Air Quality and

Climate Change (CalNex) field study, J. Geophys. Res., 118, 5830-5866, doi:10.1002/jgrd.50331, 2013.

Sander S. P., Friedl, R. R., Golden, D. M., Kurylo, M. J., Huie, R. E., Orkin, V. L., Moortgat, G. K., Ravishankara, A. R., Kolb, C. E., Molina, M. J., and Finlayson-Pitts, B. J.: Chemical kinetics and photochemical data for use in atmospheric studies, National Aeronautics and Space Administration, Jet Propulsion Laboratory California Institute of Technology Pasadena, California, 2003.

Sarwar, G., Luecken, D., Yarwood, G., Whitten, G., and Carter, W. P. L.: Impact of an updated carbon bond mechanism on predictions from the Community Multiscale Air Quality Model, J. Appl. Meteorol. Climatol., 47, 3-14, doi:10.1175/2007JAMC1393.1, 2008.

Sarwar, G., Fahey, K., Napelenok, S., Roselle, S., and Mathur, R.: Examining the impact of CMAQ model updates on aerosol sulfate predictions. In: The 10th Annual CMAS Models-3 User's Conference, October, Chapel Hill, NC, 2011.

Seethala, C. and Horvath, Á.: Global assessment of AMSR-E and MODIS cloud liquid water path retrievals in warm oceanic clouds, J. Geophys. Res., 115, D13202, doi:10.1029/2009JD012662, 2010.

Seinfeld, J. H. and Pandis, S. N.: Atmospheric chemistry and physics: From air pollution to climate change, 2 ed., John Wiley & Sons, Inc, 2006.

Shrivastava, M. K., Lane, T. E., Donahue, N. M., Pandis, S. N., and Robinson, A. L.: Effects of gas particle partitioning and aging of primary emissions on urban and regional organic aerosol concentrations, J. Geophys. Res., 113, D18301, doi:10.1029/2007JD009735, 2008.

Shrivastava, M., Zelenyuk, A., Imre, D., Easter, R., Beranek, J., Zaveri, R. A., and Fast, J.: Implications of low volatility SOA and gas-phase fragmentation reactions on SOA loadings and their spatial and temporal evolution in the atmosphere, J. Geophys. Res., 118, 3328-3342, doi:10.1002/jgrd.50160, 2013.

Sihto, S. L., Kulmala, M., Kerminen, V. M., Maso, M. D., Petaja, T., Riipinen, I., Korhonen, H., Arnold, F., Janson, R., Boy, M., Laaksonen, A., and Lehtinen, K. E. J.: Atmospheric sulphuric acid and aerosol formation: implications from atmospheric measurements for nucleation and early growth mechanisms, Atmospheric Chemistry and Physics, 6, 4079-4091, 2006.

Smith, S. R., Legler, D. M., and Verzone, K. V.: Quantifying uncertainties in NCEP Reanalyses using high-quality research vessel observations, J. Climate, 14, 4062-4072. doi: http://dx.doi.org/10.1175/1520-0442(2001)014<4062:QUINRU>2.0.CO;2, 2001.

Smith S. J., van Aardenne, J., Klimont, Z., Andres, R., Volke, A., Delgado Arias, S.: Anthropogenic sulfur dioxide emissions: 1850-2005. Atmos Chem Phys., 11, 1101-1116. doi:10.5194/acp-11-1101-2011, 2011.

Stainer, C. O., Donahue, N., and Pandis, S. N.: Parameterization of secondary organic aerosol mass fractions from smog chamber data, Atmos. Environ., 42, 2276-2299, doi:10.1016/j.atmosenv.2007.12.042, 2008.

Stevens, B., Giorgetta, M., Esch, M., Mauritsen, T., Crueger, T., Rast, S., Salzmann, M., Schmidt, H., Bader, J., Block, K., Brokopf, R., Fast, I., Kinne, S., Kornbluech, L., Lohmann, U., Pincus, R., Reichler, T., and Roeckner, E.: Atmospheric component of the MPI-M Earth System Model: ECHAM6, J. Adv. Model. Earth Syst., 5, 146-172, doi:10.1002/jame.20015, 2013.

Sokolov, A. P., Schlosser, C. A., Dutkiewicz, S., Paltsev, S., Kicklighter, D., Jacoby, H. D., Prinn, R. G., Forest, C. E., Reilly, J. M., Wang, C., Felzer, B., Sarofim, M. C., Scott, J., Stone, P. H., Melillo, J. M., and Cohen, J.: The MIT Integrated Global System Model (IGSM) Version 2: Model description and baseline evaluation, Rep. 124, Joint Program on the Sci. and Policy of Global Change, 46 pp., Mass. Inst. of Technol., Cambridge, July 2005.

Sorjamaa, R. and Laaksonen, A.: The effect of H2O adsorption on cloud drop activation of insoluble particles: a theoretical framework, Atmos. Chem. Phys., 7, 6175-6180, 2007.

Spracklen, D. V., Carslaw, K. S., Kulmala, M., Kerminen, V.-M., Mann, G. W., and Sihto, S.-L.: The contribution of boundary layer nucleation events to total particle concentrations on regional and global scales, Atmos. Chem. Phys., 6, 5631-5648, 2006.

Stephens, G. L.: Cloud feedbacks in the climate system: A critical review, J. Climate, 18(2), 237-273, 2005.

Stier, P., Feichter, J., Kinne, S., Kloster, S., Vignati, E., Wilson, J., Ganzeveld, L., Tegen, I., Werner, M., Balkanski, Y., Schulz, M., Boucher, O., Minikin, A., and Petzold, A.: The aerosol-climate model ECHAM5-HAM, Atmos. Chem. Phys., 5, 1125-1156, doi:10.5194/acp-5-1125-2005, 2005.

Taylor, K. E: Summarizing multiple aspects of model performance in a single diagram, J. Geophys. Res., 106, 7183-7192, 2001.

Textor, C., Schulz, M., Guibert, S., Kinne, S., Balkanski, Y., Bauer, S., Berntsen, T., Berglen, T., Boucher , O., Chin, M., Dentener, F., Diehl, T., Easter, R., Feichter, H., Fillmore, D., Ghan, S., Ginoux, P., Gong, S., Grini, A., Hendricks, J., Horowitz, L., Huang, P., Isaksen, I., Iversen, I., Kloster, S., Koch, D., Kirkevag, A., Kristjansson, J. E., Krol, M., Lauer, A., Lamarque, J. F., Liu, X., Montanaro, V., Myhre, G., Penner, J., Pitari, G., Reddy, S., Seland, Ø., Stier, P., Takemura, T., and Tie, X.: Analysis and quantification of the diversities of aerosol life cycles within AeroCom, Atmos. Chem. Phys., 6, 1777-1813, doi:10.5194/acp-6-1777-2006, 2006.

Tilmes, S., Lamarque, J.-F., Emmons, L. K., Kinnison, D. E., Ma, P.-L., Liu, X., Ghan, S., Bardeen, C., Arnold, S., Deeter, M., Vitt, F., Ryerson, T., Elkins, J. W., Moore, F., Spackman, R., and Martin, M. V.: Description and evaluation of tropospheric chemistry and aerosols in the Community Earth System Model (CESM1.2), Geosci. Model Dev., 8, 1395-1426, doi:10.5194/gmd-8-1395-2015, 2015.

Tsimpidi, A. P., Karydis, V. A., Zavala, M., Lei, W., Molina, L., Ulbrich, I. M., Jimenez, J. L., and Pandis, S. N.: Evaluation of the volatility basis-set approach for the simulation of organic aerosol formation in the Mexico City metropolitan area, Atmos. Chem. Phys., 10, 525-546, doi:10.5194/acp-10-525-2010, 2010.

Tsigaridis. K., Krol, M., Dentener, F. J., Balkanski, Y., Lathiere, J., Metzger, S., Hauglustaine, D. A., and Kanakidou, M.: Change in global aerosol composition since preindustrial times, Atmos. Chem. Phys., 6, 5143-5162, 2006.

Usoskin, I. G. and Kovaltsov, G. A.: Cosmic ray induced ionization in the atmosphere: full modeling and practical applications, J. Geophys. Res., 111, D21206, doi:10.1029/2006JD007150, 2006.

van Dingenen, R. and Raes, F.: Ternary nucleation of methane sulphonic acid, sulphuric acid and water vapour, J. Aerosol Sci., 24, 1-17, doi:10.1016/0021-8502(93)90081-J, 1993.

Van Pelt, R. S. and Zobeck, T. M.: Chemical constituents of fugitive dust, Environ. Monit. Assess., 130, 3-16, doi:10.1007/s10661-006-9446-8, 2007.

Vehkamaki, H., Kulmala, M., Napari, I., Lehtinen, K. E. J., Timmreck., C., Noppel, M., and Laaksonen, A.: an improved parameterization for sulfuric acid-water nucleation rates for tropospheric and stratospheric conditions, Journal of Geophysical Research-Atmospheres, 107(D22), 4622, doi:10.1029/2002JD002184, 2002.

Wang, H., Easter, R. C., Rasch, P. J.,Wang, M., Liu, X., Ghan, S. J., Qian, Y., Yoon, J.-H., Ma, P.-L., and Vinoj, V.: Sensitivity of remote aerosol distributions to representation of cloud–aerosol interactions in a global climate model, Geosci. Model Dev., 6, 765-782, doi:10.5194/gmd-6-765-2013, 2013.

Wang, K., Zhang, Y., Nenes, A., and Fountoukis, C.: Implementation of dust emission and chemistry into the Community Multiscale Air Quality modeling system and initial application to an Asian dust storm episode, Atmos. Chem. Phys., 12, 10209-10237, doi:10.5194/acp-12-10209-2012, 2012.

Wang, K., Yahya, K., Zhang, Y., Wu, S.-Y., and Grell, G.: Implementation and initial application of a new chemistry-aerosol option in WRF/Chem for simulation of secondary organic aerosols and aerosol indirect effects, Atmos. Environ., 115, 716-732, 2014a.

Wang, K., Yahya, K., Zhang, Y., Christian, H., George, P., Christoph, K., Alma, H., Roberto, S. J., Juan, L. P., Pedro, J.-G., Rocio, B., Paul, M., and Ralf, B.: A multi-model assessment

for the 2006 and 2010 simulations under the Air Quality Model Evaluation International Initiative (AQMEII) phase 2 over North America: part II. Evaluation of column variable predictions using satellite data, Atmos. Environ., 115, 587-603, http://dx.doi.org/10.1016/j.atmosenv.2014.07.044, 2014b.

Wang, M. and Penner, J. E.: Aerosol indirect forcing in a global model with particle nucleation, Atmos. Chem. Phys., 9, 239-260, 2009.

Washenfelder, R., Young, C., Brown, S., Angevine, W., Atlas, E., Blake, D., Bon, D., Cubison, M., De Gouw, J., Dusanter, S., Flynn, J., Gilman, J. B., Graus, M., Griffith, S., Grossberg, N., Hayes, P. L., Jimenez, J., Kuster, W., Lefer, B. L., Pollack, I., Ryerson, T., Stark, H., Stevens, P. S., and Trainer, M.: The glyoxal budget and its contribution to organic aerosol for Los Angeles, California, during CalNex 2010, J. Geophys. Res., 116, D00V02, doi:10.1029/2011JD016314, 2011.

Warner, J. C., Armstrong, B., He, R., and Zambon, J. B.: Development of a coupled ocean-atmosphere-wave-sediment transport (COWAST) modeling system, Ocean Modelling, 35, 230-244, doi:10.1016/j.ocemod.2010.07.010, 2010.

Williams, J. E., Scheele, M. P., van Velthoven, P. F. J., Cammas, J.-P., Thouret, V. Galy-Lacaux, C., and Volz-Thomas, A.: The influence of biogenic emissions from Africa on tropical tropospheric ozone during 2006: a global modeling study, Atmos. Chem. Phys., 9, 5729-5749, 2009.

Wu, R., and Kirtman, B. P.: Roles of Indian and Pacific Ocean air-sea coupling in tropical atmospheric variability, Clim. Dyn., 25, 155-170, 2005.

Wu, R., and Kirtman, B. P.: Regimes of seasonal air-sea interaction and implications for performance of forced simulations, Clim. Dyn., 29, 393-410, 2007.

Xie, S., Liu, X., Zhao, C., and Zhang, Y.: Sensitivity of CAM5-simulated arctic clouds and radiation to ice nucleation parameterization, J. Climate, 26, 5981-5999, doi:10.1175/JCLI-D-12-00517.1, 2013.

Yahya, K., Wang, K., Gudoshava, M., Glotfelty, T., and Zhang, Y.: Application of WRF/Chem over the Continental U.S. Under the AQMEII Phase II: Comprehensive Evaluation of 2006 Simulation, Atmos. Environ., 115, 733-755, 2014.

Yahya, K., Wang, K., Zhang, Y., Hogrefe, C., Pouliot, G., and Kleindienst, T.: Application of WRF/Chem version 3.4.1 over North America under the AQMEII Phase 2: evaluation of 2010 application and responses of air quality and meteorology-chemistry interactions to changes in emissions and meteorology from 2006 to 2010, Geosci. Model Dev., 8, 2095-2117, doi:10.5194/gmd-8-2095-2015, 2015.

Yarwood, G., Rao, S., Yocke, M., and Whitten, G. Z.: Updates to the carbon bond mechanism: CB05, Report to the U.S. Environmental Protection Agency, RT-04-00675, 2005.

Young, P. J., Archibald, A. T., Bowman, K. W., Lamarque, J.-F., Naik, V., Stevenson, D. S., Tilmes, S., Voulgarakis, A., Wild, O., Bergmann, D., Cameron-Smith, P., Cionni, I., Collins, W. J., Dalsøren, S. B., Doherty, R. M., Eyring, V., Faluvegi, G., Horowitz, L. W., Josse, B., Lee, Y. H., MacKenzie, I. A., Nagashima, T., Plummer, D. A., Righi, M., Rumbold, S. T., Skeie, R. B., Shindell, D. T., Strode, S. A., Sudo, K., Szopa, S., and Zeng, G.: Pre-industrial to end 21st century projections of tropospheric ozone from the Atmospheric Chemistry and Climate Model Intercomparison Project (ACCMIP), Atmos. Chem. Phys., 13, 2063-2090, doi:10.5194/acp-13-2063-2013, 2013.

Yu, F.: Ion-mediated nucleation in the atmosphere: Key controlling parameters, implications, and look-up table, J. Geophys. Res., 115, D03206, doi: 10.1029/2009JD012630, 2010.

Yu, F., Luo, G., Liu, X., Easter, R. C., Ma, X., and Ghan, S. J.: Indirect radiative forcing by ion-mediated nucleation of aerosol, Atmos. Chem. Phys., 12, 11451-11463, 2012.

Yu, F., Wang, Z., Luo, G., and Turco, R. P.: Ion-mediated nucleation as an important global source of tropospheric aerosols, Atmos. Chem. Phys., 8, 2537-2554, 2008.

Zambon, J. B., He, R., and Warner, J. C.: Investigation of Hurricane Ivan using the Coupled Ocean-Atmosphere-Wave-Sediment Transport (COAWST) Model, Ocean Dynamics, 64(11), pp. 1535-1554, doi:10.1007/s10236-014-0777-7, 2014.

Zaveri, R. A., Easter, R. C., and Peters, L. K.: A computationally efficient multicomponent equilibrium solver for aerosols (MESA), J. Geophys. Res., 110, D24203, doi: 10.1029/2004JD005618, 2005.

Zaveri, R. A., R. C. Easter, J. D. Fast, and L. K. Peters: Model for Simulating Aerosol Interactions and Chemistry (MOSAIC), J. Geophys. Res., 113, D13204, doi:10.1029/2007JD008782, 2008.

Zender, C. S., Bian, H., and Newman, D.: The mineral Dust Entrainment And Deposition (DEAD) model: Description and 1990s dust climatology, J. Geophys. Res., 108(D14), 4416, doi: 10.1029/2002JD002775, 2003.

Zhang, G. J., and McFarlane, N. A.: Sensitivity of climate simulations to the parameterization of cumulus convection in the Canadian Climate Centre general circulation model, Atmosphere-Ocean, 33, 407-446, 1995.

Zhang, K. M., and A. S. Wexler: An Asynchronous Time-Stepping (ATS) integrator for atmospheric applications: Aerosol dynamics, Atmos. Environ., 40, 4574-4588, 2006.

Zhang, Q., Jimenez, J. L., Canagaratna, M. R., Allan, J. D., Coe, H., Ulbrich, I., Alfarra, M. R., Takami, A., Middlebrook, A. M., Sun, Y. L., Dzepina, K., Dunlea, E., Docherty, K., DeCarlo, P. F., Salcedo, D., Onasch, T., Jayne, J. T., Miyoshi, T., Shimono, A., Hatakeyama, S., Takegawa, N., Kondo, Y., Schneider, J., Drewnick, F., Borrmann, S., Weimer, S., Demerjian, K., Williams, P., Bower, K., Bahreini, R., Cottrell, L., Griffin, R. J., Rautiainen, J., Sun, J. Y., Zhang, Y. M., and Worsnop, D. R.: Ubiquity and dominance of oxygenated species in organic aerosols in anthropogenically-influenced Northern Hemisphere midlatitudes, Geophys. Res. Lett., 34, L13801, doi:10.1029/2007GL029979, 2007.

Zhang, Q., Quan, J., Tie, X., Huang, M., and Ma, X.: Impacts of aerosol particles on cloud formation: Aircraft measurements in China, Atmospheric Environment, 45, 665-672, 2011.

Zhang, Q. Streets, D. G., He, K., Wang, Y., Richter, A., Burrows, J., Uno, I., Jang, C., Chen, D., Yao, Z., and Lei, Y.: NO_x emission trends for China, 1995-2004: The view from the ground and the view from space, J. Geophys. Res., 112, D22306, doi:10.1029/2007JD008684, 2007.

Zhang, Q., Streets, D. G., Carmichael, G. R., He, K. B., Huo, H., Kannari, A., Klimont, Z., Park, I. S., Reddy, S., Fu, J. S., Chen, D., Duan, L., Lei, Y., Wang, L. T., and Yao, Z. L.: Asian emissions in 2006 for the NASA INTEX-B mission, Atmos. Chem. Phys., 9, 5131-5153, doi:10.5194/acp-9-5131-2009, 2009.

Zhang, Y., Bischof, C. H., Easter, R. C., and Wu, P.-T.: Sensitivity analysis of a mixed-phase chemical mechanism using automatic differentiation, J. Geophys. Res., 103 (D15), 18,953-18,979, 1998.

Zhang, Y., Seigneur, C., Seinfeld, J. H., Jacobson, M., Clegg, S. L., Binkowski, F. S.: A comparative review of inorganic aerosol thermodynamic equilibrium modules: similarities, differences, and their likely causes, Atmos. Environ., 34, 117-137, 2000.

Zhang, Y., Pun, B., Vijayaraghavan, K., Wu, S.-Y., Seigneur, C., Pandis, S. N., Jacobson, M. Z., Nenes, A., and Seinfeld, J. H.: Development and application of the Model of Aerosol Dynamics, Reaction, Ionization, and Dissolution (MADRID), J. Geophys. Res., 109, D01202, doi:10.1029/2003JD003501, 2004.

Zhang, Y., McMurry, P. H., Yu, F., and Jacobson, M. Z.: A comparative study of nucleation parameterizations: 1. Examination and evaluation of the formulations, J. Geophys. Res., 115, D20212, doi: 10.1029/2010JD014150, 2010a.

Zhang, Y., Pan, Y., Wang, K., Fast, J. D., and Grell, G. A.: WRF/Chem-MADRID: Incorporation of an aerosol module into WRF/Chem and its initial application to the TexAQS2000 episode, J. Geophys. Res., 115, D18202, doi:10.1029/2009JD013443, 2010b.

Zhang, Y., Chen, Y., Sarwar, G., and Schere, K.: Impacts of gas-phase mechanisms on weather research forecasting model with chemistry (WRF/Chem) predictions: Mechanism

implementation and comparative evaluation, J. Geophys. Res., 117, D01301, doi: 10.1029/2011JD015775, 2012a.

Zhang, Y., Karamchandani, P., Glotfelty, T., Street, D. G., Grell, G., Nenes, A., Yu, F., and Bennartz, R.: Development and initial application of the global-through-urban weather research and forecasting model with chemistry (GU-WRF/Chem), J. Geophys. Res., 117, D20206, doi:10.1029/2012JD017966, 2012b.

Zhang, Y., Vijayaraghavan, K., Wen, X.-Y., Snell, H. E., and Jacobson, M. Z.: Probing into regional ozone and particulate matter pollution in the United States: 1. A 1 year CMAQ simulation and evaluation using surface and satellite data, J. Geophys. Res. 114, D22304, http://dx.doi.org/10.1029/2009JD011898, 2009.

Zhang, Y., Zhang, X., Wang, L.-T., Zhang, Q., Duan, F.-K., and He, K.-B.: Application of WRF/Chem over East Asia: Part I. Model Evaluation and Intercomparison with MM5/CMAQ, Atmospheric Environment, in press, 2015a.

Zhang, Y., Zhang, X., Wang, K., Zhang, Q., Duan, F.-K., and He, K.-B.: Application of WRF/Chem over East Asia: Part II. Model Improvement and Sensitivity Simulations, Atmospheric Environment, in press, 2015b.

Zhang, Z. and Platnick, S.: An assessment of differences between cloud effective particle radius retrievals for marine water clouds from three MODIS spectral bands, J. Geophys. Res., 116, D20215, doi: 10.1029/2011 JD016216, 2011.

Zuend, A., Marcolli, C., Peter, T., and Seinfeld, J. H.: Computation of liquid-liquid equilibria and phase stabilities: implications for RH-dependent gas/particle partitioning of organic-inorganic aerosols, Atmos. Chem. Phys., 10, 7795-7820, doi:10.5194/acp-10-7795-2010, 2010.